CASCADED CONTROL FOR IMPROVED BUILDING HVAC PERFORMANCE

A Dissertation

by

CHRISTOPHER ROBIN PRICE

Submitted to the Office of Graduate and Professional Studies of
Texas A&M University
in partial fulfillment of the requirements for the degree of

DOCTOR OF PHILOSOPHY

Chair of Committee,	Bryan Rasmussen
Committee Members,	Douglas Allaire
	Juan Carlos Baltazar
	Reza Langari
Head of Department,	Andreas Polycarpou

December 2018

Major Subject: Mechanical Engineering

ABSTRACT

As of 2011 buildings consumed 41% of all primary energy in the U.S. and can represent more than 70% of peak demand on the electrical grid. Usage by this sector has grown almost 50% since the 1980s and projections foresee an additional growth of 17% by 2035 due to increases in population, new home construction, and commercial development. Three-quarters of building energy is derived from fossil fuels making it a large contributor of the country's CO_2 and NO_x output both of which greatly affect the environment and local air quality. Up to half of energy used by the building sector is related to Heating, Ventilation, and Air-Condition systems. Focusing on improving building HVAC control therefore has a large aggregate effect on US energy usage with economic and environmental benefits for end users.

This dissertation develops cascaded loop architectures as a solution to common HVAC control issues. These systems display strong load-dependent nonlinearities and coupling behaviors that can lead to actuator hunting (sustained input oscillations) from standard PI controllers that waste energy and cost money. Cascaded loops offer a simple way to eliminate hunting and decouple complex HVAC systems with minimal *a priori* knowledge of system dynamics. As cascaded loops are easily implementable in building automation systems they can be readily and widely adopted in the field.

An examination of the current state of PI control in HVAC and discussion of coordinated, optimal control strategies being developed for reduced energy usage are discussed in Chapter 1. The following two chapters outline the structure and benefits of the cascaded architecture and demonstrate the same using a series of simulation case studies. Implementation approaches and parameterizations of the architecture are explored in Chapter 4 with a derivation showing that the addition of an additional feedback path (i.e., inner loop

control) provides more design freedom and ultimately allows for improved control. Finally, Chapter 5 details results from initial cascaded loop implementation at three campus buildings. Results showed improved control performance and an elimination of identified hunting behavior.

DEDICATION

To Momther, Dadther, and Sistair. Your love and support made this possible.

ACKNOWLEDGMENTS

Firstly, I would like to offer my sincere thanks to my advisor Dr. Bryan Rasmussen. Without your help, guidance, and mentorship this work would not have been possible. You were always supportive and I cannot thank you enough for the opportunities that you gave me. I would also like to thank Dr. Douglas Allaire, Dr. Juan Carlos Baltazar, and Dr. Reza Langari for their time and service participating in my committee.

To my labmates (or Terra Mystica league depending on who you ask), thanks all of you for making the lab a wonderful and fun place to work. Your support and help were invaluable in completing this work. Your patience while listening to me talk about golf tournaments, darts, and other boring topics are also greatly appreciated.

A special thanks to Chris Dieckert at Texas A&M Utilities and Energy Services. Your help in granting access and learning the building operations made an entire chapter of this dissertation possible.

CONTRIBUTORS AND FUNDING SOURCES

Contributors

This work was supported by a dissertation committee consisting of Dr. Bryan Rasmussen (advisor), Dr. Douglas Allaire of of the Department of Mechanical Engineering, Dr. Reza Langari of the Department Engineering Technology & Industrial Distribution, and Dr. Juan Carlos Baltazar of the Department of Architecture.

Funding Sources

Funding for this work was made possible through several sources. Views expressed in this thesis are those of the author and are not representative of supporting organization.

- *Jun. 2013 - Dec. 2014:* Work was performed under the sponsorship of the U.S. Department of Commerce, National Institute of Standards and Technology (NIST), Grant Number: 60NANB12D209. The views expressed are those of the authors and are not representative of the U.S. Department of Commerce, NIST.
- *Jan. 2015 - Aug. 2015:* Research was indirectly supported by the US Department of Energy, Office of Energy Efficiency and Renewable Energy, Advanced Manufacturing Office, Industrial Assessment Center (IAC) Program Award Number: DE-EE0005527. Any opinions, findings, and conclusions or recommendations expressed in this material are those of the authors and do not necessarily reflect the views of the US Department of Energy.
- *Sep. 2015 - Dec. 2016:* Research was indirectly supported by a grant from South-Central Partnership for Energy Efficiency as a Resource (SPEER) through the IAC as part of a pilot program. Views expressed in this material are those of the authors and do not necessarily reflect the views of SPEER.

- *Jan. 2017 - Aug. 2018:* Research was supported by the National Science Foundation (NSF) under Grant Number: CMMI-1563361. Any opinions, findings, and conclusions or recommendations expressed in this material are those of the authors and do not necessarily reflect the views of the NSF.
- *Sep. 2017 - Aug. 2018:* Work was also supported by the American Society of Heating, Refrigeration and Air-Conditioning Engineers (ASHRAE) for the academic year starting in August 2017 through the competitive Grant-In-Aid award.

NOMENCLATURE

Building Technology

AHU	Air Handling Unit
ASHRAE	American Society of Heating, Refrigerating and Air-Conditioning Engineers
EEV	Electronic Expansion Valve
HVAC	Heating, Ventilation, and Air-Conditioning
LD/HD	Low/High Demand
TRV	Thermostatic Radiator Valve
TU	Terminal Unit
TXV/TEV	Thermostatic Expansion Valve
VAV	Variable Air Volume
VCC	Vapor Compression Cycle

Building Automation

APOGEE	Building automation software used by Texas A&M University Utilities
CHW	Chilled Water
PPCL	Powers Process Control Language
SCHW	Building Supply Chilled Water
SP	Duct Static Pressure
SPD	Fan/Pump Speed
VLV	Valve Position

Control Terms

AMIGO	Approximate $\mathcal{M}$-constrained Integral Optimization PI Tuning Method
FDD	Fault Detection and Diagnosis
I/O	Input/Output
LPF/HPF	Low/High Pass Filter
LPV	Linear Parameter Varying Model
LQR	Linear Quadratic Regulator Control
MIMO	Multi-Input-Multi-Output Control
MPC	Model Predictive Control
PID	Proportional-Integral-Derivative Control
SISO	Single-Input-Single-Output Control

Error Metrics

IAE	Integrated Absolute Error
MAE	Maximum Absolute Error
MSE	Mean Square Error
RMS	Root Mean Square Error

Analysis Terms

CDD	Cooling Degree Days
LFT	Linear Fractional Transformation
LMI	Linear Matrix Inequality
NGM	Nonlinear Gap Metric
QAD	Quarter-Amplitude Damping
RGA	Relative Gain Array
ZOH	Zero Order Hold

TABLE OF CONTENTS

LIST OF FIGURES

FIGURE Page

LIST OF TABLES

1. INTRODUCTION AND LITERATURE REVIEW

Improving energy efficiency in the building sector plays an important role in reducing total United States energy consumption. As of 2011 buildings consumed 41% of all primary energy in the U.S. (Figure 1.1) [1] and can represent more 70% of peak demand on the electrical grid [2]. Usage by this sector has grown almost 50% since the 1980's and projections foresee an additional growth of 17% by 2035 due to increases in population, as well as new home and commercial construction [1]. Three-quarters of building energy is derived from fossil fuels making it a large contributor of the country's CO_2 and NO_x output both of which greatly effect the environment and local air quality [1, 3, 4].

Almost 90% of a persons lifetime is estimated to occur indoors where rooms must be conditioned to insure comfort and productivity [5, 6]. Indeed, half of all energy used by buildings is related to just three operations: Heating, Ventilation, and Air-Conditioning (HVAC) (Figure 1.1). These processes also account for a significant part of expenditures

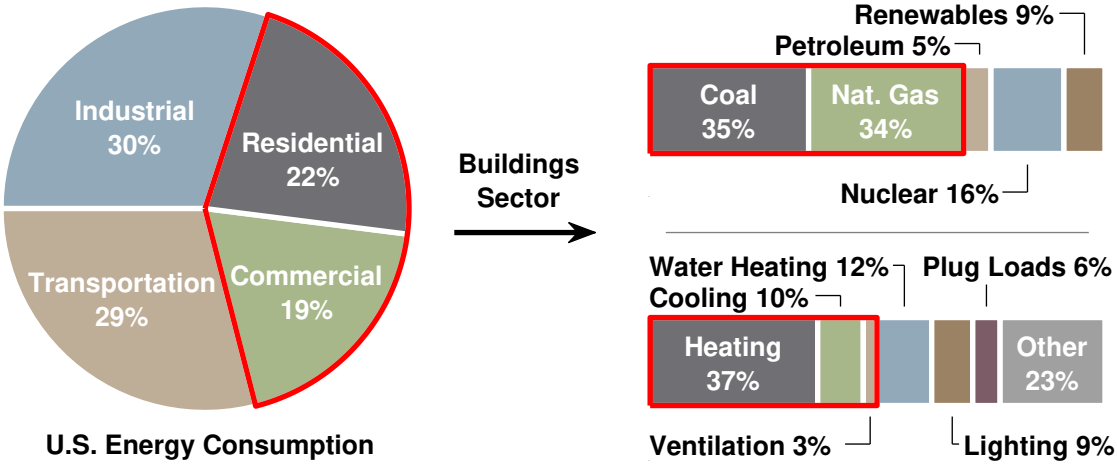

Figure 1.1: Buildings use 41% of all primary energy in the United States with 75% coming from fossil fuels. Half of that energy is used by HVAC systems (Figure adapted from [1]).

where splits are 23.4%, 14.3%, and 3.7% respectively [1]. Focus on building HVAC control can therefore have a large aggregate effect not only on building energy consumption but US energy usage as a whole with economic and environmental benefits for end users.

There is a large potential for HVAC energy savings through improved control and sensing. In the residential sector, more than 25% energy savings are possible through a combination of improved maintenance and continuous commissioning, a process of constantly ensuring a building meets its design efficiency rating [7]. For equivalent programs, the commercial sector could save more than 15% [8]. There are also energy savings associated with updating sensing and controls of building systems. Improvements such as central management systems, occupancy sensing, and demand controlled ventilation have potential to cut more than 30% of total building energy usage [9].

At the individual building level, energy savings may be equivalent to only a few hundred dollars per year in electricity cost savings. Due to the large number of buildings on the electrical grid, however, HVAC efficiency savings in the building sector are large en masse. Although there will always be efficiency savings from improved technology used in new construction, the majority of savings will be realized through better controls and/or retrofits of existing buildings. For example, approximately 80% of all US buildings were constructed before 2000 [10] with turnover of existing stock only 2-5% [11]. Because of stricter energy policy standards implemented in the last several decades, new buildings tend to use less energy [12] meaning that improvements to older construction will represent the majority of possible energy savings. With this in mind, the goals of this dissertation are to develop a cascaded control architecture to improve building HVAC component control. As it utilizes standard control techniques and is easily implementable in building automation software, it will enable widespread improvements in existing building control programs and can easily be incorporated into new systems as well.

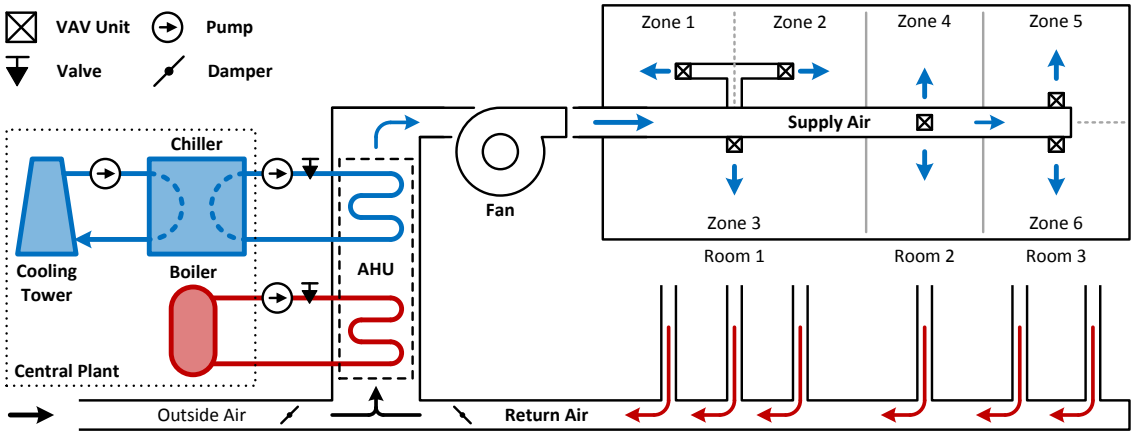

Figure 1.2: Example HVAC system diagram for a small building. Although responsible for only three rooms, there are a large number of subsystems, actuators and sensors.

1.1 Issues with Building Control*

Control of HVAC systems has some unique characteristics that make capturing potential savings difficult. Take for example the simplified schematic of an HVAC system for a small office building shown in Figure 1.2. This building has three main rooms divided into six zones inside a footprint of less than 3,500 square feet. Heating and cooling is accomplished by a centralized air-conditioning system. Supply air is circulated by a variable-speed fan responsible for maintaining static pressure in a series of ducts. Air flow into each zone is regulated by Variable Air Volume (VAV) boxes that modulate damper position to control flow based on heating load in each zone as well as minimum ventilation requirements such as ASHRAE Standard 62.1 [13]. Supply air temperature is regulated by an Air Handling Unit (AHU) that passes a combination of return and outside air over a set of coils. Hot and/or cold water is passed through these coils by pumps and valves connected to boiler and chiller systems. The chiller may further be connected to a centralized cooling tower that rejects heat to the environment. As can be seen, HVAC is an extremely

*Some material from this section was adapted by permission from Springer Nature: Chapter 4 - HVAC System Modeling and Control: Vapor Compression System Modeling and Control by B. Rasmussen, C. Price, J. Koeln, B. Keating, and A. Alleyne in Intelligent Building Control Systems ©2018 Springer.

Table 1.1: List of Sensing and Actuation Points for Example Building in Figure 1.2.

Sensors	Actuators
Zone Temperature (1-6)	VAV Dampers (1-6)
Zone Ventilation Rate (1-6)	Fan Speed
Supply Air Temperature	Supply Water Pumps
Supply Air Duct Pressure	Cold Water Valve
Supply Air Humidity	Hot Water Valve
Outside Air Temperature	Outside Air Damper
Return Air Temperature	Return Air Damper

broad term covering many different subsystems and actuators. Control of these systems must be very modular in order to ensure adequate performance of these desperate systems.

Apparent from the description above, HVAC systems will typically consist of numerous subsystems, sensors, and actuators. The example in Figure 1.2 consists of six VAV units, one supply fan, one AHU, and dampers that are connected downstream of a central heating and cooling plant. Control of the these systems involves approximately 17 sensors and 13 actuators summarized in Table 1.1. The issue of scale becomes even more pronounced when dealing with large buildings that have multiple AHUs and dozens of zones or with campuses consisting of multiple buildings. For example, the campus at Texas A&M has more than 200,000 sensors and actuators spread over 200 buildings covering approximately 14 million gross square feet [14]. The sheer number of control loops means that, in most cases, controls are never altered from factory settings or are marginally tuned at best. An effective control design for HVAC systems must therefore be easy to implement and tune as well as be modular enough to work with a broad range of systems.

Nonlinearities in HVAC systems and actuators make regulation difficult when using standard linear control techniques. Actuators themselves come in two main categories that effect how energy is used: obstruction and displacement. Obstruction actuators include

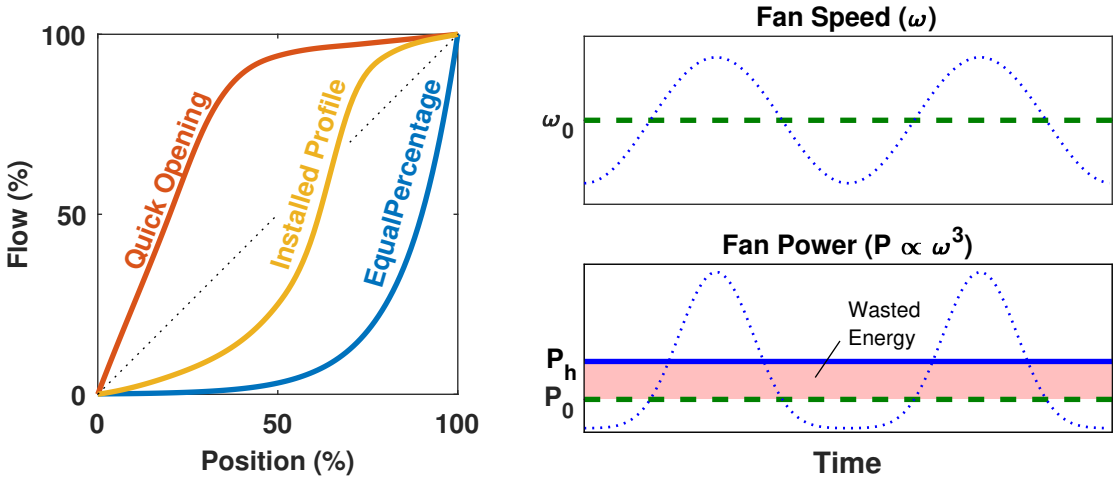

(a) (b)

Figure 1.3: (a) Valve flow profiles to reduce nonlinear behavior in an installed system. (b) Actuators with hunting behavior use more energy (P_h) than when at a constant speed (P_0) due to affinity laws. Adapted with permission from [15] ©2018 Springer.

the most well known HVAC components such as valves and dampers. These components open and close to impinge flow of a working fluid (e.g. air, water, refrigerant, etc.) and thereby control the rate of energy transfer. For example, an air conditioning expansion valve reduces outlet superheat of an evaporator by opening to allow more refrigerant flow. Obstruction actuators are inherently wasteful; energy must be spent to pressurize a working fluid and deliver it to its destination. That effort is squandered if the delivered pressure produces excess flow. Displacement actuators, however, actively consume electricity to displace the fluid. Such actuators include components such as fans, pumps, and compressors. While most energy consumption in an HVAC system will take place in these components, their use is necessary but can be minimized through control.

Both types of actuators can have nonlinear performance characteristics in terms of flow and energy consumption. Valves and dampers typically have a nonlinear relationship between position and flow (Figure 1.3(a)). While valves can be intentionally designed to have specific flow characteristics [16, 17], many are sized incorrectly or have the wrong

profile to provide any real benefit. These nonlinear attributes mean that actuators will have different effects on a system depending on conditions, leading to poor performance for static controllers in some ranges typically manifesting as undesired oscillations known as hunting. Operation of fans, pumps, and compressors can be described by well known affinity laws such as Equation 1.1 where there are cubic and quadratic relationships between power ($\dot{W}$), pressure (P), flow rate ($\dot{V}$), and speed (ω). These relationships mean that 10% reduction in fan and/or pump speed can reduce power input by more than 25%. Small reductions, therefore, in the use of these components can reap large energy savings.

$$\frac{\dot{W}_1}{\dot{W}_2} = \left(\frac{\omega_1}{\omega_2}\right)^3 \quad \& \quad \frac{P_1}{P_1} = \left(\frac{\omega_1}{\omega_2}\right)^2 \quad \& \quad \frac{\dot{V}_1}{\dot{V}_2} = \frac{\omega_1}{\omega_2} \tag{1.1}$$

HVAC actuators also display many classic nonlinear behaviors. Hysteresis is the dependence of an actuators output on time and previous input. For HVAC systems, faulty or loose linkages may cause immediate action in one direction but delayed action in another. This effect also manifests as actuator drift where position settings stray over time. Actuators can experience stiction effects whereby large input is required to start motion. This causes excessive input as controllers must wind up to overcome initial resistance. HVAC systems are also prone to faults and failures in sensing and control. Communication of temperature, occupancy, and ventilation data for multiple rooms and systems requires a large number of sensors any of which can fail or provide erroneous readings. Detailed descriptions of the behavior of specific HVAC equipment can be found in [18].

Other nonlinear HVAC effects stem from fundamental properties of heat and mass transfer. The main heat transfer modes used by HVAC systems for temperature control (free/forced convection and radiation) all display complex and time varying properties. Also, because the relationship between temperature differentials (e.g. ΔT in Equation 1.2) and actuator flow rates is multiplicative, HVAC systems have dynamics that are heavily de-

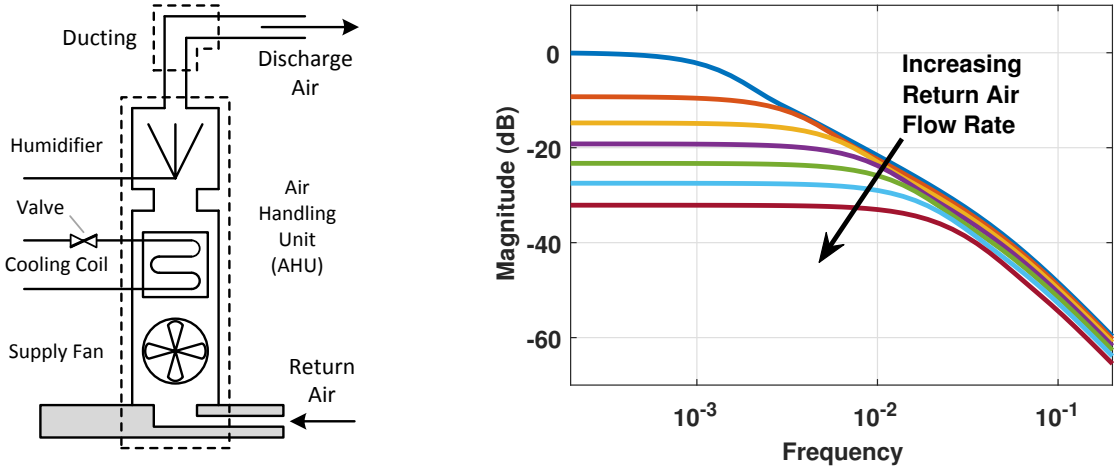

(a) (b)

Figure 1.4: (a) An AHU consists of a cooling coil, fan, ducting, and sometimes a humidifier. (b) For the model from Chapter 3, AHU dynamics can see a 40x range for steady-state gain over operating conditions. Adapted with permission from [15] ©2018 Springer.

pendent on system operating conditions. This is the case with Air Handling Units (AHUs) which can see large changes in dynamic response with load (Figure 1.4). Another example is Variable Air Volume (VAV) dynamics that are dependent on the relative difference between the supply air, current room air, and outside air temperatures as well as the current system static pressure and damper position as in Equation 1.2 from [19].

$$C_{rm} \cdot \frac{dT_{rm}}{dt} = \rho_a \cdot c_{p,a} \cdot \underbrace{\dot{V}(P_s, \theta)}_{\text{VAV Flow}} \cdot \underbrace{(T_s - T_{rm})}_{\Delta T_{rm}} + \alpha_{rm} \cdot \underbrace{(T_{oa} - T_{rm})}_{\Delta T_{oa}} + Q_{dis} \tag{1.2}$$

Each of the nonlinearities discussed play a part in a phenomenon known as actuator hunting, an issue that is well documented in the HVAC field (see [20], [21], or [22] for examples). Hunting manifests as large, relatively fast oscillations of the actuator (e.g. valves, dampers, fans, etc.) due to system control. Slow, period variations due to factors such as outside air temperature or solar loads are not considered hunting (Figure 1.5). Nonlinearity causes the dynamic characteristics of an HVAC system to vary significantly with operating

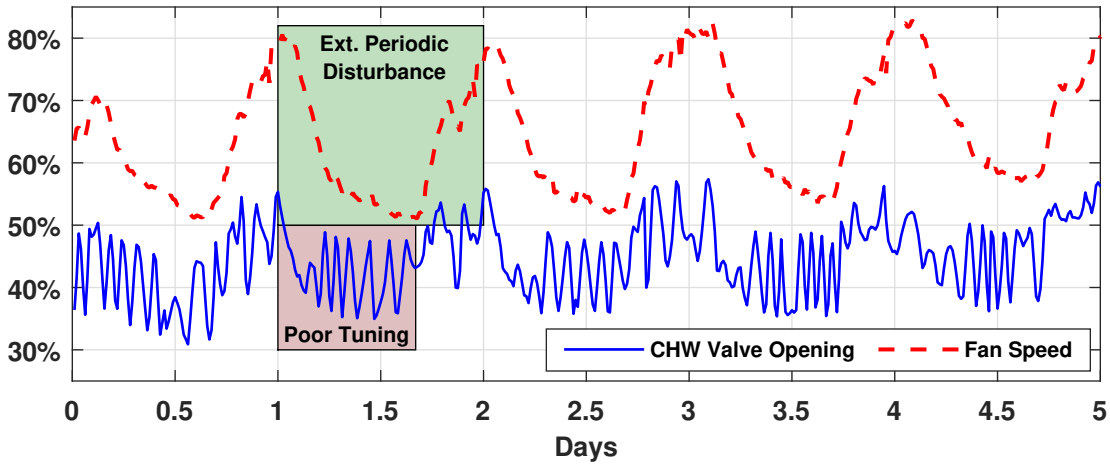

Figure 1.5: Hunting behavior is oscillatory behavior due to poor control. Slow, periodic disturbances such as weather conditions are not considered hunting.

condition. These changes have profound effects on control gains based on when a system is tuned. As system conditions move away from those under which tuning occurred, stability and performance will degrade. This causes oscillations in actuator control and can even affect up and downstream systems whose outputs will also begin to fluctuate. Combined, these effects result in unstable environmental conditions that reduce occupant comfort. In most cases, hunting is easily identifiable by inspection but automated detection methods do exist that have explicit criteria for magnitude and frequency [22].

Hunting actuators have several adverse effects that result in wasted energy and resources. As demonstrated in Figure 1.3(b), nonlinear power consumption in displacement actuators results in more energy being used when hunting occurs as there is more consumption above the mean input than below. The majority of cost savings will however be from reduced system maintenance. There is a small, infrequent cost saving due to reduced wear on the actuator resulting in less replacement of failed components. The larger cost savings will be from eliminating seasonal tuning of HVAC controls. Many institutions, including Texas A&M University, employ technicians to re-tune controllers biannually

or when hunting is detected. By reducing hunting and developing a control strategy that works effectively year-round, significant labor cost savings can be realized.

1.2 Detection of Poorly Performing HVAC Systems

Detection and identification of the root cause of performance issues in physical systems is known as Fault Detection and Diagnosis (FDD). Research into automating the FDD process has been very active in the aerospace, process control, and automotive fields (among many others) for decades [23]. Early HVAC FDD only began to appear during the 1980s and mainly focused on the operation of refrigeration systems and air handling units. FDD is especially important to building systems where it is estimated faults waste 5-30% of energy consumed by commercial buildings [24]. HVAC FDD can be purely used for diagnosis of faulty behavior but can also be used as part of a predictive maintenance program known as prognostication [23]. FDD methods can be based on modeling (either physics or statistics based) or complicated rule sets that are similar to fuzzy logic control. Comprehensive reviews of FDD methods can be found in [23, 24, 25, 26].

Fault detection methods are primarily focused on equipment issues meaning there is comparatively little research on detection of poorly performing control systems. In fact, there is no standard methodology in the HVAC industry that will verify a controller has been tuned properly [27]. In process control, the most common Control Performance Assessment (CPA) metric is the Harris Index [28] that compares performance to a theoretical Minimum Variance Controller. In practice however, this index can be too computationally complex for HVAC systems where there are often significant hardware limitations. Other CPA metrics use a variety of indices to determine performance ranging from dynamic response analysis or integral based error calculation to statistical methods. One method proposed by [29] for HVAC systems uses only superficial knowledge of a system to distinguish between sluggish or oscillatory responses and plant failure. An array of CPA indices

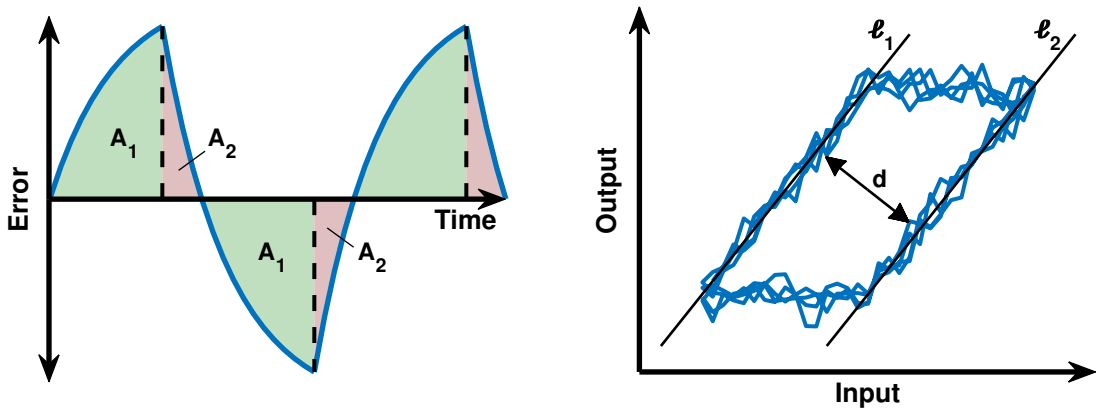

(a) (b)

Figure 1.6: (a) The ratio $A_1/A_2 \gg 1$ indicates actuator stiction (Figure adapted from [29]). (b) A method from [31] uses shape of an input-output plot to identify valve stiction.

were evaluated in [27] to identify metrics better suited for the HVAC field including the normalized Harris Index and exponentially weighted moving averages.

Beyond simple performance evaluation, detection of hunting behavior and/or poor control begins with identifying oscillations in the control signal. There are several methods that seek to automate this process by using a combination of common properties. This is usually a combination of calculating auto-correlation functions, detecting zero crossings, and integrated error functions (for more detail see Chapter 5). Alternatively, the method used to identify hunting in building systems in this dissertation uses the magnitude and time between consecutive sign changes to determine the presence of oscillations [30].

In [32], the symmetry of control error is used to determine the cause of oscillations. As seen in Figure 1.6(a), each half-period is divided and the ratio of the areas before and after the peak is computed. Aggressive or poorly tuned control tends to be sinusoidal resulting in a ratio of one, while stiction issues result in a ratio much greater than one. The method proposed by [31], also uses a metric to determine the presence of valve stiction. Each half period is fit assuming sinusoidal and triangular responses. The Stiction Index

(SI) is then the ratio of Mean Square Errors (MSE) for each fit defined by Equation 1.3. The approach proposed by [33] uses the cross-correlation between the input and output signals. Depending on the type of correlation (odd or even), the cause of oscillation can be determined as either stiction or due to an external oscillation disturbance. A more graphical approach was proposed by [34] by observing the shape of a two-axis input-output plot as in Figure 1.6(b). The shape of that plot is typically a parallelogram where stiction strongly affects the distance (d) between ℓ_1 and ℓ_2.

$$SI = \frac{MSE_{sin}}{MSE_{sin} + MSE_{Tri}} \tag{1.3}$$

From the discussion above, there are no currently available methods that can comprehensively identify and diagnose poor control performance in HVAC systems. A combination of methods can be employed to monitor performance and then systematically eliminate causes such as stiction or external disturbances. Having eliminated other causes, the root issue of poor controller performance can be established.

1.3 Traditional Building Control Strategies*

As in most fields, control of HVAC systems began with mechanically based regulation. Until the advent of computer technology, thermostats utilized bimetallic strips and relay control, also known as "bang-bang" control, to regulate temperature. Thermostats relied on the difference in thermal expansion between the two metals to operate a switch powering heating and cooling equipment. Although effective, this type of control can only regulate temperature between a substantial dead-band (Figure 1.7(a)). Such on/off control also extends to compressor and fan control. Typical refrigeration cabinets found in supermarkets and convenience stores use this strategy and are toggled by local thermostats. However

*Some material from this section was adapted by permission from Springer Nature: Chapter 4 - HVAC System Modeling and Control: Vapor Compression System Modeling and Control by B. Rasmussen, C. Price, J. Koeln, B. Keating, and A. Alleyne in Intelligent Building Control Systems ©2018 Springer.

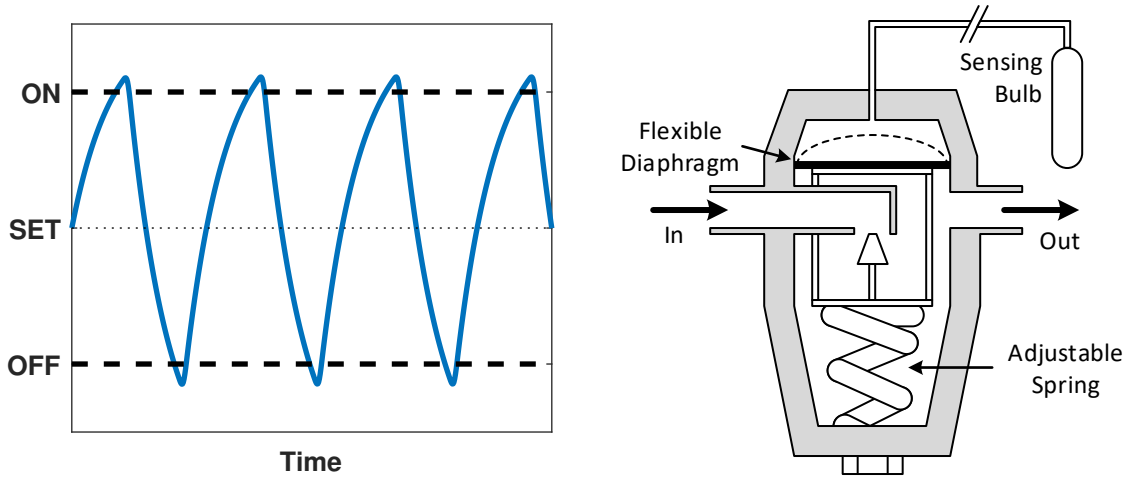

(a) (b)

Figure 1.7: (a) On/off control regulates HVAC equipment within a deadband. (b) TXV diagram showing the flexible diaphragm, sensing bulb, and adjustable setpoint spring.

on/off of control has documented issues with synchronization for parallel systems which can lead to higher electrical demand and poor temperature regulation [35, 36].

Other mechanical devices offer the ability to provide more analog control. For example, Vapor Compression Cycle (VCC) systems can regulate evaporator pressure using a mechanical valve known as a Pressure Regulating Valve (PRV). The valve uses a flexible diaphragm to adjust valve stem position based on fluctuations in system pressure. PRVs provide superior pressure disturbance rejection but are only suitable for applications with stable load requirements. The Thermostatic Expansion Valve (TEV or TXV) is an extension of a PRV that uses a sensing bulb filled with saturated refrigerant at the evaporator outlet to adjust valve position. As the evaporator discharge temperature changes, pressure inside the bulb fluctuates causing pressure differentials across the flexible diaphragm and thereby metering refrigerant. This configuration makes the TXV a superheat regulating device allowing it to adjust to changes in system demand. Due to the physical separation of the bulb and valve, these valves will often display hunting behavior [37]. A schematic of a TXV is shown in Figure 1.7(b) to demonstrate key principles mechanical control.

Over the past few decades, mechanical control devices have steadily been replaced by digital equivalents. These devices offer the ability to provide adjustable, remote, and modular control for many HVAC systems. For example, Electronic Expansion Valves (EEVs) for VCC systems use stepper motors to precisely change valve position based on digitally acquired signals. Likewise, Variable Frequency Drive (VFD) technology allows compressors, motors, and fans to operate at intermediate speeds based on system demand. Not surprisingly, digitization and miniaturization of technology has lead to the expansion of digital control strategies for HVAC systems.

1.3.1 PID Control

Despite large amounts of research and the development of many advanced control strategies in the past few years, the most dominant control strategies used today are still on/off and Proportional-Integral-Derivative (PID). One survey of 11,000 process controllers in refining, chemical, and paper industries found that 97% of all control loops were PID in structure [38]. PID is also extremely prevalent in Building Automation Controls (BAC) that are used for centralized HVAC management [22]. From Equation 1.4, a PID controller is made of three parts: a proportional component that directly responds to system error, an integral part that eliminates steady-state error, and a derivative component that prevents violent changes in control input. PID control is low order, versatile, and easily implementable. Note that the 'D' term is rarely used in most HVAC controllers due to its sensitivity to noise and perceived implementation difficulty. Despite its simplicity, PID has demonstrated effective control in a wide range of applications and even acceptable performance despite improper tuning. A future decline in the use of PID control seems unlikely as many advanced control strategies still utilize PID for local control underneath supervisory controllers and optimization algorithms [39].

$$u(t) = k_p \cdot e(t) + k_i \cdot \int_0^\infty e(t)dt + k_d \cdot \frac{d}{dt}e(t) \tag{1.4}$$

1.3.2 Simple PID Tuning

The main barrier for implementing PID control is determining the correct control gains for desired performance. The popularity of PID control has led to the development of dozens of parameter tuning methods, see [40] and [41]. Because PID tuning is such a vast field, the remainder of this section will focus on traditional and recent developments in PID control and tuning for HVAC systems. For more general PID tuning techniques see references like [42] or [43].

The tuning method created by Ziegler and Nichols [44] is by far the most ubiquitous procedure used in HVAC control today [45, Chapter 7]. The tuning method was developed based on the need for a general procedure that could provide decent performance for large numbers of first order process control loops. The method is based on the principle of Quarter-Amplitude Damping (QAD) where successive error peaks in a system response are reduced by 25% in magnitude. QAD may however be undesirable for many applications as it is inherently oscillatory with a damping ratio of only approximately $\zeta = 0.2$ (see Figure 1.8(a)).

Ziegler and Nichols developed their method based on two closed-loop system characteristics: ultimate proportional gain and period. Ultimate gain (K_u) is the point at which proportional only control causes sustained oscillation in the measured variable. The period of the oscillation (P_u) is known as the ultimate period. Experimentally, it was found that QAD occurs for proportional gains approximately half the ultimate gain while "optimal" choices for integral and derivative gains were fractions of the oscillation period. With such large proportional gains, Z-N tuned PID controllers are very susceptible to hunting behavior, especially in HVAC systems that have constantly varying dynamics. Ziegler and Nichols were themselves aware of this drawback and even suggested detuning of the proportional gain for worst-case conditions. Despite limited usefulness beyond first order

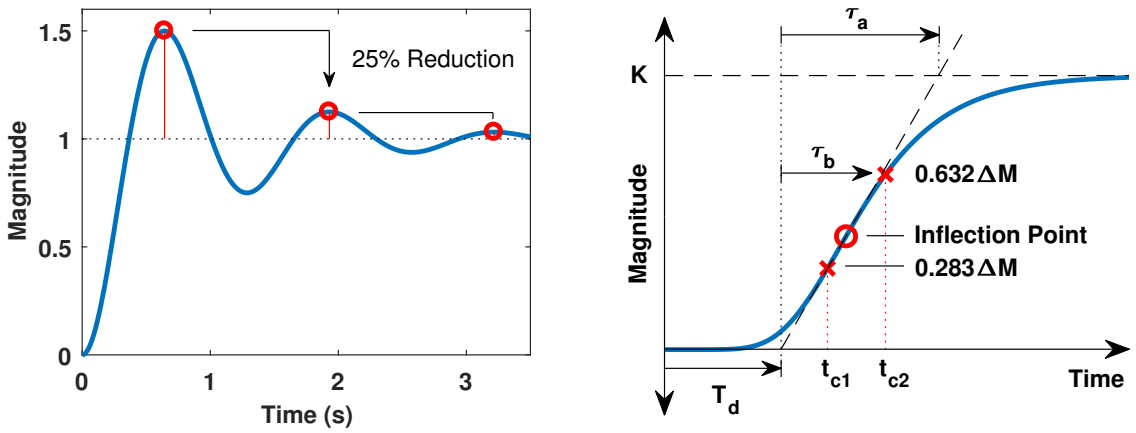

(a) (b)

Figure 1.8: (a) The Ziegler-Nichols method is based on Quarter-Amplitude Damping where successive peaks are reduced by 25%. (b) Important open loop response characteristics for first order identification.

systems and known hunting issues, the Z-N method is still by far the most prevalent tuning procedure used today because its simplicity lends itself as a good starting point for tuning.

The drawbacks of the closed-loop Z-N method spawned several improvements and/or similar methods. Modifications of the original Z-N gains have been proposed that do not aim for QAD (e.g. responses with reduced or no overshoot). These procedures are very similar to the original Z-N method, in some cases using normalized process gain ($\bar{K} = K_{ss}/K_u$) and dead-time ($\bar{T}_d = T_d/\tau$) to select gains [46] or using Nyquist analysis to adjust the Z-N gains for certain stability properties [47]. Other methods, like Tyreus-Luyben [48], use the same closed loop tuning technique but arrive at inherently different ratios of K_u and P_u for tuning the PID gains. Each of the methods discussed require that the closed loop system be pushed to a condition close to instability. In processes where sustained oscillation is difficult to achieve and/or detrimental to the system, closed-loop identification methods have been developed that only require underdamped oscillation to characterize the system [49]. Information about the decaying oscillations can be used to estimate the ultimate gain and period from which PID gains can be selected.

For systems where oscillations of any kind required by the closed loop tuning methods discussed are impractical, open loop tuning methods can be used. These tests utilize data from a step test to gather information about the process to be controlled. A step test is conducted by first setting the control system to a 'manual' mode and letting both the control and output signals stabilize at a constant value. The control signal is then stepped with enough magnitude to induce a measurable response in the output signal. Ziegler and Nichols developed rules for step tests or what they termed 'process-reaction curves'. Two response characteristics are used to determine PID values: 1) reaction rate (R) which is the slope of the response curve at its inflection point and 2) apparent lag (T_d) which is the time given by the intersection of a tangent drawn from the inflection point to the x-axis (see Figure 1.8(b)). Ratios of R and T_d are then used to fix the PID gains [44]. Although this open-loop Z-N method avoids pushing a process near instability in the tuning process, it is still geared towards results with QAD.

More detailed models of the process response can be used to characterize the open loop response by finding values for the parameters in Equation 1.5, known as a First Order Plus Dead Time (FOPDT) model. For Fit '**a**' in Figure 1.8(b), the inflection point is used to generate a tangent line from which the time delay (T_d) is found as in the Z-N open loop method. The time constant (τ_a) is then taken as the difference between the delay and the intersection of the tangent with the steady-state gain. This first method can however significantly overestimate the time constant. An improved method, Fit '**b**', sets the time constant equal to the time at which the curve crosses $0.632K$ with the delay calculated as before. While better, both fits rely on identifying and establishing a tangent to the inflection point which can be an imprecise process depending on data resolution. A third fit, Fit '**c**', does not utilize the inflection point but instead uses times t_{c1} and t_{c2} to find τ_c and T_d by Equation 1.6. Graphical representations for each of these open loop fitting methods can be found in Figure 1.8(b) and in-depth background can be found in [50].

$$P(s) = \frac{Ke^{-T_d s}}{\tau s + 1} \tag{1.5}$$

$$\tau = \frac{3}{2}(t_{c2} - t_{c1}) \qquad \& \qquad T_d = t_{c2} - \tau \tag{1.6}$$

Many open loop tuning methods take advantage of first order model fits to select PID gains. Published 11 years after the Z-N method, the Cohen and Coon method [51] can be used with the first order model discussed before. Despite the improved modeling over the Z-N method, the C-C method is still subject to robustness limitations as it is also designed for QAD in the tuned response. The Chien-Hrones-Reswick method uses an open loop characterization similar to the original Z-N method but with the system time constant used explicitly. This method is more powerful than most as it offers different gains for disturbance rejection and setpoint regulation as well as adjustments for responses with 0% or 20% overshoot [47].

For processes where a FOPDT model does not provide an accurate representation of the dynamics, other model types and associated rules have been developed. In [47], tuning rules for plant models such as Integrator Plus Dead Time (IPDT), First Order Integrator Plus Dead Time (FOIPDT), and Unstable FODPT plants are discussed. Accommodations for PID control are made in each case, for example with IPDT and FOIPDT models no additional integrator is required in the controller to eliminate steady-state error as an integrator is already contained in the plant dynamics. Methods for higher order plants such as the Second Order Plus Dead Time (SOPT) models have also been developed [49]. Representations for each of these models are given in Table 1.2 and tuning methods for each and many other model types can be found in [52].

Early tuning rules were primarily developed based on empirical testing and assumptions about what characterized an 'optimal' response. In fact, the original paper presented by Ziegler and Nichols reproduced plots from circular chart recorders using what they

Table 1.2: Example Process Models Used for PID Tuning.

IPDT	FOIDPT	UFOPDT	SOPDT
$\frac{Ke^{-T_d s}}{s}$	$\frac{Ke^{-T_d s}}{s(\tau s+1)}$	$\frac{Ke^{-T_d s}}{\tau s-1}$	$\frac{Ke^{-Tds}}{\tau^2 s^2+2\zeta\tau s+1}$

called a typical industrial process. Sense then many techniques have sought to outline a more rigorous definition of optimality. Typically this involves minimizing the magnitude of different cost functions including Integrated Absolute Error (IAE), Integrated Time weighted Absolute Error (ITAE), or Integrated Square Error (ISE) each defined in Equation 1.7. The choice of cost function used for determining a tuning formula can greatly a affect the resulting closed loop response. Some tuning formulas that use these metrics are the Fertick method [53], Ciancone and Marlin [54], and Lopez et al. [55].

$$IAE = \int_0^\infty |e(t)|dt, \qquad IAE = \int_0^\infty t|e(t)|dt, \qquad ISE = \int_0^\infty e^2(t)dt \tag{1.7}$$

The simple closed and open loop tuning methods discussed in this section are by no means exhaustive. There are dozens of other methods and refinements aimed at improving and simplifying the tuning process for specific models and industries. There is a large amount of literature available comparing the performance of different methods including [48], [56], and [57].

1.3.3 Advanced PID Tuning

Beyond empirical tuning rules, there are a host of tuning methods that utilize more advanced controls analysis to tune PID controllers. One such strategy relies on what is known as Internal Model Control. As seen in Figure 1.9(a), IMC design uses an assumed plant model $\hat{G}$ to augment the controller and feedback paths. The IMC procedure involves

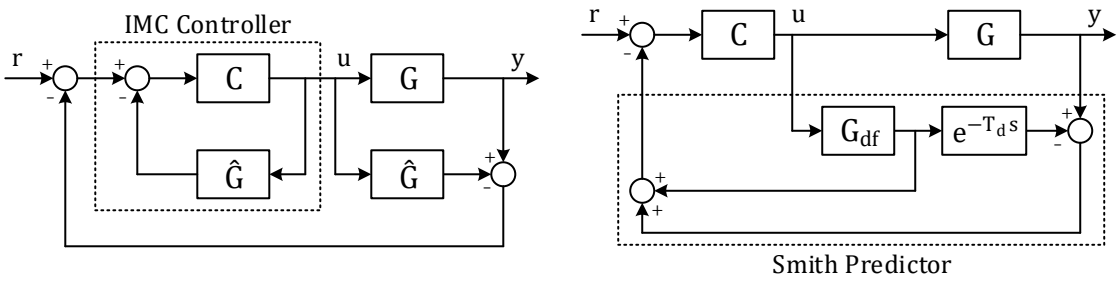

(a) (b)

Figure 1.9: (a) IMC design augments the controller and feedback loop with an assumed ideal plant model $\hat{G}$. (b) A Smith Predictor uses a delay free model to predict the response of a system with significant time delay.

first factoring $\hat{G}$ into its minimum and non-minimum phase components, $\hat{G}_-$ and $\hat{G}_+$ respectively, then augmenting $\hat{G}_-^{-1}$ with a stable filter to ensure causality. The original controller C can then be recovered by using the structure of the IMC controller according to Equation 1.8. When the assumed plant structure is first or second order, the recovered controller has the same structure as PI/PID controllers from which gains can be extracted. Detailed derivation of IMC rules and PID related structures can be found in [58].

$$C_{imc} = \frac{\hat{G}_-^{-1}}{(\lambda s + 1)^n} \quad \Rightarrow \quad C = \frac{C_{imc}}{1 + \hat{G} C_{imc}} \tag{1.8}$$

Often presented together, an equivalent to IMC is the direct synthesis method. Controllers are determined by first specifying the desired closed loop transfer function $G_{cl}(s)$, then using an identified plant model G to solve the closed loop transfer function for the required controller to achieve the closed loop response (Equation 1.9). For combinations of first and second order models for the plant and closed loop response, the resulting controller will be a PID structure [57].

$$C_{ds} = \frac{1}{G} \cdot \frac{G_{cl}}{1 - G_{cl}} \tag{1.9}$$

A special case of direct synthesis design (and IMC design) is when the plant model contains an input delay. That delay will appear in the resulting controller making it a non-PID structure. Using the first-order Taylor series expansion of the delay ($e^{-T_d s} \approx 1 - T_d s$) recovers a PID type control that includes knowledge of the delay. Incorporating the delay into the loop is related to Smith Predictor design, a method often used to control systems with significant time delay [59]. From the block diagram in Figure 1.9(b), a Smith Predictor is seen to compare a delay free model of the plant dynamics (G_{df}) with the reference signal. The predictor also compares the actual output with with a delayed model plant to prevent output drift and reject disturbances. In this way, Smith Predictors can be used to reduce delay effects while maintaining closed loop performance. An excellent example of Smith Predictor design can be found in [60].

IMC and direct synthesis can both be used to derive what is known as the Simple-IMC PID tuning rules developed by [61]. The procedure used direct synthesis to find PID gains for generalized identified model structures (e.g. first and second order with time delay). However, the resulting integral time was too slow to adequately reject load disturbances. To combat this, integral time is adjusted slightly to balance setpoint tracking and disturbance rejection. Simple-IMC provides gains for what is known as the interacting form PID controller (Equation 1.10). Equation 1.11 gives gains for the more standard non-interaction form of a PID controller. Models and settings required to obtain gains for other variations of PID control are also discussed in [61]. In general, S-IMC tuned controllers have better performance than traditional tuning rules especially for second order systems.

$$\text{Interacting PID:} \quad C(s) = K_c \left(\frac{\tau_I s + 1}{\tau_I s} \right) (\tau_D s + 1) \tag{1.10}$$

$$k_p = \frac{\tau_I + \tau_D}{\tau_I} K_c \quad , \quad k_i = \frac{K_c}{\tau_I} \quad , \quad k_d = K_c \tau_D \tag{1.11}$$

Similar methods to IMC seek to further simplify the tuning process and/or provide a measure of adjustability to the process. Lambda tuning was developed for processes with long dead times but is mostly used in the pulp and paper industries [62]. Tuning uses a desired closed loop transfer function like Equation 1.12 to explicitly solve for the PI controller form. Control gains then have a variable (λ) that can be used to adjust performance, i.e. smaller λ values mean faster closed loop responses. The Haalman Method is similar only an ideal loop transfer function G_ℓ is determined instead of the closed loop equation being specified. One specific choice is Equation 1.13, although this leads to total cancellation of process poles and zeros which can lead to control issues [63].

$$G(s) = \frac{e^{-T_d s}}{1 + \lambda T s} \qquad (1.12) \qquad\qquad G_\ell(s) = \frac{2e^{-T_d s}}{3T_d s} \qquad (1.13)$$

In a series of papers [64, 65], Astrom and Hagglund developed a method known as the M-constrained Integral Gain Optimization (MIGO) method and a simplified approximation (AMIGO). The MIGO method is based on the inverse relationship between integrated error and the integral gain ($IE = \int_0^\infty e(t)\,dt = 1/k_i$). Controllers are therefore optimized by maximizing integral gain subject to a robustness constraint specified on the Nyquist curve. The simple AMIGO rules were derived based on a nominal robustness level and results from a large test batch of plants that included first order, time delayed, and underdamped second order dynamics. Although the AMIGO rules inherently provide a known level of robustness and better performance than most traditional methods discussed, they can still lead to hunting PID controllers due to static nonlinearity [21].

A different kind of tuning procedure was developed for HVAC system in [66] that uses the Hermite-Biehler Theorem to identify stability regions for PID gains at particular load conditions that also guarantee a minimum phase margin. This is done by establishing a signature requirement that uses fixed strings of permissible signs for the real part of the

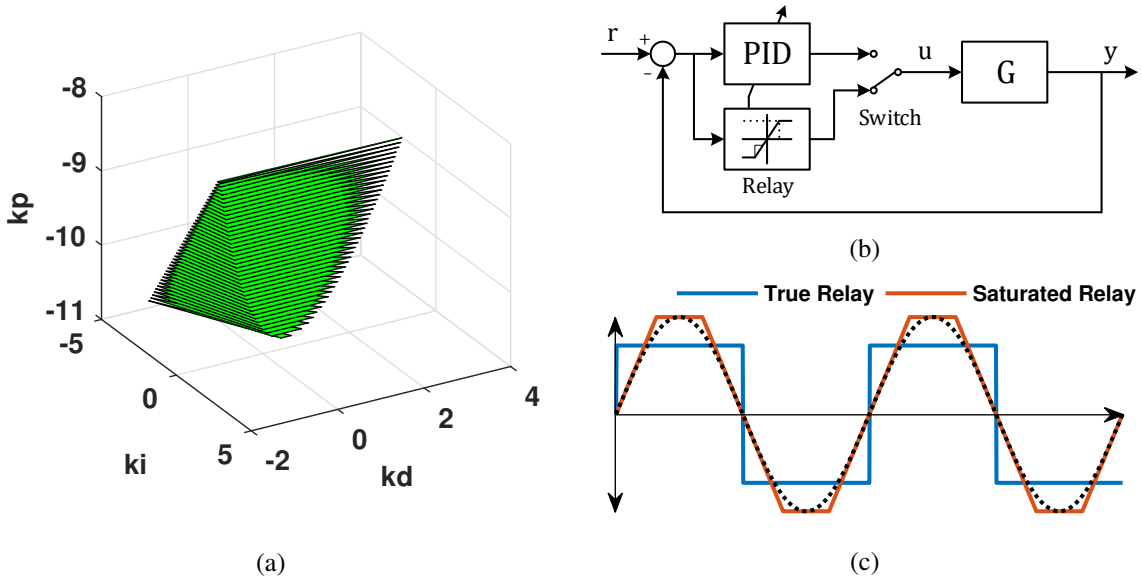

(a) (b) (c)

Figure 1.10: (a) The design procedure developed by [66] can search planes of PID gains for feasible combinations. (b) Typical setup for self-tuning PID algorithm. (c) Saturated relay feedback better approximates sinusoidal intput.

closed loop characteristic equation at its root frequencies leading to a series of linear constraints. By fixing one gain, several planes of gains can be easily generated and compiled into polytopic region of usable PID gains (see Figure 1.10(a)). Final gains are determined by searching within the polytope for gain combinations that meet design requirements. Full details on this method for continuous and discrete time plants can be found in [67].

1.3.4 Self-Tuning PID Strategies

Each of the methods discussed so far assumes that PID gains are tuned once by a control engineer and remain constant for all operation. This process involves using the identification techniques discussed before and then designing control gains off-line. Depending on success, this process has to be done several times and repeated each time the controller begins to behave poorly. To deal with changing system loads and dynamics, several automated self-tuning PID control strategies have been developed to reduce setup effort and provide periodic retuning.

Self-tuning algorithms rely on automating parameter identification and a built-in gain selection algorithm. This is done by embedding an algorithmic switch to break the control loop and then step, ramp, or pulse the input of a system while recording the response. Another method that has gained popularity is the relay feedback method proposed by [63]. This method generates a sustained oscillation in the output by including a relay block in the control loop Figure 1.10(b). From the resulting sustained oscillation, the system ultimate gain and period can be determined and used with a tuning algorithm to automatically select PID gains. Relay feedback is easily programmable and safe for closed loop identification as the relay switches control input opposite the output when it crosses the setpoint.

Pure relay feedback has a tendency to underestimate the value of ultimate gain by anywhere between 10-20%. This is because standard relay feedback relations use a Fourier approximation of the square relay signal. Greater accuracy can be achieved by using a saturation relay instead of a pure relay [68]. By introducing a slope (k) and saturation limit (h) to the relay block output, a better approximation of a sine wave is achieved (Figure 1.10(c)). Some design is required when selecting values of 'k' and 'h' to ensure accuracy of results and to generate a sustained oscillation. Modifications to the procedure are also available to account for load disturbances and nonlinearities.

While most commercial methods for self-tuning PID controllers are either step test or relay feedback based, a few other methods are used. Pseudo-Random Binary Signal identification provides greater frequency content than normal step or impulse tests that only give information about nearly steady-state conditions [69]. Given a sufficiently exciting PRBS, an accurate model of a system's frequency dynamics across a wide spectrum can be identified. Phase locked loop identification is an alternate method that uses an external control loop to regulate the phase difference between a reference signal and the measured output. This method was designed to enable better estimation of a system frequency response both in open and closed loop operation [70].

1.4 Advances in Building Control

Despite the prevalence of PID control techniques in process and building controls, there are numerous other control techniques have been developed. This section will focus on control techniques beyond PID with the understanding that many of the frameworks discussed can be augmented to tune PID controllers or use PID control as an underlying controller.

1.4.1 Model-Free Control Techniques

PID control and many of its associated tuning methods fall under the umbrella of model free control paradigms. These approaches seek to minimize the system information required to design and tune a low order controller by relying on the inherent robustness of the feedback system [70]. Most tuning methods discussed apply a set of performance criteria to a set of normalized plants and then develop generalize rules about control gains. These methods can provide adequate performance, especially when plant dynamics are similar to a system from the test set.

Methods are available that offer greater optimization of model free control gains and performance. For any optimization problem, there is an associated cost function that captures the relevant performance characteristics. A standard optimization method will use the gradient to minimize the cost function using a steepest descent algorithm. The Iterative Feedback Tuning (IFT) method allows for the generation of the gradient matrix without development of an intermediate model. This is accomplished by first recording the system response to a reference input $r(t)$ and then feeding the error signal into the system at the reference input [70]. The relevant partial derivatives needed to calculate the gradient can then be generated from the resulting signals.

The Newton Procedure is an improved optimization method that uses the Hessian to determine the location of critical points. Using IFT to find the system's Hessian matrix

would require additional system responses making on-line identification lengthy and more difficult. To address this, the Controller Parameter Cycling (CPC) algorithm perturbs each input of a system to directly calculate components of the gradient and Hessian matrices [70]. This method constructs relevant Newton parameters piecewise making it a slightly more involved process while still maintaining the benefits of the model free approach.

Many HVAC controllers take advantage of operator knowledge of system limitations and occupant comfort to create a set of rules governing system operation. Rules are typically triangular or trapezoidal weighting/membership functions that describe a series of system states. Functions for input states are usually related to comfort and are descriptive with labels such as hot, warm, comfortable, and cool. Output states are signals to system actuators and as such will have descriptions like low, medium, and high. The input and output weighting functions are blended to fix the system state and generate the appropriate actuation. Rules sets, also known as knowledge bases, create the foundation for a Fuzzy Logic Controller (FLC) which does not require explicit mathematical models.

FLC has been applied to a wide range of HVAC systems from temperature control for potato cold storage to compressor control for residential HVAC systems [71]. Fuzzy self-tuning valve control for single and multi-evaporator vapor compression systems showed significant improvement over PID control over a wide range of operating conditions. Fuzzy control has also been used in the automotive industry for independent occupant climate control using factors such as engine coolant temperature, speed, and temperature setpoint. In [72], the heating performance of a fuzzy controller was compared to PID and on/off controllers with varying dead bands. The FLC was found to consume the least energy, saving approximately 30-70% depending on the comparison. FLC can also be used to create an adaptive fuzzy PID controller as in [73] where parallel fuzzy P, fuzzy I, and fuzzy D controllers showed improved performance over traditional PID control and other fuzzy PID methods.

There are many other model-free paradigms developed for use with HVAC systems. In [74] a 'human in the loop' approach has been used to show preliminary energy savings. Occupants interacted with a smartphone application to give basic comfort data. Researchers displayed aggregate data in the app and speculated users would moderate their preferences based on group comfort. The method also included a subroutine to drift the temperature towards outside conditions over time. Another model-free comfort optimization proposed to use additional sensor streams to regulate temperature [75] within a building zone. By monitoring many points within a multi-room zone, energy usage could be optimized while preserving occupant comfort throughout a building.

1.4.2 Model-Based Control Techniques

Model-free methods offer good performance with minimal development cost. However, the greatest energy efficiency savings will come by using techniques that can solve convex optimization problems using knowledge of system dynamics and building interconnections. The following section details common model-based methods used in the HVAC field to provide improved performance and energy savings.

The simplest model-based techniques use approximation to improve performance. For example, in [21] the functions in Equation 1.14 are used to characterize static-nonlinearity of an AHU. The shape of the function can be adjusted using β_1 and β_2 to generate curves similar to Figure 1.3(a). Because the function is invertible, it can be used directly in the feedback path to reduce performance degradation with operating conditions. As discussed in the previous section, Internal Model Control (IMC), uses an assumed plant model and desired plant dynamic to generate a controller. The assumed plant model can be low order, which gives PID equivalents, or higher order for more complex designs.

$$f(u|\beta_1,\beta_2) = \frac{1-e^{-\beta_2 z}}{1-e^{\beta_2}} \qquad \text{where} \qquad z(u|\beta_1) = \frac{1-e^{-\beta_1 u}}{1-e^{\beta_1}} \tag{1.14}$$

Using measured disturbance signals to improve performance is known as feedforward control. In [76], an inverse model of dual-duct AHU dynamics was used in parallel with a PID controller. The inverse feedforward term predicted the appropriate input to meet the desired reference while the PI controller worked to reject modeling errors and disturbances. The feedforward architecture was also used as a fault detection method as output from the PI controller becomes very large when faults were present. In [77], the benefits of static and dynamic feedforward terms in temperature control were compared. Both feedforward controllers provided better control with dynamic feedforward yielding the best results.

There has been a lot of development in optimal control techniques for HVAC systems with the stated goal of reducing electricity usage further and eventually reaching net-zero-energy buildings. At their most basic level, optimal controllers seek to reduce the magnitude of a specified cost function. There are many options for cost functions but standard options include penalties on output errors and control input. For example, Equation 1.14 is the cost associated with Linear Quadratic Regulator (LQR) control where Q and R are weighting matrices that can be used to effect the performance of the resulting controller. Other cost functions can be based on performance norms such as $\mathcal{L}_2$ or $\mathcal{L}_\infty$ that penalize total energy used by a system and worst-cast performance respectively [78].

$$J(x,u) = \int_0^\infty (x^T Q x + u^T R u)\ dt \tag{1.15}$$

Examples of optimal control techniques on HVAC control design are numerous. Room temperature control via a VCC air conditioning unit is discussed in [79] where superheat and room temperature control were combined into a Multi-Input-Multi-Output controller using an LQG synthesis (i.e. LQR with Kalman Filter). Similarly, the dynamics of a heating system were analyzed and controlled using $\mathcal{H}_\infty$ synthesis in [80]. Optimal tuning

has also been used to generate tuning rules for PID controllers as in [81] where gains were adaptively tuned to regulate AHU discharge air temperature.

Often exact dynamics of an HVAC system are not know completely due to unmeasured disturbances, unmodeled dynamics, and/or modeling errors. Design of controllers with guaranteed performance despite these issues is known as robust control. Model uncertainty can be captured by using filters to create a bounding cone around the frequency response of the plant (Figure 1.11(a)). Using classic loop shaping techniques (i.e. high loop magnitude at low frequency for reference tracking and small at high frequencies for disturbance rejection), a controller can be found that guarantees performance despite limited plant knowledge. Parametric uncertainty is when the structure of a plant model is correct, but values of parameters vary within a constrained set. Both unstructured and parametric uncertainty can be grouped and placed in an upper Linear Fractional Transformation (LFT) configuration (Figure 1.11(b)) for use with optimal control techniques like $\mathcal{H}_\infty$. The uncertain and disturbance inputs are bundled together when using an $\mathcal{H}_\infty$ control approach to design for worst-case disturbances and modeling errors.

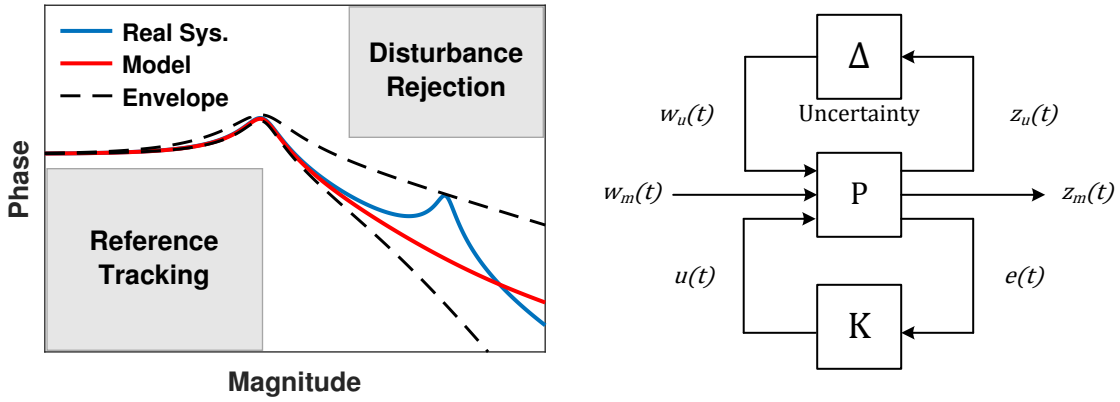

(a) (b)

Figure 1.11: (a) Loop shaping for uncertain systems ensures model envelope avoids regions defined by disturbance rejection and reference tracking criteria. (b) Model uncertainties (Δ) are collected into an upper LFT to be used with optimal tuning techniques.

This type of robust control design has been done for many HVAC systems. For example, in [82] a robust PID controller was designed for a VAV system where parameters in a FOPDT model where shown to vary more than 300% over the damper input range. With the integral gain fixed, the intersection of PD gains that satisfy sensitivity performance criteria in the presence of multiplicative uncertainty were found. The complete operation of an experimental reheat unit was controlled using a robust MIMO $\mathcal{H}_\infty$ controller in [83]. Additive uncertainty was included in each of five subsystems and weights were added to scale the normalized inputs and outputs. The controller was compared to decentralized PI control and found to have significant performance improvements due to direct compensation for dynamic coupling and time varying dynamics.

Another approach to robust control is to solve the optimal problem in terms of Linear Matrix Inequalities (LMIs) given in standard form given by Equation 1.16. LMIs have become increasingly popular in controls as many control problems can be recast as an LMI. The main advantage of LMIs is that they are convex, numerically stable, and solvable even for large systems [84]. Also, optimization problems with LMI constraints lend themselves naturally to multiple objectives and time varying systems which are just additional constraints on the optimization. Treating changing dynamics of a system as a polytopic set involves solving a set of simultaneous LMIs. Solutions to a set of LMIs have guaranteed performance for systems within the region defined by the polytopic set. This type of approach has been used to design robust controllers for HVAC equipment including air-conditioning [85] and heat pump systems [86].

$$A(x) = A_0 + x_1 A_1 + \cdots + x_n A_n < 0 \tag{1.16}$$

As discussed, HVAC systems display many nonlinear characteristics. Although robust control design can reduce the effect of nonlinearity in a system, it often results in more

conservative performance. A different approach involves describing HVAC system dynamics as a large set of linear systems with time varying parameters. This description is known as the Linear Parameter Varying (LPV) modeling approach that has been applied to many HVAC systems, see [87] and [88] for example. LPV models typically will take the form of Equation 1.17 where $\rho(t)$ is an unknown parameter that effects the system dynamics. Synthesis of controllers to deal with LPV systems fall into several main categories: polytope description, Linear Fractional Transformation (LFT), and gridding techniques. Each technique can be cast as a LMI which can be used in convex optimizations [89].

$$\begin{cases} \dot{x} = A(\rho(t))x(t) + B(\rho(t))u(t) \\ y = C(\rho(t))x(t) + D(\rho(t))u(t) \end{cases} \tag{1.17}$$

LPV modeling lends itself towards the popular HVAC control strategy of gain scheduling. This technique uses a set of linearized plant models to develop a family of controllers. During operation, the control parameters can be interpolated or hard-switched as the system transitions to a different operating point. Often this leads to better performance than robust approaches especially in neighborhoods close to the linearization point. As LPV and gain scheduling can utilize standard linear controllers, they have been used prolifically for HVAC control spanning systems from hydronic radiators [87] to vapor compression cycle systems [90, 91].

The strategy that has the most intense focus in recent building controls today is Model Predictive Control (MPC). The goal of MPC is to coordinate often disparate, coupled building systems in order to decrease overall energy usage while still maintaining occupant comfort. MPC uses system models to simulate dynamics along a receding time horizon and predict optimal control actions at each time step (Figure 1.12). Cost functions for MPC are usually quadratic [92] although for buildings systems they are typically related

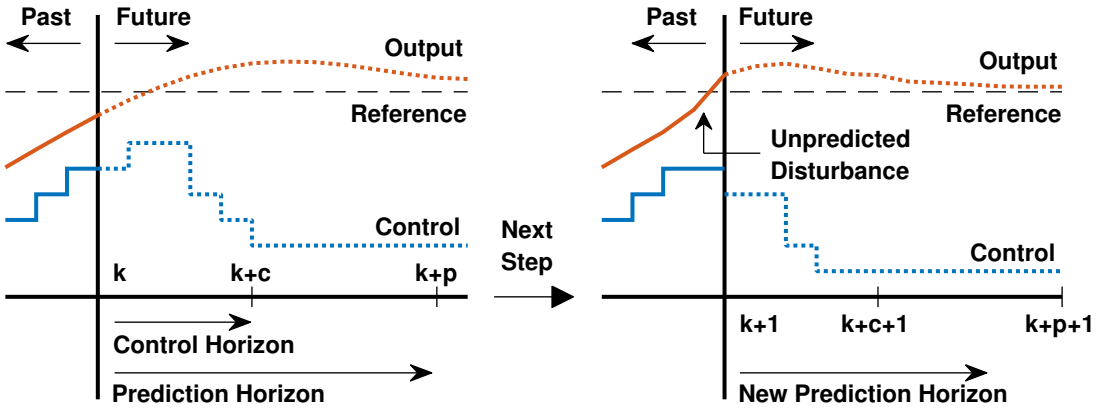

Figure 1.12: At time $t = k$, an MPC controller optimizes the control to produce the best system output. At the next time step ($t = k + 1$), this process is repeated given new data and models.

to the monetary cost of running an HVAC system and avoided productivity loss due to discomfort (see [93] for example). MPC has always been promising in simulation [94] but has increasingly been shown effective on various experimental HVAC systems as in [95], [96], and [97]. MPC is subset of Generalized Predictive Control (GPC) which use similar horizon techniques for control optimization. In particular, GPC can be used to adapt PID gains instead of directly changing the plant input signal. GPC-PID controllers have been used in diverse applications such as water level control in cooling tanks [98] and in HVAC equipment such as AHU chilled water valve control [99]. Centralized MPC has intense communication and computation demands that make implementation difficult. Strategies to limit network infrastructure include steady-state optimization (NC-OPT) [100], Decentralized MPC (DMPC) [101], and Limited-Communication DMPC (LC-DMPC) [102]. Given certain conditions, each of these methods require less communication than centralized MPC but are still able converge to the centralized optimal solution.

Inherently, the success of an MPC algorithm is heavily dependent on the system models it uses to predict along the receding horizon. There are three main methods for developing these models: physics based (white-box modeling), hybrid physics and data driven

modeling (grey-box modeling), and pure polynomial identification (black-box modeling). The choice of modeling technique depends heavily on the application. As buildings are living spaces that constantly change, real-time polynomial identification is a good option. In [30], a black-box modeling algorithm uses real time data to select the appropriate polynomial model structure and identify coefficients. The method was applied to a multi-room simulation model with several MPC algorithms. Results showed improved performance and the ability of the identification algorithm to stably interact with an MPC controller.

This review is by no means exhaustive. There are many techniques with limited experimental results that have shown promise in simulation including neural networks and genetic algorithms as in [103]. The main control technique used in the vast majority of buildings today is still PID control with MPC algorithms and gain scheduling algorithms becoming more widespread. This chapter is meant to provide the insight that a controller that uses the best parts of PID will be more readily adopted by the HVAC field, especially if it can be used as an underlying architecture for more advanced supervisory algorithms.

1.5 Outline of Dissertation Research

The remainder of this dissertation will explore the use of cascaded PID controllers for HVAC control. This architecture has multiple benefits including feedback linearization and input-output decoupling. As it uses simple PID control loops that are built into many building automation languages, it is readily adoptable in the field. In the remaining chapters, this dissertation will: introduce the structure, discuss tuning procedures for maximizing benefits, prove better performance, and discuss results from on-campus implementation in building HVAC systems.

2. CASCADED CONTROL

At its most basic level, cascaded control is the nesting of one feedback control loop inside another [63]. The structure of the cascaded loop in most literature is some variation on the block diagram given in Figure 2.1 where the outer loop generates an intermediate reference signal for the inner loop controller. Nested loops are particularly helpful when a system has several distinct dynamics between the controlled and process variables (e.g. long delays or time constants). The architecture can also be used to reject disturbances before they spill into other control loops. Typically cascaded control is used on systems with multiple possible feedback signals with the dynamics of selected inner loop signal being approximately five times faster than the process variable. The addition of multiple loops can make implementation of cascaded control more complex, however there are methods available to automate commissioning such as in [104].

Nested loops have been used in a variety of HVAC applications for the past several decades [105]. Several aspects of Air Handling Unit (AHU) control have seen improvement from using the architecture. In [106], cascaded control on duct pressure using differential supply and return air flow rate as the intermediate variable showed greater stability than either direct pressure control or differential control separately. Also important was that the nested loop still utilized feedback from the pressure sensor, allowing it to reject

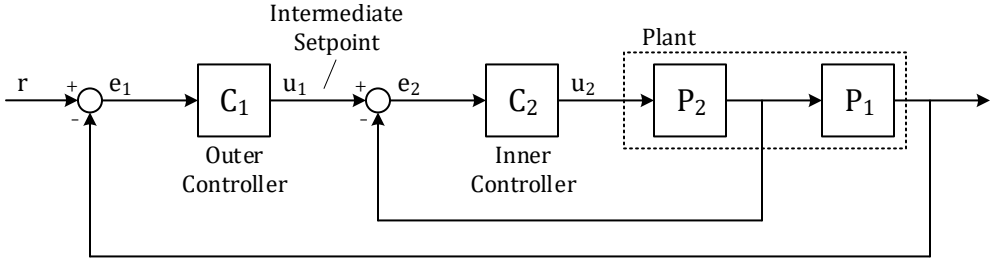

Figure 2.1: General block diagram of a cascaded control loop used in literature.

disturbances from infiltration or exhaust airflow. AHU discharge/exit air temperature was controlled in [107] with a PI and P cascaded loop augmented with a learning neural network. This structure created an adaptive cascaded loop that showed improved temperature regulation but required significant training data and did not respond quickly to sudden changes in cooling load. In [108], a cascaded architecture using non-interacting and PD control was used to decouple temperature and relative humidity control of AHU exit air. Simulation results showed that within a given time span, the controller could vary temperature or humidity while maintaining the other.

Cascaded control also showed significant improvement of superheat control in vapor compression systems. In [109], a mechanical Thermostatic Expansion Valve (TEV) was augmented with a stepper motor to adjust the pressure setpoint stem based on superheat at the evaporator outlet. The architecture vastly reduced variation in system responses at high and low flow conditions and improved overall system response. The architecture was also implemented with an Electronic Expansion Valve (EEV) where the valve stem was controlled directly by a stepper motor. Authors later discovered that when used with multi-evaporator systems, cascaded control could reduce coupling [110]. Similar improvement was discovered in [111] while using refrigerant mass flow as the intermediate variable. This solution is however more difficult to implement as mass flow sensors are more expensive and less common than pressure sensors in VCC systems.

The cascaded architecture is widely utilized in a variety of other fields. The structure is commonly used for robust motor speed regulation using outer loop control to generate a supply current setpoint for the inner loop. In [112] this structure was augmented with PI observers to eliminate issues of parameter uncertainty and external disturbances. Cascaded loops are even seen in robotic systems, as in [113] where it was used for position tracking and torque control of a four-arm pneumatic muscle tool tip machine. It is also used in navigation control as in [114] where a three-layer cascaded loop that used LQR stabilizing

state feedback, input-output decoupling control, and PD control to manage the flightpath of a robotic helicopter.

This chapter will highlight the additional benefits of cascaded control beyond disturbance rejection. As shown, cascaded control can significantly reduce variations in system dynamics, eliminate unwanted oscillations (hunting), and decouple multi-input-multi-output (MIMO) dynamics. This is accomplished by defining the structure of the cascaded loop and several performance metrics that can quantify the architectures benefits. The types of systems and signals that can utilized this structure are also outlined.

2.1 Structure*

In addition to all the benefits discussed before, cascaded control has recently been shown to effectively linearize inherent and load-dependent nonlinearities for a broad range of HVAC systems [115, 116]. The specific form for the cascaded loop used in this dissertation is shown in generalized block diagram form in Figure 2.2. The architecture consists of a fast inner loop controller with proportional gain k_L and an outer loop PI controller with gains k_p and k_i with respective control signals u_i and u_o. The system nonlinearity is contained within the inner control loop which, as shown later, will approximately linearize the system dynamics for the outer loop controller. Plant dynamics are given in Equation 2.1 and consist of a unitary transfer function $G(s)$ and a dynamic nonlinear gain $\psi(\sigma)$ which is dependent on the operating condition 'σ' assumed to vary between 0 for low load and 1 for high load situations. This plant configuration is related to the Hammerstein modeling approach which has been widely used in the HVAC field [117, 118]. The system has one input and at most two distinct outputs which may, or may not, have separate nonlinearities.

*Material in Sections 2.1-2.4 is adapted with permission from "Effective Tuning of Cascaded Control Loops for Nonlinear HVAC Systems", C. Price and B. Rasmussen, Proceedings of the 2015 Dynamic Systems and Control Conference, vol. 2, ©2015 ASME and "Optimal Tuning of Cascaded Control Architectures for Nonlinear HVAC Systems", C. Price and B. Rasmussen, Science and Technology for the Built Environment, vol. 23(8), pp. 1190-1202, ©2017 ASHRAE.

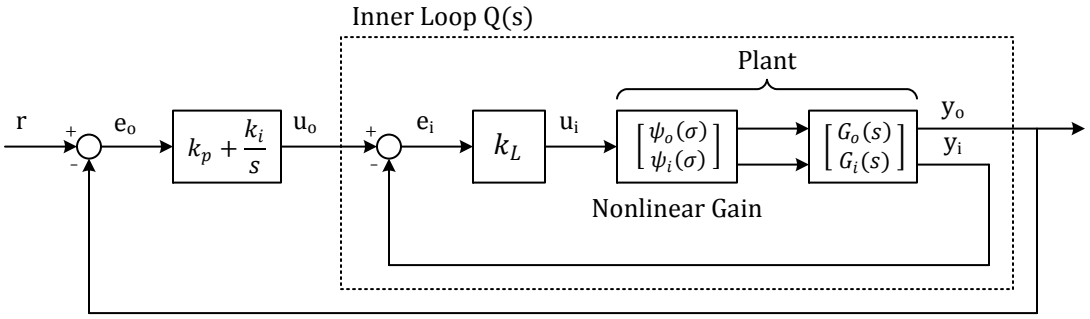

Figure 2.2: Block diagram of a general cascaded loop for the process $G(s)$ with a single input and at most two outputs. Variables relating to the inner and outer loops have subscripts "i" and "o" respectively.

This architecture is extremely modular in that the inner and outer loops can take feedback on the same or different outputs which can have separate load dependent gains.

$$G(s) = \begin{bmatrix} \psi_i(\sigma) G_i(s) \\ \psi_o(\sigma) G_o(s) \end{bmatrix} \tag{2.1}$$

The cascaded loop provides nonlinearity compensation by placing the system nonlinearities in the numerator and denominator of the inner loop transfer function (Equation 2.2). This structure allows the nonlinearities to counteract each other, reducing their overall effect on the system dynamics provided that both $\psi_o(\sigma)$ and $\psi_i(\sigma)$ are monotonic with respect to load condition and have slopes with the same sign. Such nonlinear trends are common in HVAC systems that seek to control temperatures through flow control methods such as variable air volume boxes or air-handling units. The linearization behavior of the cascaded controller is demonstrated by Figure 2.3 where the effects of the inner loop control are applied to a generic, first-order system with a single nonlinearity. As the inner loop gain increases, the relative difference between operating conditions 'A' and 'B' is reduced and the dynamic response of the system is quickened across all conditions.

$$L(s, k_L, \sigma) = \frac{k_L \psi_o(\sigma) G_o(s)}{1 + k_L \psi_i(\sigma) G_i(s)} \tag{2.2}$$

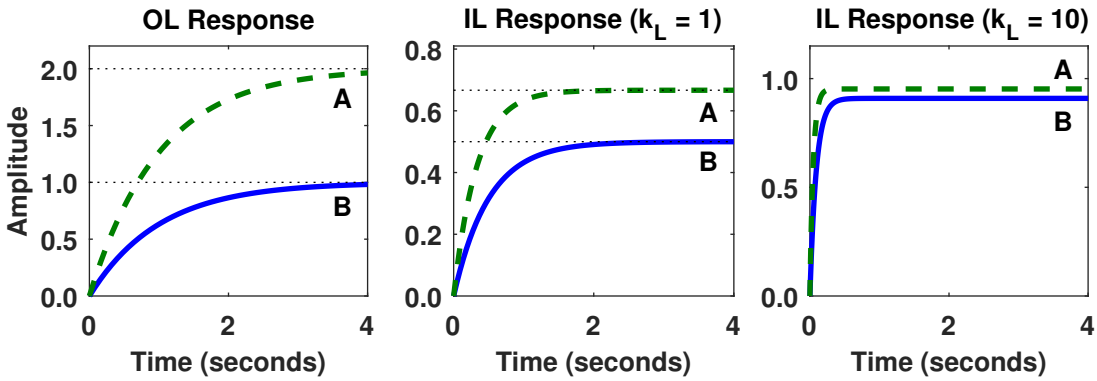

Figure 2.3: The inner loop (IL) controller of the cascaded architecture reduces differences in steady-state gains between operating conditions 'A' and 'B' as well as speeds the overall response. Adapted with permission from [115] ©2015 ASME.

The main benefits of the cascaded architecture (e.g. reduced gain variation and faster response times) are realized without the need for detailed models of the system nonlinearities. As both nonlinearities inherently appear in the numerator and denominator of $L(s)$, the self-countering aspect of the inner loop control is realized regardless of the nonlinear gain structure. The model-free aspect of the cascaded control loop becomes especially important in dealing with multicomponent systems. For example, many buildings will have one or more air-handling units connected to several variable air volume boxes, each with their own control loop. Developing detailed models for each of these systems can become impractical, especially in large buildings or at large campuses with several hundred facilities [14].

The following sections outline metrics that can be used to quantify the benefits of cascaded control and their purpose when tuning loops. The linearization metrics are novel while the decoupling metrics are well known in multivariable control. Tuning procedures take advantage of these metrics to present new methods for tuning cascaded loops for improved HVAC system performance.

2.2 Linearization Metrics

To develop tuning rules and quantify the amount of linearization provided by inner loop control, the following Nonlinear Gap Metrics (NGMs) are proposed (see [115]). The NGM of the open-loop system, symbolized Υ, is defined in Equation 2.3 as the ratio of the minimum to maximum steady-state gain of the uncompensated outer loop process $\psi_o(\sigma)G_o(0)$ over all operating conditions 'σ'. This open-loop NGM provides a measure of how much steady-state variation is present in the inner loop dynamics and is taken as the degree of nonlinearity in the original system. The metric will vary between values of 0 and 1 depending on how gains differ between conditions. Many HVAC systems have steady-state gain variations of an order of magnitude or more, resulting in $\Upsilon < 0.1$.

$$\Upsilon = \frac{\min\limits_{\forall\sigma} \psi_o(\sigma)G_o(0)}{\max\limits_{\forall\sigma} \psi_o(\sigma)G_o(0)} \tag{2.3}$$

The linearizing effect of the inner loop gain is captured by the closed-loop NGM given by Equation 2.4. This metric, symbolized $\Gamma(k_L)$, is the ratio of the smallest and largest steady-state gains of the inner loop transfer function $L(0, k_L, \sigma)$ over all operating conditions for a particular inner loop gain. Greater nonlinearity compensation is indicated by $\Gamma(k_L)$ values near 1 due to reduced variation in system gains. The closed-loop NGM provides a measurement to compare the amount of linearization achieved by the inner loop proportional control and the original nonlinearity of the system.

$$\Gamma(k_L) = \frac{\min\limits_{\forall\sigma} L(0, k_L, \sigma)}{\max\limits_{\forall\sigma} L(0, k_L, \sigma)} \tag{2.4}$$

The values of Υ and $\Gamma(k_L)$ can be used to select an inner loop gain or adjust weighting variables in optimal tuning methods due to the following important properties. Properties 1

and 2 show that there always exists an inner loop gain that will improve the linearization of the system and Property 3 implies that closed-loop gap metric will have two basic shapes. Property 4 shows that linearization from cascaded control is only achievable if ψ_i and ψ_o have the same monotonic trend with respect to operating conditions. From a practical standpoint, these properties show that an HVAC technician could safely tune inner loop gains by starting with an initial small value for k_L and then gradually increase the gain until desired performance is achieved. Each property is stated below with a short proof:

Property 1: The closed-loop gap metric $\Gamma(k_L)$ approaches the open loop gap metric Υ for small inner loop gains k_L.

For $k_L > 0$, let the maximum and minimum values of $L(0, k_L, \sigma)$ occur at the operating conditions specified by Equation 2.5. These relations can be used to rewrite the closed-loop gap metric as shown in Equation 2.6.

$$\underline{\sigma} = \underset{\forall\sigma}{\operatorname{argmin}}\, L(0, k_L, \sigma) \qquad \& \qquad \bar{\sigma} = \underset{\forall\sigma}{\operatorname{argmax}}\, L(0, k_L, \sigma) \tag{2.5}$$

$$\Gamma(k_L) = \frac{\psi_o(\underline{\sigma}(k_L))}{\psi_o(\bar{\sigma}(k_L))} \cdot \frac{1 + k_L\psi_i(\bar{\sigma}(k_L))}{1 + k_L\psi_i(\underline{\sigma}(k_L))} \tag{2.6}$$

As inner loop gain becomes small ($k_L \to 0$), the dynamics of the inner loop will be dominated by the numerator of the inner loop control (Equation 2.7). This implies that the inner loop will be minimized and maximized at the extremes of the outer loop nonlinearity (Equation 2.8).

$$\lim_{k_L \to 0} L(0, k_L, \sigma) = k_L\psi_o(\sigma)G_o(0) \tag{2.7}$$

$$\underline{\sigma}^* = \lim_{k_L \to 0} \underline{\sigma}(k_L) = \underset{\forall\sigma}{\operatorname{argmin}}\, \psi_o(\sigma) \quad \& \quad \bar{\sigma}^* = \lim_{k_L \to 0} \bar{\sigma}(k_L) = \underset{\forall\sigma}{\operatorname{argmax}}\, \psi_o(\sigma) \tag{2.8}$$

Taking the limit of Equation 2.6 as the inner loop gain approaches zero and substituting for the operating conditions of Equation 2.8 shows that $\Gamma(k_L)$ approaches the open loop metric for small inner loop gains (Equation 2.9).

$$\lim_{k_L \to 0} \Gamma(k_L) = \frac{\psi_o(\underline{\sigma}^*)}{\psi_o(\bar{\sigma}^*)} = \Upsilon \tag{2.9}$$

Property 2: The slope of $\Gamma(k_L)$ is positive for small inner loop gains.

The partial derivative of Equation 2.6 with respect to k_L at a given inner loop gain is given by Equation 2.10. The limit of this partial derivative as the inner loop gain approaches zero has the form of Equation 2.11. For this quantity to be positive, the difference between the inner loop nonlinearity at the operating conditions $\bar{\sigma}^*$ and $\underline{\sigma}^*$ must be positive.

$$\frac{\partial}{\partial k_L}\Gamma(k_L) = \frac{\psi_o(\underline{\sigma})}{\psi_o(\bar{\sigma})} \cdot \frac{\psi_i(\bar{\sigma}) - \psi_i(\underline{\sigma})}{(1 + k_L \psi_i(\underline{\sigma}))^2} \tag{2.10}$$

$$\lim_{k_L \to 0} \left\{ \frac{\partial}{\partial k_L}\Gamma(k_L) \right\} = \frac{\psi_o(\underline{\sigma}^*)}{\psi_o(\bar{\sigma}^*)} \left[\psi_i(\bar{\sigma}^*) - \psi_i(\underline{\sigma}^*)\right] > 0 \tag{2.11}$$

As both $\psi_i(\sigma)$ and $\psi_o(\sigma)$ vary monotonically and have the same trends with respect to the operating condition σ, Equation 2.8 can be rewritten as Equation 2.12. This fact shows that the slope of the closed-loop metric will be positive for small k_L according to Equation 2.11.

$$\underline{\sigma}^* = \lim_{k_L \to 0} \underline{\sigma}(k_L) = \operatorname*{argmin}_{\forall \sigma} \psi_i(\sigma) \quad \& \quad \bar{\sigma}^* = \lim_{k_L \to 0} \bar{\sigma}(k_L) = \operatorname*{argmax}_{\forall \sigma} \psi_i(\sigma) \tag{2.12}$$

Property 3: The closed-loop gap metric will approach 1 if the nonlinearities are multiplicatively related.

For large values of inner loop gain, $\Gamma(k_L)$ will approach the value Ω given by Equation 2.13. This value simplifies to 1 if the inner and outer loop nonlinearities are equal or

are multiplicatively related. Otherwise, Ω can be either greater or less than the original open-loop NGM.

$$\lim_{k_L \to \infty} \Gamma(k_L) = \frac{\psi_o(\underline{\sigma}(k_L))}{\psi_o(\bar{\sigma}(k_L))} \cdot \frac{\psi_i(\bar{\sigma}(k_L))}{\psi_i(\underline{\sigma}(k_L))} = \Omega \tag{2.13}$$

Property 4: ψ_i and ψ_o must have the same trend with respect to operating conditions.

The closed-loop NGM also shows that cascaded control should not be used when systems have nonlinearities with differing slopes. If the inner and outer loop nonlinearities have opposite trends, the inner loop transfer function will have the extremes given by Equation 2.14 where over- and under-bars signify maximum and minimum values of ψ, respectively.

$$\begin{aligned} L_{min} &= \frac{k_L \psi_o(\underline{\sigma}) G_o(0)}{1 + k_L \psi_i(\underline{\sigma}) G_i(0)} = \frac{k_L \underline{\psi}_o G_o(0)}{1 + k_L \bar{\psi}_i G_i(0)} \\ L_{max} &= \frac{k_L \psi_o(\bar{\sigma}) G_o(0)}{1 + k_L \psi_i(\bar{\sigma}) G_i(0)} = \frac{k_L \bar{\psi}_o G_o(0)}{1 + k_L \underline{\psi}_i G_i(0)} \end{aligned} \tag{2.14}$$

This information can be used to show that the partial derivative of the closed-loop metric is always negative according to Equation 2.15. The expression is due to G being unitary and $\psi_i, \psi_o > 0$. This indicates that any inner loop control applied to such a system will result in greater nonlinearity over all operating conditions.

$$\frac{\partial}{\partial k_L} \Gamma(k_L) = \frac{\partial}{\partial k_L} \frac{L_{min}}{L_{max}} = \frac{\underline{\psi}_o}{\bar{\psi}_o (1 + k_L \bar{\psi}_i)^2} (\underline{\psi}_i - \bar{\psi}_i) < 0 \tag{2.15}$$

Given these properties, the closed-loop gap metric can have the two basic shapes shown in Figure 2.4(a). The closed-loop gap metric will have a peak, curve 'P', if the partial derivative of the inner loop transfer function (Equation 2.16) has a constant, positive real root with respect to k_L. In this case the inner loop gain should be chosen as close to the peak as possible without violating actuator saturation or stability constraints. If Equation 2.16 does not have a solution, then the metric will have an 'S' shaped curve and the

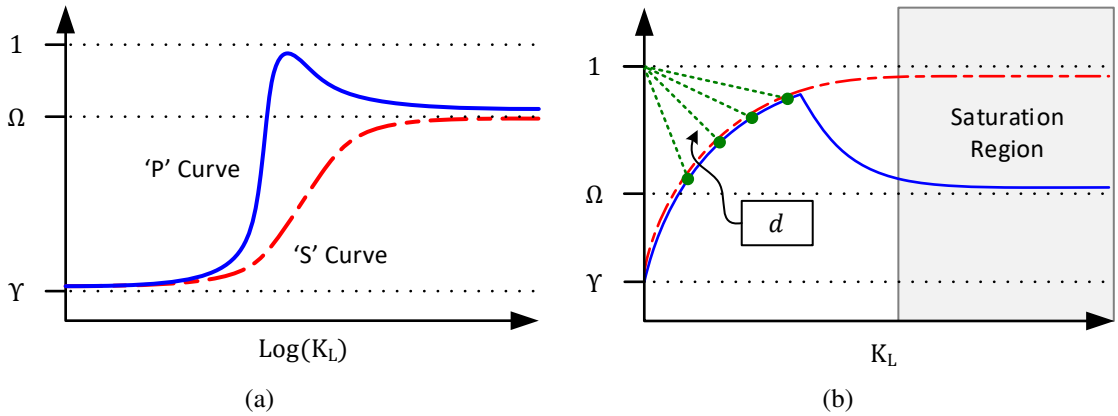

Figure 2.4: (a) The closed-loop NGM $\Gamma(k_L)$ has two distinct shapes that determine how inner loop gain is selected. (b) Points on the closed-loop NGM curve are similar to a Pareto optimal front. Inner loop gain should minimize control effort but maximize linearization.

inner loop gain should be made as large as possible. Gains can be further tuned by interpreting the closed-loop NGM as a Pareto optimal front. As in Figure 2.4(b), the distance d of Equation 2.17 is a weighted distance between the NGM curve and the point $(0, 1)$ which represents "perfect" linearization with no control effort. The formula can therefore be used to balance linearization effect with actuation constraints on the inner loop gain. Selected values of k_L are used directly or as target gains for optimal tuning methods.

$$(1 + k_L\psi_i(\sigma))\frac{\partial}{\partial\sigma}\psi_o(\sigma) = k_L\psi_o(\sigma)\frac{\partial}{\partial\sigma}\psi_i(\sigma) \tag{2.16}$$

$$d(k_L) = \sqrt{\alpha_1(1 - \Gamma(k_L))^2 + \alpha_2\left(\frac{k_L}{k_{L,max}}\right)^2} \tag{2.17}$$

2.3 Decoupling Metrics*

A starting point for controlling Multi-Input-Multi-Output (MIMO) systems has traditionally been attempting to use Single-Input-Single-Output (SISO) controllers for the

*Material in this section is adapted with permission from "Decoupling of MIMO Systems Using Cascaded Control Architectures with Application for HVAC Systems", C. Price and B. Rasmussen, Proceedings of the American Control Conference, pp. 2907-2912, ©2017 IEEE.

input-output (I/O) pairs of a system. This approach can work well for some plants provided that they are diagonally dominant with minimal cross term effects. In many cases, however, individual inputs can have strong effects on multiple system outputs. Coupling can act as a strong disturbance for SISO controllers and significantly degrade performance to the point of instability.

The degraded performance of SISO controllers on MIMO systems has led to the development of many decoupling control techniques. These methods seek to untangle the I/O pairs and allow for the design of simple SISO controllers for the new, decoupled relationships. This can be done using simple feed-forward terms such as a Static Decoupling Matrix [119] or by intense analysis of the I/O relationships to determine pairings that yield the least coupling [120].

Decoupling methods all require detailed knowledge of system dynamics or, at a minimum, steady-state behavior at the desired frequency. Depending on the size of the system and the complexity of its dynamics, generating detailed models can be time consuming, if not impractical. These types of controllers also must be updated each time the system is augmented or altered. The addition of new components or even a slight alteration can significantly reduce the performance of decoupling controllers.

For highly coupled systems, application of MIMO control techniques can provide better performance than modified SISO techniques. Popular control choices include $\mathcal{H}_2$, $\mathcal{H}_\infty$, and Model Predictive Control (MPC). MIMO control design seeks to use complete knowledge of system dynamics to formulate optimal controllers. However, as with decoupling controllers, detailed models are required and controllers are sensitive to system modifications. MIMO controllers also tend to be computationally expensive as they are typically high order. See references like [121] for details on the complexity of MIMO control.

Cascaded control has shown the ability to decouple the dynamics of multi-evaporator Vapor Compression Cycle (VCC) systems [110]. The following section provies detailed

analysis of how cascaded control can decouple input/output (I/O) pairs and how it can be used as a model-free MIMO decoupling approach. The section will present decoupling metrics used in literature and detail the behavior of cascaded control for I/O separation.

2.3.1 Relative Gain Array

The Relative Gain Array (RGA) is a non-singular, complex matrix developed by [122] as a measure for the interactions between inputs and outputs of MIMO systems. The matrix is defined in Equation 2.18 where '$\circ$' denotes the Schur (element-by-element) matrix product. The RGA has important properties including independence from I/O scaling and row/column sums of one. The selection of I/O pairs according to [121] should prefer pairings such that the rearranged system has an RGA matrix close to identity near the closed-loop bandwidth and avoids pairings with negative elements on the RGA diagonal. Large elements indicate strong sensitivity to plant uncertainty while negative pairings indicate open loop instability.

$$RGA(X) \triangleq \Lambda(X) = X \circ (X^{-1})^T \tag{2.18}$$

An associated metric known as the RGA Number is defined in Equation 2.19 for diagonal controllers. The sum norm here indicates the sum of the absolute values of all matrix elements. A completely decoupled system will have an RGA Number of zero while poorly conditioned systems with large RGA elements will necessarily result in large RGA numbers. Controllers seeking to decouple a system for diagonal control should therefore seek to minimize the RGA Number.

$$RGA\#(X) \triangleq N(X) = \|\Lambda(X) - I\|_{\text{sum}} \tag{2.19}$$

Previous research has shown that cascaded control can reduce the magnitude of the RGA Number for coupled systems. This remainder of this section will use the RGA matrix

and RGA number to demonstrate how this architecture provides model-free decoupling of highly coupled systems.

2.3.2 Asymptotic Decoupling Behavior

Let the coupled system be given in state-space representation as Equation 2.20. Note that this system includes non-zero D matrices indicating that the cascaded decoupling effect will be realized even for systems that are not strictly proper. The only restriction placed on the system is that coupled outputs be completely observable and controllable.

$$\begin{cases} \dot{x} = & Ax + Bu_i \\ y_i = & C_i x + D_i u_i \\ y_o = & C_o x + D_o u_i \end{cases} \tag{2.20}$$

The inner loop control of the cascaded architecture can be written as Equation 2.21 where K_L is a real diagonal matrix with positive entries $k_{L,i}$ and u_o is the control signal coming from the outer loop PID controller. Substitution and matrix algebra give the final form where $K^* = (I + K_L D_i)^{-1} K_L$.

$$\begin{aligned} u_i = & \; K_L(u_o - y_i) \\ = & \; (I + K_L D_i)^{-1} K_L (u_o - C_i x) \\ = & \; K^*(u_o - C_i x) \end{aligned} \tag{2.21}$$

Further substitution yields Equation 2.22 which is the state-space representation for the inner loop process.

$$\begin{cases} \dot{x} = & [A - BK^*C_i]\, x + BK^* u_o \\ y_o = & [C_o - D_o K^* C_i]\, x + D_o K^* u_o \end{cases} \tag{2.22}$$

Using the Matrix Inversion Lemma (see [121] Appendix A) and the matrix identify of Equation 2.23, the transfer function form of the coupled inner loop dynamics can be expressed as Equation 2.24.

$$I - (I + P)^{-1}P = (I + P)^{-1} \tag{2.23}$$

$$L(s) = \left\{K_L^{-1}G_o(s)^{-1} + G_i(s)G_o(s)^{-1}\right\}^{-1} \tag{2.24}$$

The transfer function of the inner loop control reveals the asymptotic decoupling behavior of the cascaded architecture. When $|K_L| << 1$, the inner loop dynamics are the same as that of the open loop system Equation 2.25 (i.e. the outer loop process). For small values of inner loop gain, therefore, the RGA and RGA Number of the inner loop are equal to that of the open loop response. Conversely, when $|K_L| >> 1$ and the inner and outer loops take feedback on the same signal ($G_i(s) = G_o(s)$), the inner loop transfer function will approach identity (Equation 2.26). This means that given unlimited control, the inner loop will completely decouple the system dynamics. Note that this decoupling is achieved regardless of frequency and results in an RGA number of zero. When $G_i(s) \neq G_o(s)$, the coupling will approach a level determined by the combination $G_i(s)^{-1}G_o(s)$. Careful selection of the inner loop signal can minimize the asymptotic coupling.

$$\lim_{|K_L|\to 0} L(s) = K_L G_o(s) \tag{2.25}$$

$$\lim_{\substack{|K_L|\to\infty \\ G_i(s)=G_o(s)}} L(s) = I \tag{2.26}$$

2.3.3 Intermediate Behavior

In many cases, intelligent selection of the inner loop gains will significantly reduce system coupling with minimal gain. Re-writing the RGA Number as Equation 2.27 shows how it responds to intermediate values of inner loop gain. Note that here, δ represents the impulse function and X^{ij} is the matrix X with i-th and j-th row and column removed.

$$N(X) = \sum_{i,j} \left| (-1)^{i+j} \cdot \frac{x_{ij} \det X^{ij}}{\det X} - \delta(i-j) \right| \tag{2.27}$$

The value of the RGA Number for the inner loop process will be finite given two criteria: the entries of a steady-state gain matrix $G(j\omega)$ are finite in magnitude and the determinant of the gain matrix is not zero. For the inner loop control, the first requirement means that there are no integrator states, i.e. no poles at the origin. The second requirement mandates that the system maintain distinct I/O relationships. Should the determinant pass through zero or change signs for a given inner loop gain, this indicates that multiple control directions have merged and the system has lost rank at the desired frequency.

The behavior of the relative gain number will therefore be smooth provided there are no inner loop gains for which the system gain matrix loses rank. Monte-Carlo analysis of hundreds of random systems indicated that in most cases the RGA will decrease with increasing inner loop gain excluding peaks caused by loss of rank and asymptotic behavior if $G_i(s) \neq G_o(s)$. Figure 2.5(a) shows several expected RGA number profiles generated from those random systems. Selection of inner loop gains should utilize the RGA number to avoid certain values of K_L gains at frequencies where loss of rank occurs while balancing decoupling effect, actuator saturation constraints, and system stability.

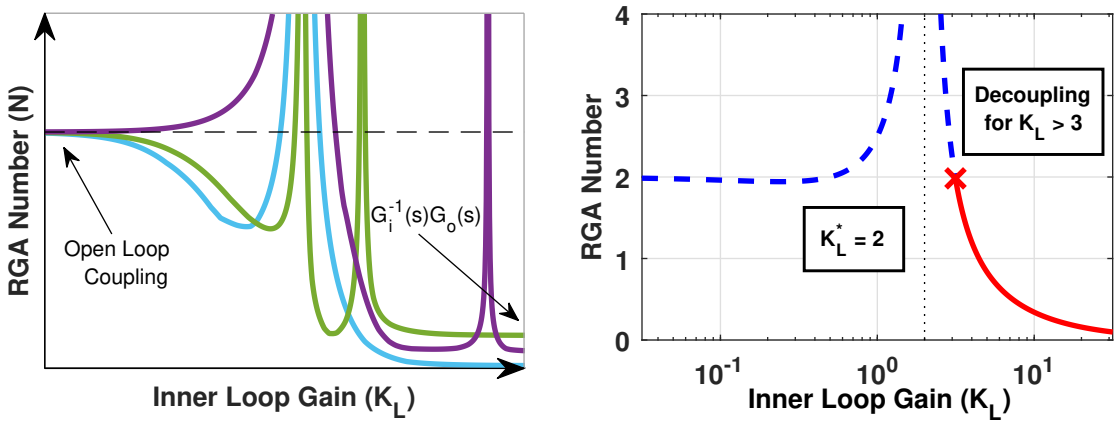

(a) (b)

Figure 2.5: (a) Common RGA Number profiles of random systems. Coupling begins at open loop RGA number and approaches total decoupling for large inner loop gains if $G_i(s) = G_o(s)$. (b) RGA number plot for the system in Equation 2.28. ©2017 IEEE.

As an example, consider the simple system given by Equation 2.28 where coupling occurs only in the system output matrix C. The determinant of the steady-state inner loop process is shown by Equation 2.29 which indicates that a sign change occurs at $K_L^* = 2$. This means that there will be only one asymptotic peak in the RGA Number curve near inner loop gain values of K_L^*. Designing a cascaded controller for this system should avoid gains in that area, specifically aiming for gain values of $K_L > 3$ (see Figure 2.5(b)).

$$\begin{cases} \dot{x} = \begin{bmatrix} -1 & 0 \\ 0 & -2 \end{bmatrix} x + Iu \\ y = \begin{bmatrix} 1 & -1 \\ 0 & -1 \end{bmatrix} x \end{cases} \tag{2.28}$$

$$\det\left(G_{IL}(0)\right) = \frac{K_L^2}{(K_L - 2)(K_L + 1)} \tag{2.29}$$

2.4 Simple Tuning Rules

Having defined metrics and their behavior, the task becomes how to use them to tune a cascaded controller for the desired performance. The following section details simple tuning rules that can be used for field implementation of cascaded controllers. Selection of the inner loop gain can be done using the linearization metric analysis from Section 2.2 or RGA analysis from Section 2.3. Having selected a k_L gain, tuning of the outer loop controller can be accomplished using any standard tuning method in one of the three following cases. Special care should be taken when using step response tuning methods as these procedures assume an S-shaped process curve with no overshoot and will often over-tune outer loop gains for underdamped second order systems (Figure 2.6).

2.4.1 Case 1: $G_i(s)$ & $G_o(s)$ Have Similar Time Scales

In this case, the outer loop tuning procedure is a successive loop closure. This is accomplished by applying the inner loop controller, then tuning the outer loop gains using

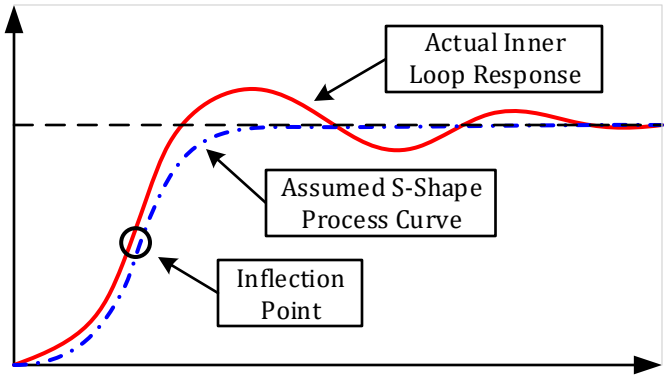

Figure 2.6: Step-response tuning procedures should not be used to tune outer loop gains as they produce aggressive PID gains. Adapted with permission from [115] ©2015 ASME.

any standard method. Because variation in the inner loop steady-state gain is now reduced significantly, gains determined using this process will be similar no matter the conditions under which the outer loop is tuned. This procedure is essentially tuning the closed loop characteristic equation of Equation 2.30.

$$\Delta_{cl}(s) = 1 + \left(\frac{k_p s + k_i}{s}\right)\left(\frac{k_L \psi(\sigma) G_i(s)}{1 + k_L \psi(\sigma) G_i(s)}\right) G_o(s) = 0 \tag{2.30}$$

2.4.2 Case 2: $G_i(s)$ & $G_o(s)$ Have Different Time Scales

Tuning when the inner and outer loop processes display disparate time scales simplifies the selection of outer loop gains. Due to the separation, the inner loop process can be taken as a static gain equal to the steady-state gain $L(0)$. Because the inner loop gain was chosen to minimize the relative difference between $L(0)$ over all operation conditions using $\Gamma(k_L)$, such an assumption will produce similar outer loop gains no matter when the tuning takes place. This case is equivalent to tuning the characteristic equation of Equation 2.31.

$$\Delta_{cl}(s) = 1 + \left(\frac{k_p s + k_i}{s}\right) \cdot L(0) \cdot G_o(s) = 0 \tag{2.31}$$

2.4.3 Case 3: Feedback on Same Signal ($G_i(s) = G_o(s)$)

In this special case, both inner and outer loops take feedback on the same signal. Manipulation of the closed loop characteristic equation yields the expression of Equation 2.32 which has the appearance of a traditional PI controller with gains k_1 and k_2 given by Equation 2.33. Because the inner and outer loop gains are highly coupled, successive loop closure will not capture the interaction between the two loops. This means that the cascaded controller should be tuned by first finding a nominal PI controller and then using Equation 2.33 to find the final outer loop gains using the selected inner loop gain. As this process does not involve first applying the inner loop control, the final cascaded gains will depend on when the loop is tuned. For example, tuning in low system gain conditions will lead to more aggressive outer loop gains. Tuning will therefore be an iterative process as performance must be evaluated to determine the final gains.

$$\Delta_{cl}(s) = 1 + \frac{k_1 s + k_2}{s} \cdot \psi(\sigma) \cdot G(s) = 0 \tag{2.32}$$

$$\begin{cases} k_1 = k_L(k_p + 1) \\ k_2 = k_L k_i \end{cases} \tag{2.33}$$

2.5 Tuning with $\mathcal{H}_\infty$ Synthesis

As a starting point for optimal selection of cascaded loop gains, an attempt to cast the tuning process as an $\mathcal{H}_\infty$ synthesis problem was made. Typically, a system is transformed into a generalized control configuration like that of Figure 2.7(b). In this representation, the closed-loop transfer function from w to z is given by the Lower Fractional Transformation (LFT) $z = F_\ell(P, K)w$. The control synthesis problem therefore seeks to minimize the norm of the lower LFT. The $\mathcal{H}_\infty$ system norm definition of Equation 2.34 means that this problem will seek to minimize the maximum singular value of the system.

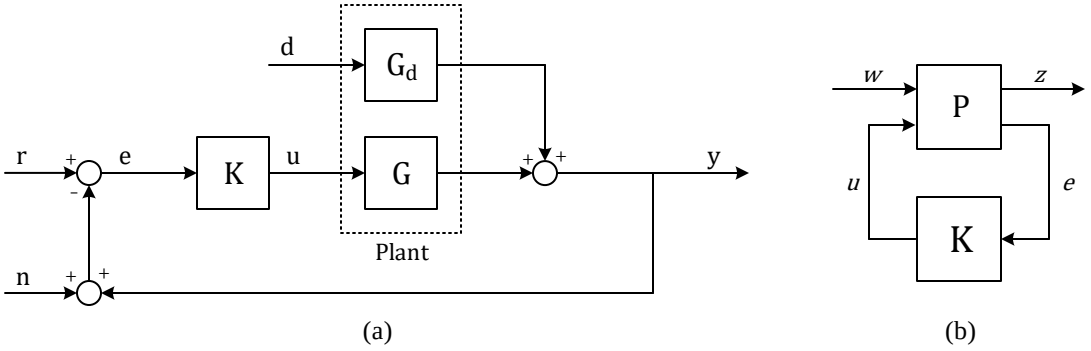

Figure 2.7: For $\mathcal{H}_\infty$ synthesis, the block diagram from (a) is transformed into the generalized control from of (b).

$$\| F_\ell(P,K) \|_\infty = \max_\omega \bar{\sigma}\left(F_\ell(P,K)(j\omega)\right) \tag{2.34}$$

The next step in typical $\mathcal{H}_\infty$ synthesis is the specification of design objectives in terms of norm constraints. This is done with weighting functions on the inputs and outputs of the system that seek to warp singular values in the regions of interest. For example, for worst case error tracking a simple first order low-pass filter can be used to reduce the size of singular values above a design cut-off frequency. Once the weight system is constructed, the optimal $\mathcal{H}_\infty$ controller can be found iteratively using solutions to Riccati equations or using a Linear Matrix Inequality approach.

The $\mathcal{H}_\infty$ synthesis formulation, was found to be a poor choice for tuning of cascaded control gains. As mentioned, dynamic weighting functions are typically used to shape a systems singular values in order to specify controller performance. However, the addition of non-static weighting functions will increase the order of the resulting controller. In order to maintain the cascaded control structure, only static weights can be used with the consequence of losing the ability to tune the regions of performance for the resulting inner and outer loop gains. This observation lead to the following section where a more suitable methodology for tuning of cascaded control gains is presented.

2.6 LQ Optimal Tuning*

The previous sections outline simple rules for initial tuning of a cascaded controller. In many cases, however, tighter and/or more robust control can be required. To deal with this, this section presents an optimal tuning framework for selecting cascaded control gains that take advantage of the metrics discussed previously.

Tuning the loops of a cascaded controller can be cast as a linear quadratic (LQ) cost minimization problem. LQ control is a state-space optimal control method that seeks to minimize the quadratic cost function J of Equation 2.35 where x and u are vectors containing the state variables and control inputs, respectively. The weighting matrices Q and R allow the cost function to be adjusted based on performance requirements and actuation constraints. LQ designed controllers have an inherent level of robustness due to guaranteed stability criteria of 60° phase margin and a gain margin of at least $1/2$. This method, including the state space techniques used in the following analysis, are well-covered in many common control textbooks including [59].

$$J = J(x, u) = \int_0^\infty (x^T Q x + u^T R u) dt \tag{2.35}$$

The plant of Equation 2.1 can be expressed in state-space form as in Equation 2.36 where $x \in \mathbb{R}^n$ and $y \in \mathbb{R}^m$. If $n \neq m$ (i.e. there are more state variables than inputs) the cascaded tuning problem can be formulated as a linear quadratic regulator (LQR) problem subject to output feedback control. To utilize this method, the state equations must be altered slightly. Under the transformation of Equation 2.37, the state-space representation of $G(s)$ becomes Equation 2.38. The last two entries in the new state vector x_T are now the two cascaded loop outputs y_i and y_o.

*Material in this section is adapted with permission from "Optimal Tuning of Cascaded Control Architectures for Nonlinear HVAC Systems", C. Price and B. Rasmussen, Science and Technology for the Built Environment, vol. 23(8), pp. 1190-1202, ©2017 ASHRAE.

$$G(s) = \begin{cases} \dot{x} = & Ax + Bu_i \\ y = & Cx = \begin{bmatrix} y_i \\ y_o \end{bmatrix} \end{cases} \tag{2.36}$$

$$x_T = Tx = \begin{bmatrix} x_1 & x_2 & \cdots & x_{n-2} & y_i & y_o \end{bmatrix}^T \tag{2.37}$$

$$\begin{cases} \dot{x}_T &= TAT^{-1}x_T + TBu_i = A_T x_T + B_T u_i \\ y_T &= CT^{-1}x_T = C_T x_T = \begin{bmatrix} \vec{0}_{2\text{x}(n-2)} & I \end{bmatrix} x_T \end{cases} \tag{2.38}$$

In order for the system output to match the feedback signals required in the cascaded control loop, the transformed system of Equation 2.38 will be augmented with an integrator on the outer loop output signal y_o. This addition leads to the final state-space form of Equation 2.39. From Equation 2.40, the output of this new augmented system is seen to be the required input for the inner loop control signal of the cascaded loop when the reference signal is taken as an arbitrary constant (i.e. $r \equiv 0$).

$$\begin{cases} \dot{x}_a = \begin{bmatrix} A_T & \vec{0}_{n\text{x}1} \\ [\vec{0}_{1\text{x}(n-1)} & 1] \quad 0 \end{bmatrix} x_a + \begin{bmatrix} B_T \\ 0 \end{bmatrix} u_i = A_a x_a + B_a u_i \\ y_a = \begin{bmatrix} y_i \\ y_o \\ \int y_o \, dt \end{bmatrix} = \begin{bmatrix} \vec{0}_{3\text{x}(n-3)} & I_3 \end{bmatrix} x_a = C_a x_a \end{cases} \tag{2.39}$$

$$\begin{aligned} u_o &= k_p(r - y_o) + k_i \textstyle\int (r - y_o)\, dt \\ u_i &= -k_L(y_i - u_o) \\ &= -k_L y_i - k_L k_p(y_o - r) - k_L k_i \textstyle\int (y_o - r)\, dt \\ &= -k_1 y_i - k_2(y_o - r) - k_3 \textstyle\int (y_o - r)\, dt \end{aligned} \tag{2.40}$$

The LQR problem with static output feedback amounts to minimizing the quadratic cost function of Equation 2.35 subject to the control input structure of Equation 2.40. Many solutions have been proposed for this problem all of which iteratively solve the simultaneous equations of Equation 2.41 where $A_c = A_a B_a K C_a$ is the closed-loop system matrix. The initial condition $x(0)$ is arbitrary and is, therefore, typically chosen to be on

the unit sphere for regulation problems. Convergence of the LQ optimization problem is guaranteed if the system is output feedback stabilizable, C has full row rank, R positive definite, and Q positive semidefinite with $(\sqrt{Q}, A)$ detectible. The complete method and convergence criteria are outlined in [123] which also includes several examples as well as sample code.

$$\begin{array}{ll} (I) & 0 = A_c^T P + P A_c + C_a^T K^T R K C_a + Q \\ (II) & 0 = A_c S + S A_c^T + x(0) x^T(0) \\ (III) & K = R^{-1} B_a^T P S C_a^T (C_a S C_a^T)^{-1} = \begin{bmatrix} k_1 & k_2 & k_3 \end{bmatrix} \end{array} \tag{2.41}$$

The weighting matrices Q and R in Equation 2.41 should be selected so as to increase the linearization effect of the inner loop control while balancing the total amount of actuation. Results can be adjusted using the open- and closed-loop NGMs outlined in the previous section. Once the desired solution has been calculated, the final cascaded control gains can be recovered from the nominal gain K using Equation 2.42.

$$k_L = k_1, \quad k_p = \frac{k_2}{k_L}, \quad k_i = \frac{k_3}{k_L} \tag{2.42}$$

The setup for the LQR output feedback problem transforms and augments the original system dynamics. This process effectively pulls the inner loop feedback gain through the summation block of the inner control loop as shown in Figure 2.8. The above iterative procedures may in some cases allow for the inner loop gain ($k_L = k_1$) to tend toward zero or even change signs. Such results will essentially zero any inner loop feedback signal and reduce the cascaded architecture to a traditional PI controller. Therefore, only weights that produce positive gains should be considered. In situations where the Q and R weights result small inner loop gain or a sign change, the LQ optimization is indicating that PI control might be better suited for such applications.

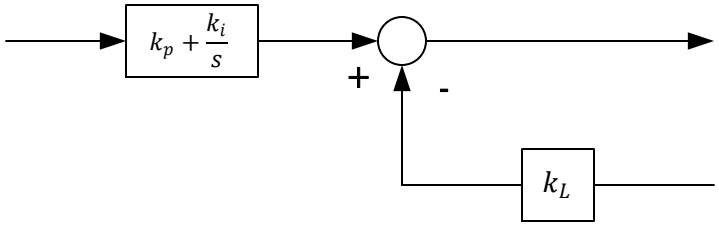

Figure 2.8: The setup for the LQ optimization process effectively pulls k_L through the inner loop summation block.

2.6.1 Special Case: Feedback on a Single Signal

The formulation above changes slightly in the case that both the inner and outer loops take feedback on the same signal. For this configuration, the inner loop control signal has the form of Equation 2.43. The LQR output feedback problem can be solved using the same iterative techniques as before except that only two nominal gains will be determined (i.e. k_1 and k_2). The inner loop gain should be chosen using the NGM analysis outlined in the previous section. The outer loop PI control gains can then be recovered from the LQR tuning using Equation 2.44.

$$u_i = -k_L(k_p + 1)y - k_L k_i \int y\, dt = -k_1 y - k_2 \int y\, dt \tag{2.43}$$

$$k_p = \tfrac{k_1}{k_L} - 1, \quad k_i = \tfrac{k_2}{k_L} \tag{2.44}$$

2.6.2 Special Case: LQR with Full-State Feedback

When the number of states equals the number of outputs (i.e. $n = m$) the LQR problem reduces to a full-state feedback problem. In this case, the quadratic cost function is guaranteed to be convex in terms of the control gains and minimization algorithms can be applied. Specifically, the Linear Matrix Inequalities (LMIs) of Equation 2.45 can be used to find the optimal quadratic cost and associated control gains [84]. For a given cost 'γ'

a state feedback controller exists provided that an $x \in \mathbb{S}^n$ (symmetric), $\gamma \in \mathbb{R}$ (real), and $W = KX \in \mathbb{R}^{1\text{x}n}$ exist. The result from solving the LQR problem using standard Ricatti equations is therefore γ^* or the minimum cost for which the LMIs of Equation 2.45 have a solution.

$$\begin{array}{ll} (I) & (A_{ai}X + B_{ai}W) + (A_{ai}X + B_{ai}W)^T + x_{i0}x_{i0}^T < 0 \\ (II) & \mathrm{tr}(Q^{1/2}X(Q^{1/2})^T) + \mathrm{tr}(Y) < \gamma \\ (III) & \begin{bmatrix} -Y & R^{1/2}W \\ (R^{1/2}W)^T & -X \end{bmatrix} < 0 \end{array} \tag{2.45}$$

The LMI approach has the main advantage of offering a means to robustly optimize system performance. The dynamics of all HVAC systems can be classified as being roughly first- or second-order which explains the prevalence of lumped-capacitance models in the field. This consistency allows for the set of all possible response characteristics for a given HVAC system to be classified as a polytopic set. Therefore, LMI (I) of Equation 2.45 can be solved simultaneously over several operating conditions 'i'. Specifically, conditions at the extremes of the operating ranges of the HVAC system can be thought of as existing on the convex hull of all possible responses. Results using LMI solution techniques will therefore guarantee a given quadratic performance over the range of operating conditions.

2.7 Discrete Time Considerations

Analysis from the previous sections has been conducted in the continuous time domain. However, modern controllers are implemented with digital hardware in discrete time. This section provides a brief overview of the effects discrete time design has on cascaded control using first and second order systems with Zero-Order Hold (ZOH) sampling.

The ZOH equivalent of a first order continuous time system is given by Equation 2.46. Solving for the closed loop expression of the inner loop control gives the maximum allow-

able inner loop gain for stability (Equation 2.47). This maximum is a strictly decreasing function with respect to the dimensionless parameter aT where T is the sampling time. The benefits of cascaded control therefore vary strictly with sampling time. This intuitive result suggests that given Nyquist frequency requirements (i.e. $aT < 2$), nearly all of the cascaded controllers benefits can be realized in discrete time for first order systems.

$$G_{zoh}(z) = Z\left\{\frac{1-e^{-sT}}{s}\left(\psi(\sigma)\frac{a}{s+a}\right)\right\} = \psi(\sigma)\cdot\frac{1-e^{-aT}}{z-e^{-aT}} \tag{2.46}$$

$$K_L^* = \frac{1}{\psi_{max}}\cdot\frac{1+e^{-aT}}{1-e^{-aT}} \tag{2.47}$$

The ZOH approximation of a second order system is given in Equation 2.48 where $\phi = \arccos(\zeta)$. For the three damping cases (under, critically, and over-damped) stability limits of inner loop gain were analyzed using the Jury stability test for discrete time systems (see [124]) which are given in Equation 2.49. The polynomial $f(z)$ is the system characteristic equation which will be dependent on the inner loop gain. As seen in Figure 2.9 where $\omega_n = 1$ and $\psi(\sigma) = 1$, in general if the sampling frequency is faster than the Nyquist requirement, only one of three Jury conditions determines the maximum allowable inner loop gain. In this region, the constraint is strictly decreasing with sampling time indicating that most potential linearization effect can be achieved in discrete time design given proper sampling. Specific Jury test conditions can be found in Appendix A.

$$\begin{aligned} G_{zoh}(z) &= Z\left\{\frac{1-e^{-sT}}{s}\left(\frac{\psi(\sigma)\omega_n^2}{s^2+2\zeta\omega_n s+\omega_n^2}\right)\right\} \\ &= \psi(\sigma)\left\{1-\frac{z-1}{\sqrt{1-\zeta^2}}\cdot\frac{z\sqrt{1-\zeta^2}+e^{-\zeta\omega_n T}\sin(\omega_n\sqrt{1-\zeta^2}T-\phi)}{z^2-2ze^{-\zeta\omega_n T}\cos(\omega_n\sqrt{1-\zeta^2}T)z+e^{-2\zeta\omega_n T}}\right\} \end{aligned} \tag{2.48}$$

$$f(z) = z^2 + a_1 z + a_0 \text{ is stable if: } \begin{cases} (1) & |a_0| > 1 \\ (2) & 1 + a_1 + a_0 > 0 \\ (3) & 1 - a_1 + a_0 > 0 \end{cases} \tag{2.49}$$

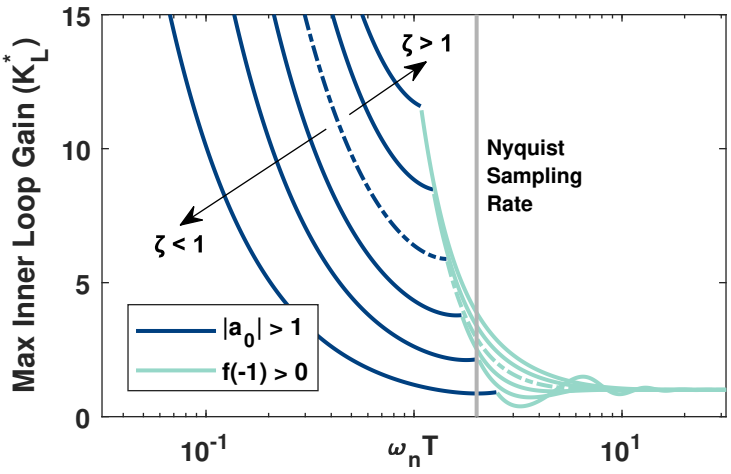

Figure 2.9: A single Jury stability test condition determines the maximum allowable inner loop gain given proper sampling. That condition strictly decreases with sampling time.

Another issue when dealing with real systems is the effect of time delay on control. To analyze its effect, the following assumptions are made about the delayed system: 1) inner loop dynamics are faster than the outer loop, 2) inner loop time delay is less than outer loop delay, 3) continuous time gains are tuned during 'high' system gain conditions for conservative control, and 4) time delay is in the feed forward path.

As an example, consider the dynamics given in Equation 2.50. Bode plots for standard PI control and for a cascaded control with $G_i(s) = G_o(s)$ are shown in Figure 2.10(a). From the plots, the differences in magnitude across operating conditions shrink substantially at low frequencies with cascaded control. This makes the crossover frequency more consistent during varying conditions and delays. The initial crossover point for both controllers are vary similar (0.9 vs. 0.5 rad/s). Comparisons of control responses indicate that the cascaded controller is no more sensitive to time delays than traditional PI control.

$$G(s) = \frac{\psi(\sigma)}{10s+1} \quad \text{where} \quad \psi(\sigma) = 1 + 9\sigma^2 \tag{2.50}$$

For extremely long delays (e.g. approaching the system fundamental time constant), cascaded control begins to develop resonant peaks in its bode phase and magnitude plots

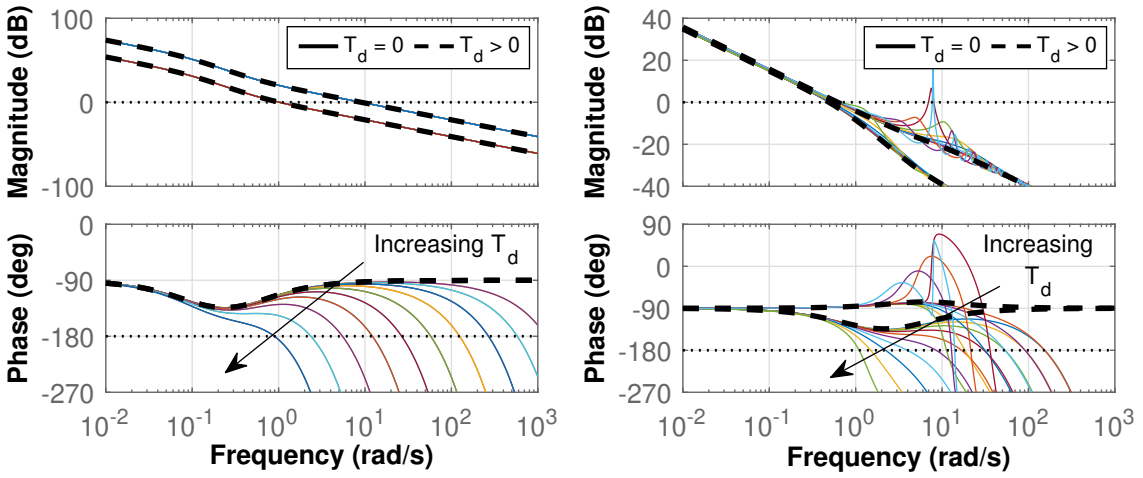

(a) (b)

Figure 2.10: (a) Bode plot for increasing time delay with PI control of system 2.50. (b) Bode plot for a cascaded control configuration.

(Figure 2.10(b)). Peaks appear due to the time delay being incorporated into the dynamics of the inner loop transfer function. As delay increases, its effect becomes larger. Once the delay becomes large enough, the peak may push the crossover frequency by an order of magnitude or more. In practice, however, controlling a system whose time delay is longer than its characteristic time constant is impractical without special approaches such as Smith predictors.

2.8 Summary

This chapter presented a specific form of cascaded control that utilizes a proportional inner loop and PI outer loop structure. Previous literature used cascaded control solely for disturbance rejection and assumed distinct time scale differences between nested loops. Using a new Nonlinear Gap Metric, this chapter highlights the ability of cascaded control to linearize load dependent nonlinearities of a system. Relative Gain Array analysis also showed that for MIMO systems, cascaded control can decouple input-output pairs. These benefits were realized without exact knowledge of the systems nonlinearity making the

cascaded structure very modular. Improved performance was also seen for inner and outer loop feedback on the same signal indicating that cascaded control can be used for systems that do not display the rule-of-thumb dynamic separation.

The linearization and decoupling behaviors of cascaded control were used to develop tuning procedures for selecting inner and outer loop gains. Simple tuning rules allow for quick implementation in the field while an optimal LQ framework allows for robust tuning across multiple operation conditions using LMIs. Issues with establishing an H_∞ framework were also discussed.

3. BENEFITS OF CASCADED CONTROL IN PRACTICE

In the previous chapter, the benefits cascaded control and methods for tuning loop gains were presented. This chapter will demonstrate these advantages and procedures through a series of case studies. Example systems highlight critical behavior while experimental and simulation results show how Heating, Ventilation, and Air-Conditining (HVAC) systems control is improved by the cascaded architecture.

The first case study shows how inner loop control reduces the envelope of responses over all operating conditions using an example second-order system. This is followed by an analysis of MIMO decoupling behavior using an identified structured multi-evaporator refrigeration system model. The next several case studies use simulation models of common HVAC equipment to demonstrate improved performance with cascaded control. Finally, the optimal tuning of a thermal expansion valve control for an experimental heat pump system is presented.

3.1 Case Study #1: Nonlinear Second Order Dynamic System*

To illustrate the differences between traditional tuning methods, simple cascaded tuning rules, and the proposed LQ optimal approach from the previous chapter, consider the nonlinear second-order system given by Equation 3.1. In this example, the inner loop dynamics are first order with a faster response than the outer loop, second order dynamics. Both processes share a single nonlinear gain from their common input to respective output ($\psi_o = \psi_i$) that is quadratic with respect to operating condition and varies by an order of magnitude for $\sigma \in [0, 1]$. These conditions are common in many HVAC systems including air handlers [21] and refrigeration systems [90] that use flow to control temperature.

*This case study is adapted with permission from "Optimal Tuning of Cascaded Control Architectures for Nonlinear HVAC Systems", C. Price and B. Rasmussen, Science and Technology for the Built Environment, vol. 23(8), pp. 1190-1202, ©2017 ASHRAE.

Table 3.1: Gains for Example 2nd Order System Controllers

Controller	Tuning Method	σ	k_L	k_p	k_i
PI	Skogestad IMC	0	—	3.6	2.6
		1	—	0.36	0.26
Cascaded	Successive Loop Closure with Skogestad IMC	0	5	12.8	25.2
		1	0.5		
	LQ with NGM	0	8	8.7	12.9

$$G(s) = \psi(\sigma) \begin{bmatrix} G_i(s) \\ G_o(s) \end{bmatrix} = (9\sigma^2 + 1) \begin{bmatrix} \frac{5}{s+5} \\ \frac{2}{s^2+3s+2} \end{bmatrix} \tag{3.1}$$

Traditional PI control seeks to regulate the process $\psi(\sigma)G_o(s)$ over all operating conditions. As shown in Table 3.1, the nonlinear gain can cause PI gains to vary significantly depending on the operating conditions in which the system is tuned. These variations in many cases lead to hunting behavior, the phenomenon discussed in detail in Chapter 1. Tuning of cascaded control loops using Successive Loop Closure (SLC) with standard tuning methods still sees large but reduced variations. As seen in Table 3.1 and Figure 3.1(a), changing system dynamics result in a wide range of closed loop Nonlinear Gap Matric (NGM) values for different inner loop gains. In the worst case, SLC tuning realizes less than half of the linearizing effect of the inner loop control with $\Gamma = 0.4$ for $k_L = 0.5$.

The spread of closed-loop responses for each controller and tuning method over the range of all operating conditions is shown in Figure 3.1(b) along with example responses for $\sigma = 0.25$. As shown, the spread of PI control responses is quite significant and contains both severely underdamped and overdamped characteristics. The control spread of the SLC tuned cascaded controller is much smaller than that of the PI controller; however, that spread is heavily dependent on the conditions in which the controller is tuned. The LQ method allows tuning for higher inner loop gains and greater nonlinearity compensation

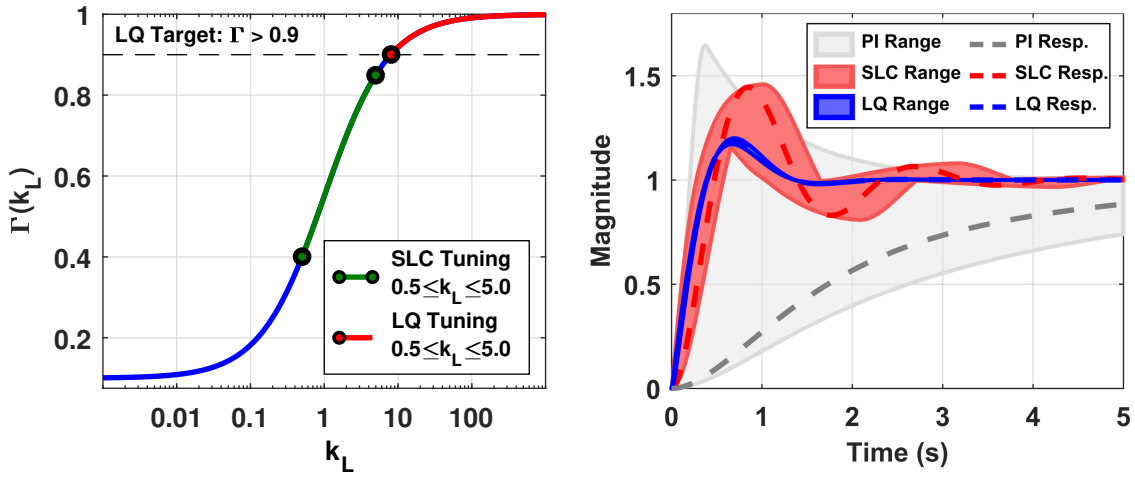

(a) (b)

Figure 3.1: (a) Closed loop NGM profile for example system. (b) The spread of closed-loop responses is significantly reduced by cascaded control.

while balancing the response of the outer loop controller. Overall, the proposed quadratic tuning method provides much more consistent performance while still maintaining stability of the closed-loop. State-space models and final weights can be found in Appendix B.

3.2 Case Study #2: Decoupling Multi-Evaporator Dynamics*

To understand how the cascaded architecture can decouple dynamics of a MIMO system, a simplified model of a multi-evaporator water chiller is analyzed. This model is based off of the experimental Vapor Compression Cycle (VCC) system from [110] where cascaded control improved performance at startup and during operation. The system used R-134a refrigerant and water as the primary and secondary fluids respectively. Rooms are represented by small water tanks and outside weather conditions by a large reservoir tank. Disturbances to the room, e.g. infiltration or occupancy, are mimicked by variable speed pumps that cycle water from the warm reservoir and by small water heaters.

*This case study is adapted with permission from "Decoupling of MIMO Systems Using Cascaded Control Architectures with Application for HVAC Systems", C. Price and B. Rasmussen, Proceedings of the American Control Conference, pp. 2907-2912, ©2017 IEEE.

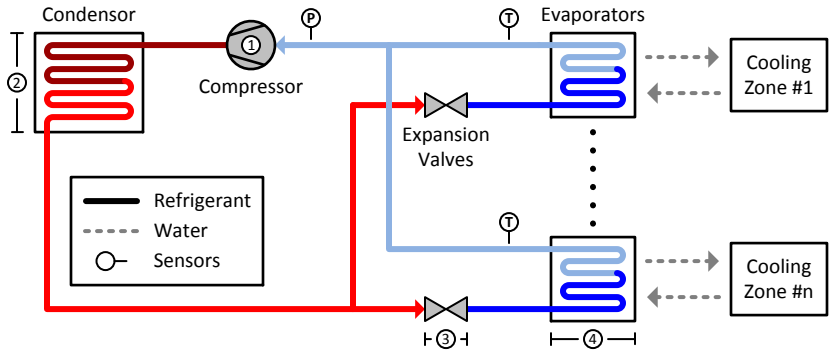

Figure 3.2: The small-scale water chiller system uses a VCC to cool two 'room' water tanks. The cycle consists of (1) compression, (2) condensation, (3) evaporation, and (4) evaporation. Adapted with permission from [125] ©2017 IEEE.

Room tank temperatures are controlled by passing water through evaporators that are part of the VCC cycle shown in Figure 3.2. The VCC cycle consists of refrigerant undergoing compression, condensation, expansion, and evaporation. Control of a VCC seeks to regulate the amount of refrigerant superheat at each evaporator outlet. Excessively high superheating reduces overall efficiency while unevaporated refrigerant can damage the compressor. Therefore control designs that can robustly regulate superheat to only a few degrees are desired.

The dynamics of multi-evaporator VCC systems can be highly coupled for several reasons. Pressure throughout the system is inherently coupled due to the physical connection of refrigerant lines. Also many systems use only a single common pressure sensor located downstream of the evaporators to reduce instrumentation costs. As each control input causes change in pressure, control of one evaporator necessarily affects the others. Valve movements also affect the flow of refrigerant throughout the system. Changes in mass flow rate in one evaporator cause fluctuations in flow rate elsewhere.

The following simplified model is based on an understanding of the physics of coupled variables [118, 120] and can be used to capture the dominant coupling effects in a multi-evaporator VCC system. The dynamics of the 'n' evaporator exit temperatures ($\vec{x}_1$) and

the response of the common pressure state (x_2) are each assumed to be first order. Each control input affects not only the associated temperature state but also the common pressure state. Output for a traditional PI/PID control structure is the difference between the exit temperatures and the estimated saturation temperature which is related to the shared pressure state by a lookup table. The simplified state space representation of these dynamics is given by Equation 3.2 where L_1, B_1, B_2, and C_2 are all positive, nxn diagonal matrices.

$$\begin{cases} \dot{x} = \begin{bmatrix} -L_1 & 0 \\ 0 & l_2 \end{bmatrix} \begin{bmatrix} \vec{x}_1 \\ x_2 \end{bmatrix} + \begin{bmatrix} -B_1 \\ \vec{1}_{1\text{x}n} B_2 \end{bmatrix} u_i \\ y_o = \begin{bmatrix} I & -C_2 \vec{1}_{n\text{x}1} \end{bmatrix} x \end{cases} \tag{3.2}$$

As the system matrices are known explicitly, a closed-form solution for the open loop transfer function can be expressed as Equation 3.3. Note that all coupling terms in the transfer function come from the second part of this expression.

$$\begin{aligned} G(0) &= -\begin{bmatrix} I & -C_2 \vec{1}_{n\text{x}1} \end{bmatrix} \begin{bmatrix} -L_1 & 0 \\ 0 & -l_2 \end{bmatrix}^{-1} \begin{bmatrix} -B_1 \\ \vec{1}_{1\text{x}n} B_2 \end{bmatrix} \\ &= -L_1^{-1} B_1 - \underbrace{\frac{1}{l_2} C_2 \vec{1} B_2}_{\text{Coupling Terms}} \end{aligned} \tag{3.3}$$

Further, the coupling terms have rank one allowing the use of the matrix identify of Equation 3.4 to determine the closed-form solution for the open loop RGA matrix (Equation 3.5) where $Z = B_2 B_1^{-1} L_1$. This expression will be used for comparison of several configurations of a cascaded controller.

$$(X+Y)^{-1} = X^{-1} - \frac{1}{1 + \text{tr}\,(YX^{-1})} X^{-1} Y X^{-1} \tag{3.4}$$

$$\text{RGA}_{\text{OL}} = I + \left(\frac{1}{l_2[l_2 + \text{tr}\, Z]} \right) \left\{ (\text{tr}\, Z) I - Z \vec{1} \right\} Z \tag{3.5}$$

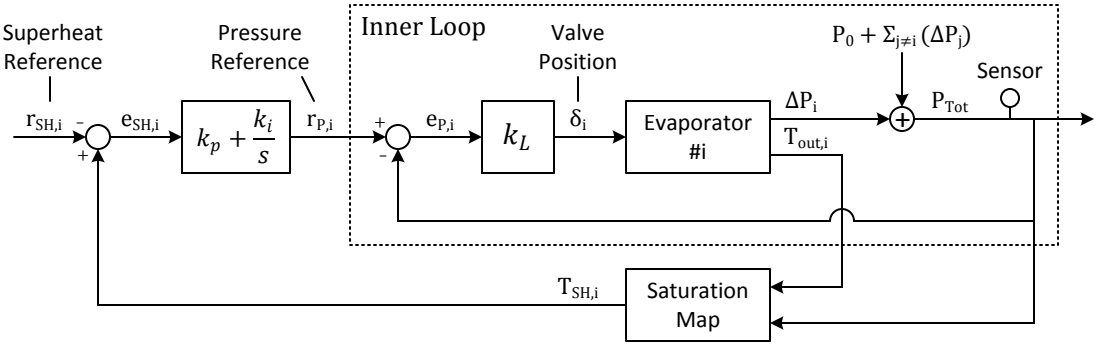

Figure 3.3: Block diagram for simplified multi-evaporator VCC system model where 'P_0' denotes initial system pressure and 'Δ' changes in system variables. ©2017 IEEE.

Consider the inner loop feedback signal given by Equation 3.6. When $D_i = 0$, the resulting inner loop control signal (Equation 3.7) is analogous to pressure feedback with a single common sensor. This type of feedback is shown in block diagram by Figure 3.3. For large inner loop gains, the inner loop transfer function becomes singular indicating that the RGA Number will approach infinity. This behavior is seen in the explicit inner loop transfer function (Equation 3.8). Note that although the transfer function approaches that of the open loop system (Equation 3.3) for small inner loop gain, the singular coupling terms grow as a function of the diagonal inner loop control matrix K_L. A plot of the RGA Number curve with single pressure feedback is shown in Figure 3.4. The model used was identified from experimental data with the structure discussed before and $C_2 = I$.

$$y_i = \begin{bmatrix} \vec{0} & C_2 \vec{1}_{n\text{x}1} \end{bmatrix} x + D_i u_i \tag{3.6}$$

$$u_P = \begin{bmatrix} k_{L,a}(u_{o,a} - x_2) \\ k_{L,b}(u_{o,b} - x_2) \\ \vdots \\ k_{L,n}(u_{o,n} - x_2) \end{bmatrix} = K_L \left(u_o - \begin{bmatrix} \vec{0} & \vec{1}_{n\text{x}1} \end{bmatrix} x \right) \tag{3.7}$$

$$Q_P(0) = -L_1^{-1} B_1 K_L + \underbrace{\frac{1}{l_2 + \operatorname{tr} B_2 K_L} \left[L_1^{-1} B_1 K_L - I \right] \vec{1} B_2 K_L}_{\text{Coupling Terms}} \tag{3.8}$$

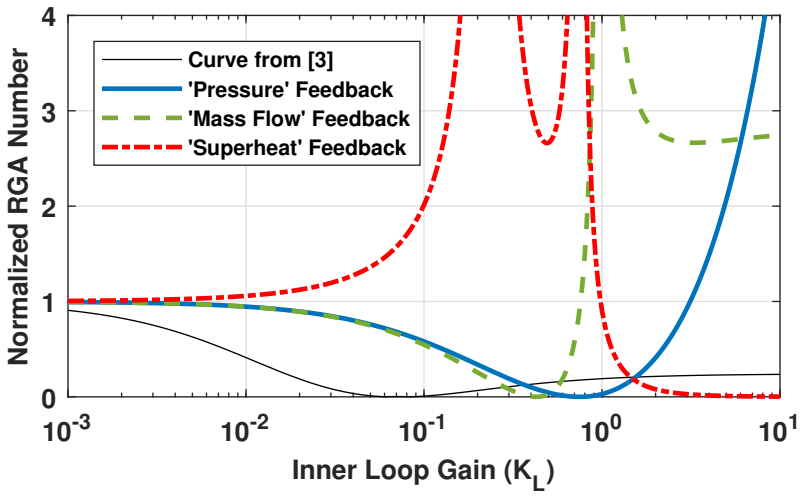

Figure 3.4: RGA number profiles for several cascaded control configurations for the simplified multi-evaporator VCC model. ©2017 IEEE.

Despite lacking asymptotic decoupling, the common pressure feedback signal can reduce coupling in the simplified evaporator dynamics with only moderate gains. Note that the coupling terms in Equation 3.8 are completely eliminated from the inner loop transfer function when individual inner loop gains are selected as $k^*_{L,i} = l_{1,i}/b_{1,i}$. Further, a single finite inner loop gain value could approximately decouple the system provided that evaporator dynamics are sufficiently similar. This behavior is reflected in Figure 3.4 where steady-state decoupling approaches zero for $k_{L,i} \approx 0.7$.

When $D_i = I$ in Equation 3.6, the feedback signal has analogies to a mass flow feedback loop with sensors for each evaporator; a configuration previously used by [111] to linearize a VCC system. The output equation is a result of mass flow through a VCC system being dependent on both valve position and system pressure. This feedback signal differs from the single pressure feedback in that the inner loop transfer function is invertible. However, the resulting asymptotic RGA Number is greater than with the original system. Despite this, moderate inner loops can still completely decouple the system with slightly lower inner loop gain.

This analysis helps to understand the response of the cascaded controller from [110]. That controller used separate evaporator pressure sensors to decouple evaporator dynamics. After an initial reduction in RGA number, the coupling increased to some intermediate (but improved) coupling number determined by $G_i(s)^{-1}G_o(s)$. From the analysis above, the dip is due to the inner loop gain approaching a value K_L^* determined by the dynamics of the evaporators and the rise is due to the inner and outer loop taking feedback on separate signals.

An alternative loop configuration that guarantees asymptotic decoupling takes inner and outer loop feedback on the same signal, i.e. superheat. This control structure requires minimal implementation as it adds only a single proportional loop to the control software. Using the superheat signal gives the inner loop dynamics given by Equation 3.9 where B is the open loop input matrix. Solving for the determinant of the steady-state gain matrix yields expression Equation 3.10 for a two evaporator system. From this expression, the denominator of the determinant has 'n' roots indicating 'n' peaks in the RGA Number with respect to K_L. This shape is also shown in Figure 3.4. Selection of the inner loop gain should avoid these roots and place inner loop gain outside the troughs, i.e. $K_L \geq 1$.

$$\dot{x} = \begin{bmatrix} -L_1 + B_1 K_L & -B_1 K_L C_2 \vec{1}_{n\text{x}1} \\ -\vec{1}_{1\text{x}n} B_2 K_L & -l_2 + \operatorname{tr} B_2 K_L C_2 \end{bmatrix} x + B K_L u_o \tag{3.9}$$

$$\det(L_{sh}(0)) = \frac{l_2 + \operatorname{tr}(L_1 B_1^{-1} B_2 C_2)}{\left(l_2 + \operatorname{tr}(L_1 B_1^{-1} B_2 C_2)\right) + \left(l_2 \operatorname{tr}(K_L^{-1} L_1 B_1^{-1}) + \det(L_1 K_L^{-1} B_1^{-1})\right)[l_2 - \operatorname{tr}(K_L B_2 C_2)]} \tag{3.10}$$

The inner loop feedback signals and their associated RGA Number profiles illustrate how cascaded control can be used to decouple system dynamics. As shown, each signal offers decoupling for different inner loop gains. Selection of sensor, signals, and inner loop gains can therefore be balanced against system actuation and control constraints to achieve decoupling. For example, while superheat feedback with a single sensor can asymptoti-

cally decouple system dynamics, Electronic Expansion Valves (EEVs) typically have slow response rates. Other inner feedback signals, e.g. pressure feedback, may therefore be more appropriate given system actuator response characteristics.

These considerations are in addition to the linearization effects of the cascaded control loop shown in [86]. Analysis of the Nonlinear Gap Metrics used to tune inner loop gains showed that under certain cases, increasing inner loop gain could improve linearization provided by the cascaded architecture. Depending on the system, a situation can therefore arise where decoupling and linearization considerations are in conflict; changing inner loop gain my slightly reduce coupling but allow more nonlinearity. For systems with coupled and nonlinear behavior such as HVAC systems, cascaded control can reduce both given proper tuning.

3.3 Case Study #3: Fan Speed Control for Linearization*

The remaining case studies shift away from simplified examples towards physical models and/or experimental systems. The next two case studies will focus specifically on room temperature control using two methods: direct fan control and Variable Air Volume (VAV) dampers. Room air temperature regulation in multi-zone buildings is usually accomplished by supplying constant temperature conditioned air to a room at variable flow rates. Regulation of the supply air temperature is done by the Air Handling Unit (AHU), a system that is the subject of a later case study. These devices typically contain a supply fan, cooling coil, and a humidifier, although the effects of humidity control are not considered in this section. The conditioned air is then connected to room zones through internal duct work. By modulating supply fan speed, the volume flow rate of air into a room may be

*This case study is adapted with permission from "Compensation of HVAC System Nonlinearities Using Cascaded Control Architecture", C. Price and B. Rasmussen, Proceedings of the Dynamic Systems and Control Conference, vol. 2, ©2014 ASME and "HVAC Nonlinearity Compensation Using Cascaded Control Architectures", C. Price, S. Liang, and B. Rasmussen, ASHRAE Transactions, vol. 121, pp. 217-231, ©2015 ASHRAE.

controlled directly. For larger systems, terminal boxes located before each control zone may have individual fans as opposed to a single, central unit.

This case study considers a single zone, lumped capacitance model of room temperature dynamics [19]. Equation 3.11 details how heat transfer through the building envelope is dependent on the difference between the room (T) and outside air temperature (T_{oa}) as well as the heat transfer coefficient of the walls. Infiltration (H_{inf}) was considered as a constant heat load on the building while the internal gains (H_{hg}) varied on an approximate occupant schedule for a typical work day. The dynamics of the motor and fan are governed by Equation 3.12 and traditional affinity laws, respectively. The torque and back-EMF constants, k_t and k_e respectively, are based on those of a typical two horse power motor [126] while the fan inertia is that of an appropriately sized axial fan.

$$C\frac{dT_a}{dt} = \rho_a c_{p,a}\dot{V}_a(T_s - T_a) + UA(T_{oa} - T_a) + H_{hg} + H_{inf} \tag{3.11}$$

$$RJ\dot{\omega} + k_t k_e \omega = k_t V_{in} \tag{3.12}$$

Although these equations are linear ordinary differential equations, the dynamics depend on operating conditions. Equation 3.11 evolves based on differences between the supply, outside, and room air temperatures meaning that its response characteristics will vary with operating conditions. As room temperatures evolves depending on these differences, response characteristics will vary according to weather conditions, supply air temperature, and zone temperature set points. Figure 3.5 shows how the steady-state gains and time constants of the systems dominate first order response vary depending on cooling demand (as measured by fan load). For a room temperature of $20°$C ($68°$F), outside air temperature was calculated to allow steady-state to occur at the initial fan input. A constant step change in fan speed was then introduced and response data collected. As shown, steady-state gains more than double across the operating range while time constants in-

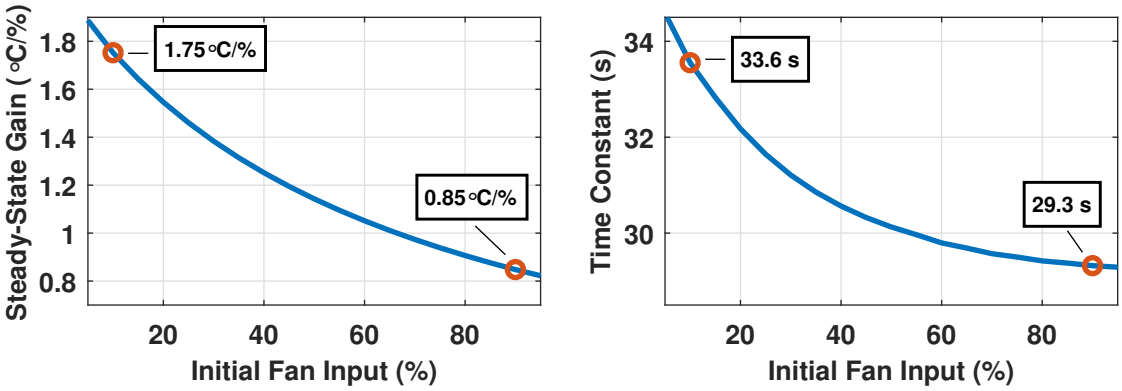

(a) (b)

Figure 3.5: (a) Steady-state gains for the fan system vary by more than double across all operating conditions. (b) The system time constant also varies by approximately 14%.

crease by approximately 15%. Control gains will therefore vary depending on when the system was tuned. This means that if the system is tuned in low gain conditions, it will become too aggressive as response gains increase. This operational dependence therefore has a large contribution in HVAC system hunting.

To compensate for these changing nonlinear gains, the cascaded loop of Figure 3.6(a) was implemented in simulation. In a slight departure from the loop implemented on the VCC system in [109], feedback for the inner and outer loops will both be on room temperature. As shown by Equation 3.13, the nonlinear gain function $\psi(\omega)$ still appears in both the numerator and denominator of the inner loop transfer function. This placement will offset the nonlinear gain without knowledge of its structure. Additionally, the inner loop gain will approach unity as the proportional gain k_L increases. The cascaded loop inherently reduces system nonlinearities while also shrinking the range of steady-state gains. The loop will therefore operate more consistently across all cooling load conditions while eliminate fan speed hunting.

$$L(s) = \frac{k_L \psi(\omega) G(s)}{1 + k_L \psi(\omega) G(s)} \tag{3.13}$$

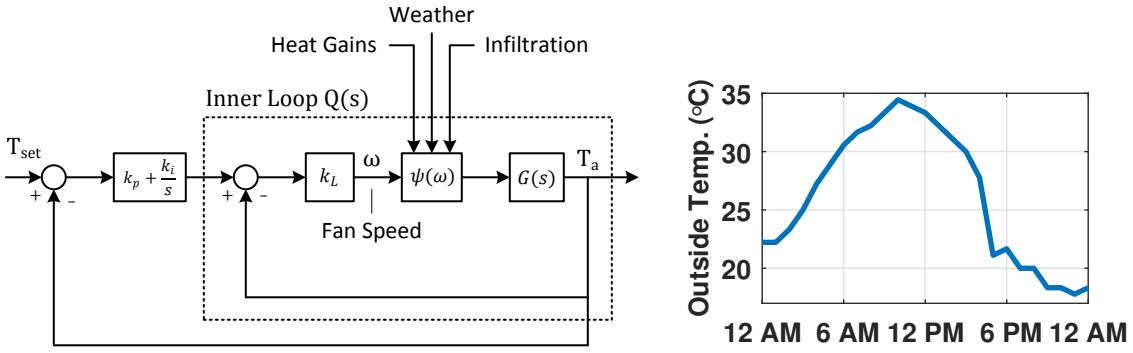

(a) (b)

Figure 3.6: (a) The proposed cascaded loop takes inner and outer loop feedback on room temperature. (b) Outside air temperature input for fan cascaded and PI loop simulations.

Simulations used the outside air temperature profile shown in Figure 3.6(b) with results shown graphically by Figure 3.7 and summarized in Table 3.2. As shown, around 5 PM the combination of a sudden decrease in outside air temperature and low internal heat load caused the system to transition to the large gain characteristics on the left side of the axes in Figure 3.5. After that time, the PI controller tuned in high demand conditions (HDPI) begins to cause oscillations in room air temperature and stable waves in fan speed of 100 rpm after 8 PM. The PI controller tuned in low demand conditions (LDPI) does not display the same hunting behavior but does struggle to regulate room temperature. These two controllers highlight the full range of possible performance seen with traditional control loops and their associated tuning procedures. While a technician may attempt to tune gains during "moderate" cooling loads, such conditions are difficult to identify in practice. This often leads to detuning of controllers to avoid hunting issues and gains that are close to the LDPI example. The cascaded controller shows similar regulation performance to the HDPI controller but eliminates the fan speed hunting seen in later hours. As the fan speed varies between 10% and 90% of its maximum value, the simulation captures both high and low demand conditions. The cascaded loop provides the best performance across

all conditions while eliminating fan speed hunting showing that a single controller can be used to regulate the system under all conditions.

Table 3.2: Fan Control Case Study Results

Error Metric	Low Demand PI	High Demand PI	Cascaded Control
Root Mean Square Error (RMS)	1.15°C (2.07°F)	0.76°C (1.37°F)	0.85°C (1.53°F)
Mean Bias Error (MBE)	0.34°C (0.61°F)	0.15°C (0.27°F)	0.17°C (0.31°F)
Hunting	No	Yes	No

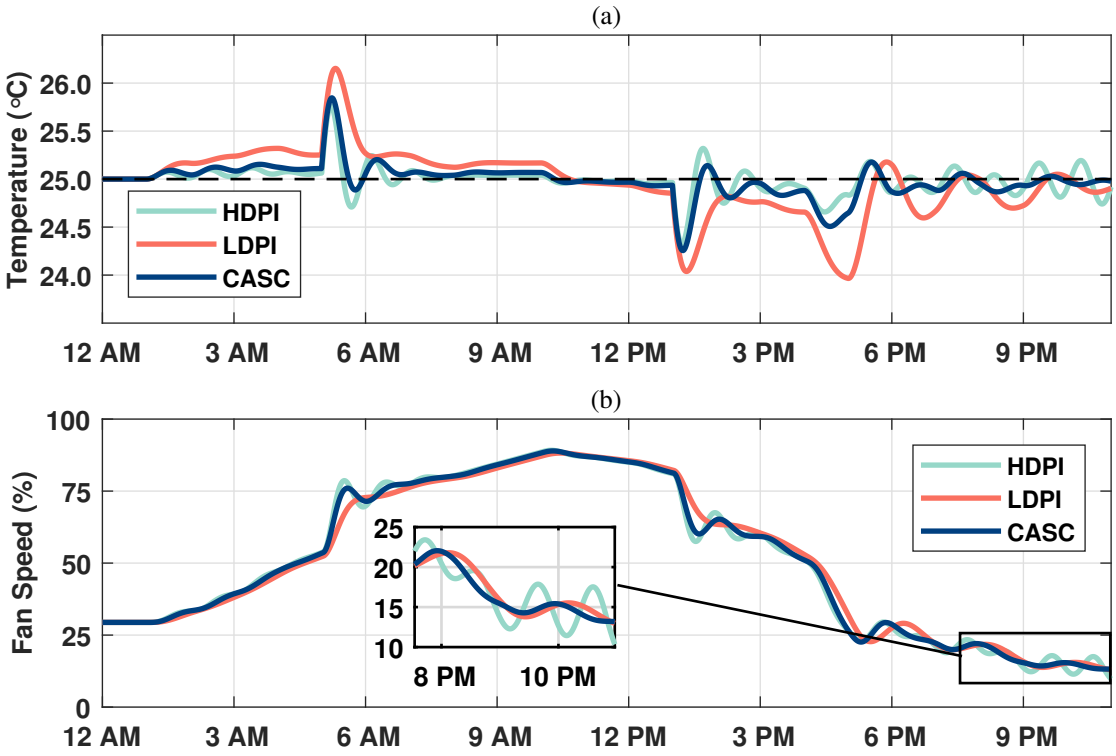

Figure 3.7: Results for fan control case study show oscillatory PI behavior starting around 2 PM with stable oscillations after 8 PM. Cascaded control eliminated hunting behavior.

3.4 Case Study #4: VAV Terminal Box Control*

The previous case study has shown that the cascaded loop can improve the performance of systems with non-constant, nonlinear response characteristics controlled by positive displacement actuators. The predominate configuration in commercial buildings is however the Variable Air Volume (VAV) system where is conditioned air supplied to building zones through duct work that ends at Terminal Unit (TU) boxes located in each zone. As each room may require different amounts of air, TU boxes contain dampers that obstruct the flow of air. A separate control loop regulates the static pressure in the ducts by regulating the supply fan speed to ensure adequate flow.

Damper characteristics introduce an additional nonlinearity to the system dynamics of the previous section. As shown in Figure 3.8(a), the relationship between damper po-

*This case study is adapted with permission from "Compensation of HVAC System Nonlinearities Using Cascaded Control Architecture", C. Price and B. Rasmussen, Proceedings of the Dynamic Systems and Control Conference, vol. 2, ©2014 ASME and "HVAC Nonlinearity Compensation Using Cascaded Control Architectures", C. Price, S. Liang, and B. Rasmussen, ASHRAE Transactions, vol. 121, pp. 217-231, ©2015 ASHRAE.

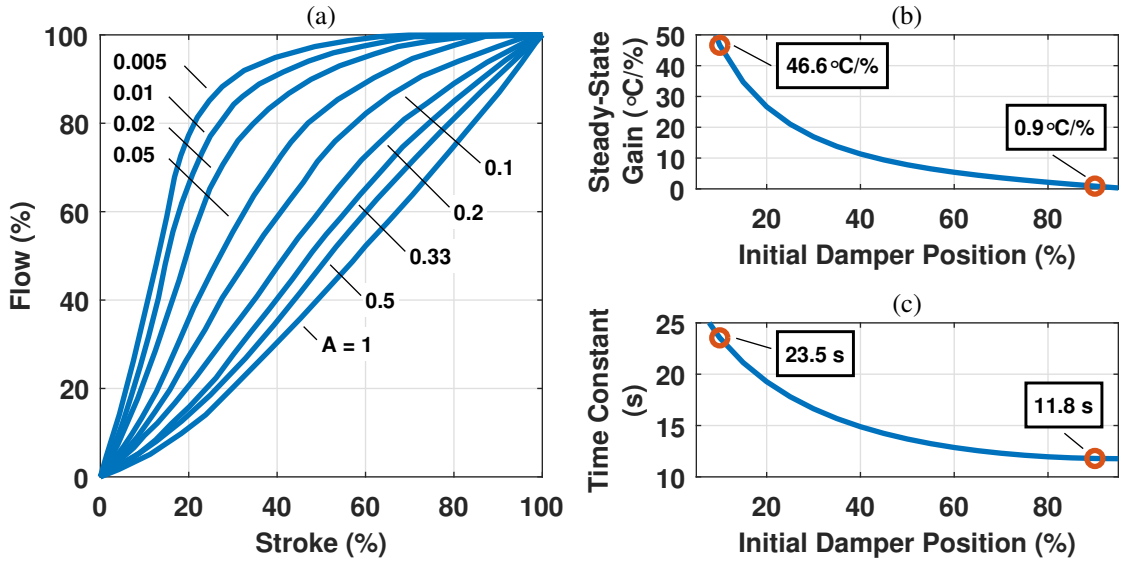

Figure 3.8: (a) Parallel blade damper characteristics (reproduced from [45, Chapter 7]). (b) System steady-state gains vary in magnitude by over 50 times. (c) System time response more than doubles over the operating range.

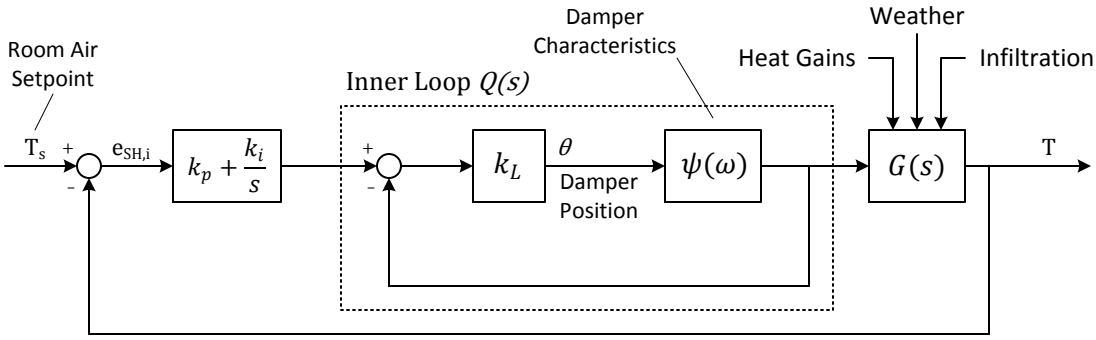

Figure 3.9: Cascaded control for the VAV system regulates volumetric air flow rate, eliminating the nonlinear damper characteristics and improving overall performance.

sition and volumetric flow rate depends on the ratio between total system pressure loss and the pressure drop across an individual terminal unit. The relationship in most cases is highly nonlinear and will result in damper hunting if tuned carelessly. For the simulations presented in this section, the damper characteristics are based roughly on those of the 'A = 0.05' curve with the relationship given by Equation 3.14 where θ is the angle of the damper opening. The addition of damper nonlinearities has a profound effect on the systems response characteristics. The steady-state gain to a step input change in damper position now varies in magnitude by over 50 times while the time constant more than doubles. This change has a large effect on the magnitude of control gains depending on when the controller is tuned.

$$V(\theta) = -V_{max}(\theta^2 - 2\theta) \tag{3.14}$$

Elimination of the primary nonlinearity in the VAV systems leads to the cascaded loop shown in Figure 3.9. This architecture will require the addition of a flow averaging sensor to measure volumetric flow rate. However these sensors are relatively inexpensive and often come prepackaged with many TU boxes. The inner loop control will regulate the volume flow rate of air through the terminal box with set points generated by the outer loop

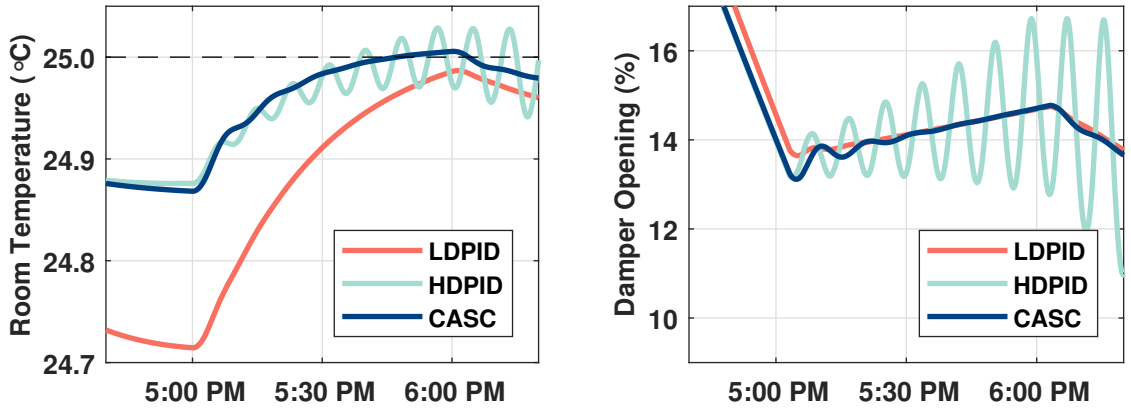

(a) (b)

Figure 3.10: Around 5 PM, system gains become large enough that the high demand PID controller begins to hunt. The cascaded controller displays no hunting while having similar performance.

PID controller. This configuration is what [127] refers to as a pressure independent control loop, named for the way the control eliminates variations in flow rate due to changes in system static pressure. Beyond this, the cascaded configuration has the same linearizing properties as the previous section due to the placement of the nonlinear gain in the inner loop transfer function (Equation 3.15). Therefore the impact of the damper characteristics will be greatly reduced, improving overall performance.

$$L(0) = \frac{k_L \psi(\theta)}{1 + k_L \psi(\theta)} \tag{3.15}$$

Simulations were conducted using the outside air disturbance and internal heat gains from Case Study #3. From the detail plots of Figure 3.10 and the data in Table 3.3, traditional PID damper control can be seen to suffer from the same issues as fan speed control. Around 5 PM, the PID controller tuned in high demand (HDPID) causes damper position to begin oscillating steadily with magnitudes increasing well over 5%. The PID controller tuned in low demand (LDPID) displays no hunting but shows poor regulation when com-

Table 3.3: VAV System Case Study Results

Error Metric	Low Demand PID	High Demand PID	Cascaded Control
Root Mean Square Error (RMS)	1.124°C (0.223°F)	0.545°C (0.981°F)	0.047°C (0.085°F)
Maximum Absolute Error (MAE)	0.446°C (0.803°F)	1.968°C (3.542°F)	0.268°C (0.482°F)
Hunting	No	Yes	No

pared to the other controllers. Cascaded control displays similar mean performance to the high demand PID controller without hunting. This is why the RMS error for the cascaded controller is much lower than the two traditional PID controllers. These simulations show that the cascaded controller is able to compensate for actuator nonlinearities without requiring knowledge of the actuator dynamics before implementation. The simulations also show that the cascaded controller is able to work with HVAC systems that both positively displace and obstruct the flow of cold air for room temperature control.

3.5 Case Study #5: Air Handling Unit Control*

Both the previous case studies focused on control of room temperature by modulating the flow rate of chilled air into a designated zone. The supply air temperature itself is controlled by the Air Handling Unit (AHU) shown schematically in Figure 3.11. In cooling mode, warm return air is mixed with outside air required for ventilation. Air is then passed through the unit by the supply fan and across a heat exchanger. Chilled water is passed though the heat exchanger to absorb heat from the air in a forced convection process. The flow rate of water into the heat exchanger is modulated with a valve whose position is controlled by a stepper motor. In this way discharge air temperature can be controlled based

*This case study is adapted with permission from "HVAC Nonlinearity Compensation Using Cascaded Control Architectures", C. Price, S. Liang, and B. Rasmussen, ASHRAE Transactions, vol. 121, pp. 217-231, ©2015 ASHRAE.

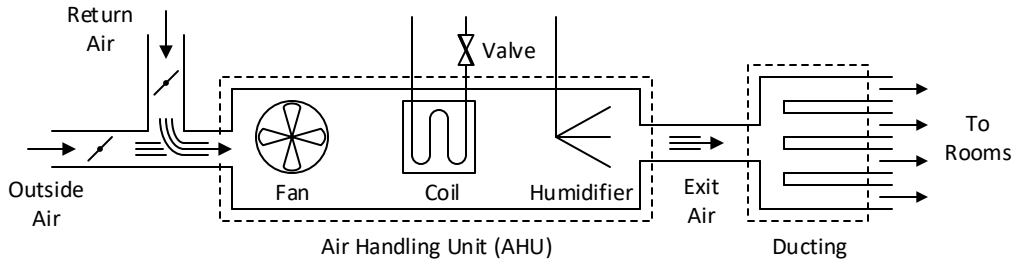

Figure 3.11: Diagram of a typical Air Handing Unit (AHU) and its components.

on the required demand. Most building HVAC systems use a simple PI control loop to regulate the discharge air temperature. A survey of AHU chilled water valves on the campus of Texas A&M University has shown that this approach has serious implementation issues with 65% of sampled units displaying hunting behavior [22]. This section expands on previous results and further demonstrates the ability of a cascaded control loop to compensate for the nonlinearities in the AHU dynamics.

The basic heat transfer process is modeled based on equations from [128]. A finite volume approach divides the cooling coil into N sections along its travel. The individual water and coil temperature dynamics are calculated using Equations 3.16 and 3.17 respectively. The water temperature is influenced by convective heat transfer with the coil wall as well as the temperature and flow rate (q) of water entering the finite volume. Section temperature also depends on convection between the coil wall and the air passing over a section. The exit temperature of air leaving a finite volume is calculated by Equation 3.18 with the final discharge air temperature calculated using an average of all N sections. This model was shown to have good agreement with experimental data by [129].

$$C_w \cdot \frac{\partial T_w}{\partial t} + c_{p,w} \cdot q(\delta) \cdot \frac{\partial T_w}{\partial x} + h_w \cdot P_t(T_w - T_c) = 0 \tag{3.16}$$

$$C_c \cdot \frac{\partial T_c}{\partial t} + c_{p,a} \cdot \dot{m}_a \cdot \varepsilon_a \cdot (T_c - T_{a,in}) + \kappa_w(T_c - T_w) = 0 \tag{3.17}$$

$$T_{a,out} = T_{a,in} + \varepsilon_a(T_c - T_{a,in}) \tag{3.18}$$

The fluid dynamics involved with the air and water flows are modeled using several approaches. Water-side flow uses the Churchill Correlation given by Equation 3.19 to calculate the friction factor for laminar and turbulent flow. The Gnielinski Factor is used to calculate the Nusselt number using the Reynolds and Prandtl numbers. For the three cases of laminar, transition, and turbulent flow, the Nusselt number is calculated by assuming a constant value of 4.364, estimating using an empirical polynomial, or computing using Equation 3.20 respectively. The convection heat transfer coefficient, h_w, for the water can then be determined from the definition of the Nusselt number. Air-side flow characteristics use the Colburn J-factor analogy (Equation 3.21) to calculate the convective heat transfer coefficient, h_a, of the air. This information is used to calculate the air flow NTU value from which the heat transfer effectiveness can be calculated by Equation 3.22.

$$ff = 2\left\{\left(\frac{8}{Re}\right)^{2} + \left[2.457\ln\left[\left(\frac{7}{Re}\right)^{0.9} + 0.27\frac{\epsilon}{D}\right]^{-1} + \left(\frac{37530}{Re}\right)^{16}\right]^{-1.5}\right\}^{\frac{1}{12}} \tag{3.19}$$

$$Nu = \frac{\left(\frac{ff}{8}\right)(Re - 1000)\,Pr}{1 + 12.7\left(\frac{ff}{8}\right)^{1/2}\left(Pr^{2/3} - 1\right)} \tag{3.20}$$

$$J_h = \frac{hPr^{2/3}}{c_p G} \tag{3.21}$$

$$\varepsilon_a = 1 - e^{-NTU_a} \tag{3.22}$$

The above equations demonstrate the highly complex, nonlinear dynamics of forced convection. Despite the complexity, system responses to step changes in chilled water flow rate are predominately first order, allowing them to be classified as before. Open loop simulations with 72°F (22°C) entering and 55°F (12.8°C) exiting air temperatures were conducted using a range of return air flow rates corresponding to valve openings between 10% and 90% open. Over this range, step changes in valve position resulted in steady-state

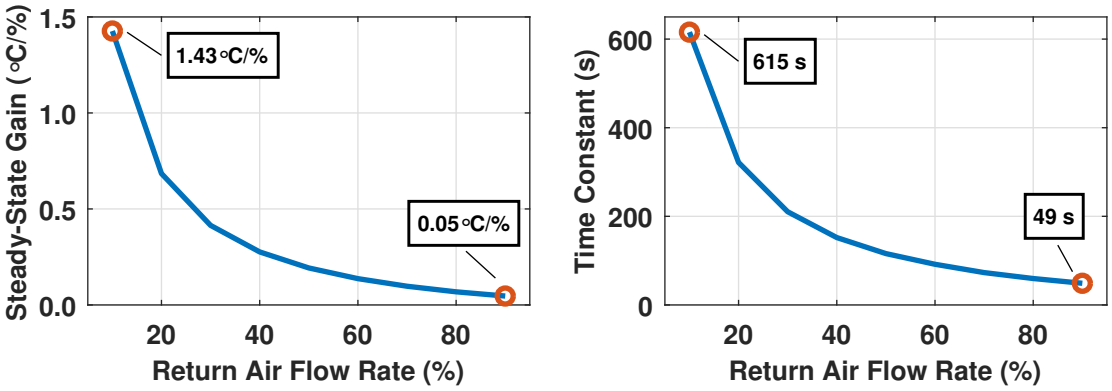

(a) (b)

Figure 3.12: The steady-state gain and time constant for the AHU simulation model each vary by an order of magnitude over all operating conditions.

gains that vary in magnitude by over 30 times and time constants that increase in duration by over 12 times (Figure 3.12). The previous sections have shown that this type of variation leads to actuator hunting as the system moves away from the tuning conditions. Therefore the prevalence of hunting in chilled water valves is not surprising.

To increase the accuracy of the simulations, additional implementation factors were included. As sensors in HVAC systems typically report readings in quantized values, temperature feedback was discretized in 0.1°F (0.056°C) intervals. This in effect creates dead zones in which there is no sensible change in the controlled output and, consequently, no change in actuator position. A range of controller sampling rates were also considered with the simulations using a period of five seconds. Results showed that there is an interaction between sensor quantization and controller sampling rate. Depending on the degree of quantization, degradation of control performance with decreased sampling time may be masked. If temperatures remain within a discretized block, decreased sampling will have no effect on performance.

Simulations used real data collected at the Utilities Business Office (UBO) on the campus of Texas A&M University. Return air temperatures as well as the demand signal

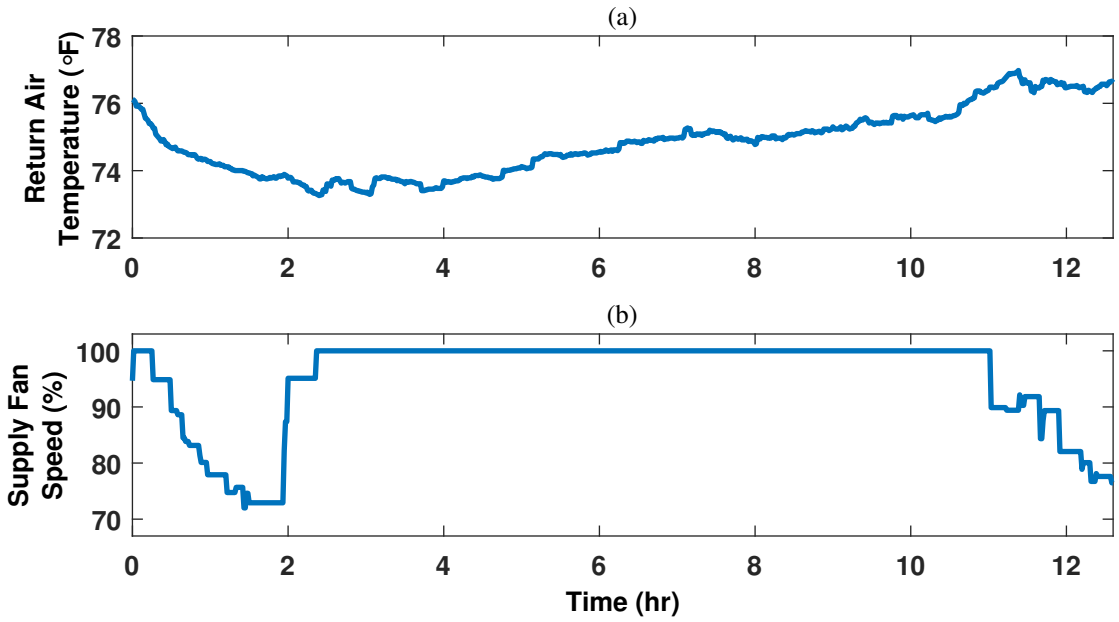

Figure 3.13: The return air temperatures (a) and supply fan speeds (b) used in the AHU simulations were recorded on 05/21/2014 at the Utilities Business Office at Texas A&M University in College Station, Texas from 6 AM to 7 PM.

to the supply fan are shown by Figure 3.13. As the model parameters given by [128] are for a much smaller AHU than the one used in the UBO building, maximum air and water flow rates were tuned to allow matching percentages of flow rates and valve positions with real data. Despite the difference in scale, the underlying physics of the real and model systems remain the same. In this way, the simulation provides insight into the performance of traditional PI control of chilled water valves and the benefits of the cascaded approach.

Despite the complicated dynamics, a cascaded loop with inner and outer loop feedback on discharge air temperature is able to eliminate the chilled water valve hunting seen in Figure 3.14. As shown, the PI Controller tuned in high demand conditions (HDPI) begins to show sustained oscillations when the valve position drops below approximately 50% open. This region has significantly higher response gains than those under which the controller was tuned. The HDPI controller therefore overestimates the required actuation

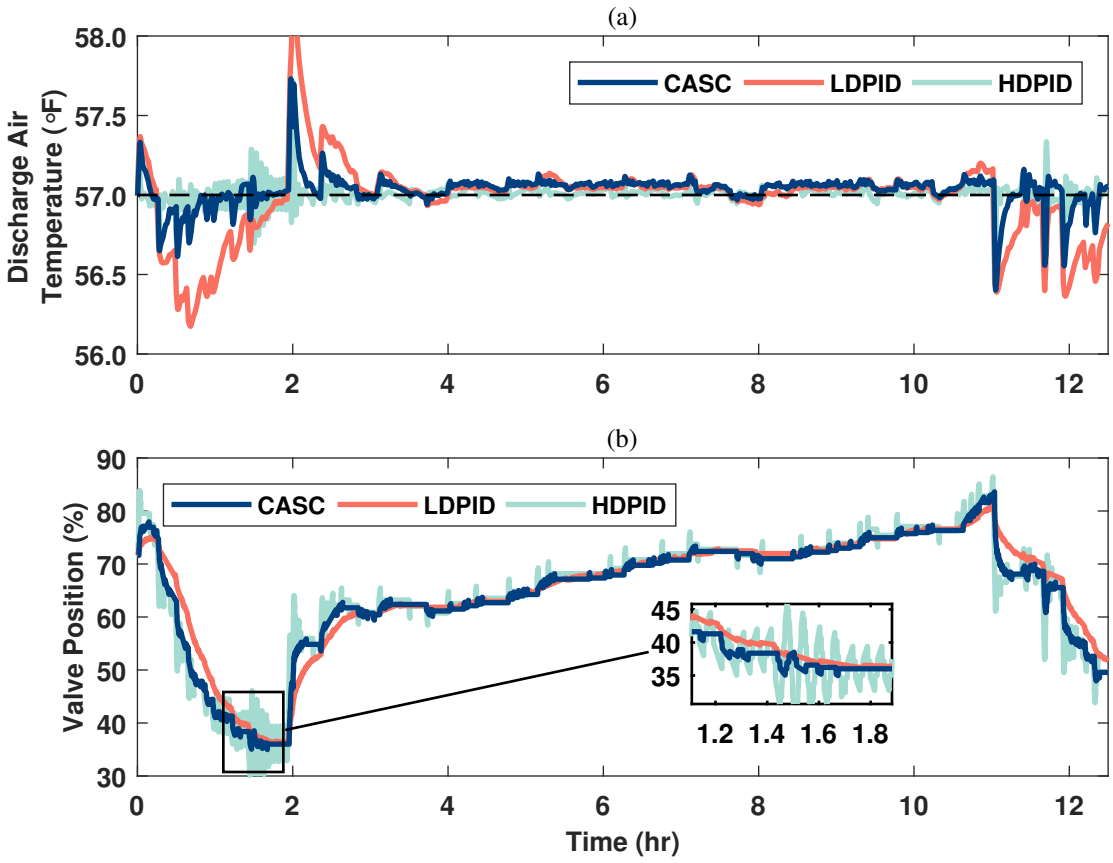

Figure 3.14: The discharge air temperature (a) and valve position (b) of the AHU simulations show that the high demand PI controller hunts in low demand conditions. The cascaded controller eliminates hunting without sacrificing performance.

leading to the observed hunting behavior. In contrast, the LDPI controller is much less aggressive due to the larger system gains present when the controller was tuned. While the LDPI controller does not show hunting behavior, it struggles to tightly regulate the discharge air temperature, resulting in large RMS and MAE errors. Without knowledge of the nonlinear dynamics, the cascaded loop was able to eliminate valve hunting and maintain comparable mean error values to the HDPI controller. These simulation results show that the cascaded loop is able to adequately control the system for the entire range of operating conditions. Results are summarized in Table 3.4.

Table 3.4: AHU Simulation Results for Data Collected On 5/19/2014

Error Metric	Low Demand PI	High Demand PI	Cascaded Control
Root Mean Square Error (RMS)	0.249°F (0.138°C)	0.062°F (0.034°C)	0.089°F (0.049°C)
Maximum Absolute Error (MAE)	1.23°F (0.68°C)	0.55°F (0.31°C)	0.73°F (0.41°C)
Total Valve Travel (%)	214	999	474
Hunting	No	Yes	No

3.6 Case Study #6: Radiator Valve Control*

The previous case studies have established that cascaded loops are able to compensate for nonlinearities associated with temperature dynamics, actuator characteristics, and forced convection. Each system was used in cooling mode to reject disturbance from heating gains. This, however, represents only half the HVAC picture as in cold weather rooms need to be heated to maintain a comfortable working environment. A common heating system is the hydronic radiator that passes high temperature hot water through a heat exchanger located in each room. Unlike the air handling unit, warming is accomplished by a combination of free convection and radiative heat transfer, not by forced convection. The flow rate of water through the heat exchanger is controlled by a Thermostatic Radiator Valve (TRV) whose position is modulated by a stepper motor. The valve allows heat dissipation to the room to be controlled in relation to heating demand.

Finite volume approximations of N sections along the radiator travel were used to model the heat transfer process [87]. This model was developed and validated by [130]. Each section has dynamics expressed by Equation 3.23. The first term on the right hand

*This case study is adapted with permission from "Compensation of HVAC System Nonlinearities Using Cascaded Control Architecture", C. Price and B. Rasmussen, Proceedings of the Dynamic Systems and Control Conference, vol. 2, ©2014 ASME and "HVAC Nonlinearity Compensation Using Cascaded Control Architectures", C. Price, S. Liang, and B. Rasmussen, ASHRAE Transactions, vol. 121, pp. 217-231, ©2015 ASHRAE.

side expresses the heat transfer between individual finite volumes and captures the dependence on hot water flow rate (q). The second term gives the heat radiated from the finite volume to the room. The magnitude of this value is calculated in relation to a nominal condition under which the inlet, outlet, and room temperatures are 70°C (158°F), 50°C (122°F), and 20°C (68°F) respectively. These values give rise to the nominal power dissipation of the radiator (Φ_0) and the mean temperature difference calculated by Equation 3.24. The total heat radiated to the room is then calculated by Equation 3.25 which represents a summation of heat transfer by each finite volume. Room dynamics, given in Equations 3.26 and 3.27, are similar to those used for the fan and VAV controlled systems with the addition of the building envelope temperature.

$$\frac{C_r}{N} \cdot \frac{dT_n}{dt} = c_w q(T_{n-1} - T_n) - \frac{\Phi_0}{N}\left(\frac{T_n - T_a}{\Delta T_{m,0}}\right)^{1.3} \tag{3.23}$$

$$\Delta T_{m,0} = \frac{T_{in,0} + T_{out,0}}{2} - T_0 \tag{3.24}$$

$$H = \frac{\Phi_0}{N}\sum_{i=1}^{N}\left(\frac{T_n - T_a}{\Delta T_{m,0}}\right)^{1.3} \tag{3.25}$$

$$C_e\dot{T}_e = UA \cdot (T_{oa} - T_e) + UA \cdot (T_a - T_e) \tag{3.26}$$

$$C\dot{T}_a = UA \cdot (T_e - T_a) + H \tag{3.27}$$

Nonlinearities in the radiator system are dominated by the heat transfer process. The valve relationship between opening and water flow rate is given by Equation 3.28 which characterizes a typical TRV [87]. In this equation, the coefficient of the quadratic term is dominated by the coefficient of the linear term. Because of this, the valve map is nearly linear and contributes little to the overall nonlinear behavior of the system. The radiator response characteristics display heavy reliance on operating condition as with the cooling systems. Response steady-state gains to a step change in valve position vary by an order of magnitude over the valve working range while the time constant more than doubles. This accounts for the prevalence of valve hunting in TRV controlled systems.

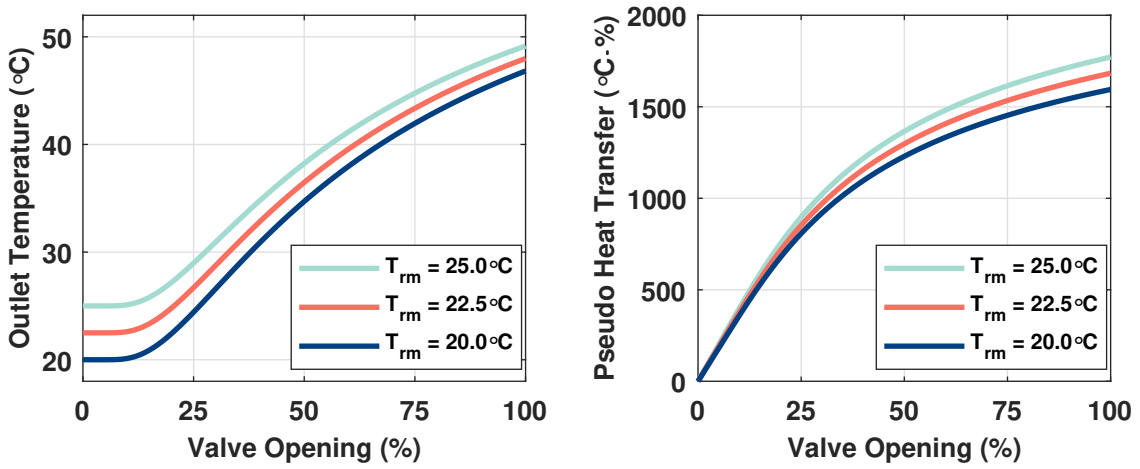

(a) (b)

Figure 3.15: (a) Radiator outlet temperature equalizes with room temperature at low flow rates. (b) Estimating heat transfer to the room recovers observability for the inner loop controller over all valve positions.

$$q(\delta) = (-3.4x10^{-4})\delta^2 + 0.75\delta \tag{3.28}$$

The radiator system has interesting dynamics that require a slight variation of the cascaded loop. The inner loop control was first applied to the radiator outlet temperature as the dominant nonlinearities stem from the heat transfer process. At low flow rates, however, supply water is able to equalize in temperature with the surrounding room air leading to the flat regions observed in Figure 3.15(a). Feedback on outlet temperature alone will have a section between approximately 0% and 15% valve opening where there is a total loss of observability. To correct for this issue, the cascaded loop of Figure 3.16 applies the inner loop control on an estimation of heat transfer to the room. By multiplying the valve position (δ) by the change in temperature across the radiator (Equation 3.29), measurable output is attained for all operating regions as seen in Figure 3.15(b). Feedback on this estimated variable will place the nonlinear gain function of the heat transfer process in the numerator and denominator of the inner loop transfer function, thereby reducing

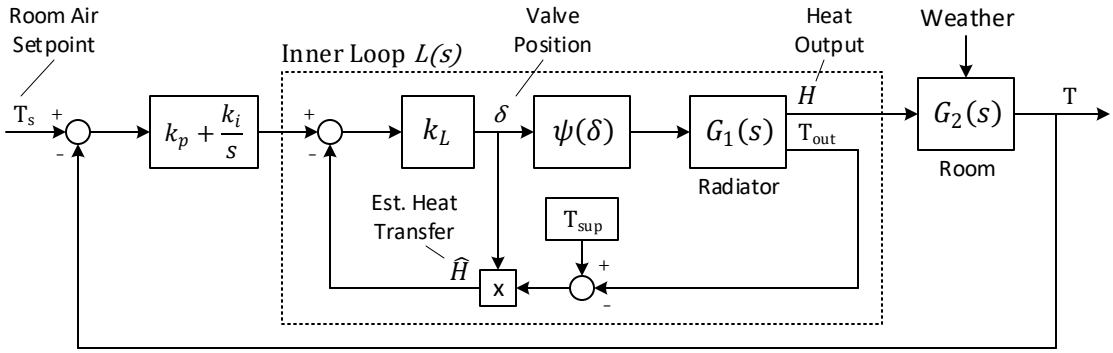

Figure 3.16: The proposed cascaded loop uses an estimation of heat radiated to the space as the inner loop feedback signal. This configuration will compensate for the nonlinearities associated with radiative heat transfer.

its effects. This is accomplished without the need for a valve map or a model of the heat transfer dynamics. The proposed loop will require the addition of a temperature sensor at the radiator outlet but as such a sensor is relatively inexpensive, this represents a minimal implementation cost.

$$\hat{H} = \delta(T_s - T_{out}) \tag{3.29}$$

Simulations follow the same procedure as those used by [87]. Only disturbances due to fluctuation in outside air temperature are considered with the basic profile given by Figure 3.17(a). In low heat demand conditions, the initial outside air temperature is 20°C (68°F) while in high heat demand, the initial temperature is -12°C (10.4°F). Results show that in low demand, a PI controller tuned during high heat demand (HDPI) displays hunting behavior. As shown in Figure 3.17(c), this controller over estimates the required heat and floods the radiator with hot water. This causes room temperature to rise above the set point and the valve to completely close. This process is repeated constantly over the simulation and is clearly a form of valve hunting. The cascaded controller is able to offer similar performance to the HDPI controller without hunting and avoiding the large initial overshoot of 2°C (3.6°F) of the low heat demand PI controller (LDPI). In high heating

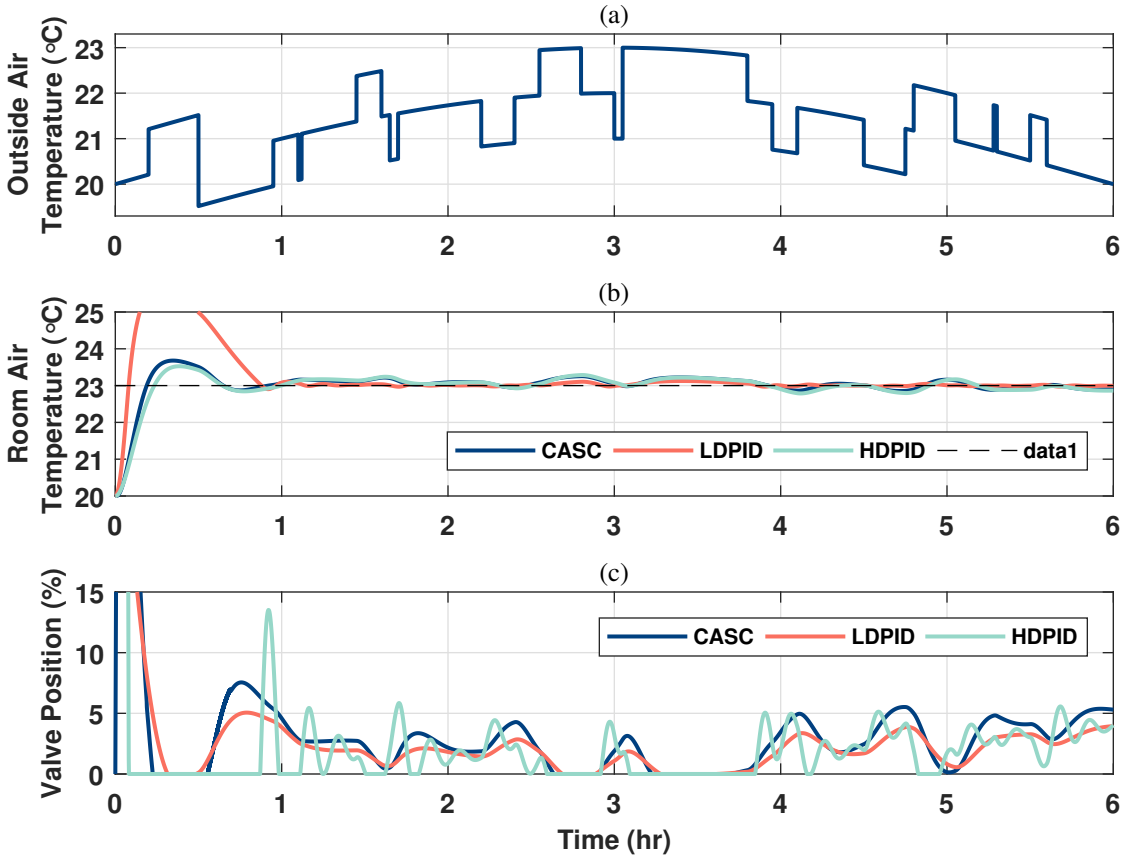

Figure 3.17: Simulation results for hydronic radiator case study: (a) Outside air temperature (reproduced from [86] with permission). (b) Room temperature. (c) Valve position.

demand, the LDPI controller struggles to regulate temperature, running a mean of -0.3°C (-0.5°F) below its set point. While the HDPI controller offers the best performance under these conditions, the cascaded controller has comparable RMS error and in fact is better able to balance room temperature around the desired set point. These simulations show that traditional PI control requires a seasonal retuning to offer consistent performance throughout the year. The single cascaded controller is able to offer equivalent performance to the best PI controller in both low and high demand conditions. This means that a single controller can be used for the entire year, eliminating labor costs associated with semiannual tuning of HVAC control loops. Results are summarized by Tables 3.5 and 3.6.

Table 3.5: Radiator Simulation Results for Low Heat Demand Conditions

Error Metric	Low Demand PI	High Demand PI	Cascaded Control
Root Mean Square Error (RMS)	0.400°C (0.720°F)	0.707°C (1.273°F)	0.391°C (0.704°F)
Maximum Bias Error (MBE)	-0.006°C (0.68°F)	0.209°C (0.376°F)	-0.053°C (0.095°F)
Hunting	No	Yes	No

Table 3.6: Radiator Simulation Results for High Heat Demand Conditions

Error Metric	Low Demand PI	High Demand PI	Cascaded Control
RMS	0.629°C (1.132°F)	0.439°C (0.790°F)	0.482°C (0.868°F)
MBE	-0.301°C (-0.542°F)	-0.110°C (-0.198°F)	-0.033°C (-0.059°F)

3.7 Case Study #7: Optimal Tuning of Heat Pump EEV Controller*

The power of the LQ optimal tuning framework with full state feedback control discussed in Chapter 2 is demonstrated experimentally through the tuning of an electronic expansion valve (EEV) on a residential grade heat pump system. Heat pumps are a subset of vapor compression cycle (VCC) systems and have become increasingly popular in the past few years [131]. VCC systems typically consist of four main components: a compressor, a condenser, an expansion valve, and an evaporator. Refrigerant cycling through these components goes through four main stages: (1) compression, (2) condensation, (3) expansion, and (4) evaporation. The components and processes for a heat pump are shown in Figure 3.18(a). Control of VCC systems involves regulation of evaporator superheat which is defined as the difference between the refrigerant temperature and the saturation temperature at the evaporator exit. As heat transfer is most efficient during liquid-vapor transition, superheat ideally should be kept small. However, two-phase flow entering the

*This case study is adapted with permission from "Optimal Tuning of Cascaded Control Architectures for Nonlinear HVAC Systems", C. Price and B. Rasmussen, Science and Technology for the Built Environment, vol. 23(8), pp. 1190-1202, ©2017 ASHRAE.

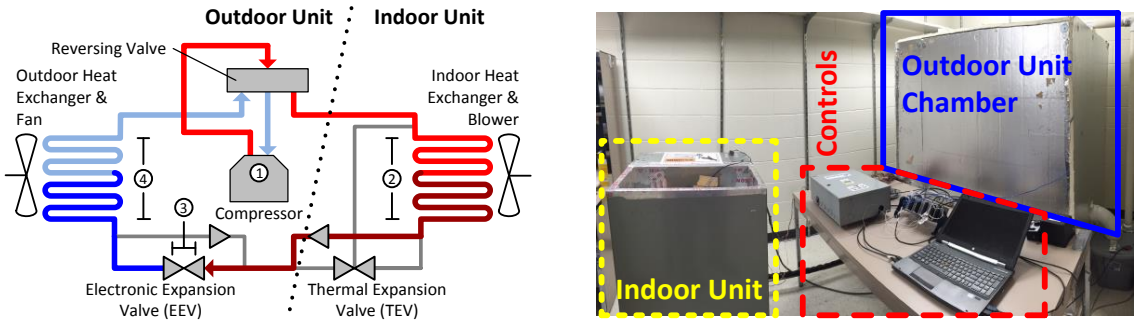

(a) (b)

Figure 3.18: (a) System diagram for a residential heating and cooling system in heat pump mode. (b) Experimental heat pump system showing the outdoor unit temperature chamber, indoor unit, and controls.

compressor can cause catastrophic damage leading to typical superheat set-points of a few degrees.

Refrigerant superheat is controlled by modulating the opening of an expansion valve located at the entrance of the evaporator. The valve controls the mass flow of refrigerant into the evaporator and, therefore, has an effect on the magnitude of the superheat. Several types of expansion valves exist on the market with varying degrees of expense and technology. The EEV is of particular importance as it has enabled modern control techniques to be applied to superheat control. EEVs use a stepper motor to control the position of the valve needle and thereby regulate flow. Direct control of the valve's position allows for the integration of several system sensors into the control algorithm such as temperature and pressure in the evaporator and condenser.

The heat pump cycle is the reverse of the familiar air conditioning cycle. To heat an indoor space, heat is absorbed from outside air then transported and released inside the building. As the temperature of the refrigerant passing though the outdoor evaporator must be colder than the ambient air, several issues arise. When the coil temperature approaches $0°C$ ($32°F$), condensate can form and freeze on the evaporator fins. Frost growth

significantly decreases the efficiency of the heat pump cycle and is the topic of extensive research [132, 133]. Excessively cold temperatures reduce the efficiency of the cycle by increasing the load on the compressor and impairing heat transfer. The tuning presented here avoids these issues by ensuring that ambient temperatures stay above freezing.

The experimental system used for this tuning is a residential grade dual heat pump and air-conditioning system with a rated capacity of three tons. The system's indoor unit consists of a heat exchanger, three stage blower, and thermal expansion valve (TEV). The outdoor unit package contains a heat exchanger, compressor, variable speed fan, and an EEV. Switching between heating and cooling modes is accomplished by a reversing valve that alters the flow of refrigerant through the system. The outdoor unit has been encased in a temperature controlled, insulated chamber to simulate outdoor conditions. Several openings and small electronics fans located in the walls of the chamber allowed heating load on the system to be varied. The EEV used in heating mode has linear flow characteristics and a full travel of 250 steps with a maximum travel time of 16.6 seconds. However, the valve is essentially saturated below 30 steps and only has an effective control range of approximately 50 steps [134]. Despite the limited actuation ability, the cascaded control loop was still able to significantly improve overall performance. System sensing and control were accomplished using Labview and Matlab Simulink software. All components are highlighted in Figure 3.18(b).

Heat pump system dynamics were identified through a series of EEV step tests under the different load conditions outlined by Table 3.7. For each condition, the system was allowed to reach steady state with the ambient temperature in the outdoor unit chamber at around $3°$C ($37.5°$F). The valve position was then varied and the resulting responses in evaporator superheat and discharge pressures were recorded. Steady-state gain models as well as second-order single input, two output dynamic models were identified to be used with NGM and LQ tuning methods, respectively. These models capture how system

Table 3.7: Heat Pump System Identification Test Conditions

Demand	Outdoor Fan Speed (%)	Indoor Blower Speed (Stage)	Compressor Speed (rpm)
Low	25	1	1800
Mid	50	2	3525
High	75	3	5300

dynamics vary as the system operating conditions change. The identified models for each condition can be found in Appendix B.

The cascaded loop used for the heat pump system will take inner loop feedback on evaporator pressure and outer loop feedback on refrigerant superheat. This is the same structure used by [109] which was applied to a single evaporator, VCC water chiller system. On that system the inner loop pressure control greatly reduced variation in system dynamics across operating conditions as well as improved disturbance rejection. The identified heat pump steady-state models were used to find the nonlinear gain models of Equation 3.30 for the inner and outer loops signals. Using these models and the definition of Equation 2.4, the NGM curve for this cascaded control structure was generated (Figure 3.19(a)). As shown, cascaded control will provide more linearization than the open-loop for inner loop gains less than 1.73 with the most linearization provided by $k_L = 0.63$. To provide flexibility in the LQ tuning process, a closed-loop gap metric value of $\Gamma > 0.9$ was targeted (i.e. $0.44 \leq k_L \leq 0.87$). This target reflects most of the achievable linearization of the cascaded loop.

$$\begin{aligned} \psi_i(\sigma) &= 0.57\sigma^2 - 1.35\sigma + 0.89 \\ \psi_o(\sigma) &= 0.24\sigma^2 - 0.48\sigma + 0.74 \end{aligned} \qquad \text{for} \qquad 0 \leq \sigma \leq 1 \tag{3.30}$$

After applying the state transformation of Equation 2.37 and augmenting the dynamics with an integrator on superheat error as in Equation 2.39, the LQ tuning method for this

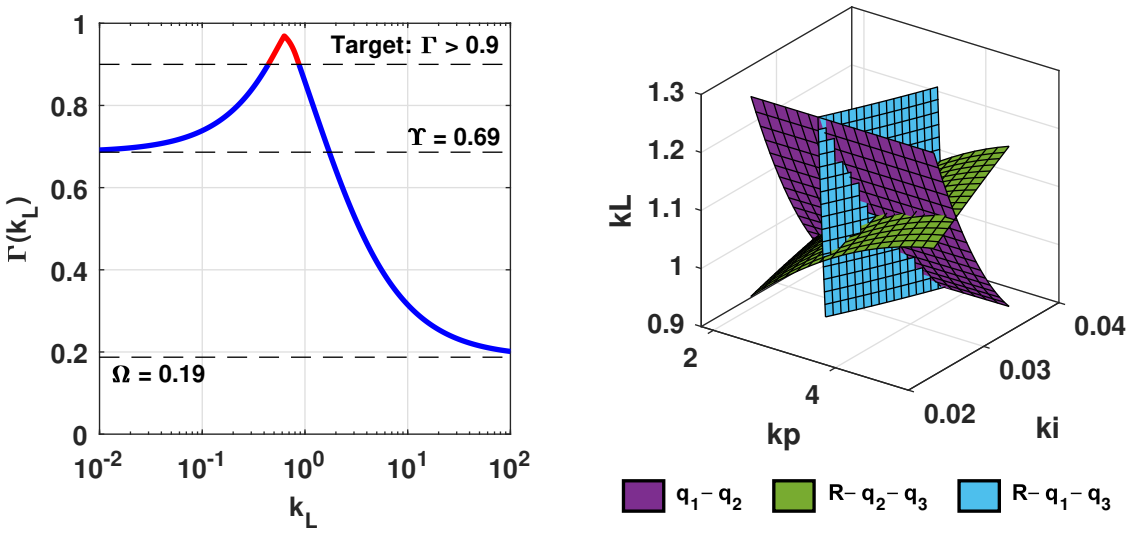

(a) (b)

Figure 3.19: (a) Closed-loop NGM plot for the heat pump system. Tuning goal with LQR for inner loop gain is $\Gamma > 0.9$ which corresponds to $0.45 \leq k_L \leq 1.73$. (b) Three-dimensional (3D) plot of how gains vary with respect to LQR weights.

cascaded control structure will have four distinct weights: the three diagonal elements of the state weighting matrix Q and the control input weight R. The general strategy for selecting these weights takes into account the goals of the cascaded control loop. As the cascaded controller seeks to reduce errors in superheat control, the weight on this state (q_1) should be large. Errors in evaporator pressure are secondary and will be masked by the outer loop integral controller. The weight on the evaporator pressure state (q_2) should, therefore, be smaller than q_1. The steady-state value of the outer loop integrator (i.e. integrated superheat error) is not important in terms of the LQ cost function. This state is used to compensate for steady-state errors in the proportional control of the inner loop pressure control. Therefore, the weight on the integrator state should be made small. The final weight, R, is used to limit the aggressiveness of the control action. Given that the EEV on the experimental system has a slow response time and coarse step sizes, control should be expensive and R large. These general strategies are summarized in Table 3.8.

Table 3.8: LQ Weight Strategies for Heat Pump Loop Tuning

Weight	Variable Influenced	Magnitude
q_1	Evaporator Superheat	Large
q_2	Evaporator Pressure	Less than q_1
q_3	Superheat Integrator	Small
R	Valve Position	Large

Using these general strategies, the LQ weights were initially selected to be as in Equation 3.31. For these nominal weights, a plot like that of Figure 3.19(b) was generated using the full state feedback LMIs of Equation 2.45. The plot shows how varying combinations of weights affects the three cascaded control gains and can be used to determine which weight to adjust. For example, the inner loop gain with the nominal weights is too large. Both R and q_3 can reduce the inner loop gain but R has a stronger effect. This process was repeated until the final weights Q^* and R^* were found (Equation 3.32). These weights correspond to the cascaded control gains of $k_L = 0.75$, $k_p = 1.5$, and $k_i = 0.01$.

$$Q = \begin{bmatrix} 10 & 0 & 0 \\ 1 & 0 & 0 \\ 0 & 0 & 1.0e\text{-}2 \end{bmatrix}, \quad R = 1 \qquad (3.31)$$

$$Q^* = \begin{bmatrix} 10 & 0 & 0 \\ 1 & 0 & 0 \\ 0 & 0 & 3.2e\text{-}3 \end{bmatrix}, \quad R^* = 66 \qquad (3.32)$$

The LQ optimally tuned cascaded controller was tested against the performance of two PI controllers tuned under the high- and low-demand conditions given in Table 3.7. The experimental testing procedure created a change in operating conditions by stepping compressor speed from 2000 to 2500 rpm at 600 seconds and 2500 to 2000 rpm at 1500 seconds. Both indoor and outdoor fans were set at 50% of their maximum speeds and the outdoor chamber air temperature was set to $37°$F ($2.8°$C). These conditions represent a mid-range system demand. As shown in Figure 3.20, the optimally tuned cascaded controller significantly outperforms both PI controllers. Initially all three controllers have

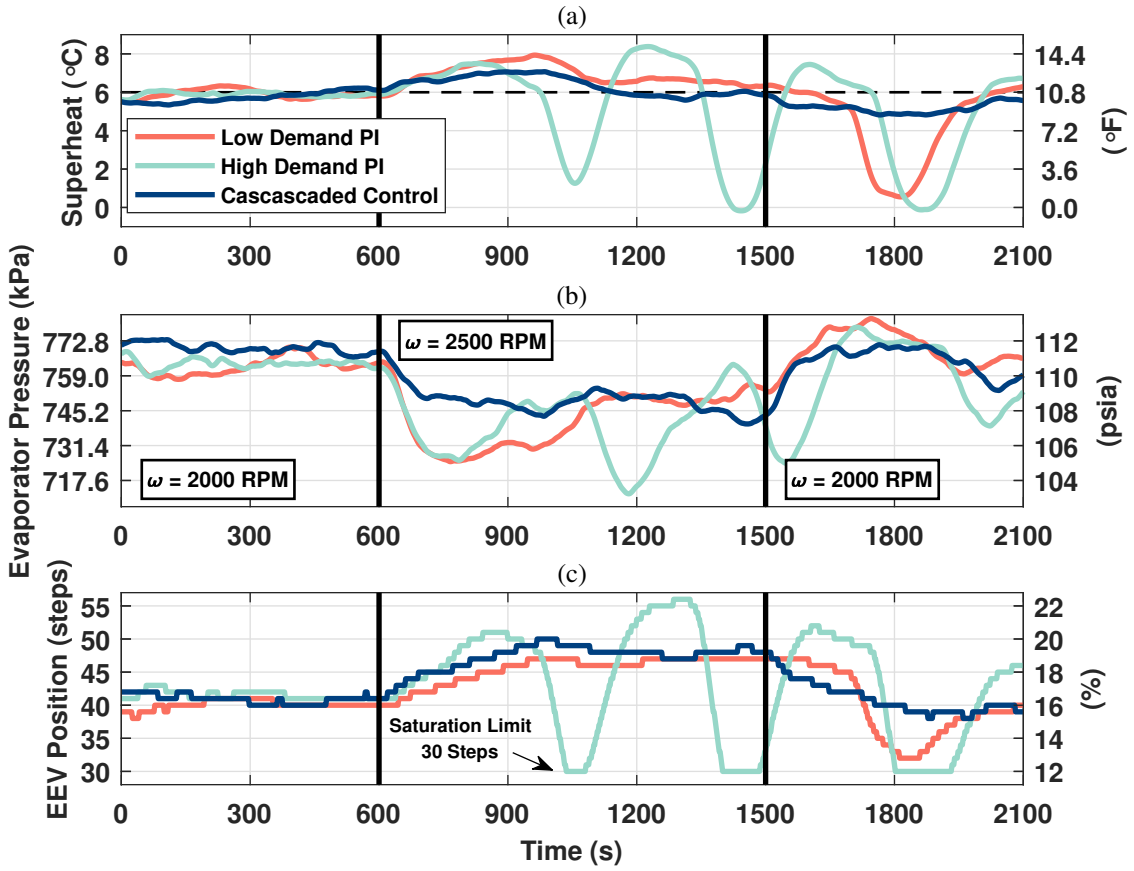

Figure 3.20: Experimental test results comparing traditional PI control of heat pump EEV with cascaded control tuned using proposed LQ method. Compressor speed step-up occurred at 600 seconds and step-down at 1500 seconds.

equivalent performance keeping evaporator superheat at $6°$C ($10.8°$F). After the compressor speed steps up at 600 seconds, the PI controller tuned for high load conditions opens the expansion valve too quickly and by too much. This has the effect of flooding the evaporator with refrigerant and setting up oscillations in the superheat response as the controller begins to hunt, eventually saturating the valve position three times. The PI controller tuned for low heat demand conditions has a much better response to the initial ramp of compressor speed. However, the controller reacts too slowly to the compressor speed drop at 1500 seconds causing the evaporator to nearly lose superheat.

The cascaded controller outperforms the PI controllers in the experimental test for three key reasons. From Figures 3.20(a) and 3.20(b), evaporator pressure is seen to respond much more quickly to changes in compressor speed than superheat. The fast inner loop control operating on pressure is therefore better able to respond to changes in compressor speed which strongly effects evaporator pressure. Control on pressure also helps to mitigate time delay issues associated with surface mount thermocouples. Both traditional PI controllers are limited in their response to system disturbances by the transient heat transfer between the refrigerant, the pipe walls, and the sensor itself. The cascaded controller also performs better because the inner loop gain was selected to reduce variations in system dynamics through its linearizing effect. This allows the outer loop controller to avoid the hunting behavior seen with the traditional PI controllers during compressor speed changes. Finally, the LQ tuning method also contributes in improving the controller performance. By utilizing the LMI formulation of the LQ method, the selected control gains provide robustness to changing operating conditions.

3.8 Summary of Case Study Results

This chapter highlights several benefits of cascaded control and the proposed tuning procedures. The first two case studies used examples to show how cascaded control can linearize load dependent nonlinearities and decouple MIMO systems. The next four case studies used models of typical HVAC systems to show that cascaded control can linearize and improved performance for a variety of nonlinearities and systems. The final case study used an experimental heat pump system to test the proposed optimal tuning procedure from Chapter 2 on a real system. While cascaded control generally used more control effort than a detuned PI controller, it avoided hunting seen with high demand PI controllers. The more aggressive cascaded control may consume slightly more energy but it linearizes system responses, enabling supervisory controllers to reduce total building energy consumption.

4. PERFORMANCE EVALUATION OF CASCADED CONTROL

This section analyzes cascaded control performance using two main methods. The first is the Dual-Youla parameterization that describes the interconnection of all stabilizing plants and controllers in terms of a nominal condition. The second is a Linear Parameter Varying (LPV) description of HVAC dynamics, discussed in Chapter 1, that will be used to determine the limits of performance improvements provided by the cascaded architecture.

The Youla parameterization of a controller involves a reformulation of the controller such that it incorporates input from a stable filter Q [135]. Allowing this filter to vary in RH_∞ will describe all stabilizing controllers for a given plant. This method facilitates performance optimization and adaptive control techniques as variations in the Youla parameter can be made online without sacrificing system stability. A dual concept can be used to reformulate the plant in terms of a stable filter S that describes all plants that are stabilized by a given nominal controller. Together, these two parameters easily lend themselves to robustness and performance analysis.

In [135], two main control approaches for the Youla parameterization are described. The first involves nesting Q filters to the controller over time when performance degrades or desired responses change. This approach is essentially an iterated approximation of the plant dynamics and the associated optimal controller. Nesting in this way can lead to very complicated control structures as well as high order systems. Another approach would be to identify differences between a model and actual plant dynamics, essentially continuously estimating the S filter. This online estimation can then be used to update the Q parameter in real time according to some update algorithm.

The Youla parameterization has been incorporated into many control algorithms. In [136], a gain scheduled controller was developed for a multiple-evaporator air conditioning

system. Using the Youla formulation, guarantees on system stability and performance were outlined as well as a bound on reference signal rate changes. The method has also been incorporated into Iterative Learning Control (ILC) designs for robotic manipulators. For example, in [137] PD controllers for a six degree of freedom robot manipulator were coupled with an ILC whose form was determined in part by the Youla parameterization. Other applications include fault tolerant control design [138] and damping control for power systems [139].

This section will measure performance using an H_∞ framework. The H_∞ system norm captures the worst case performance of a system over all frequencies and input/output directions. As HVAC systems must ensure occupant comfort given any conditions, minimizing the H_∞ norm provides a suitable metric. The $\mathcal{H}_\infty$ framework has been well developed with numerous texts discussing norm calculation and control synthesis as in [121].

The remainder of this chapter outlines the Dual-Youla parameterization for a generalized control connection and uses the result to derive a soft-implementation framework for phased cascaded control implementation. Evaluation of performance between PI and cascaded control is discussed based on a combination of controller blending techniques. Finally, analysis of the cascaded architecture is done to show that cascaded control performance will be equal or better than traditional HVAC PI controllers.

4.1 Cascaded Control as Static Feedback

The Youla parameterizations in the following sections are greatly simplified by the controller being described as a static feedback system. For PI and cascaded control, this involves shifting the integrator from the controller to the plant dynamics which requires some manipulation of the nominal system. First, consider the cascaded inner loop feedback expression of Equation 4.1 after full substitution of signal definitions. As seen, to describe cascaded control as static feedback the plant must be augmented with an integra-

tor state for the outer loop error. This is accomplished by adding an additional state to the plant that integrates outer loop error using the output matrices $\bar{C}_{P,o}$ and $\bar{D}_{P,o}$ from the initial system $\bar{P}_0$. The outputs of this augmented plant P can now be manipulated so that $e = \begin{bmatrix} e_o & y_i & \int e_o \, dt \end{bmatrix}^T$ as in Equation 4.2. This expression is for continuous time systems but a similar process can be done for discrete systems.

$$\begin{aligned} u_i &= k_L(u_o - y_i) \\ &= k_L \left\{ (k_{p1} e_o + k_{i1} \textstyle\int e_o \, dt) - y_i \right\} \\ &= k_L k_{p1} e_o + k_L k_{i1} \textstyle\int e_o \, dt - k_L y_i \end{aligned} \tag{4.1}$$

$$P_0 : \left[\begin{array}{c|cc} A_{P0} & B_{P0} \\ \hline C_P & D_P \end{array}\right] = \left[\begin{array}{cc|c} \bar{A}_{P0} & 0 & \bar{B}_{P0} \\ \bar{C}_{P,o} & 1 & \bar{D}_{P,o} \\ \hline \bar{C}_P & 0 & \bar{D}_P \\ 0 & 1 & 0 \end{array}\right] \tag{4.2}$$

A nominal PI controller K_0 operating on y_o (i.e. the outer loop signal) can therefore be written as the output feedback controller in Equation 4.3 with gains k_{p0} and k_{i0}. Similarly, a cascaded controller can also be cast as output feedback problem. From Equation 4.1 the cascaded controller K_1 can be expressed as Equation 4.4 where the gains are combinations of the cascaded control gains k_{p1}, k_{i1}, and k_L. These static descriptions can now be used in the following sections. Note that this process is similar to that from Chapter 2.6 except that the no restriction on the reference signal will be used.

$$K_0 : \left[\begin{array}{c|ccc} 0 & 0 & 0 & 0 \\ \hline 0 & k_{p0} & 0 & k_{i0} \end{array}\right] \tag{4.3}$$

$$K_1 : \left[\begin{array}{c|ccc} 0 & 0 & 0 & 0 \\ \hline 0 & k_L k_{p1} & -k_L & k_L k_{i1} \end{array}\right] \tag{4.4}$$

4.2 Dual Youla Parameterization for Stability Analysis

The following section outlines the derivation of Youla parameterizations for stability analysis of a general plant and static output feedback controller with dynamics given by

Equations 4.5 and 4.6. These expressions will be combined in the next section to find the Dual Youla structure of a generalized cascaded loop interconnection.

$$P_0 : \left[\begin{array}{c|c} A_{P0} & B_{P0} \\ \hline C_{P0} & D_{P0} \end{array}\right] \qquad (4.5) \qquad\qquad K_0 : \left[\begin{array}{c|c} 0 & 0 \\ \hline 0 & D_{K0} \end{array}\right] \qquad (4.6)$$

4.2.1 Derivation of J_K Block

The Youla parameterization for stability analysis of a controller breaks the system K into two parts (J_K and Q) as in Figure 4.1(a). The first step in deriving expressions for both systems is to find coprime factors for the interconnection of the nominal systems P_0 and K_0. Left and right coprime factors are defined in Equation 4.7 must must satisfy the double Bezout relations given in Equation 4.8. Note that the following definitions follow those outlined in [135, Chapter 2] for a general stabilizing controller.

$$\begin{aligned} G = NM^{-1} = \tilde{M}^{-1}\tilde{N} \qquad & N, M, \tilde{N}, \tilde{M} \in \boldsymbol{RH}_\infty \\ K = UV^{-1} = \tilde{V}^{-1}\tilde{U} \qquad & U, V, \tilde{U}, \tilde{V} \in \boldsymbol{RH}_\infty \end{aligned} \qquad (4.7)$$

$$\begin{bmatrix} \tilde{V} & -\tilde{U} \\ -\tilde{N} & \tilde{M} \end{bmatrix} \begin{bmatrix} M & U \\ N & V \end{bmatrix} = \begin{bmatrix} M & U \\ N & V \end{bmatrix} \begin{bmatrix} \tilde{V} & -\tilde{U} \\ -\tilde{N} & \tilde{M} \end{bmatrix} = \begin{bmatrix} I & 0 \\ 0 & I \end{bmatrix} \qquad (4.8)$$

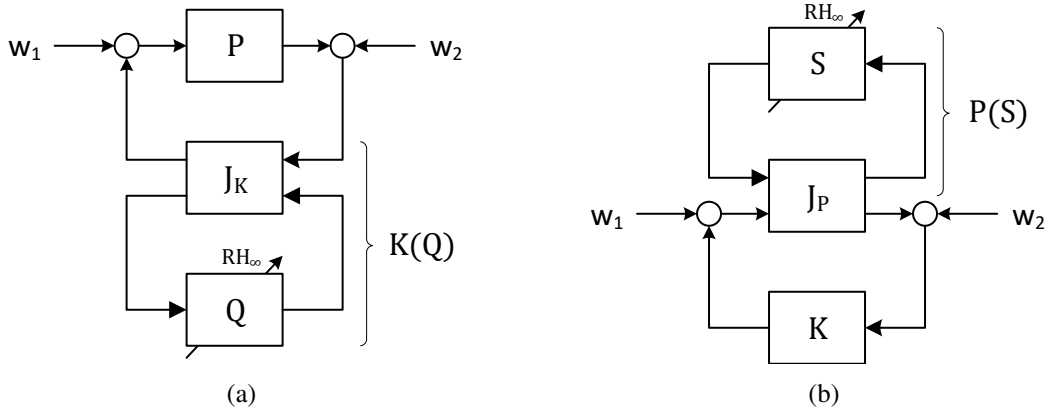

Figure 4.1: Block diagrams of the Youla parameterization of the controller (a) and plant (b). When combined, these systems define the Dual Youla parameterization of a system.

Coprime factors for the P_0 and K_0 are given in Equations 4.9 & 4.10 where $Y_{00} = (I - D_{K0}D_{P0})^{-1}$ and $Z_{00} = (I - D_{P0}D_{K0})^{-1}$. Note that F_P is a design variable required for the stability of the coprime factorization and can be selected using any technique that stabilizes the system $A_{P0} + B_{P0}F_P$.

$$\begin{bmatrix} M & U \\ N & V \end{bmatrix} = \left[\begin{array}{c|cc} A_{P0} + B_{P0}F_P & B_{P0} & 0 \\ \hline F_P & I & D_{K0} \\ C_{P0} + D_{P0}F_P & D_{P0} & I \end{array}\right] \tag{4.9}$$

$$\begin{bmatrix} \tilde{V} & -\tilde{U} \\ -\tilde{N} & \tilde{M} \end{bmatrix} = \left[\begin{array}{c|cc} A_{P0} + B_{P0}Y_{00}D_{K0}C_{P0} & -B_{P0}Y_{00} & B_{P0}Y_{00}D_{K0} \\ \hline F_P - Y_{00}D_{K0}C_{P0} & Y_{00} & -Y_{00}D_{K0} \\ Z_{00}C_{P0} & -Z_{00}D_{P0} & Z_{00} \end{array}\right] \tag{4.10}$$

The J_K block has the form of Equation 4.11 from [135, Chapter 2]. To use this definition, three systems must be derived: $\tilde{V}^{-1}$, V^{-1}, and $-V^{-1}N$. Details for each of these parameters are given by Equations 4.12−4.14. Combining all of these expression gives Equation 4.15.

$$J_K = \begin{bmatrix} UV^{-1} & \tilde{V}^{-1} \\ V^{-1} & -V^{-1}N \end{bmatrix} = \begin{bmatrix} K_0 & \tilde{V}^{-1} \\ V^{-1} & -V^{-1}N \end{bmatrix} \tag{4.11}$$

$$\tilde{V}^{-1} = \left[\begin{array}{c|c} A_{P0} + B_{P0}Y_{00}D_{K0}C_{P0} & -B_{P0}Y_{00} \\ \hline F_P - Y_{00}D_{K0}C_{P0} & Y_{00} \end{array}\right]^{-1} = \left[\begin{array}{c|c} A_{P0} + B_{P0}F_P & B_{P0} \\ \hline Y_{00}^{-1}F_P - D_{K0}C_{P0} & Y_{00}^{-1} \end{array}\right] \tag{4.12}$$

$$V^{-1} = \left[\begin{array}{c|c} A_{P0} + B_{P0}F_P & 0 \\ \hline C_{P0} + D_{P0}F_P & I \end{array}\right]^{-1} = \left[\begin{array}{c|c} 0 & 0 \\ \hline 0 & I \end{array}\right] \tag{4.13}$$

$$-V^{-1}N = \left[\begin{array}{c|c} A_{P0} + B_{P0}F_P & B_{P0} \\ \hline -(C_{P0} + D_{P0}F_P) & -D_{P0} \end{array}\right] \tag{4.14}$$

$$J_K = \left[\begin{array}{c|cc} A_{P0} + B_{P0}F_P & 0 & B_{P0} \\ \hline Y_{00}^{-1}F_P - D_{K0}C_{P0} & D_{K0} & Y_{00}^{-1} \\ -(C_{P0} + D_{P0}F_P) & I & -D_{P0} \end{array}\right] \tag{4.15}$$

4.2.2 Derivation of Q Block

The expression for a specific Q to transform the nominal controller K_0 to a new controller K_1 can be found using Equation 4.16. The expression will be broken into two parts: $\tilde{V}(K_1-K_0)$ and $(I-G_0K_1)^{-1}\tilde{M}^{-1}$. Derivations for each part are given by Equations 4.17 and 4.18. Note that $Y_{01} = (I - D_{K1}D_{P0})^{-1}$ and $Z_{01} = (I - D_{P0}D_{K1})^{-1}$.

$$\begin{aligned} Q &= \tilde{V}(K_1 - K_0)V(Q) \\ &= \tilde{V}(K_1 - K_0)(I - G_0K_1)^{-1}\tilde{M}^{-1} \end{aligned} \tag{4.16}$$

$$\begin{aligned} \tilde{V}(K_1 - K_0) &= \left[\begin{array}{c|c} A_{P0} + B_{P0}Y_{00}D_{K0}C_{P0} & -B_{P0}Y_{00} \\ \hline F_P - Y_{00}D_{K0}C_{P0} & Y_{00} \end{array}\right] \left[\begin{array}{c|c} 0 & 0 \\ \hline 0 & D_{K1} - D_{K0} \end{array}\right] \\ &= \left[\begin{array}{c|c} A_{P0} + B_{P0}Y_{00}D_{K0}C_{P0} & -B_{P0}Y_{00}(D_{K1} - D_{K0}) \\ \hline F_P - Y_{00}D_{K0}C_{P0} & Y_{00}(D_{K1} - D_{K0}) \end{array}\right] \end{aligned} \tag{4.17}$$

$$\begin{aligned} &(I - G_0K_1)^{-1}\tilde{M}^{-1} = \\ &= \left[\begin{array}{c|c} A_{P0} & B_{P0}D_{K1} \\ \hline -C_{P0} & I - D_{P0}D_{K1} \end{array}\right]^{-1} \left[\begin{array}{c|c} A_{P0} + B_{P0}Y_{00}D_{K0}C_{P0} & B_{P0}Y_{00}D_{K0} \\ \hline Z_{00}C_{P0} & Z_{00} \end{array}\right]^{-1} \\ &= \left[\begin{array}{c|c} A_{P0} + B_{P0}D_{K1}Z_{01}C_{P0} & B_{P0}D_{K1}Z_{01} \\ \hline Z_{01}C_{P0} & Z_{01} \end{array}\right] \left[\begin{array}{c|c} A_{P0} & -B_{P0}D_{K0} \\ \hline C_{P0} & Z_{00}^{-1} \end{array}\right] \\ &= \left[\begin{array}{c|c} A_{P0} + B_{P0}D_{K1}Z_{01}C_{P0} & B_{P0}(D_{K1}Z_{01}Z_{00}^{-1} - D_{K0}) \\ \hline Z_{01}C_{P0} & Z_{01}Z_{00}^{-1} \end{array}\right] \\ &= \left[\begin{array}{c|c} A_{P0} + B_{P0}D_{K1}Z_{01}C_{P0} & B_{P0}Y_{01}(D_{K1} - D_{K0}) \\ \hline Z_{01}C_{P0} & Z_{01}Z_{00}^{-1} \end{array}\right] \end{aligned} \tag{4.18}$$

$$Q = \left[\begin{array}{c|c} A_{P0} + B_{P0}D_{K1}Z_{01}C_{P0} & B_{P0}Y_{01}(D_{K1} - D_{K0}) \\ \hline -F_P + Y_{01}D_{K1}C_{P0} & Y_{01}(D_{K1} - D_{K0}) \end{array}\right] \tag{4.19}$$

Important relationships used to find this expression are given in Equation 4.20. These relationships are also used in the next sections to find the final forms for J_P and S.

$$\begin{aligned} D_{K1}Z_{01}Z_{00}^{-1} - D_{K0} &= Y_{01}(D_{K1} - D_{K0}) \\ -Y_{00}(D_{K1} - D_{K0})Z_{01} &= Y_{01}(D_{K1} - D_{K0})Z_{00} \end{aligned} \tag{4.20}$$

4.2.3 Derivation of J_P Block

The Youla parameterization of the plant (Figure 4.1(b)) uses the definition of Equation 4.21 to find J_P. Derivations for the three systems $\tilde{M}^{-1}$, M^{-1}, and $-M^{-1}U$) are given in Equations 4.22−4.24 which are used to find the final expression in Equation 4.25.

$$J_P = \begin{bmatrix} -M^{-1}U & M^{-1} \\ \tilde{M}^{-1} & NM^{-1} \end{bmatrix} = \begin{bmatrix} -M^{-1}U & M^{-1} \\ \tilde{M}^{-1} & P_0 \end{bmatrix} \tag{4.21}$$

$$\tilde{M}^{-1} = \left[\begin{array}{c|c} A_{P0} + B_{P0}Y_{00}D_{K0}C_{P0} & B_{P0}Y_{00}D_{K0} \\ \hline Z_{00}C_{P0} & Z_{00} \end{array}\right]^{-1} = \left[\begin{array}{c|c} A_{P0} & -B_{P0}D_{K0} \\ \hline C_{P0} & Z_{00}^{-1} \end{array}\right] \tag{4.22}$$

$$M^{-1} = \left[\begin{array}{c|c} A_{P0} + B_{P0}F_P & B_{P0} \\ \hline F_P & I \end{array}\right]^{-1} = \left[\begin{array}{c|c} A_{P0} & -B_{P0} \\ \hline F_P & I \end{array}\right] \tag{4.23}$$

$$-M^{-1}U = \left[\begin{array}{c|c} A_{P0} & -B_{P0} \\ \hline -F_P & -I \end{array}\right]\left[\begin{array}{c|c} A_{P0} + B_{P0}F_P & 0 \\ \hline F_P & D_{K0} \end{array}\right] = \left[\begin{array}{c|c} A_{P0} & -B_{P0}D_{K0} \\ \hline -F_P & -D_{K0} \end{array}\right] \tag{4.24}$$

$$J_P = \left[\begin{array}{c|cc} A_{P0} & B_{P0}D_{K0} & -B_{P0} \\ \hline F_P & -D_{K0} & I \\ -C_{P0} & Z_{00}^{-1} & D_{P0} \end{array}\right] \tag{4.25}$$

4.2.4 Derivation of S Block

The expression for a filter S to augment the nominal plant can be found using Equation 4.26. As before, the expression will be broken into two parts: $V^{-1}(I - P_1K_0)^{-1}$ and $(P_1 - P_0)M$. Derivations for each part are given by Equations 4.27 & 4.28 with the final form given by Equation 4.29. Note that $Y_{10} = (I - D_{K0}D_{P1})^{-1}$ and $Z_{10} = (I - D_{P1}D_{K0})^{-1}$.

$$\begin{aligned} S &= \tilde{M}(S)(P_1 - P_0)M \\ &= V^{-1}(I - P_1K_0)^{-1}(P_1 - P_0)M \end{aligned} \tag{4.26}$$

$$\begin{aligned} V^{-1}(I - P_1K_0)^{-1} &= \left[\begin{array}{c|c} 0 & 0 \\ \hline 0 & I \end{array}\right] \left[\begin{array}{c|c} A_{P1} & B_{P1}D_{K0} \\ \hline -C_{P1} & I - D_{P1}D_{K0} \end{array}\right]^{-1} \\ &= \left[\begin{array}{c|c} A_{P1} + B_{P1}D_{K0}Z_{10}C_{P1} & B_{P1}D_{K0}Z_{10} \\ \hline Z_{10}C_{P1} & Z_{10} \end{array}\right] \end{aligned} \tag{4.27}$$

$$\begin{aligned} (P_1 - P_0)M &= \left[\begin{array}{cc|c} A_{P1} & 0 & B_{P1} \\ 0 & A_{P0} & B_{P0} \\ \hline C_{P1} & -C_{P0} & D_{P1} - D_{P0} \end{array}\right] \left[\begin{array}{c|c} A_{P0} + B_{P0}F_P & B_{P0} \\ \hline F_P & I \end{array}\right] \\ &= \left[\begin{array}{ccc|c} A_{P1} & 0 & B_{P1}F_P & B_{P1} \\ 0 & A_{P0} & B_{P0}F_P & B_{P0} \\ 0 & 0 & A_{P0} + B_{P0}F_P & B_{P0} \\ \hline C_{P1} & -C_{P0} & (D_{P1} - D_{P0})F_P & D_{P1} - D_{P0} \end{array}\right] \\ &= \left[\begin{array}{cc|c} A_{P1} & (A_{P1} - A_{P0}) - (B_{P1} + B_{P0}F_P) & B_{P1} - B_{P0} \\ 0 & A_{P0} + B_{P0}F_P & B_{P0} \\ \hline C_{P1} & (C_{P1} - C_{P0}) + (D_{P1} - D_{P0})F_P & D_{P1} - D_{P0} \end{array}\right] \end{aligned} \tag{4.28}$$

$$S = \left[\begin{array}{cc|c} A_{P1} + B_{P1}D_{K0}Z_{10}C_{P1} & B_{P1}Y_{10}(Y_{00}^{-1}F_P - D_{K0}C_{P0}) & B_{P1}Y_{10}Y_{00}^{-1} \\ 0 & A_{P0} + B_{P0}F_P & B_{P0} \\ \hline Z_{10}C_{P1} & Z_{10}D_{P1}F_P - Z_{10}(C_{P0} + D_{P0}F_P) & Z_{10}(D_{P1} - D_{P0}) \end{array}\right] \tag{4.29}$$

This final form was found by eliminating uncontrollable/unobservable modes, applying simple state transformations, and using the identify $I + D_{K0}Z_{10}(D_{P1} - D_{P0}) = Y_{10}Y_{00}^{-1}$.

An assumption about how the plant parameters vary will greatly simplify analysis in the following sections. HVAC systems typically have two types of nonlinearities: static and dynamic. These variations typically manifest as changes in steady-state gain and system time constants. Both of these changes can be captured assuming that only the

A and B matrices vary meaning that $C_{P0} = C_{Pi}$ and $D_{P0} = D_{Pi}$. This also leads to the implicit assumption that the state dimension of the system is constant over HVAC operating conditions. Equation 4.30 contains identities resulting from this assumption and Equation 4.31 the resulting simplified form for S.

$$Z_{00} = Z_{10} \quad \& \quad Z_{01} = Z_{11} \quad \& \quad Y_{00} = Y_{10} \quad \& \quad Y_{01} = Y_{11} \tag{4.30}$$

$$S = \left[\begin{array}{cc|c} A_{P1} + B_{P1}D_{K0}Z_{00}C_{P0} & B_{P1}(F_P - Y_{00}D_{K0}C_{P0}) & B_{P1} \\ 0 & A_{P0} + B_{P0}F_P & B_{P0} \\ \hline Z_{00}C_{P0} & -Z_{00}C_{P0} & 0 \end{array}\right] \tag{4.31}$$

4.3 Stability of the Dual Youla Parameterization

As stated in Theorem 4.2 from [135, Chapter 3], the Dual Youla parameterization $(G(S), K(Q))$ is stable if and only if the pair (Q, S) is stabilizing. This theorem is based on the result shown in Equation 4.32 where the Redheffer Star-Product $\mathcal{S}(J_P, J_K)$ is an anti-diagonal pass-through matrix after uncontrollable and unobservable states have been removed. Stability of the parameterization therefore involves determining if either of the conditions in Equation 4.33 are true.

$$\begin{aligned} \mathcal{S}(J_P, J_K) &= \left[\begin{array}{cc|cc} A_{P0} + B_{P0}Y_{00}D_{K0}C_{P0} & -B_{P0}(F_P - Y_{00}D_{K0}C_{P0}) & 0 & -B_{P0} \\ 0 & A_{P0} + B_{P0}F_P & 0 & B_{P0} \\ \hline F_P - Y_{00}D_{K0}C_{P0} & F_P - Y_{00}D_{K0}C_{P0} & 0 & I \\ -Z_{00}C_{P0} & -Z_{00}C_{P0} & I & 0 \end{array}\right] \\ &= \left[\begin{array}{c|cc} 0 & 0 & 0 \\ \hline 0 & 0 & I \\ 0 & I & 0 \end{array}\right] \end{aligned} \tag{4.32}$$

$$\begin{bmatrix} I & -Q \\ -S & I \end{bmatrix}^{-1} \quad \text{or} \quad \begin{bmatrix} (I - QS)^{-1} & -Q(I - SQ)^{-1} \\ S(I - QS)^{-1} & (I - SQ)^{-1} \end{bmatrix} \quad \in \boldsymbol{RH}_\infty \tag{4.33}$$

The expression of interest for stability is therefore Equation 4.34 where $D_\delta = D_{K1} - D_{K0}$. This system is stable (i.e. $\in \boldsymbol{RH}_\infty$) if all eigenvalues of the A matrix are in the left half plane or in the unit circle for continuous and discrete time systems respectively.

$$\left[\begin{array}{ccc|cc} A_{P0}+B_{P0}D_{K1}Z_{01}C_{P0} & 0 & 0 & 0 & B_{P0}Y_{01}D_\delta \\ 0 & A_{P1}+B_{P1}D_{K0}Z_{00}C_{P0} & B_{P1}(F_P - Y_{00}D_{K0}C_{P0}) & B_{P1} & 0 \\ 0 & 0 & A_{P0}+B_{P0}F_P & B_{P0} & 0 \\ \hline F_P - Y_{01}D_{K1}C_{P0} & 0 & 0 & I & -Y_{01}D_\delta \\ 0 & -Z_{00}C_{P0} & Z_{00}C_{P0} & 0 & I \end{array}\right]^{-1} \tag{4.34}$$

To check requirements for the Dual Youla parameterization of an output feedback system only the A matrix of Equation 4.34 is required. To simplify analysis, the design parameter is chosen to be $F_P = Y_{01}D_{K1}C_{P0}$. This choice stabilizes the Youla parameterization by design (i.e. the new controller K_1 stabilizes the nominal system) and makes Q a static gain. Derivation of the required system matrix is given by Equation 4.35.

$$\begin{aligned} A - BD^{-1}C &= A - \begin{bmatrix} B_{P1} & 0 \\ B_{P0} & 0 \end{bmatrix} \begin{bmatrix} I & -Y_{01}D_\delta \\ 0 & I \end{bmatrix} \begin{bmatrix} 0 & 0 \\ -Z_{00}C_{P0} & Z_{00}C_{P0} \end{bmatrix} \\ &= \begin{bmatrix} A_{P1}+B_{P1}D_{K1}Z_{01}C_{P0} & 0 \\ B_{P0}Y_{01}D_\delta Z_{00}C_{P0} & A_{P0}+B_{P0}Y_{00}D_{K0}C_{P0} \end{bmatrix} \end{aligned} \tag{4.35}$$

The matrix above is block diagonal meaning the eigenvalues of the (Q,S) interconnection are given by Equation 4.36. From this expression, the eigenvalues of the interconnection are the union of the eigenvalues of the nominal system with the nominal plant and the eigenvalues of the perturbed plant with the new controller. The first condition is stable by design while the second needs to be tested over the set of possible plants. Note that the stability of the varying plant with the nominal controller is implied as it was used to establish the plant parameterization. Essentially, the stability of the Youla parameterization depends on the cascaded controller stabilizing the plant over its expected variations.

$$\lambda(\mathcal{F}_\ell(S,Q)) = \lambda(A_{P1} - B_{P1}D_{K1}Z_{01}C_{P0}) \cup \lambda(A_{P0} - B_{P0}D_{K0}Z_{00}C_{P0}) \tag{4.36}$$

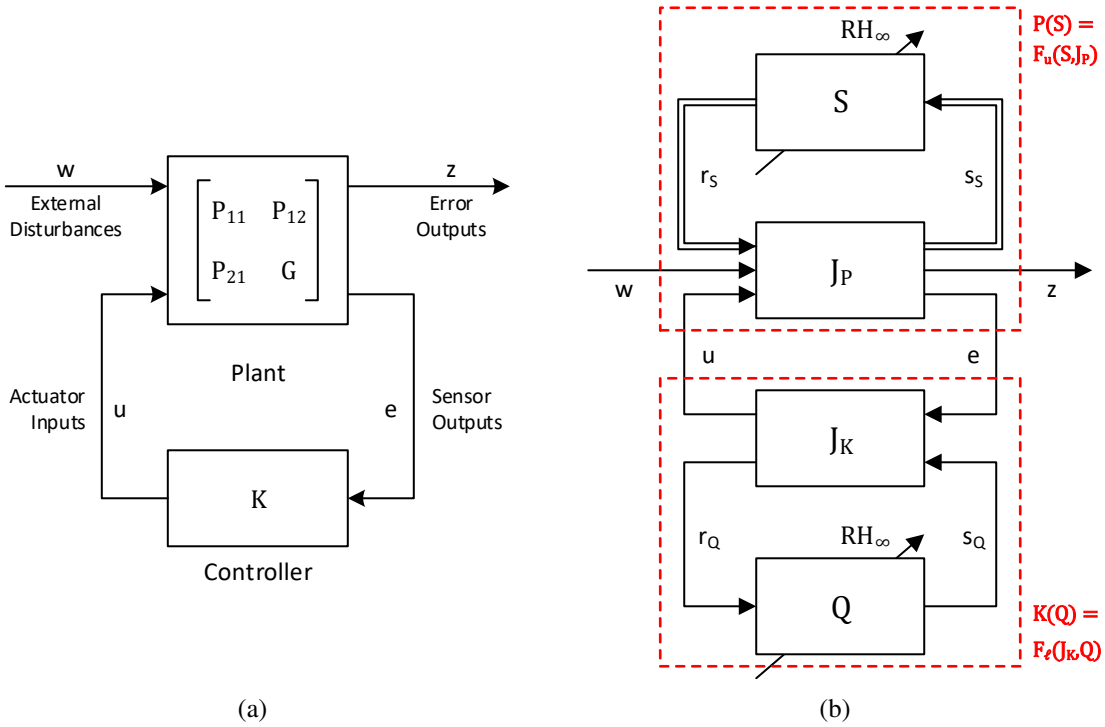

Figure 4.2: (a) Generic plant-controller connection used for Dual Youla parameterization. (b) As Q and S vary in RH_∞ all stable system interconnections are described.

4.4 Dual Youla Parameterization for Performance Analysis

Having found criteria for stability of a PI to cascaded control transition, this section develops the Dual Youla parameterization for performance analysis of the system in Figure 4.2(a). A generic description of a plant and controller interconnection for the block diagram is given by Equations 4.37 & 4.38 where plant transfer functions P_{11}, P_{12}, P_{21}, and G describe the input and output relationships of the control system. The assumption $D_{P0,22} = 0$ requires only that there is no instantaneous feed-through of actuator input u to the sensor output, a common trait of many HVAC systems. Subscripts for the plant C and D matrices have been shortened because of the assumption that only the A and B matrix parameters vary.

$$P_0 : \left[\begin{array}{c|cc} A_{P0} & B_{P0,1} & B_{P0,2} \\ \hline C_{P1} & D_{P11} & D_{P12} \\ C_{P2} & D_{P21} & 0 \end{array}\right] \qquad (4.37) \qquad K_0 : \left[\begin{array}{c|c} 0 & 0 \\ \hline 0 & D_{K0} \end{array}\right] \qquad (4.38)$$

Typical signal definitions for a feedback system are given in Equation 4.39 where r_s is a reference input, d is a disturbance input, and n is sensor noise. Sensor/feedback signals are outer loop error ($r_s - y_o$) and the inner loop signal (y_i) used for cascaded control. The error outputs are outer loop error and the control signal (u_i) which sets up the trade-off of balancing tracking error with control effort.

$$w = \begin{bmatrix} r_s \\ d \\ n \end{bmatrix} \quad \& \quad z = \begin{bmatrix} r_s - y_o \\ u_i \end{bmatrix} \quad \& \quad e = \begin{bmatrix} r_s - y_o \\ y_i \end{bmatrix} \qquad (4.39)$$

Having established the structure of the plant and controllers, the Youla parameterizations from the previous section can be used to derive the Dual Youla representation of the output feedback system as in Figure 4.2(b). The parameterization of this system will initially involve both signals z and e meaning that the controller K_0 must be written as Equation 4.40 so that it operates only on feedback from the signal e. Taking the plant from Equation 4.37 and the design variable $F_P = \begin{bmatrix} F_{P1} & F_{P2} \end{bmatrix}$, the controller Youla parameters are given by Equations 4.41 and 4.42.

$$\hat{K}_0 : \begin{bmatrix} 0 & 0 \\ 0 & K_0 \end{bmatrix} = \left[\begin{array}{c|cc} 0 & 0 & 0 \\ \hline 0 & 0 & 0 \\ 0 & 0 & D_{K0} \end{array}\right] \qquad (4.40)$$

$$J_K : \left[\begin{array}{c|cc|cc} A_{P0} + B_{P0,1}F_{P1} + B_{P0,2}F_{P2} & 0 & 0 & B_{P0,1} & B_{P0,2} \\ \hline F_{P1} & 0 & 0 & I & 0 \\ F_{P2} - D_{K0}D_{P21}F_{P1} - D_{K0}C_{P2} & 0 & D_{K0} & -D_{K0}D_{P21} & I \\ -(C_{P1} + D_{P11}F_{P1} + D_{P12}F_{P2}) & I & 0 & -D_{P11} & -D_{P12} \\ -(C_{P2} + D_{P21}F_{P1}) & 0 & I & -D_{P21} & 0 \end{array}\right] \qquad (4.41)$$

$$Q: \left[\begin{array}{c|cc} A_{P0}+B_{P0,2}D_{K1}C_{P2} & 0 & B_{P2}(D_{K1}-D_{K0}) \\ \hline -F_{P1} & 0 & 0 \\ -F_{P2}+D_{K1}C_{P2} & 0 & (D_{K1}-D_{K0}) \end{array}\right] \tag{4.42}$$

These expressions can be greatly simplified by the design parameter F_P. In particular, choosing $F_{P1} = 0$ and $F_{P2} = D_{K1}C_{P2}$ will make all states in Q unobservable. After eliminating those states, the controller Youla parameter is therefore only a static gain equal to the difference between the nominal controller (PI) and some new stabilizing state feedback controller D_{K1}. This selection also has an effect on the J_K parameter in that the first input of the Q block will be multiplied by zero and the first output of Q is always zero. This means the third input and output of J_K can be eliminated. With these eliminations, the J_K block has additional unobservable/uncontrollable states that can also be removed leading to the final reduced forms of Equations 4.43 and 4.44. This form is the same as if the parameterization was done for the connection of the system (A_{P0}, $B_{P0,2}$, C_{P2}, 0) and K_0.

$$\begin{aligned} J_K: &\left[\begin{array}{c|cc|c} A_{P0}+B_{P0,2}D_{K1}C_{P2} & 0 & 0 & B_{P0,2} \\ \hline 0 & 0 & 0 & 0 \\ (D_{K1}-D_{K0})C_{P2} & 0 & D_{K0} & I \\ -C_{P2} & 0 & I & 0 \end{array}\right] \\ &= \left[\begin{array}{c|cc} A_{P0}+B_{P0,2}D_{K1}C_{P2} & 0 & B_{P0,2} \\ \hline (D_{K1}-D_{K0})C_{P2} & D_{K0} & I \\ -C_{P2} & I & 0 \end{array}\right] \end{aligned} \tag{4.43}$$

$$Q: \left[\begin{array}{c|c} 0 & 0 \\ \hline 0 & D_{K1}-D_{K0} \end{array}\right] \tag{4.44}$$

Similar to the controller parameterization, the plant parametrization requires that the controller be cast as $\hat{K}_0$. Using the same design parameter F_P, the plant Youla parameters are given by Equations 4.45 and 4.46.

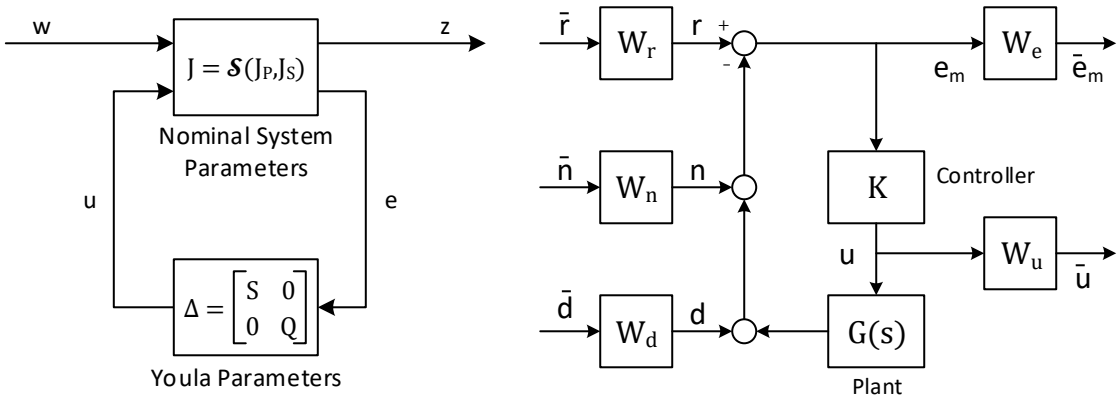

(a) (b)

Figure 4.3: (a) The compact Dual Youla formulation places all plant-controller variations in one system Δ. (b) A typical control system input and output filter configuration.

$$J_P : \left[\begin{array}{c|cc|cc} A_{P0} & 0 & B_{P0,2}D_{K0} & -B_{P0,1} & -B_{P0,2} \\ \hline 0 & 0 & 0 & I & 0 \\ D_{K1}C_{P2} & 0 & -D_{K0} & 0 & I \\ \hline -C_{P1} & I & -D_{P12}D_{K0} & D_{P11} & D_{P12} \\ -C_{P2} & 0 & I & D_{P21} & 0 \end{array}\right] \tag{4.45}$$

$$S : \left[\begin{array}{cc|cc} A_{P1} + B_{P1,2}D_{K0}C_{P2} & B_{P1,2}(D_{K1} - D_{K0})C_{P2} & B_{P1,1} & B_{P1,2} \\ 0 & A_{P0} + B_{P0,2}D_{K0}C_{P2} & B_{P0,1} & B_{P0,2} \\ \hline C_{P1} + D_{P12}D_{K0}C_{P2} & -* & 0 & 0 \\ C_{P2} & -* & 0 & 0 \end{array}\right] \tag{4.46}$$

The final step in the Dual Youla derivation is to gather the Youla parameters as in Figure 4.3(a). This involves finding the Redheffer Star-Product $J = \mathcal{S}(J_P, J_K)$, see [78, Chapter 10] and combining systems S and Q into a single diagonal system Δ. In the final forms of Equations 4.47 and 4.48 where $D_\Delta = D_{K1} - D_{K0}$, all plant variations and controller augmentations can be captured by the Δ system in terms of a nominal plant and controller interconnection described by J.

$$J: \left[\begin{array}{cc|c|ccc} A_{P0}+B_{P0,2}D_{K0}C_{P2} & 0 & -(B_{P0,1}+B_{P0,2}D_{K0}D_{P21}) & 0 & 0 & 0 \\ 0 & A_{P0}+B_{P0,2}D_{K1}C_{P2} & 0 & 0 & 0 & B_{P0,2} \\ \hline -(C_{P1}+D_{P12}D_{K0}C_{P2}) & C_{P1}+D_{P12}D_{K1}C_{P2} & D_{P11}+D_{P12}D_{K0}D_{P21} & I & 0 & D_{P12} \\ \hline 0 & 0 & I & 0 & 0 & 0 \\ (D_{K1}-D_{K0})C_{P2} & 0 & D_{K0}D_{P21} & 0 & 0 & I \\ -C_{P2} & 0 & D_{P21} & 0 & I & 0 \end{array}\right] \tag{4.47}$$

$$\Delta: \left[\begin{array}{cc|ccc} A_{P1}+B_{P1,2}D_{K0}C_{P2} & B_{P1,2}D_{\Delta}C_{P2} & B_{P1,1} & B_{P1,2} & 0 \\ 0 & A_{P0}+B_{P0,2}D_{K1}C_{P2} & B_{P0,1} & B_{P0,2} & 0 \\ \hline C_{P1}+D_{P12}D_{K0}C_{P2} & -* & 0 & 0 & 0 \\ C_{P2} & -* & 0 & 0 & 0 \\ 0 & 0 & 0 & 0 & D_{\Delta} \end{array}\right] \tag{4.48}$$

Both J and Δ introduce additional states to the plant-controller systems. The number of Youla parameters Δ_i should be minimized in order to keep the parameterization dimension low while still accurately representing system requirements. In addition, input/output filtering for robust control should be applied after the Youla parameterization so that fixed filter dynamics do not become incorporated into either Youla parameters.

4.5 Soft Implementation of Cascaded Control Using Youla Parameterization*

Analysis from the previous sections can be used to develop a method to bridge the transition from PI to cascaded control. This is important for the tuning process as gains can be tested and poor performance identified before occupant comfort is affected. The development also lays the groundwork for large scale deployment and adaptive control techniques in that it offers a way to phase in controllers over time. Ensuring occupant comfort during implementation helps to maintain working relationships with building administrators by minimizing discomfort and associated work orders.

Consider a time-invariant plant as in Equation 4.49 with $D_P = 0$ that has been augmented as before with an integrator on the outer loop feedback signal. Given the PI and cascaded controller structures of Equations 4.38 and 4.4, the an expression for the controller Youla parameters J_K and Q with $F_P = D_{K1}C_P$ are given by Equations 4.50.

*Work from this section is adapted with permission from "Soft Implementation of Cascaded Control Architectures Using the Youla Parameterization", C. Price and B. Rasmussen, Proceedings of the American Control Conference, pp. 4652-4657, ©2018 IEEE.

$$G : \left[\begin{array}{c|c} A_P & B_P \\ \hline C_P & 0 \end{array}\right] = \left[\begin{array}{cc|c} \bar{A}_P & 0 & \bar{B}_P \\ \bar{C}_{P,o} & 1 & 0 \\ \hline \bar{C}_P & 0 & 0 \\ 0 & 1 & 0 \end{array}\right] \tag{4.49}$$

$$J_K = \left[\begin{array}{c|cc} A_P + B_P D_{K1} C_P & 0 & B_P \\ \hline (D_{K1} - D_{K0}) C_P & D_{K0} & I \\ -C_P & I & 0 \end{array}\right] \;\&\; Q = \left[\begin{array}{c|c} 0 & 0 \\ \hline 0 & D_{K1} - D_{K0} \end{array}\right] \tag{4.50}$$

Let a new parameter $\bar{Q}$ be defined as in Equation 4.51. Because Q is simply a static gain and λ is a positive scalar less than one, $\bar{Q}$ is guaranteed to be RH_∞. This means that the controller parameterized by $\bar{Q}$ (i.e. $K(\bar{Q})$) will stabilize the plant G for all values of λ. By varying the value of λ slowly, the control will stably transition from nominal PI control ($\lambda = 0$) to cascaded control ($\lambda = 1$).

$$\bar{Q} = \lambda Q \quad \text{where} \quad 0 \leq \lambda \leq 1 \tag{4.51}$$

A realization of this transitional control can be found by combining the systems J_K and $\bar{Q}$ using a lower Linear Fractional Transformation (LFT) as defined in [78], an operation that is greatly simplified by $\bar{Q}$ being a static gain. Note that the resulting transitional controller given in Equation 4.52 now contains a model of the plant dynamics. At $\lambda = 0$ and $\lambda = 1$, $K(\bar{Q})$ is simply a static gain equal to K_0 and K_1 respectively. However, for all other values of λ the phased controller will have dynamics. This is a slight departure from work in the previous chapters as it requires an *a priori* knowledge of the plant. However, one advantage of working with HVAC systems is that their dynamics are dominantly first or second order making identification a simple task.

$$K(\bar{Q}) = F_\ell(J_K, \bar{Q}) = \left[\begin{array}{c|c} A_{P0} + B_{P0}(D_{K1} - \lambda D_\Delta) C_{P0} & \lambda B_{P0} D_\Delta \\ \hline (1-\lambda) D_\Delta C_{P0} & D_{K0} + \lambda D_\Delta \end{array}\right] \tag{4.52}$$

Soft implementation has several advantages when implementing cascaded control. Both the PI and cascaded controller in output feedback form use the same integrator signal, so bumpless transfer or complex integrator reset strategies are unnecessary. The tuning process is also simplified as original performance can easily be restored by returning to $\lambda = 0$. Slowly ramping into full cascaded control means issues with test gains can be spotted before the unset of poor, oscillatory, or unrecoverable behavior.

One important note about this method is the distinction between frozen and transitional stability. Although the Q-parameterization guarantees stability for each fixed value of λ, stability of the timevarying $\lambda(t)$ is not assured. In most gain scheduling literature this issue is dealt with in one of two ways: 1) variation is assumed to be 'sufficiently slow' or 2) the approach is modified to recover transitional stability. In the first approach, Q is assumed to vary slowly enough that the system essentially achieves frozen stability at each value of Q. An exact definition of the allowable rate of change is not defined and varies by system. For the second approach, see [140] for example, recovering transitional stability often comes with a trade off as faster transitional stability requires more conservative control. This distinction is also important in the Dual-Youla parameterization where both the plant and controller must vary sufficiently slowly to ensure stability. Stability of the transitional controller is investigated more in the following example.

4.5.1 Example: Radiator Valve Control

Returning to the hydronic radiator valve system from Section 3.6, the system described by Figure 4.4 is used to simulate room air temperature control. The model is based on that from [87] and will demonstrate the benefits of soft implementation of a cascaded controller. The inner loop signal for cascaded control is again estimated heat transfer $\hat{H} = \delta(T_s - T_r)$, i.e. TRV valve position multiplied by the water temperature drop across the radiator.

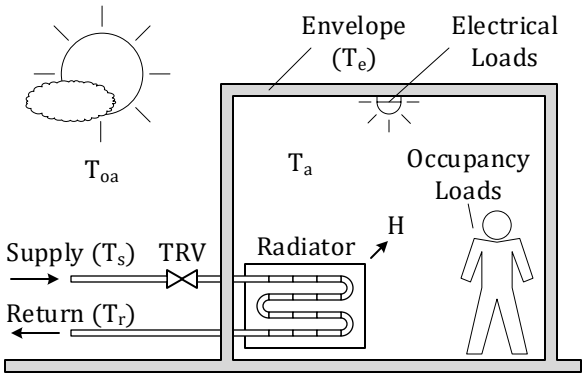

Figure 4.4: Diagram of hydronic radiator system simulation model. ©2018 IEEE.

In order to highlight differences between hard switching and a soft transition between controllers, both a nominal PI and cascaded controller were tuned using standard PI tuning and techniques from [115] respectively. Resulting tuned gains are given in Equation 4.53. Also the model from Equation 4.54 was identified from simulation data and used to generate matrices required to implement Equation 4.51. The outside air temperature signal in Figure 4.5 is used to model disturbances from sensor noise and variations in solar heating, occupancy, etc. and features a repeated 2-hour profile (i.e. before, during, and after switching).

$$\begin{gathered} k_{p0} = 6.12, \quad k_{i0} = 0.007 \\ k_{p1} = 2200, \quad k_{i1} = 1.95, \quad k_L = 0.01 \end{gathered} \tag{4.53}$$

$$\bar{G}: \left[\begin{array}{ccc|c} 0.9993 & 0 & 0 & 0.0156 \\ 0 & 1.99 & -0.9898 & 1 \\ 0 & 1 & 0 & 0 \\ \hline 0.0180 & 0 & 0 & 0 \\ 0 & 0.4461 & -0.4655 & 0 \end{array}\right] \tag{4.54}$$

Results for two switching conditions are shown in Figure 4.6. All controllers have the same response for the initial two hours (i.e. PI control) after which the hard switched case immediately changes to cascaded control. During the transition period, λ for the soft

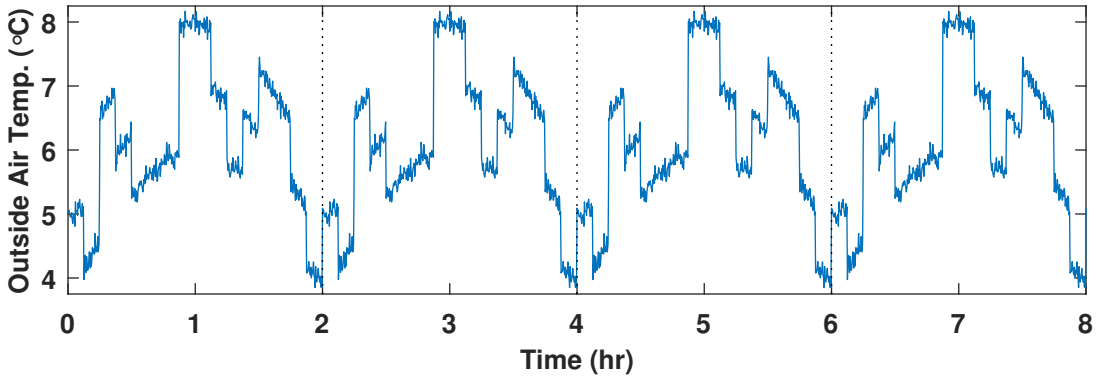

Figure 4.5: Outdoor temperature profile used as disturbance for radiator simulation model. ©2018 IEEE.

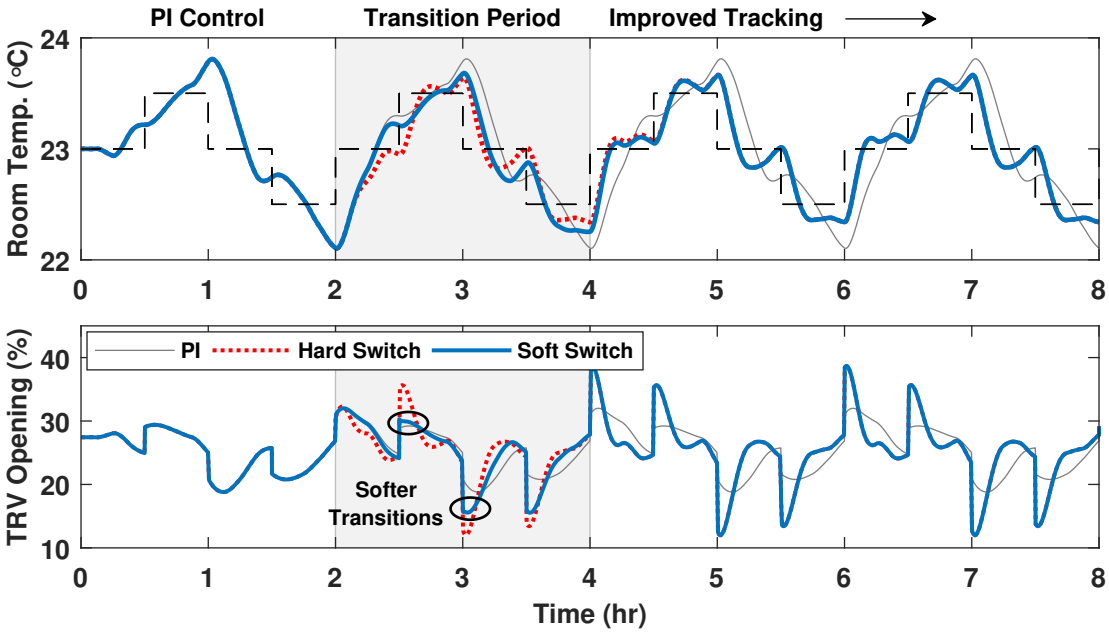

Figure 4.6: Comparison of transition techniques from PI to cascaded control. The soft switched controller uses less initial control effort than the hard switched controller making the transition easier on system resources. ©2018 IEEE.

switched controller is ramped from 0 to 1 and the response begins to converge to the hard switch case, completely merging at approximately 4.5 hrs. After the transition period, both switched controllers have improved tracking performance over the nominal PI controller.

The transition period can be used as an important step in the tuning process. The soft switched controller uses less control effort at the beginning of the transition, closely mir-

roring the PI controller. This makes the change to cascaded control easier on the system and its actuators. For this simulation, cascaded control gains were tuned beforehand allowing the hard switch to immediately achieve better performance. During a normal tuning process, however, the performance of test gains is not known. The transition period allows for issues with gains to be identified before the onset of oscillations/poor performance.

4.6 Performance Evaluation using Linear Matrix Inequalities

The previous sections outline a blending technique for soft implementation of a cascaded control loop. To evaluate the performance of this method and compare performance of PI and cascaded loops, this section will use the $\mathcal{H}_\infty$ norm framework. Evaluation of performance for a control system depends on the design requirements set by expectations and system limitations. This means that certain signals will be more important than others, conflicts between units or the relative magnitudes of signals may exist, and only certain frequencies of signals may be relevant. To deal with these issues, Equations 4.55 and 4.56 are input/output filters for signals w and z in Figure 4.2(a) and can be used to shape the design process. Filter 'w' should define the frequency content of the disturbance/reference inputs while filter 'z' should be the reciprocal of the desired frequency content of the outputs. Equation 4.57 gives the dynamics of the filtered plant.

$$\begin{cases} \dot{x}_w = A_w x_w + B_w \bar{w} \\ w = C_w x_w + D_w \bar{w} \end{cases} \tag{4.55}$$

$$\begin{cases} \dot{x}_z = A_z x_z + B_z z \\ \bar{z} = C_z x_z + D_z z \end{cases} \tag{4.56}$$

$$\begin{cases} \dot{x}_f = \begin{bmatrix} A & B_1 C_w & 0 \\ 0 & A_w & 0 \\ B_z C_1 & B_z D_{11} C_w & A_z \end{bmatrix} \begin{bmatrix} x \\ x_w \\ x_z \end{bmatrix} + \begin{bmatrix} B_1 D_w & B_2 \\ B_w & 0 \\ B_z D_{11} D_w & B_z D_{12} \end{bmatrix} \begin{bmatrix} \bar{w} \\ u \end{bmatrix} \\ \begin{bmatrix} \bar{z} \\ e \end{bmatrix} = \begin{bmatrix} D_z C_1 & D_z D_{11} C_w & C_z \\ C_2 & D_{21} C_w & 0 \end{bmatrix} x_f + \begin{bmatrix} D_z D_{11} D_w & D_z D_{12} \\ D_{21} D_w & D_{22} \end{bmatrix} \begin{bmatrix} \bar{w} \\ u \end{bmatrix} \end{cases} \tag{4.57}$$

A typical robust control problem is shown in Figure 4.3(b) where $\bar{r}$ is a reference input, $\bar{n}$ represents sensor noise, and $\bar{d}$ contains disturbance signals. Each of these signals is assumed to be white noise with unitary gain that must be shaped to meet design requirements. For HVAC systems, disturbance inputs are generally diurnal due to outside weather conditions or semi-random changes in internal heat load due to occupancy schedules. As both these signals are fairly slow, a Low Pass Filter (LPF) like Equation 4.58 can be used to approximate their behavior. Similarly, HVAC set points are typically long step changes that can be approximated with a LPF. Sensor noise is in general a small magnitude, high frequency phenomenon that can be modeled with a High Pass Filter (HPF) as in Equation 4.59.

$$G_{lpf}(s) = \frac{b}{as+1} \qquad (4.58) \qquad\qquad G_{hpf}(s) = \frac{bs}{as+1} \qquad (4.59)$$

Outputs for HVAC systems are usually temperature error and control effort. HVAC actuators are often slow and many are rate limited. Therefore high frequency errors are usually impossible to eliminate due to control limitations. This means that the output error filter should be an LPF so that the performance metric only considers low frequency errors. While the magnitude of valve or damper opening is not inherently important, rapid changes in actuation should be suppressed and therefore W_u should be a high pass filter.

After designing the input and output filters, the $\mathcal{H}_\infty$ system norm is a good choice for evaluating HVAC system performance. From Equation 4.60, the $\mathcal{H}_\infty$ is defined as the maximum singular value of a system over all frequencies and input directions. The norm can therefore be thought of as a measure of worst case performance. As building controls must guarantee occupant comfort even in the most challenging conditions, this norm is a natural choice for HVAC systems.

$$\|G(s)\|_\infty = \sup_\omega \{\sigma_{\max}(G(j\omega))\} \qquad (4.60)$$

The $\mathcal{H}_\infty$ norm is usually computed numerically by finding the smallest value γ for which the system Hamiltonian matrix has eigenvalues on the imaginary axis. This is an iterative process in which an initial guess for γ, usually large, is reduced until an answer is found with an acceptable level of accuracy. Another option is to solve for the system norm using Linear Matrix Inequalities (LMIs) where the problem is cast as a convex minimization with constraints. LMIs are computationally efficient and are able to incorporate multiple design objectives. As seen in Equation 4.61, the LMI problem can even incorporate multiple operating conditions and solve for a polytopic system norm.

$$\begin{cases} \min & \gamma \\ \text{s.t.} & P > 0 \\ & \begin{bmatrix} A_i^T P + P A_i & P B_i & C_i^T \\ B_i^T P & -\gamma I & D_i^T \\ C_i & D_i & -\gamma I \end{bmatrix} < 0 \end{cases} \tag{4.61}$$

Finally, a description of the time varying dynamics of HVAC systems and a description of controller transitions must be outlined. The simplest approach to modeling dynamic changes is identify a series of linear system models at different operating conditions and then blend their outputs according to a scheduling variable. This approach can also be applied to a network of controllers as in Figure 4.7(a). While straightforward, output blending has no guarantees of stability during transitions of the scheduling variable. Another blending approach would be to use the Dual-Youla Parameterization discussed in the previous section to identify a series of Q_i and S_i parameters and combine their outputs through the J_K and J_P blocks as in Figure 4.7(b). As linear combinations of systems in RH_∞ are themselves stable, this type of blending recovers the stability guarantees of the parameterization. Differences in these methods are explored in the following example.

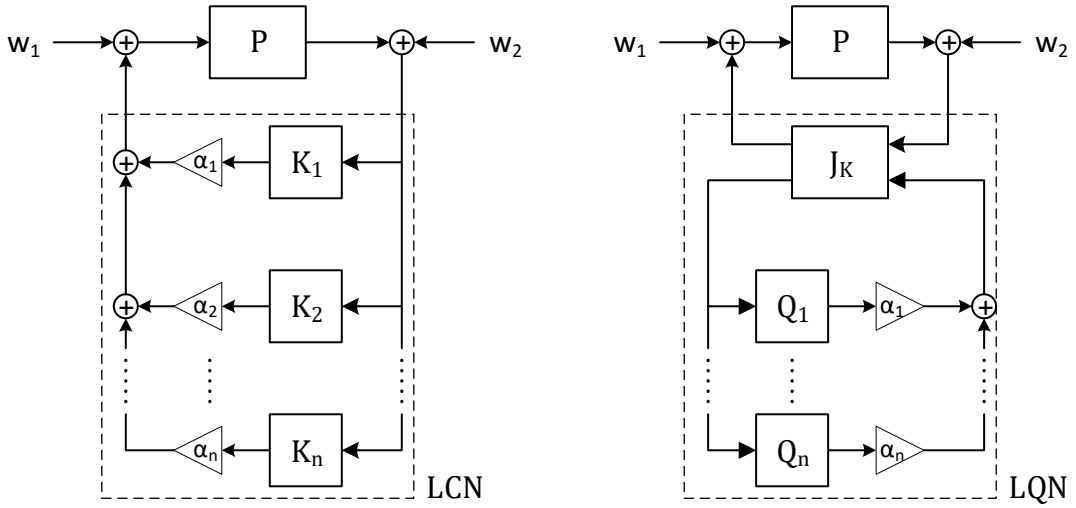

Figure 4.7: (a) A Linear Controller Network (LCN) uses linear interpolation to blend the outputs of different controllers. (b) A Linear-Q Network (LQN) blends different controllers by interpolating Youla parameters thereby recovering stability guarantees.

4.6.1 Example: AHU Discharge Air Temperature Control

This section presents a case study comparing the performance of PI and cascaded control for time varying systems with different implementations. The example system is loosely based on the AHU model from Chapter 3.5 and has the first order, time delay dynamics of Equation 4.62. A series of simulated valve step tests for a range of fan speeds were conducted for a constant discharge air temperature of $55°$F. Identified parameter models are given in Equation 4.63 for the scheduling variable $\theta \in [0, 1]$.

$$G(s, \theta) = \frac{K(\theta)}{\tau(\theta)s + 1} e^{-T_d(\theta)s} \tag{4.62}$$

$$\begin{aligned} K(\theta) &= 3.1e^{-14.8\theta} + 1.1e^{-3.3\theta} \\ \tau(\theta) &= 1437e^{-12.8\theta} + 387e^{-2.2\theta} \\ T_d(\theta) &= 100e^{-2.5\theta} + 2.5e^{-1.5\theta} \end{aligned} \tag{4.63}$$

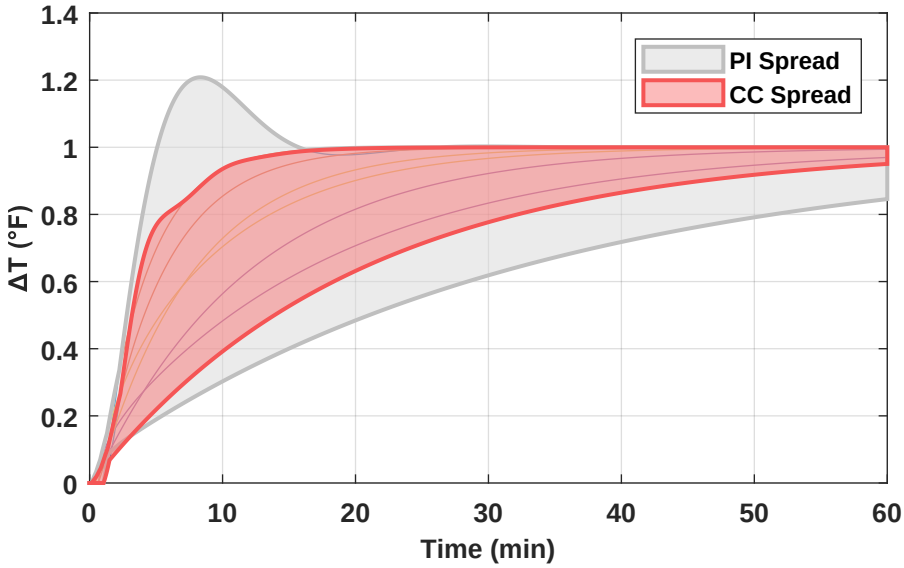

Figure 4.8: Comparison of tuned PI and cascaded control responses over the scheduling parameter θ. Cascaded control shrinks the cone of possible responses.

Analyzing building code across the Texas A&M campus shows that the minimum fan speed for all AHUs when operating is 20% to ventilation requirements. This means that the steady-state gain, time constant, and time delay will vary by factors of 18, 8, and 7 over the operating range $\theta \in [0.2, 1]$ respectively according to the model. PI and cascaded control gains were tuned in the $\theta = 0.2$ condition giving conservative gains (Equation 4.64) that avoid excessive oscillation over the operating range. A comparison of step responses is given in Figure 4.8 which shows that cascaded control reduces the envelope of possible responses. This effect will be quantified by the following H_∞ analysis.

$$\begin{aligned} \text{PI:} \quad & k_{p0} = 2.15 \quad k_{i0} = 0.8 \\ \text{CC:} \quad & k_{p1} = 0.20 \quad k_{i1} = 0.3 \quad k_L = 5 \end{aligned} \tag{4.64}$$

The closed loop system in Figure 4.3(b) requires the design of five filters: three input filters (W_r, W_n, and W_d) and two output filters (W_e and W_u). References changes for HVAC systems including AHUs are typically steps with long latency between changes. A lower bound for the reference signal period is assumed to be 15 minutes and the magnitude

is assumed to be 1°F giving the LPF of in Equation 4.65. Input disturbances are slightly faster than reference changes and must include daily weather conditions. Assuming that disturbances affect discharge temperature by $\pm 0.5^{\circ}$F with a period of 10 minutes covers these effects leading again to an LPF. Finally, sensor noise is inherently high frequency and small in magnitude. As the dynamics of the system act essentially act as an LPF, noise considerations will be neglected for this example.

$$W_r = \frac{1}{142s+1} \qquad \& \qquad W_d = \frac{1}{100s+1} \tag{4.65}$$

Output filters must be designed to penalize poor system and controller behavior. Reference tracking errors should be kept small and dissipated quickly. The desired maximum level of error is $\pm 1^{\circ}$F with an upper period bound of 10 minutes. The system will not be able to react to faster error frequencies than this limit, so the error filter should be an LPF as in Equation 4.66. When designing W_u, the steady-state magnitude of the control signal is not important for the performance problem. The control filter should therefore be an HPF to penalize sudden changes in position and avoid issues with actuation rate limiting. Many dampers and valves have travel times of 60 seconds or a maximum rate of change of 1.67%/s leading to the filter in Equation 4.66.

$$W_e = \frac{1}{100s+1} \qquad \& \qquad W_u = \frac{0.3s}{0.3s+1} \tag{4.66}$$

The plots in Figure 4.9 show the results of analyzing the example system with the designed weights, different implementation methods, and situations. In all combinations, a Youla parameterization for the varying plant dynamics is found using a nominal system $P_0(\theta)$ to create a Linear-S Network (LSN) description of the plant. Figure 4.9(a) shows results for combinations of frozen plants (i.e. θ fixed in $[0.2, 1]$) and a frozen controllers (i.e. ϕ fixed in $[0, 1]$). At each operating condition 'θ', the cascaded controller gives better

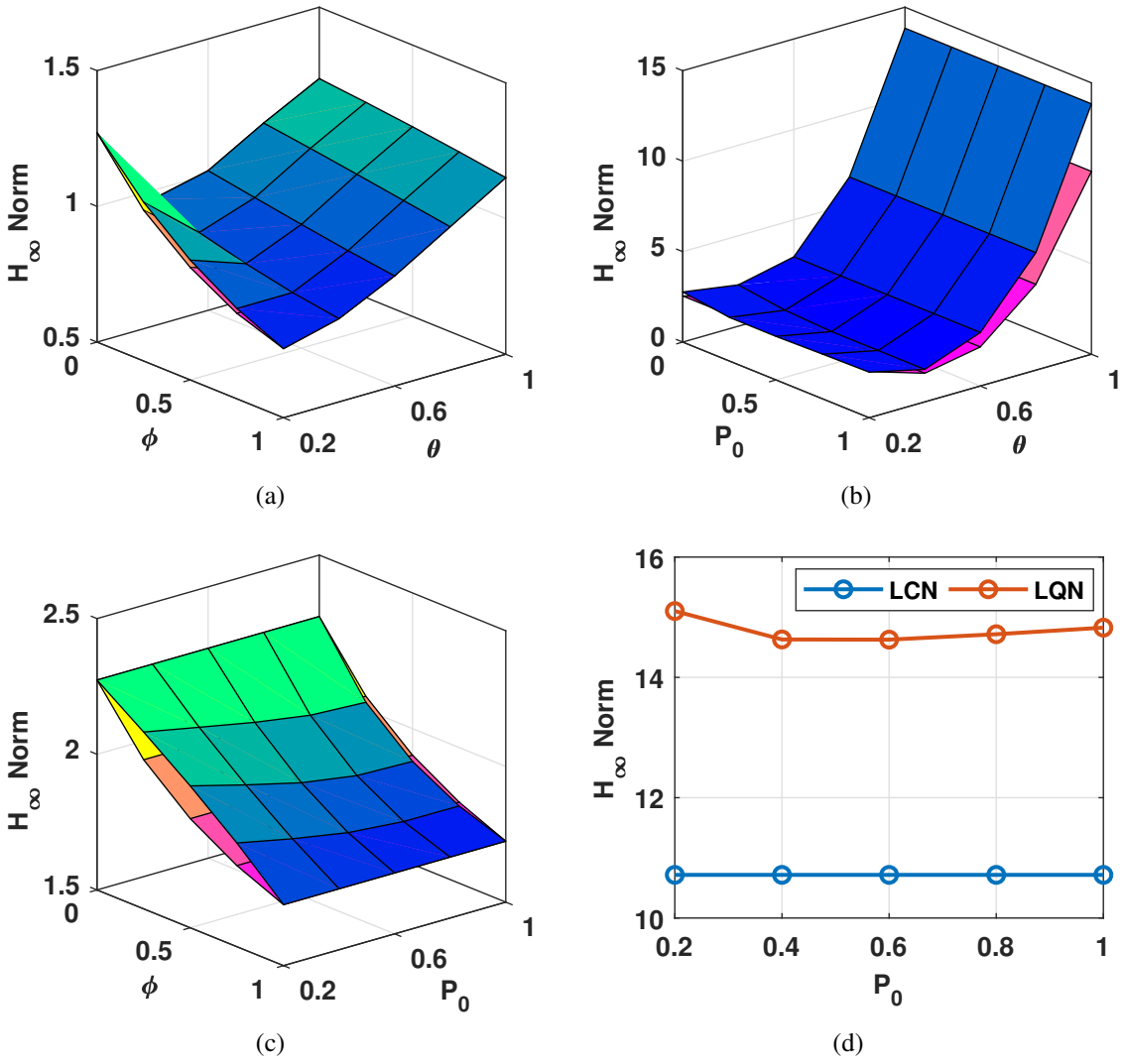

Figure 4.9: Blue color gradient is for results with LQN and pink gradient for LCN. (a) Single plant with single controller. (b) Single plant with polytopic controller. (c) Polytopic plant with single controller. (d) Polytopic plant and controller.

$\mathcal{H}_\infty$ performance over the range of controllers than PI control. Further, the norm decreases linearly as the control approaches cascaded control (i.e. $\phi \to 1$). Also shown is that there is little difference between results for controllers parameterized as Linear-Q or the much simpler Linear Controller Network (LQN and LCN).

The LMI norm outlined in the previous section can also be used to analyze the polytopic performance of the example system. In Figure 4.9(b), the plant is frozen but the controller is assumed to vary arbitrarily in $\phi \in [0, 1]$. The selection of the nominal plant appears to have little effect while the operating condition has a strong influence. When $\theta = 1$, the system has its slowest gain profile and control error will be large which is borne out in the plot. Interestingly, the LCN network appears to offer better norm results especially at high load.

Similarly, in Figure 4.9(c) the controller is frozen but the plant scheduling parameter is free to vary polytopically. Again the choice of nominal system for the plant Youla parameterization has little effect on the system performance norm. As in the frozen plant and controller case, as $\phi \to 1$ (i.e. cascaded control) the system performance improves. The LCN network again offers slightly lower performance norms when compared to the LQN network but there is essentially no difference.

The final condition tested was norm analysis for a fully polytopic plant and controller system (Figure 4.9(d)). The selection of nominal system for the plant LSN parameterization seems to have little or no effect on the norm output. The LCN network does, however clearly have better norm performance. This may indicate that for simple dynamics, like most HVAC equipment, the full Youla controller parameterization may not be necessary. As mentioned before, the LCN approach has no guarantees for stability as the controller scheduling variable ϕ varies. This trade-off is therefore system dependent and necessary when stability is paramount.

Overall, cascaded control shows a distinct improvement of system $\mathcal{H}_\infty$ performance for all conditions. Although the selection of nominal system for the LSN parameterization of the plant does not seem to effect the norm performance at a given operating condition, it does have an effect on the initial value. Therefore, the nominal plant condition should be chosen for the most common conditions to minimize modeling errors. The results also

show that, at least for this example, that while full Dual-Youla analysis of the plant and controller does provide stability guarantees, overall performance benefits are minimal. Therefore for implementation in the field, simple control interpolation between PI and cascaded control can be used.

4.7 Performance Guarantees for Cascaded Control

Results from the previous section indicate that the cascaded controller is able to offer better performance than a well tuned PI controller. This section seeks to provide a mathematical basis for this observation.

Consider the LPV system and generic static feedback controller of Equation 4.67. Here a state transformation is assumed to collect all varying parameters into the system A and B matrices. The closed loop system matrices are then given by Equation 4.68.

$$G(\theta): \left[\begin{array}{c|cc} A(\theta) & B_1(\theta) & B_2(\theta) \\ \hline C_1 & D_{11} & D_{12} \\ C_2 & D_{21} & 0 \end{array}\right] \qquad K: \left[\begin{array}{c|ccc} 0 & 0 & 0 & 0 \\ \hline 0 & k_1 & k_2 & k_3 \end{array}\right] \tag{4.67}$$

$$G_{cl}(\theta): \left[\begin{array}{c|c} A_{cl} & B_{cl} \\ \hline C_{cl} & D_{cl} \end{array}\right] = \left[\begin{array}{c|c} A(\theta) + B_2(\theta) D_K C_2 & B_1(\theta) + B_2(\theta) D_K D_{21} \\ \hline C_1 + D_{12} D_K C_2 & D_{11} + D_{12} D_K D_{21} \end{array}\right] \tag{4.68}$$

As discussed, the performance norm of a time varying closed loop system can be approximated using a polytopic LMI description as in Equation 4.61. The standard form of an LMI is given in Equation 4.69 where $F_i \in \mathbb{R}^{n \times n}$ are given and $x \in \mathbb{R}^m$ is the variable [141]. The polytopic $\mathcal{H}_\infty$ norm can be written in standard LMI form by assuming that the solution P can be written in terms of its basis matrices $P = x_1 E_1 + x_2 E_2 + \cdots + x_m E_m$ where $E_i \in \mathbb{S}^n$ and $m = n(n+1)/2$. Substitution gives Equation 4.70 in terms of its scalar LMI variables.

$$F(x) \triangleq F_0 + \sum_{i=1}^{m} x_i F_i > 0 \tag{4.69}$$

$$\begin{bmatrix} 0 & 0 & C_{cl}^T \\ 0 & -\gamma I & D_{cl}^T \\ C_{cl} & D_{cl} & -\gamma I \end{bmatrix} + \sum_{i=1}^{m} x_i \begin{bmatrix} A_{cl}^T E_i + E_i A_{cl} & E_i B_{cl} & 0 \\ B_{cl}^T E_i & 0 & 0 \\ 0 & 0 & 0 \end{bmatrix} < 0 \tag{4.70}$$

An assumption about the structure of the controller can now be made to separate contributions to the LMI that are shared by both cascaded and PI control from those only from cascaded control. Let $D_k = D_{PI} + \varepsilon D_\Delta$ where $D_{PI} = [k_p \quad 0 \quad k_i]$ and $D_\Delta = \begin{bmatrix} 0 & 1 & 0 \end{bmatrix}$. The expression above can then be written as Equation 4.71 where $A_{cl,pi}$, $B_{cl,pi}$, $C_{cl,pi}$, and $D_{cl,pi}$ are the closed loop system matrices with PI control.

$$\begin{bmatrix} 0 & 0 & C_{cl,pi}^T \\ 0 & 0 & D_{cl,pi}^T \\ C_{cl,pi} & D_{cl,pi} & 0 \end{bmatrix} + \sum_{i=1}^{m} x_i \begin{bmatrix} A_{cl,pi}^T E_i + E_i A_{cl,pi} & E_i B_{cl,pi} & 0 \\ B_{cl,pi}^T E_i & 0 & 0 \\ 0 & 0 & 0 \end{bmatrix}$$
$$+\varepsilon \left\{ \begin{bmatrix} 0 & 0 & (D_{12} D_\Delta C_2)^T \\ 0 & 0 & (D_{12} D_\Delta D_{21})^T \\ D_{12} D_\Delta C_2 & D_{12} D_\Delta D_{21} & 0 \end{bmatrix} \right.$$
$$\left. + \sum_{i=1}^{m} x_i \begin{bmatrix} (B_2(\theta) D_\Delta C_2)^T E_i + E_i(\star) & E_i(*) & 0 \\ (B_2(\theta) D_\Delta D_{21})^T E_i & 0 & 0 \\ 0 & 0 & 0 \end{bmatrix} \right\} < \gamma \begin{bmatrix} 0 & 0 & 0 \\ 0 & I & 0 \\ 0 & 0 & I \end{bmatrix} \tag{4.71}$$

The above expression essentially describes two LMIs: the $\mathcal{H}_\infty$ performance norm LMI with PI control and a second LMI containing terms due solely to inner loop feedback. Equation 4.72 gives the simplified standard form and the dependence of the second expression on the existence of ε (i.e. an inner loop feedback path).

$$W_0 + x_1 W_1 + x_2 W_2 + \cdots + x_d W_d + \varepsilon(V_0 + x_1 V_1 + x_2 V_2 + \cdots + x_d V_d) < \gamma \bar{I} \tag{4.72}$$

The above expression shows how the performance of a cascaded loop system is guaranteed to be as good or better than even a well tuned PI controller. A solution P to the PI performance problem $W_0 + \sum_{i=1}^{m} x_i W_i < \gamma \bar{I}$ gives values for the LMI scalar variables x_i. That solution determines structure of the sum $V_0 + \sum_{i=1}^{m} x_i V_i$ in Equation 4.72 when

$\varepsilon \neq 0$. When ε is allowed to vary, it acts as an additional free variable that can be selected to further minimize the system performance norm γ. While there is no guarantee that performance will improve, it is upper bounded by the original PI performance in which case the optimal inner loop gain is simply $k_L = 0$. However, the additional free variable provides an opportunity to significantly reduce the performance norm in most cases.

This observation assumes that LMI variables have previously been found such that there exists a $P < 0$ for a given performance level γ and PI control. It does not show how the performance will be affected if the inner loop feedback is included in search for the x_i variables. As before, the solution will be upper bounded this time by the ε-only minimization. This means that the expected performance of a cascaded controller will always be better than or equal to an equivalently tuned PI controller.

4.8 Summary of Cascaded Performance Evaluation

This chapter developed the Dual Youla parameterization for a general static feedback controller and used it to analyze the stability of a system with PI and cascaded control. The Youla parameterization was also used to analyze the performance of HVAC systems using an $\mathcal{H}_\infty$ framework. Input/output filters were developed that penalize poor performance while respecting actuation limitations present in most HVAC actuators. A simple case study was used to compare two different cascaded loop implementations: direct control interpolation and Youla-Q interpolation. Results showed that while the Youla interpolation recovered stability guarantees, direct interpolation provided similar performance. For field implementation on HVAC systems, direct interpolation is therefore a good option. Finally, a proof was discussed showing that cascaded control architectures provide the same or better performance than traditional PI controllers used in most building systems.

5. IMPLEMENTATION OF CASCADED CONTROL ON CAMPUS*

To identify hunting behavior and quantify benefits of the proposed cascaded control loop on real building systems, an automated method for hunting detection was developed by [30] and cascaded control was applied to several buildings at Texas A&M University. Sections 5.1 and 5.2 follow the explanations and figures presented in [30] with permission. Section 5.3 summarizes results of an HVAC control survey at Texas A&M from [30] while the remaining sections discuss implementation of cascaded control architectures in building software and present results from cascaded loop testing at three campus buildings.

5.1 Detection of Hunting Behavior

There are many causes of actuator hunting in HVAC systems and distinguishing between them is essential. As discussed in Chapter 1, buildings are inherently time varying and nonlinear systems whose dynamic characteristics can change significantly over time. Consider a Variable Air Volume (VAV) box with an air flow damper (Figure 5.1). Control gains tuned when the damper is mostly closed will be smaller than when the damper is mostly open. These differences would are not an issue if system demand was constant. HVAC systems are, however, always in flux due to highly variable loads such as weather and occupancy. Static control will therefore either barely respond or vastly overestimate required control leading to generally poor performance and/or hunting behavior.

Hunting in signals can also be caused by hunting in upstream and downstream systems. For example, oscillations in the discharge air temperature of an Air Handling Unit (AHU) will cause oscillations in the damper position of a VAV as it must adjust to compensate for the greater/lesser cooling ability of the supply air. The oscillating damper will also cause

*Material in Sections 5.1-5.3 is adapted with permission from "A Methodology for Automating the Implementation of Advanced Control Algorithms Such as Model Predictive Control on Large Scale Building HVAC Systems", R. Chintala, PhD Thesis, Texas A&M University, 2017.

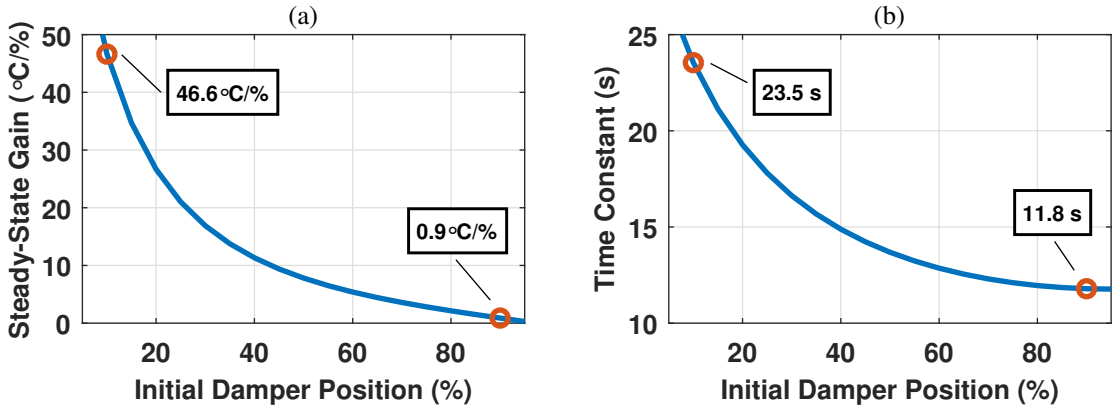

Figure 5.1: For a VAV system (a) steady-state gains vary in magnitude by over 50 times and (b) time constants more than double over all operating ranges.

hunting in AHU supply fan speed, as the duct static pressure will oscillate with damper position. Other hunting factors include actuator friction causing periodic windup in the actuation signal, poor control tuning, and oscillating disturbances.

When observing data from building systems, two distinct frequencies are observed: slow peaks due to daily variation in outside temperature and faster peaks due to any of the control hunting factors discussed above. Periodic disturbances caused by daily building usage are either random or follow a distinct schedule (e.g. weekday work hours, temperature setbacks, etc.). These disturbances will necessarily cause oscillations in the control signal but should not be identified as hunting. A detection algorithm must therefore distinguish between such normal fluctuations and hunting behavior caused by the controllers.

Hunting behavior in process industries led to the development of several oscillation detection methods. Detection of oscillations in process controls can be difficult due to a wide range of frequencies and asymmetric profiles. In [142], a combination on-line/off-line algorithm was developed that could identify oscillations and determine whether friction or control was the cause. The procedure uses the Integrated Absolute Error (IAE) of the process error signal (Equation 5.1) where the integration bounds are the time between

consecutive zero crossings of $e(t)$. When control performance is good, the time between crossings and therefore the IAE will be small. When the IAE crosses a threshold value, a 'load' disturbance is said to have occurred. When two or more load disturbances occur within a given window, hunting behavior will be identified. An extension to this method was proposed by [143] that improves diagnostic capabilities of the algorithm by analyzing the power spectrum of process data off-line. From this, distinctions between tuning issues and limit-cycles caused by nonlinearities such as valve friction can be made.

$$IAE = \int_{t_{i-1}}^{t_i} e(t)dt \tag{5.1}$$

Other off-line methods rely purely on statistical analysis of the error signal. In [144], the decay ratio of oscillations in the error signal Auto-Correlation Function (ACF) were used to detect hunting. This method has the added benefit of distinguishing between sustained and decaying oscillations. Similarly, [145] used the ACF of the inverse Fourier transform of the filtered power spectrum. Zero crossing frequency of this ACF can then be used to infer the presence of hunting. With this method multiple frequencies can be identified, helping to distinguish between causes.

5.1.1 Hunting in HVAC Systems

Each method described so far has been developed for process control. The main difficulty in detecting hunting in those industries is the wide range of frequencies present in normal operation. Buildings, however, have a much more defined band of frequencies (e.g. daily schedules) during normal operation making identification of hunting behavior easier than in process applications. A hunting algorithm for buildings must distinguish between undesired oscillations caused by control loops and daily load disturbances. The main sources for load disturbances are outside weather conditions that have period of one day and internal heat loads (e.g. occupancy, computers, etc.) that are inherently non-

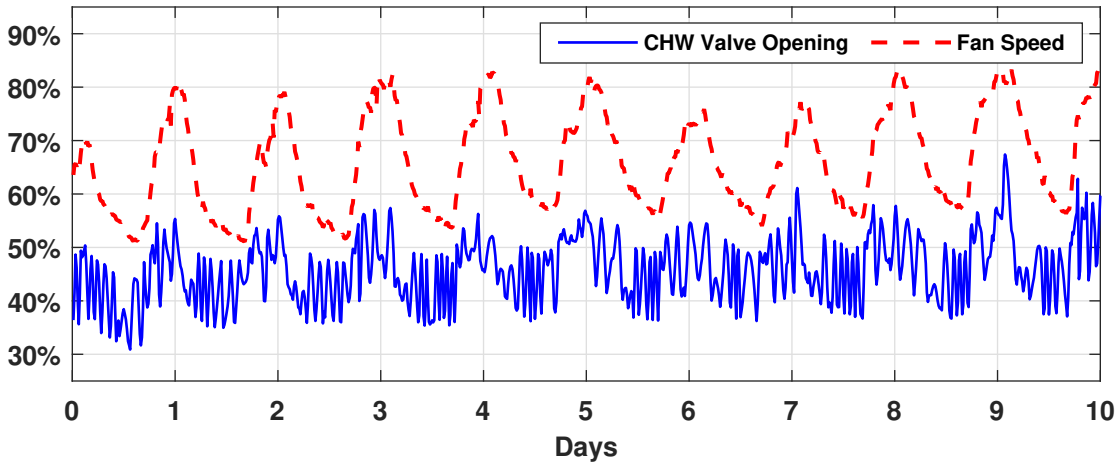

Figure 5.2: Hunting chilled water valve data from air handling unit in the Texas A&M Therapeutics Manufacturing Building. Figure from [30].

oscillatory. Internal loads will generally have a square profile with distinct step changes. Control loops regulating these loads will exhibit similar characteristics.

An example of typical oscillations in building HVAC systems is shown in Figure 5.2 where there are two distinct frequencies exhibited by the chilled water valve position and supply fan speed. The fan oscillates according to daily weather loads while the valve has oscillations at a much higher frequency. There are no load disturbances that equate with the fast frequency of the valve control which is a strong indication of hunting.

This chapter will use the algorithm proposed in [22] to identify and quantify hunting behavior in building HVAC on the Texas A&M campus. The main advantage of this algorithm is that only the control signal is required to detect hunting. This is a simplification over other methods as they require both setpoint and output signals be recorded by the building management system to calculate error.

5.1.2 Summary of Detection Algorithm

The algorithm uses two aspects of the control signal to determine whether an oscillation is hunting: amplitude and frequency. To be identified, an oscillation must fulfill three

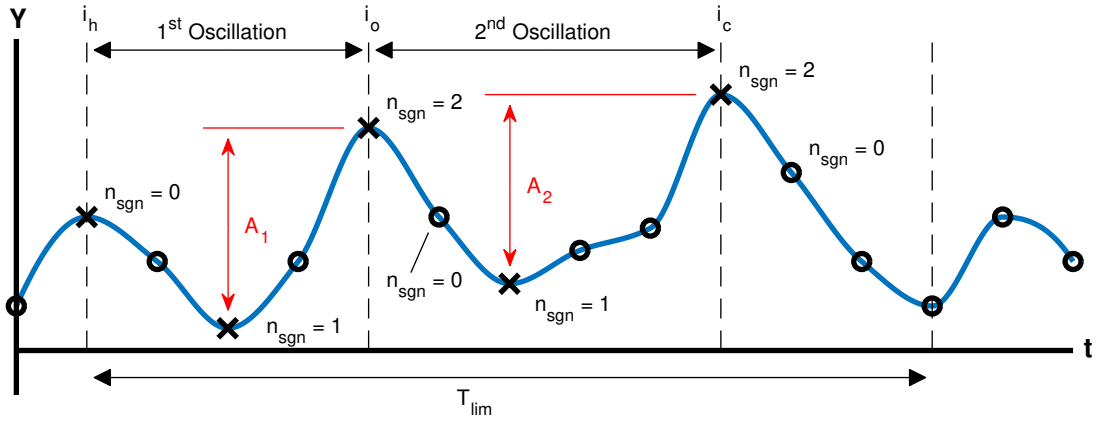

Figure 5.3: Example of the hunting algorithm used to identify and quantify hunting in building HVAC systems. Adapted from [30].

criteria: The peak-to-peak magnitude of an oscillation must be larger than the design limit A_{lim}, a threshold below which variations are considered negligible. There must also be at least n_{lim} oscillations within an observation window T_{lim} to exclude random variations due to changes in occupancy. Finally, the frequency of oscillation (f_{osc}) must be faster than daily weather/occupancy loads. Figure 5.3 shows a diagram of the hunting algorithm and a summary of major steps is provided below:

Initilzation: The algorithm begins by initializing index variables i_h, i_o, and i_c that track the location of the start of the hunting window, the last oscillation, and current index respectively. All three indices are initialized to 2 (Matlab indices begin at 1). Four other variables A_{min}, A_{max}, n_{sgn}, and n_{osc} are all created with initial values of 0. A_{max} and A_{min} track the extreme values of the control signal in the current oscillation window while n_{sgn} and n_{osc} track the number of sign changes and detected oscillations respectively. Finally an empty array H is created that will track the indices of identified hunting behavior.

Step 1 - Time Check: At each index, the current index is checked against the hunting window specified by T_{lim}. If $T_{lim} > i_c - i_h$, no hunting behavior has been detected

resulting in i_h and i_o being set to the current index i_c while n_{sgn} and n_{osc} are reset to 0. If $T_{lim} < i_c - i_h$, the algorithm proceeds to Step 2.

Step 2 - Inflection Detection: At each index i_c, the algorithm determines if there is an inflection point by calculating the future sign change ($S_+ = y[i_c + 1] - y[i_c]$) and previous sign change ($S_- = y[i_c] - y[i_c - 1]$). If $S_+ \neq S_-$, then a sign change is recorded and n_{sgn} is incremented by one. At each instance, i_c is also increased by one.

Step 3 - Oscillation Detection: When $n_{sgn} = n_{lim} = 2$, two sign changes have occurred and a possible oscillation has been detected between i_o and i_c. The algorithm then determines the upper and lower magnitudes of the signal and computes the peak-to-peak magnitude (i.e. $A = A_{max} - A_{min}$). If $A > A_{lim}$, than an oscillation has been detected, n_{osc} is incremented by one, and i_o is set to the current index i_c. If $A < A_{lim}$, the oscillation is considered insignificant and no changes are made.

Step 4 - Hunting Detection: When $n_{osc} = 2$, two significant oscillations have been detected and possible hunting behavior has been found. The algorithm computes the time difference between the beginning of the hunting window (i_h) and the end of the second oscillation (i_c). Hunting is detected if $(i_c - i_h) \leq T_{lim}$ and H is augmented with starting and ending indices of the hunting behavior as in Equation 5.2.

$$H = \left[\begin{array}{c} H \\ \hdashline [i_h \quad i_c] \end{array}\right] \tag{5.2}$$

Step 5 - Reset Variables: After two oscillations, variables are reset to advance the hunting detection window. Specifically, $i_h = i_o$ and $i_o = i_c$ move the indices to the beginning and end of the last detected oscillation respectively while n_{sgn} is reset to zero and n_{osc} is set to one. The algorithm then returns to Step 1 until the entire data set has been analyzed.

Post Processing: After the data set has been analyzed, the hunting array H is processed to remove duplicate indices and later used to create a logical index variable (i.e. a vector of

boolean values) that contains only the locations of identified hunting. The control signal is also analyzed to identify long periods of continuous zero input (more than three hours) indicating the system is in standby mode. The percentage of hunting time is then calculated by dividing the total time of identified hunting by the total operating time.

Code for the hunting algorithm can be found in Appendix D. The outputs of the function are locations of all identified periods of hunting behavior and a percentage of time spent hunting based on total operating hours. The algorithm can be used in real time or be used to analyze historical building data as in the next section.

5.1.3 Algorithm Considerations

Several algorithm variables must be considered when analyzing a data set for hunting. At the start of the algorithm, the peak-to-peak amplitude limit (A_{lim}) must be set. Larger values will make detection less sensitive by only identifying very large oscillations while a small A_{lim} may falsely identify sensor noise as hunting. The length of the hunting window must also be considered as its size will effect the frequency of oscillations detected. As discussed before, the window must be short enough to exclude frequencies associated with daily heat loads, but long enough to capture oscillations in actuator input. Both parameters must be adjusted together for successful hunting identification.

Also important is the sampling time (T_s) of the hunting data. Figure 5.4 shows the results of applying the hunting algorithm to a common data set sampled at 1-minute and 15-minute intervals. For this example A_{lim} was set to 15% and T_{lim} was set to 2 hours for each data set. As shown, while there is some aliasing of the hunting signal due to the reduced sampling rate, the detection algorithm is still able to identify similar periods of hunting behavior. The figure makes clear that the success of observing and detecting hunting is heavily dependent on T_s and consequently T_{lim}.

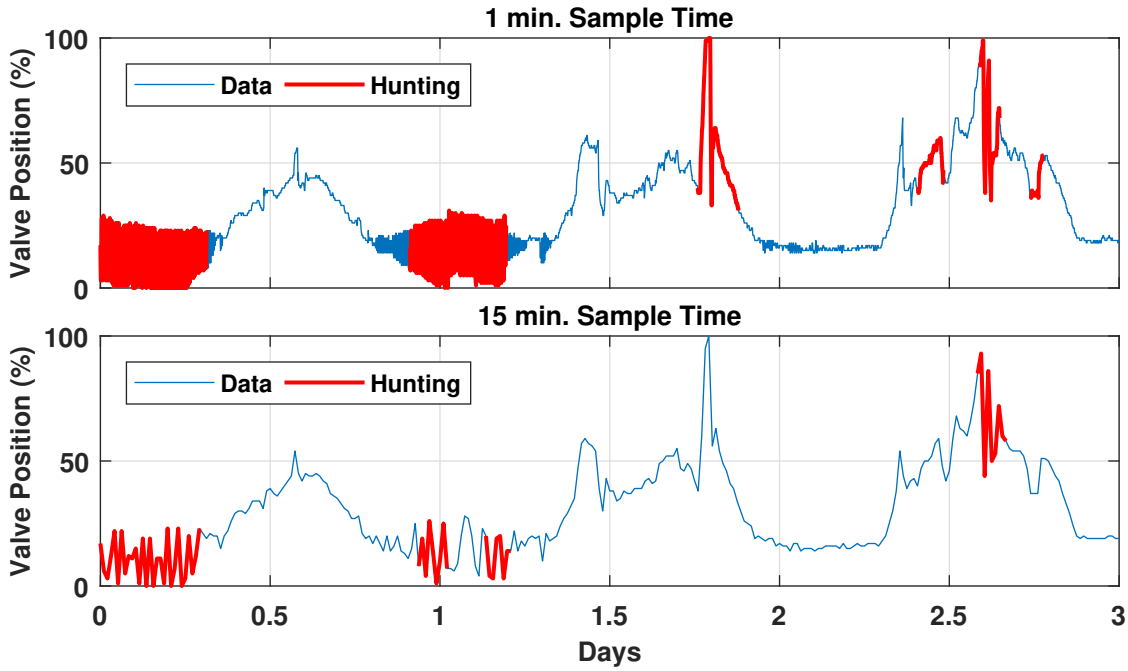

Figure 5.4: Sampling at different rates identifies the same regions as hunting behavior (adapted from [30]).

While clearly a strong tool for HVAC control performance, the algorithm should not be used for diagnosis. As discussed, hunting in one process can cause oscillations in other controllers throughout an HVAC system. Figure 5.5 shows data over a ten day period for two process variables: average building VAV damper position and AHU fan speed. As is evident, the periods of identified hunting behavior are similar for both signals. This indicates that there should always be an extra step after the detecting algorithm is complete to determine the root cause of the oscillations.

5.2 Current Building Control Technology at Texas A&M

Texas A&M became the second largest university in the United State by total enrollment starting in the 2016-2017 academic year. Due to its size, the university has a large campus with over 750 buildings spread over 5,200 acres. In order to manage building operations, the university has invested heavily in an extensive Building Automation System

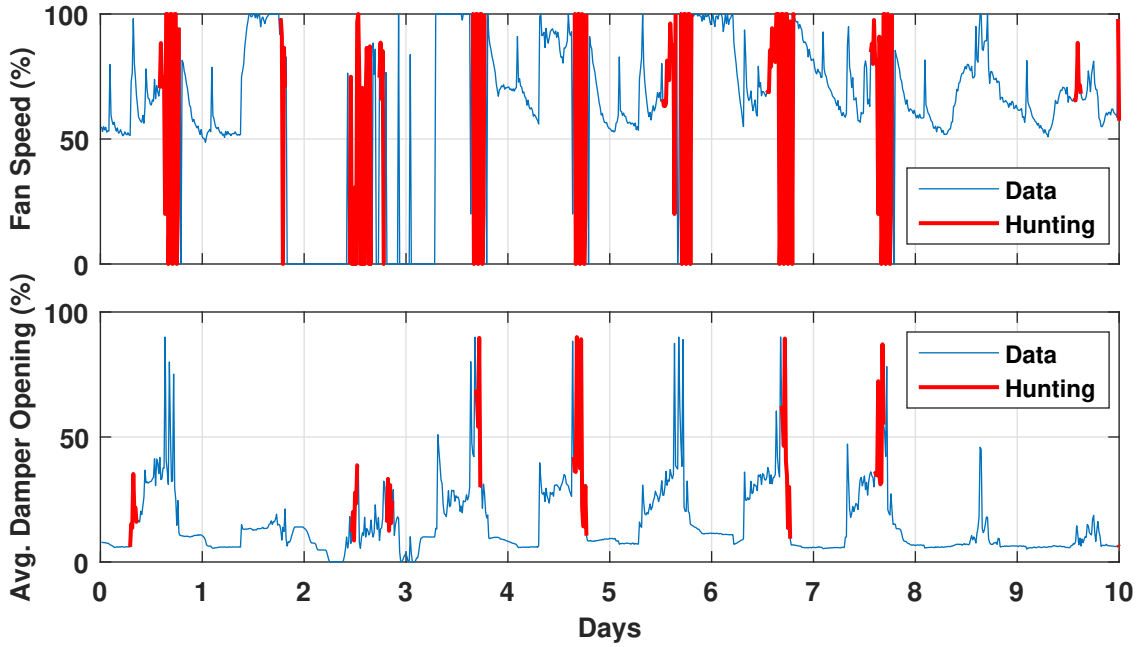

Figure 5.5: Fan speed and average damper opening data shows the occurrence and detection of simultaneous hunting (adapted from [30]).

(BAS) that centralizes and monitors over 200,000 control points across 14 million square feet of office and academic spaces.

The university currently uses Siemens APOGEE and the PPCL programing language to remotely control its HVAC equipment [146]. A digital control panel for a typical AHU is shown in Figure 5.6 highlighting key processes. For a given unit, there can be as many as seven control loops operating simultaneously: (1-2) Discharge air temperature control uses separate hot and cold supply water valve positions to regulate temperature, (3) Duct static pressure is regulated by the speed of the supply air fan, (4 - 6) Air quality parameters including CO_2, relative humidity, and outside air percentage are all controlled by affecting system setpoints, (7) Discharge air temperature setpoint is regulated by a control loop that factors in supply air quality and average VAV damper position. The last loop aims to minimize energy waste due to over pressurizing supply ducts for room air demands, an

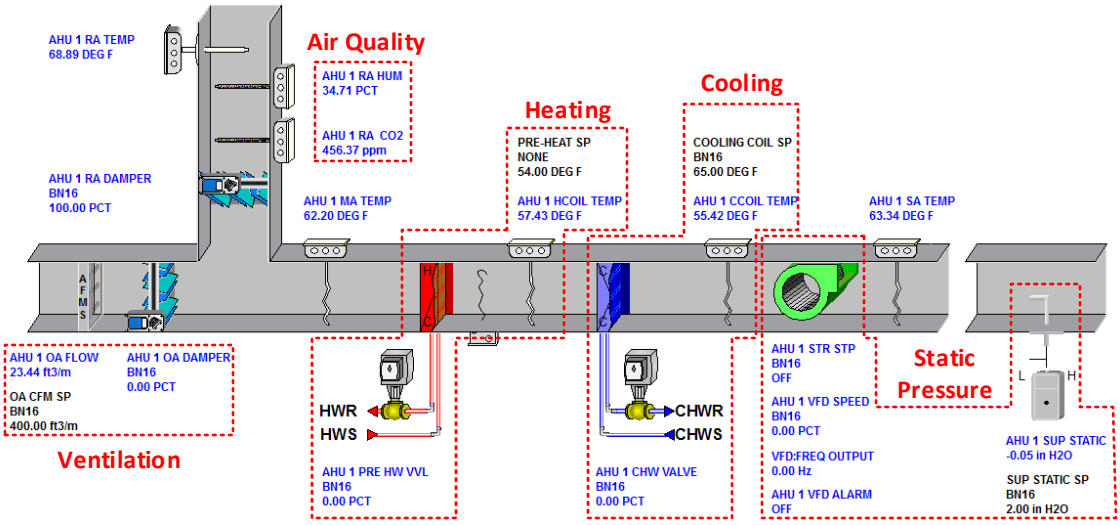

Figure 5.6: Typical APOGEE control panel configuration for an AHU at Texas A&M.

important savings consideration as the relationship between fan power and speed is cubic. The sheer number of control loops makes the use of a centralized BAC network essential.

Nearly all control loops across campus are PI/PID type controllers implemented using the PPCL LOOP command whose syntax is given as:

LOOP(type , pv , cv , sp , pg , ig , dg , st , bias , lo , hi , 0)

- **type:** refers to the direction of the controller and is either '0' for direct or '1' for indirect control. The standard definition for a direct process is one where the control variable increases in response to a rise in the system output. Alternatively, direct control corresponds to $e = y - r$ and indirect control to $e = r - y$ assuming all control gains are positive.
- **pv:** is the name of the Process Variable being regulated (temperature, flow rate, etc.).
- **cv:** is the name of the Control Variable used for actuation (opening, voltage, etc.).
- **sp:** is the name of the Set-Point signal against which **pv** is compared.

- **pg, ig, & dg:** are the proportional, integral, and derivative gains.
- **st:** is the Sampling Time of the loop. Code executes faster than **st** but the LOOP command is only executed after the sampling time has elapsed.
- **bias:** is the bias term for the LOOP command.
- **lo & hi:** are the saturation limits for the LOOP command. The algorithm has built-in anti-windup to deal with saturated control issues.

The PPCL User's Manual suggests initial values for the **pg** and **ig** gains of 1000 and 20 respectively. These are suggested as they typically provide conservative control for the vast majority of control situations. However, the fact that most PI loops on campus have these values for their control gains strongly indicates many loops never received additional tuning. As the next section will show, this is usually to the detriment of system performance and leads to either sluggish control or hunting behavior.

While ON/OFF control makes up the bulk of remaining control loops, recently commissioned buildings are being converted to use adaptive control loops. These loops use either the ADAPTM or ADAPTS statements that use internal weighting factors to update gains every sample time to minimize error. ADAPTM is a single-input, multi-output adaptive controller designed specifically for AHU supply air temperature control while ADAPTS is a general purpose controller for use with linear and non-linear processes [147]. Both algorithms require controllability, open-loop stability, and low dead-time.

In many cases, adaptive loops can provide superior performance but they are also susceptible to some common problems. At startup, ADAPT commands have a discovery period that cycles the system through many operating conditions to calibrate weighting factors. Without care, this can cause a system to enter undesirable operating states. ADAPT statements also have documented issues with sluggish reaction to setpoint changes over long periods and can experience lock-up if the control variable saturates. These difficul-

ties and the greater number of arguments in ADAPT statements (14 compared to 11) mean that ADAPT statements are often more difficult to implement and explains the persistent prevalence of PI type controllers in building HVAC systems on campus.

5.3 Survey of Campus HVAC Performance

To help establish the overall performance of current controls on campus and the prevalence of hunting in building HVAC equipment, a survey of ten buildings at Texas A&M University was conducted. In particular, the performance of AHU supply air fans and chilled water valves was analyzed. The corresponding signals used for hunting detection are fan speed and valve position.

Data for the selected buildings was collected at 15 minute intervals and the algorithm was applied with $A_{lim} = 15\%$ and $T_{lim} = 2$ hr. Table 5.1 gives the results of the campus-wide survey. Results show that hunting in HVAC controls is a widespread issue. Approximately 70% of all chilled water valves exhibited hunting for 6-78% of their operating time while 22% of supply air fans exhibited hunting for 6-26% of operating time. This indicates

Table 5.1: Results from Hunting Survey at Texas A&M University

Building	AHUs	Fans Hunting	Hunting Duration	Valves Hunting	Hunting Duration
1	3	1	11%	2	6-19%
2	10	0	-	10	33-78%
3	2	0	-	2	6-7%
4	1	1	23%	1	27%
5	5	0	-	4	7-31%
6	2	0	-	2	12-39%
7	2	0	-	0	-
8	8	7	6-26%	6	7-12%
9	6	0	-	5	14-31%
10	3	0	-	0	-

that measures aimed at minimizing hunting (e.g. cascaded control) can have a significant impact on improving HVAC performance and energy usage.

5.4 Implementation of Cascaded Control Loops in PPCL

From previous discussion of the LOOP command, the large magnitude of the recommended **pg** and **ig** gains stand out. For example, consider a discharge air temperature error of $0.1°$F. If **pg** truly equaled 1000, then an AHU valve would be commanded 100% open even though the error is quite small. Similarly, **ig** = 20 would completely saturate the valve after only 20 sample units assuming $t_s = 5$ sec. This behavior would be extremely aggressive and does not match the performance seen in loops across campus.

This discrepancy strongly indicates that there are scaling factors included in the LOOP calculation that reduce the magnitude of the control gains. To determine the exact values for these factors, data from campus buildings was used to optimally match gains to a PI controller. From the data, the form of the PPCL PI controller was determined to be Equation 5.3. This the same as a standard implementation of a discrete PI controller. The Matlab function `fmincon` was also used to determine that the relationship between k_p and **pg** as well as k_i and **ig**. As shown in Figure 5.7, the relationships given by Equation 5.4 provide an excellent match to the output of the LOOP command despite different gains and sampling times.

$$u = k_p \cdot e + k_i \cdot t_s \cdot \Sigma e \tag{5.3}$$

$$k_p = \mathbf{pg}/1000 \qquad \& \qquad k_i = \mathbf{ig}/1000 \tag{5.4}$$

Having determined the relationship between the gains in the LOOP command (**pg** and **ig**) and the control gains (k_p and k_i), the implementation of cascaded control in PPCL can be considered. Initial deployment for an AHU at the Utilities Business Office (UBO)

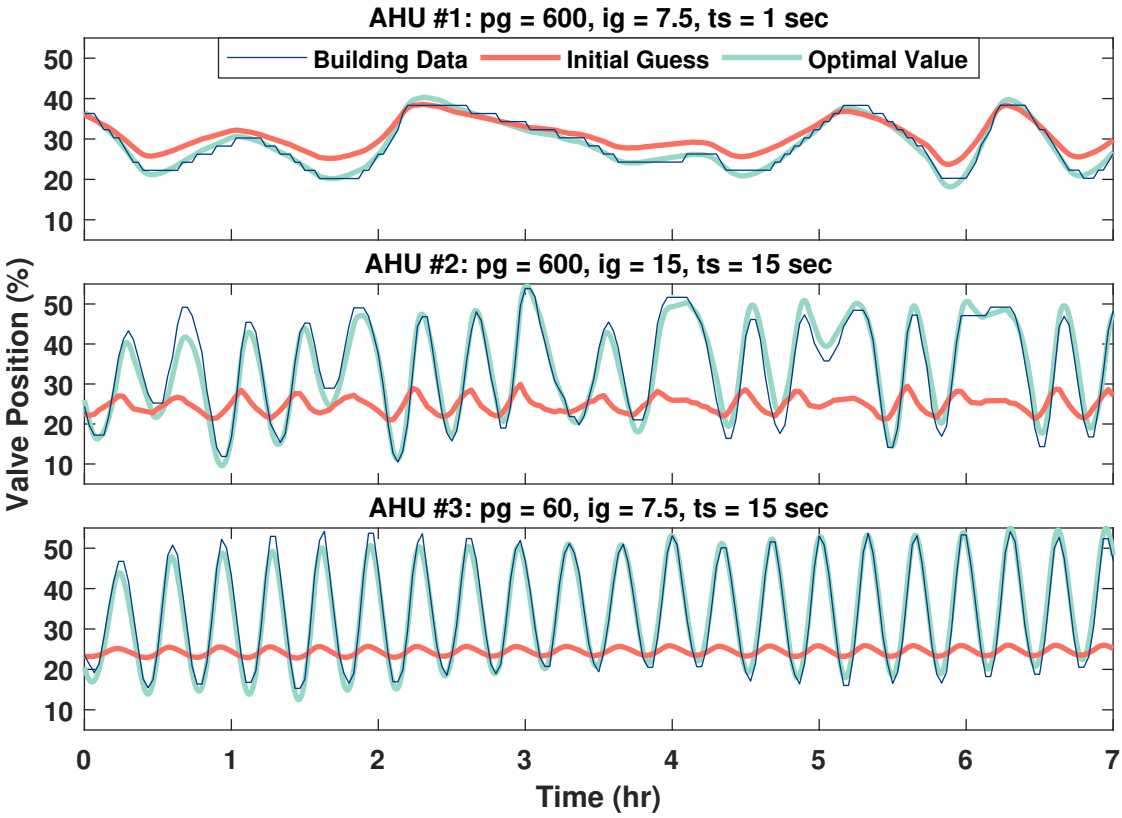

Figure 5.7: Optimization found PPCL gains that matched control output of Building 1600.

building located on the west campus at Texas A&M used Algorithm 5.1. The controller regulates Discharge Air Temperature (DAT) to its setpoint (DAT.S) using chilled water valve position (CCV). Note that the inner and outer loops are implemented using two LOOP commands and an intermediate virtual point named "AH01.DATLOOP1.ILSP" that stores the inner loop setpoint (i.e. the outer loop output). Although the LOOP command has built-in saturation and anti-windup, it will only stop integration of each LOOP independently. This becomes an issue when the inner loop (i.e. valve position) is saturated but the outer loop remains enabled. Lines 0060-0070 deal with this issue by checking if the valve is saturated and then dynamically enabling/disabling the outer loop LOOP command on line 0110 accordingly. The code is somewhat lengthly, requires creation of extra points, and has 7 tunable variables.

```
0010 C Point Name Abbreviations
0020 DEFINE(X,"AH01.")
0030 DEFINE(Y,"AH01.DATLOOP1.")
0040 DEFINE(Z,"AH01.DATLOOP2.")
0050 C Outer Loop Anti-Windup
0060 IF("%X%CCV" .GT. 1 .AND. "%X%CCV" .LT. 99) THEN SET(0,SECND2)
0070 IF(SECND2 .GT. "DISABLE.TIMER") THEN DISABL(110) ELSE ENABLE(110)
0080 C Inner Loop Control
0090 LOOP(128,"%X%DAT","%Y%ILSP","%X%DAT.S","%Y%P","%Y%I",0,"%Y%TIME
  ","%Y%BIAS",50,70,0)
0100 C Outer Loop Control
0110 LOOP(0,"%X%DAT","%X%CCV","%Y%ILSP","%Z%P",0,0,"%Z%TIME","%Z%BIAS
  ",50,70,0)
```

Algorithm 5.1: Initial PPCL Cascaded AHU Control Implementation

A different approach to cascaded control in PPCL can shorten the code and simplify its implementation. Consider the inner loop control signal given in Equation 5.5 where $e_1 = r - y_1$, $e_2 = u_1 - y_2$, B_1, and B_2 are outer and inner loop errors and biases respectively. The first two terms resemble the output of a PI controller with PI gains of $k_L k_p$ and $k_L k_i$ while the final terms are a combination of loop biases and inner loop feedback.

$$\begin{aligned} u_2 &= k_L e_2 + B_2 \\ &= k_L(u_1 - y_2) + B_2 \\ &= k_L\left[(k_p e_1 + k_i \Sigma e_1 + B_1) - y_2\right] + B_2 \\ &= \underbrace{k_L k_p(r - y_1) + k_L k_i \Sigma(r - y_1)}_{\text{PI Control}} + \underbrace{B_2 + k_L B_1 - k_L y_2}_{\text{Bias}} \end{aligned} \tag{5.5}$$

Expressed in this form, the cascaded controller can clearly be implemented as a *single* LOOP command without the need for the extra intermediate virtual point as before. This is important because inner/outer loop anti-windup issues are avoided as the new algorithm takes advantage of the built-in PPCL saturation measures. PPCL code based on this implementation for AHU control is given by Algorithm 5.2 taking into account that the outer and inner loops are reverse and direct acting respectively. The bias term is calculated and stored in a local variable ($LOC1) on line 0040 because PPCL does not allow for calculations inside of function calls. Note that the simplified code eliminates fives lines and

reduces the number of tuning variables to five. One disadvantage of this implementation is the loss of ability to have different sampling times for the inner and outer loops. Despite this, all benefits of cascaded control can still be realized even through the two loops operate at the same sampling rate.

```
0010 C Point Name Abbreviation
0020 DEFINE(X,"AH01.")
0030 C Bias Term Calculation
0040 $LOC1 = "%X%BIAS" + "%X%KL"*"%X%DAT"
0050 C Cascaded Control
0060 LOOP(0,"%X%DAT","%X%CCV","%X%DAT.S","%X%P","%X%I",0,"%X%TIME",
  $LOC1,0,100,0)
```

Algorithm 5.2: Simplified PPCL Cascaded AHU Control Implementation

The final sections of this chapter will detail results of applying cascaded control to three campus buildings. Details about the size, layout, and location of each building will be provided as well as comparisons between original PI and cascaded control. Typical building PPCL code can be found in Appendix E.

5.5 Building 1497: Utilities Business Office

Working with the staff at the Texas A&M Utilities and Energy Services, limited access to the HVAC control systems of Building 1497 was established. This building is known as the Utilities Business Office (UBO) and is located in the Veterinary Medicine quadrant. The UBO is a single-story, rectangular building consisting of ten temperature controlled zones and one unconditioned server room with the general floor plan given in Figure 5.8. The building is serviced by a single rooftop AHU consisting of a variable speed fan, chilled water coil with valve, and return/outdoor air dampers. The unit has two sensors for discharge air temperature and end static pressure. Zones 1-10 have VAV terminal boxes equipped with a hot water reheat coil and an air damper. The hot and cold water needs of the building are serviced by two dedicated loops that provide access to the universities centralized heating and cooling water supply.

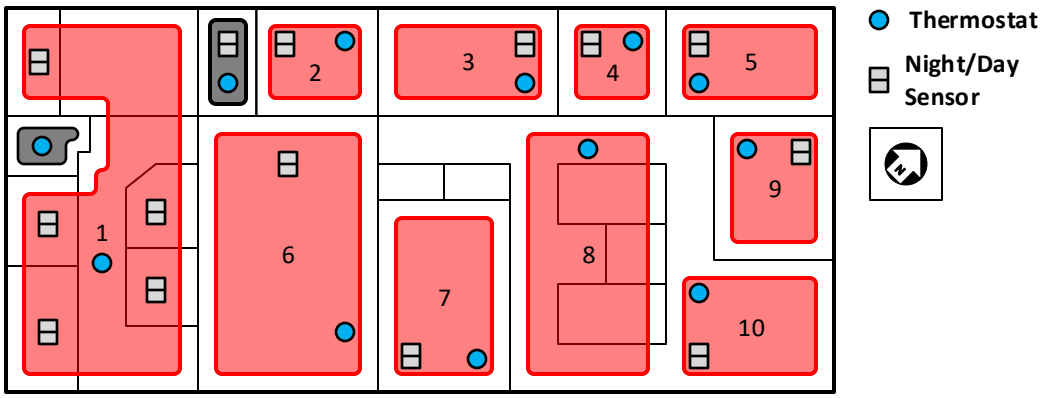

Figure 5.8: Zone layout for the Utilities Business Office at Texas A&M University.

The UBO building uses a complex, nested PI-based architecture for its HVAC control (Figure 5.9). During normal operation, PI controller (1) modulates the speed of the supply fan to maintain static pressure in the air ducts. The End Static Pressure (ESP) setpoint is the output of another PI controller (2) that compares the damper demand given by Equation 5.6 to a design setpoint $D_{set} = 60$. Room air temperature is regulated by a cascaded damper control architecture similar to the one discussed in [116]. An outer loop PI controller (3) uses room temperature error to calculate a flow demand $F_i \in [0, 100]$ that determines the flow rate required for each room. Flow demand is converted to a flow rate though linear interpolation between minimum ventilation requirements and the maximum system output. Inner loop control (4) uses local control and a flow rate sensor to match the outer loop flow setpoint. Similar to ESP control, the AHU discharge air temperature setpoint is generated by a PI controller (5) using the cooling demand calculation of Equation 5.7 and the design setpoint $C_{set} = 60$. PI controllers (6-7) modulate hot and cold water supply valves to match the exit/supply air temperature setpoint.

$$D = \frac{3}{5}\max(\theta_i) + \frac{2}{5}\left(\frac{1}{n}\sum_{i=1}^{n}\theta_i\right) \quad (5.6) \qquad C = \frac{3}{5}\max(F_i) + \frac{2}{5}\left(\frac{1}{n}\sum_{i=1}^{n}F_i\right) \quad (5.7)$$

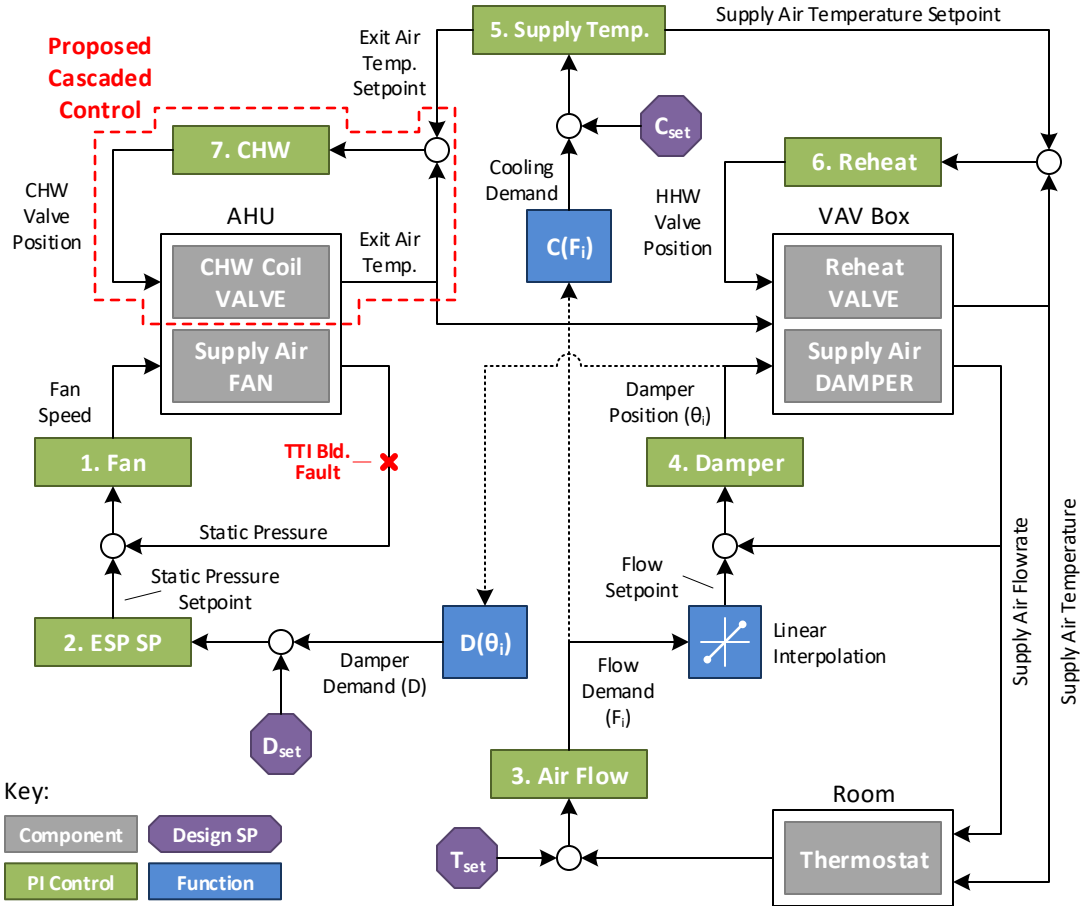

Figure 5.9: Process flow for UBO HVAC control.

UBO chilled water valve control used to regulate AHU exit air temperature has documented issues with actuator hunting. As seen in Figure 5.10, the valve had identified periods of hunting accounting for 50% of its operating time during the first half of August 2015. Oscillations are most pronounced during low load conditions such as early morning or during cool winter weather. For example, the valve hunted 57% of its operating time during the three month period of Nov. 1st, 2013 to Feb. 1st, 2014 while the valve hunted only 14% from May 1st to August 1st, 2016.

AHU exit air temperature control has three distinct hunting behaviors. Under high load, valve control typically does not hunt. In early spring, temperatures are usually warm in the afternoon but cool in the evening resulting in hunting late in the day (Figure 5.11).

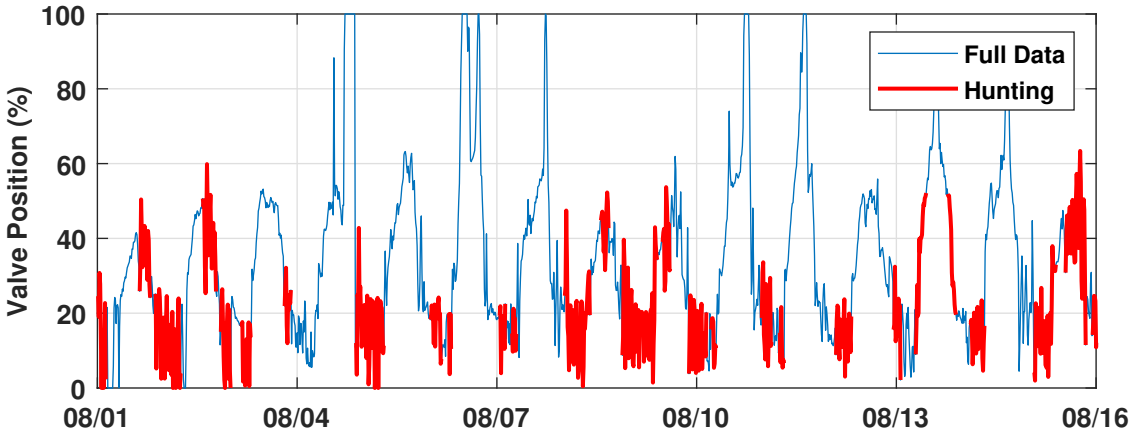

Figure 5.10: In August 2015, the UBO chilled water valve hunted (red) fully half of its operation time.

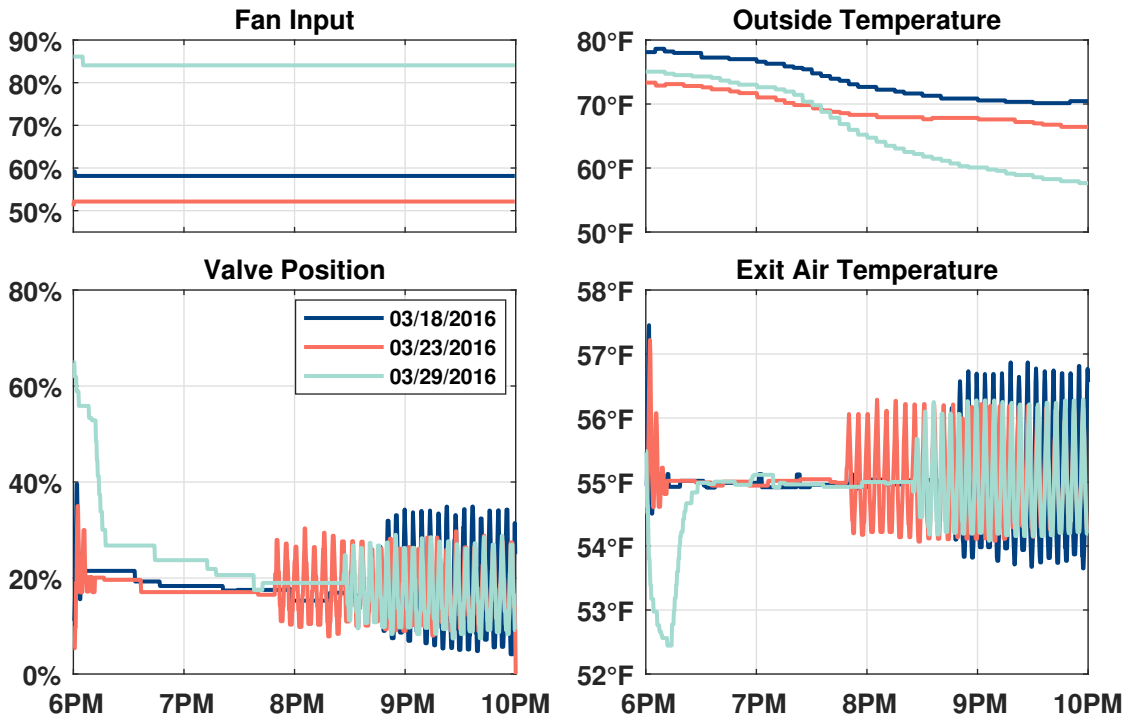

Figure 5.11: The UBO chilled water valve control often begins to hunt in late evening.

On other spring days, there is never enough load to prevent hunting behavior (Figure 5.12). This behavior indicates that control performance is strongly tied to the operating conditions of the system.

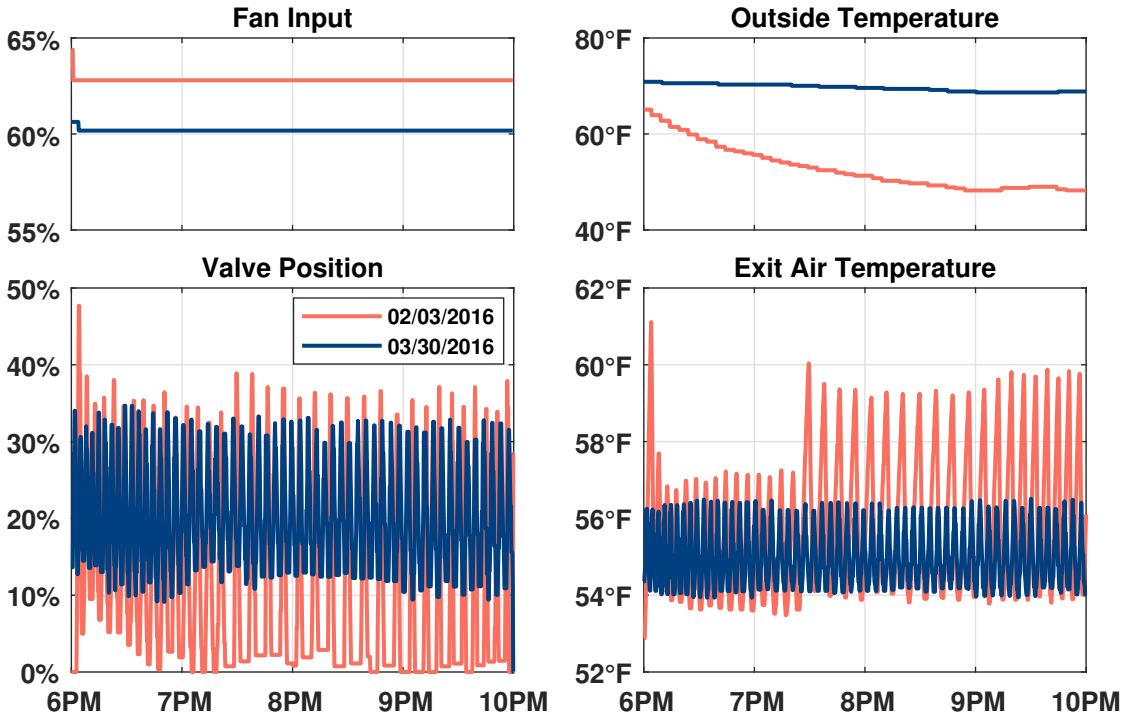

Figure 5.12: The UBO chilled water valve hunts continuously in low load conditions.

In addition to time-varying system characteristics, the chilled water valve has issues with cold water slug flow. Figure 5.13 shows that for a period of 2 hours, exit air temperature begins to chatter continuously despite little to no change in valve position. The cause of this behavior can be explained by Figure 5.14 where oscillations in primary supply water temperature lead oscillations in exit air temperature despite constant chilled water valve position at 15% open. When there is no flow, both the supply water and exit air temperatures rise. After a slug of chilled water passes through the valve, both temperatures drop with supply water leading. Some of the observed hunting behavior in the UBO building may be due to this slug flow behavior, especially in cases when the valve is almost completely closed.

Cascaded control was applied to the chilled water valve control at the UBO Building. Testing utilized Algorithm 5.1 and was conducted daily from 6-10 pm. Several step identi-

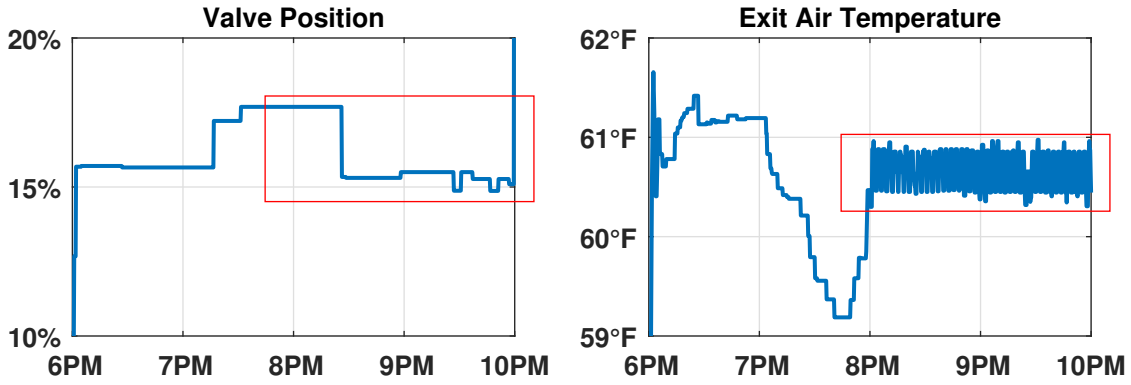

Figure 5.13: The UBO exit air temperature often begins to hunt in late evening.

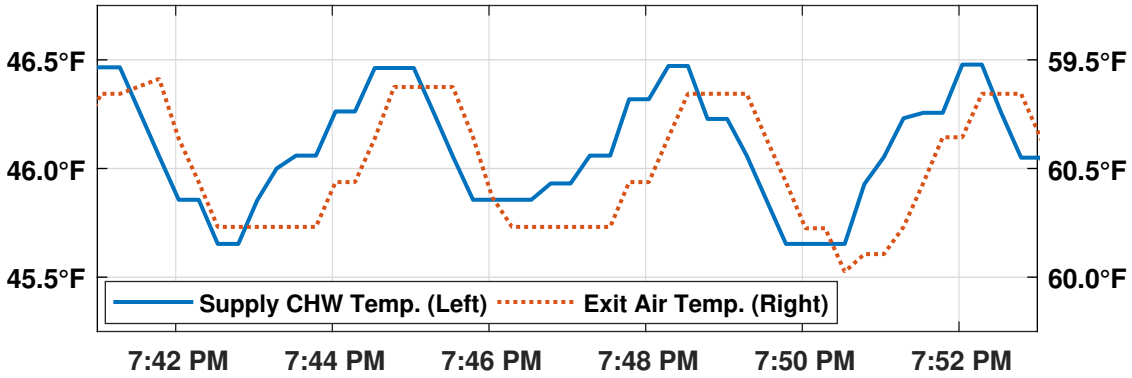

Figure 5.14: Despite constant valve position, both supply water and exit air temperatures oscillate indicating valve slug flow.

fication tests were performed on the system for a range of supply fan speeds from 20-90% to capture different loads. Cascaded gains of $k_L = 4$, $k_{pc} = 1.25$, and $k_{ic} = 0.2$ were chosen using the NGM analysis and the tuning procedure from Chapter 2. Testing began October 2015 and ran through approximately through the end of the year. Figure 5.15 shows the improved performance of cascaded control by comparing data from two days with similar load (i.e. valve openings) and outside air temperatures. Figure 5.16 shows additional results for a range of load conditions, highlighting that hunting behavior seen with the original PI controller has been eliminated without sacrificing performance.

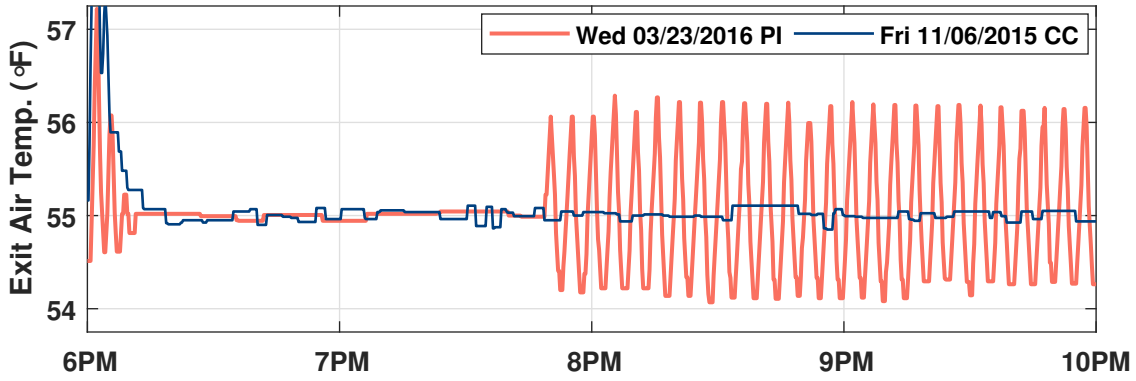

Figure 5.15: Comparison of PI and cascaded control at UBO under similar load conditions.

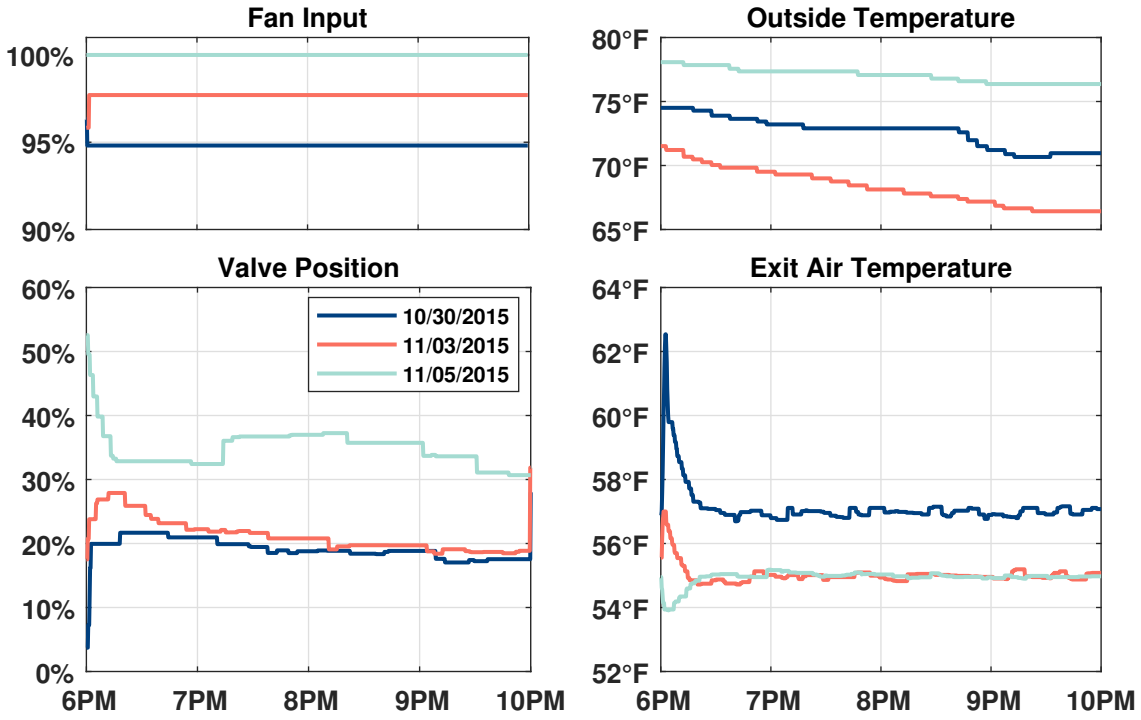

Figure 5.16: Cascaded control eliminated UBO hunting behavior seen with PI control.

5.6 Building 0474: Philosophy Department & Student Senate Offices

Completed in 1914, Building 0474 originally consisted of a half-basement and two upper stories that served as the campus YMCA [148]. As such, the lower level contained an exchange store, barber shop, and a swimming pool. The upper floors housed a two-

Figure 5.17: Basic layout of HVAC zones and exterior of the YMCA Building.

story auditorium and interfaith chapel. A fourth floor was added six years later for student and visitor lounges. After construction of a new campus natatorium in 1932, the pool was filled in and converted to a bowling alley. The construction of the Memorial Student Center in 1951 and the All Faiths Chapel in 1957 prompted the YMCA to be completely converted to an office building by filling in the two-story auditorium with an intermediate floor. A total renovation was completed in 2012 that included upgraded HVAC equipment and controls. The building currently houses the Texas A&M Philosophy Department and offices for the Student Senate. Despite being over 100 years old and undergoing many conversions, the building is still known as the YMCA Building.

In its current form, the YMCA Building has approximately 54,000 ft^2 of office space consisting of four floors with approximately 20 heating and cooling zones each (Figure 5.17). Each floor has its own AHU where return and outside air are mixed and conditioned. Every zone has a parallel fan powered VAV terminal box with hot water reheat coil. These boxes have return air ducting that draws warm air from the ceiling plenum for 'free' reheat and can use the heating coil to substitute reheat when at the minimum supply

Table 5.2: Summary of 2017 Hunting Evaluation at Building 0474.

AHU	1	2	3	4
CHW Valve	2.29%	1.05%	11.4%	2.12%
Fan Speed	2.78%	0.17%	0.32%	0.52%
DAT Setpoint	1.53%	0%	0.10%	1.00%

air flow rate. The building control system has a wide array of sensors including relative humidity, CO_2, and outside air flow rate (ventilation). The overall temperature control structure is the same as at the UBO building (see Figure 5.9) except with additional complexity due to the upgraded terminal boxes and ventilation sensors.

YMCA Building operations were transferred to a new server in the spring of 2017. Full historical trending of relevant HVAC system operating points began around August 1st with a sample time of 5 minutes. Table 5.2 gives the results of analyzing each floors AHU operation for fan and chilled water valve hunting through December 31st, 2017. Overall, control in the YMCA building does not display much hunting behavior except for the third floor where the CHW valve hunts just over 10% of its operating time.

Observations of building performance point to two main causes for the hunting behavior. First, identified hunting in AHU3 occurs almost entirely in low cooling conditions. This indicates that the PI controller was likely tuned for mid-to-high load conditions. While there may be some reduction in hunting from implementing the cascaded controllers (mainly with the third floor), the main benefits will be improved tracking performance due to more aggressive performance afforded by the cascaded architecture.

The second cause of valve hunting seems to be oscillations in the AHU discharge air temperature setpoint as with the data in Figure 5.18. Exit air temperature setpoint is set by a PI controller (see Figure 5.9) whose output can swing five or more degrees several times a day. As the CHW valve control tries to follow the setpoint changes, the resulting

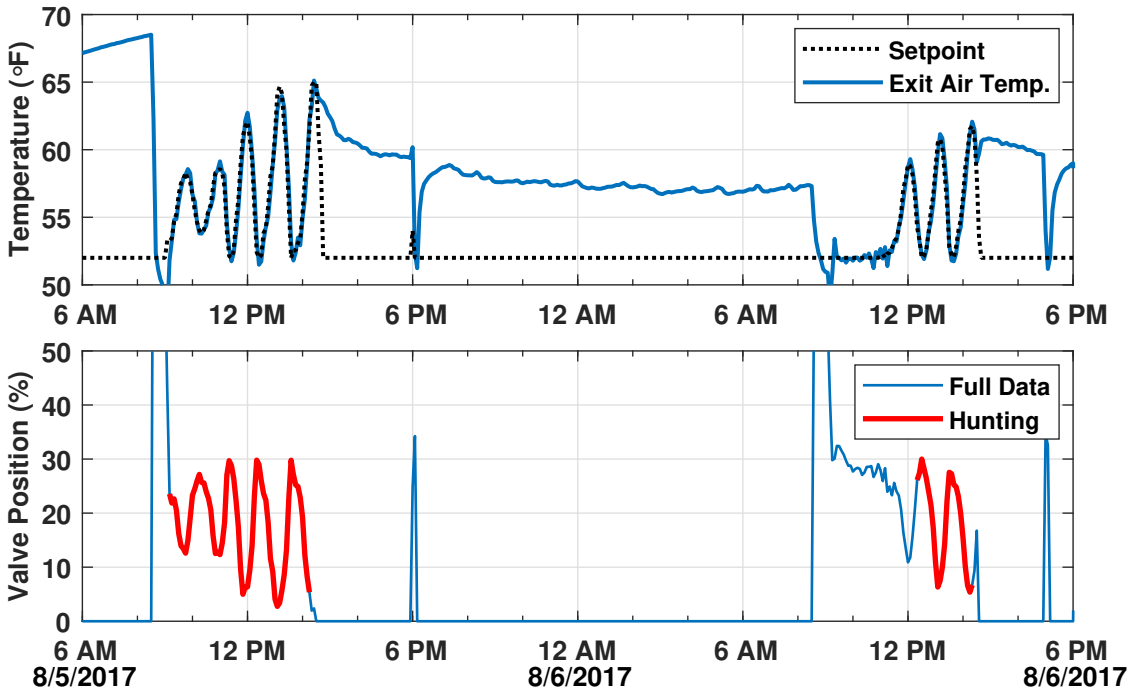

Figure 5.18: Hunting in the YMCA Building AHU exit air temperature setpoint may be identified as hunting in the chilled water valve control.

fluctuations in CHW demand cause large oscillations in chilled water valve position that can be identified as hunting. To estimate the effect setpoint hunting on the identified CHW valve control, Table 5.2 also includes the results of applying the hunting algorithm to discharge temperature setpoint with an amplitude limit of 3-5°F. As expected, a small part of the identified valve hunting overlaps with setpoint oscillations with the remainder mostly from operating in low demand conditions. While changes to the supervisory DAT setpoint PI controller were beyond the scope of this project, cascaded control was applied to the chilled water valve control. Total elimination of hunting behavior in valve control may not be realized due to the supervisory control issue, however, any reduction of valve hunting behavior can be attributed to the application of cascaded control.

Algorithm 5.2 was initially tested on the fourth floor AHU chilled water valve and later applied to the other three floors. All four original PI controllers had gains of **pg** =

1000 and **ig** = 20 with a sampling time of $t_s = 1$ second which are the recommended LOOP gains in the PPCL User's Manual. As a starting point, the inner loop gain was set at a conservative value $k_L = 0.5$ and the outer loop gains at $k_{pc} = 1$ and $k_{ic} = 0.04$. When converted to nominal gains using the relationships of Equation 2.33, $k_1 = 1$ and $k_2 = 0.02$ are equal to the original PI control gains. This choice should provide similar transient performance to the original control but with the added linearization benefits of the inner loop control. The resulting control gains (**pg**$_\mathbf{c}$ and **ig**$_\mathbf{c}$) used in Algorithm 5.2 are calculated using Equation 5.8. For the bias term, the inner loop bias is the average of the minimum and maximum valve position (i.e. $B_2 = 50\%$). The outer loop bias is the average of the minimum and maximum allowable exit/discharge air temperatures, $52°\text{F}$ and $65°\text{F}$ respectively. The bias term **B** for the PPCL code is therefore given by Equation 5.9 where **DAT** is discharge air temperature. Note that the bias term of the LOOP command has no scaling factor. Inner loop gains for all units were later increased to $k_L = 1$ starting in March 2018 to increase the level of cascaded linearization.

$$\mathbf{pg_c} = 1000 k_L k_{pc} = 500 \qquad \& \qquad \mathbf{ig_c} = 1000 k_L k_{ic} = 20 \tag{5.8}$$

$$\begin{aligned} \mathbf{B} &= B_2 + k_L(\mathbf{DAT} - B_1) \\ &= 50\% + \left(0.5\frac{\%}{°\text{F}}\right)\left(\mathbf{DAT} - \frac{65°\text{F} + 52°\text{F}}{2}\right) \\ &= 20.75\% + \left(0.5\frac{\%}{°\text{F}}\right)\mathbf{DAT} \end{aligned} \tag{5.9}$$

After initial testing on the top floor unit, cascaded control for discharge air temperature control was implemented throughout the YMCA building. To fairly compare HVAC performance before and after implementation, weather disaggregation was applied to the data using the Degree Day (DD) method. A DD is related to how long and by how much outside ambient conditions stay above or below a baseline temperature. Usually assumed

to be 65°F, this balance temperature is the ambient load condition under which a building requires no conditioning. Cooling and heating degree days, CDD and HDD respectively, can be thought of as the area above or below the balance temperature for a given outside temperature profile. The DD is therefore a useful tool to compare HVAC data as it inherently normalizes for warmer or colder weather.

System performance will be measured using two metrics: Root-Mean-Square (RMS) error and average (AVG) error. For error to be calculated, the system must be ON and in cooling mode for more than 90 minutes. These criteria are important because, particularly on weekends, AHUs will cycle ON/OFF randomly for short periods of time to maintain building air quality. These bursts are not long enough for the AHUs to reach their temperature setpoints and are not representative of the tracking ability of the valve controller. Detecting cooling mode is important as the chilled water valve can be saturated at 0% causing large error accumulation despite not being utilized. Criteria for detecting these conditions are given in Table 5.3 and cooling time is then found by the intersection of ON/OFF and the negation of HEAT detection.

Typical daily AHU results from 6AM to 6PM are shown in Figure 5.19. Each AHU tracks is discharge temperature setpoint throughout the day and displays no hunting behavior. Hunting algorithm results are givn in Table 5.4, where the hunting in AHU 3 has been reduced by 45%. Hunting percentages for all other floors are up slightly ($\sim$1%) but still small enough to not indicate an issue.

Table 5.3: Cooling Mode Detection Criteria for YMCA Building.

Condition	Criteria	Comment
ON/OFF	$\omega_i = 0$	Minimum ω_i when LOOP is active is 20%.
HEAT	$\delta_i = 0$	Identified when true continuously for 90 minutes.

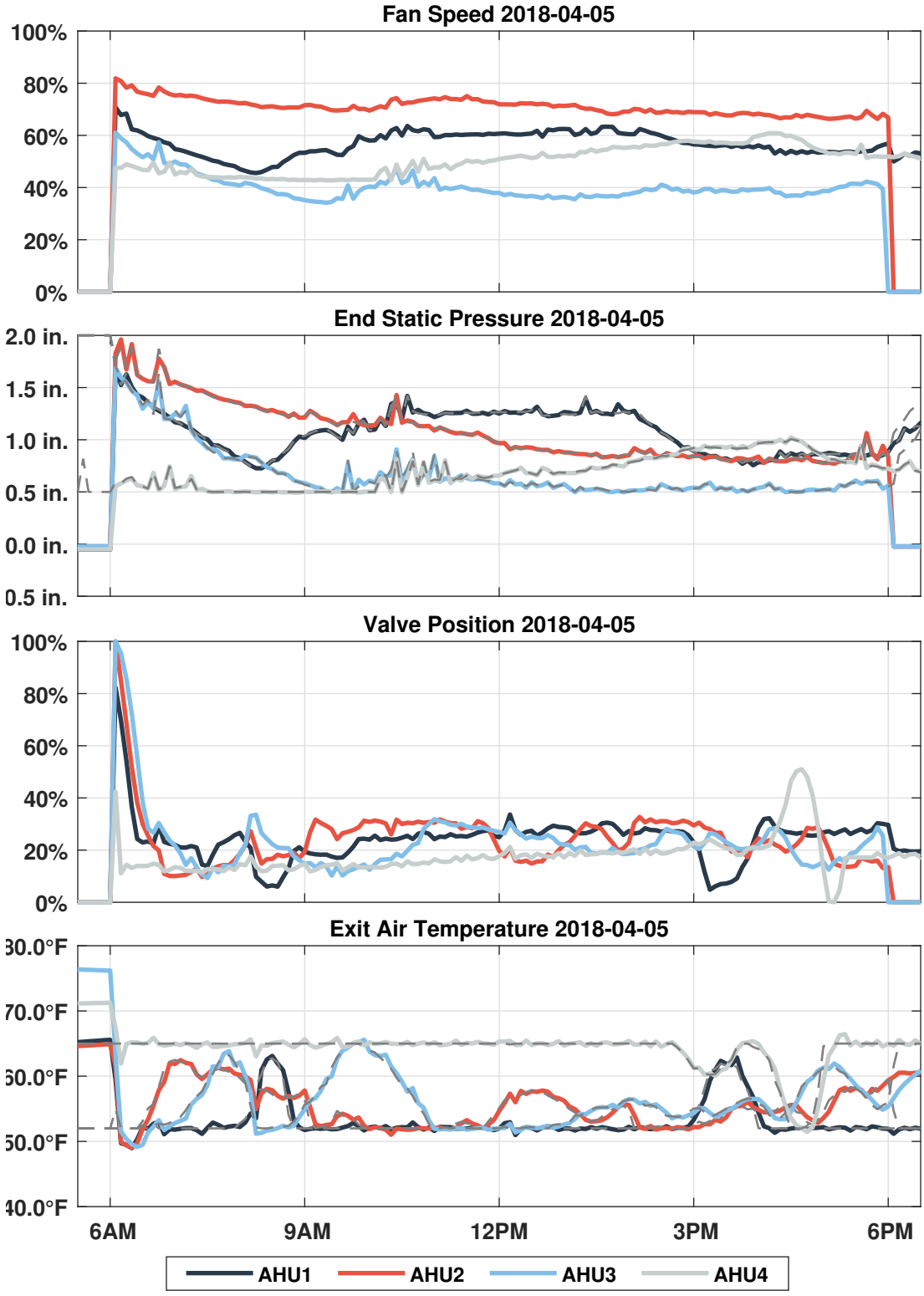

Figure 5.19: Typical performance of DAT cascaded controllers at YMCA Building.

Table 5.4: Summary of 2018 Hunting Evaluation at Building 0474.

AHU	1	2	3	4
CHW Valve	1.91%	3.79%	6.32%	3.35%
Fan Speed	1.24%	0.02%	0.42%	0.40%
DAT Setpoint	0.55%	1.11%	0.25%	1.28%

Improvements in system performance are better seen in Figures 5.20-5.23 that show PI data from 2017 and cascaded control data from 2018. For each floor, at least marginally, there is a reduction in dependence on load condition (i.e. flatter trend lines) and a tighter dispersion of error metrics with cascade control than PI control, particularly with AVG error. This is seen visually and in the decrease in standard deviation from the trend line. Improved RMS error results show that the controllers are better able to track setpoint changes while less negative AVG error values means occupants will be more comfortable rather than slightly warm (because $e = r - y$).

The minimal improvements in AHUs 1 & 4 are the results of two main issues. For AHU 1, PI data from 2017 has significantly less days in cooler weather than CC in 2018. As these conditions tend to result in more error for this unit, the 2017 trend line is smaller in this region than expected. AHU 4 data is the result of the unit being slightly undersized for observed loads. In warm weather, Unit 4 will be maxed out with the valve and supply fan operating at 100% but only slowly reaching command setpoints for static pressure and air temperature. This leads to large errors in warm weather that will be similar for both PI and CC control. However, in Figure 5.23 there does appear to be an improvement in performance in cooler conditions. Overall, cascaded control was applied successfully to all AHUs at the YMCA building and showed performance benefits without introducing control hunting issues.

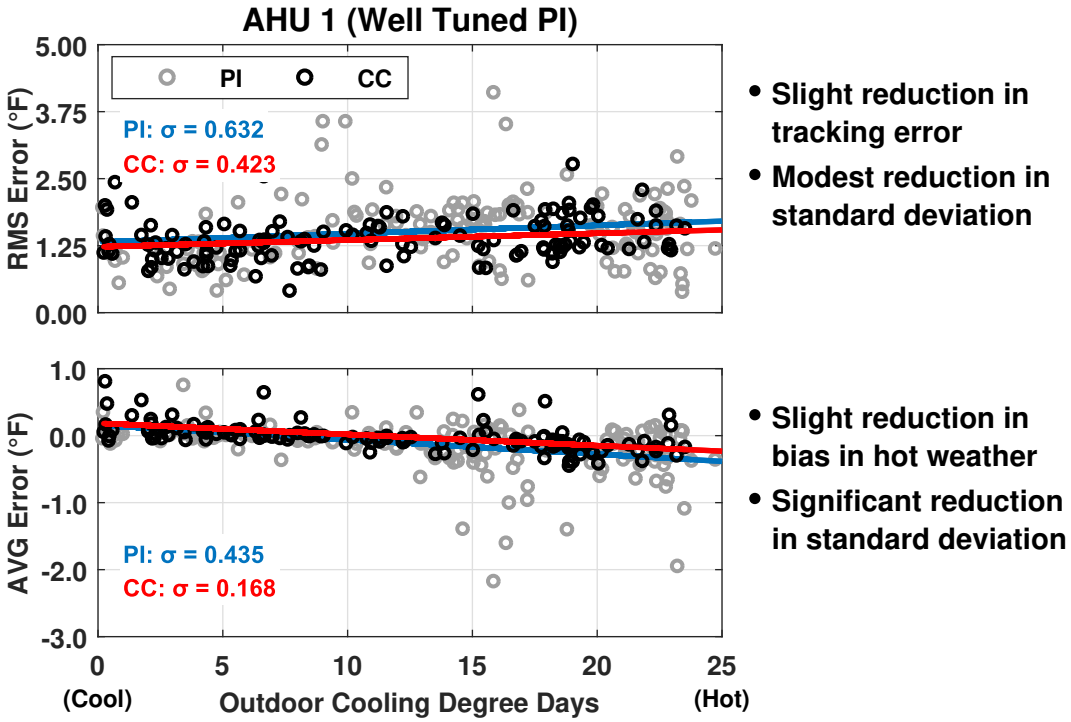

Figure 5.20: AHU 1 performance comparison between PI and cascaded control.

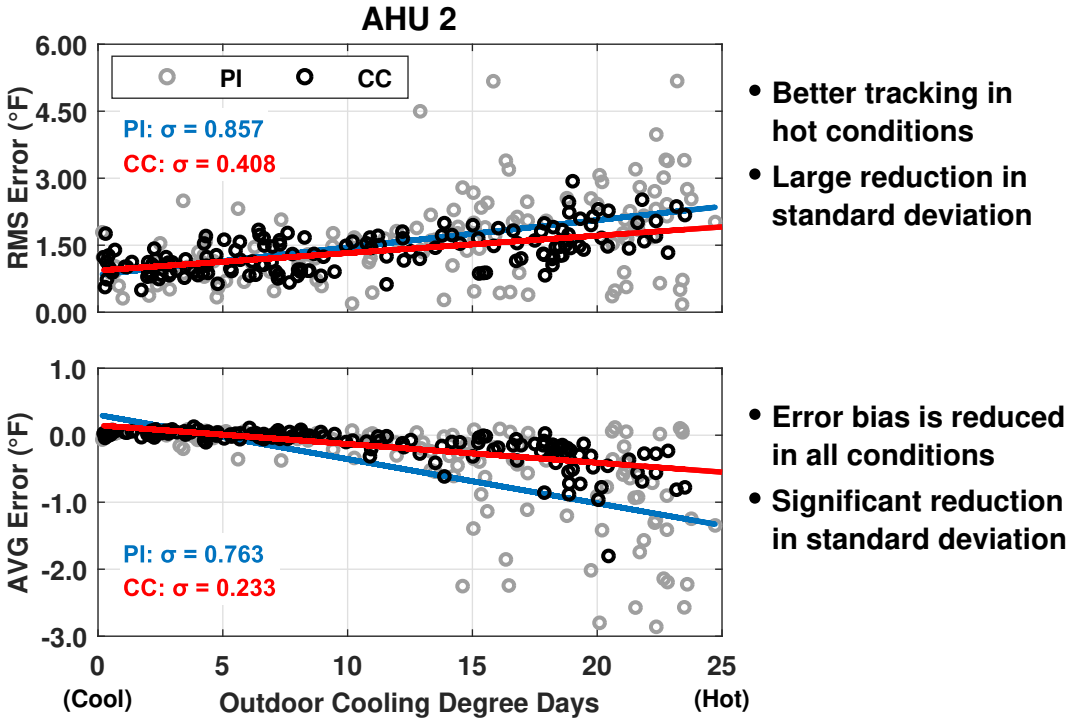

Figure 5.21: AHU 2 performance comparison between PI and cascaded control.

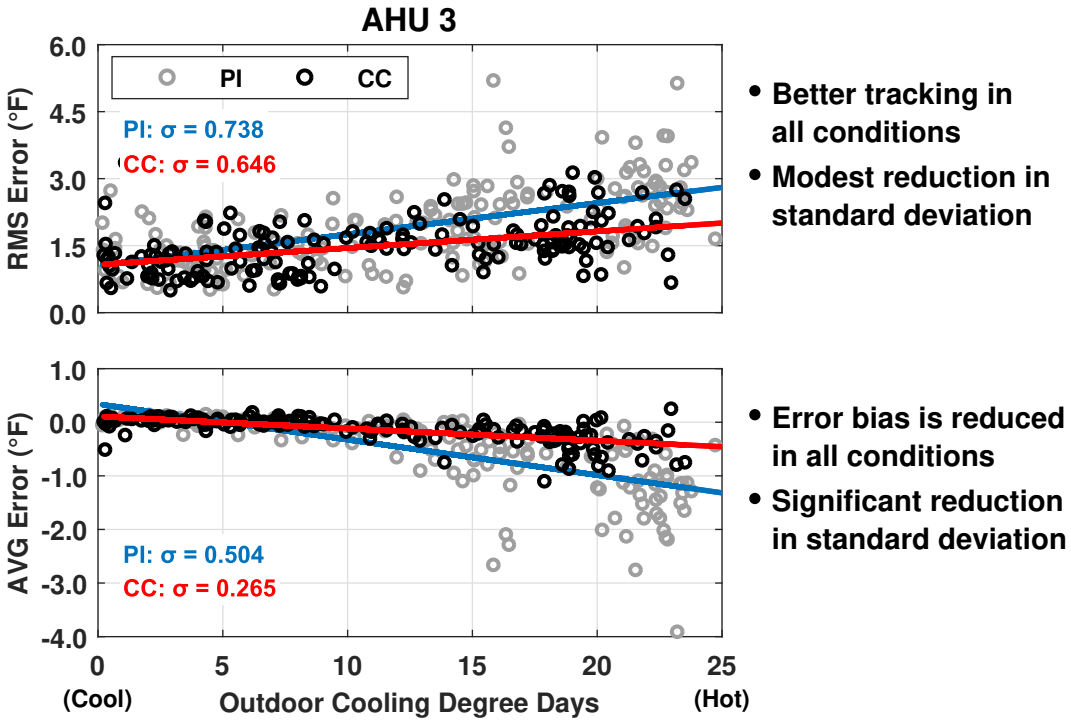

Figure 5.22: AHU 3 performance comparison between PI and cascaded control.

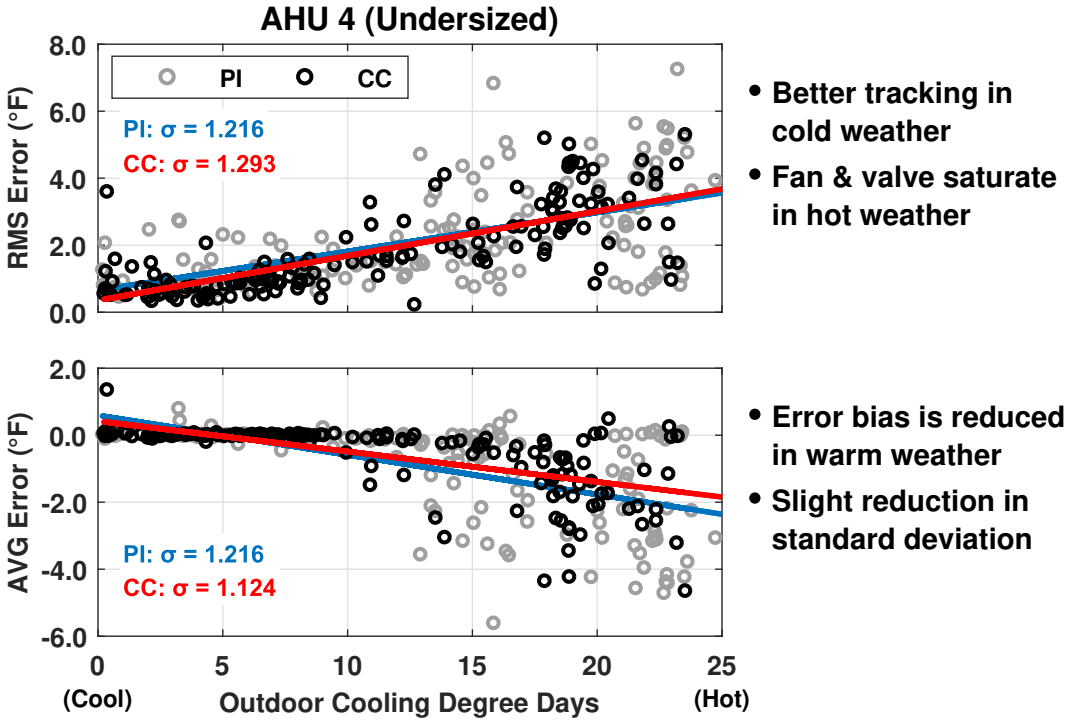

Figure 5.23: AHU 4 performance comparison between PI and cascaded control.

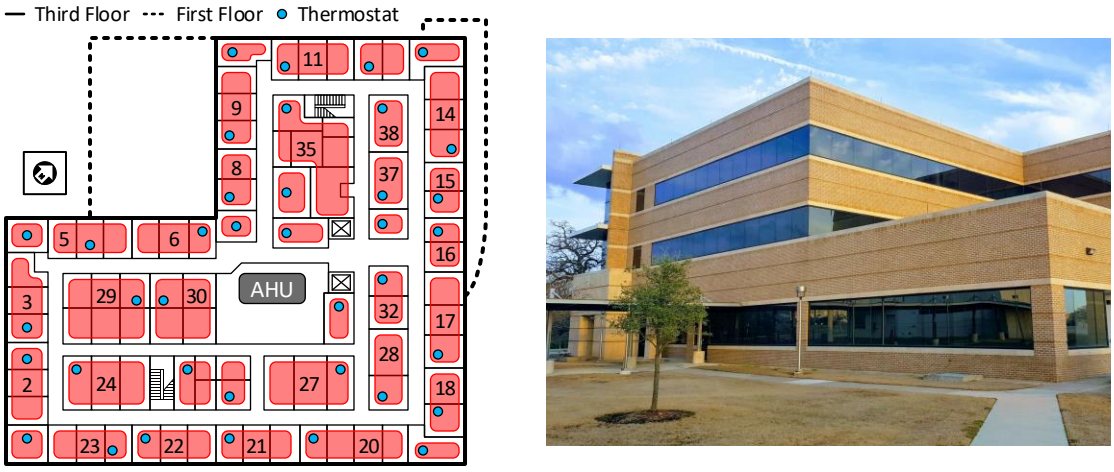

Figure 5.24: Basic layout of HVAC zones and exterior of the TTI Building.

5.7 Building 1600: Gilchrist (TTI) Building

The Gilchrist Building is an approximately 85,000 ft^2 office and research facility located in the Texas A&M Research Park on west campus. The building was completed in 1999 and consists of three floors in a mostly L-shaped configuration with additional space on the ground floor. The building hosts a branch of the Texas A&M Transportation Institute (TTI) whose mission is to develop solutions to challenges in all modes of transportation. Institute facilities at this location include a driving simulator, an eye tracking system, a hardware-in-the-loop simulation testbed, and a fully instrumented test vehicle. There are 32 heating and cooling zones on the first floor, 40 on the second and 38 on the third roughly corresponding to the floor plan given in Figure 5.24.

The Gilchrist Building utilizes a Dedicated Outdoor Air System (DOAS) for its ventilation requirements. The DOAS, also known as a fresh air unit, is functionally similar to a normal AHU except that its supply air is 100% outside air (see Figure 5.25). The system supplies preconditioned ventilation air to AHUs on every floor. Each AHU has a local cooling coil to make up for latent heat in the return air stream. Parallel fan powered

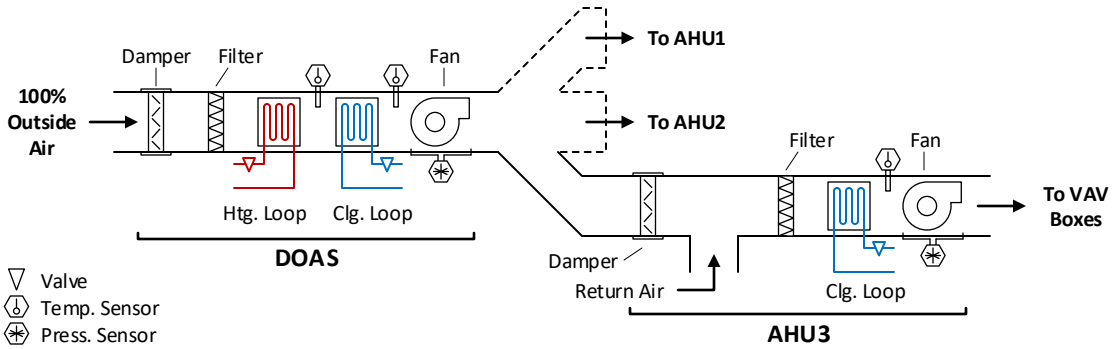

Figure 5.25: The Gilchrist Building uses a dedicated outdoor air unit for ventilation air.

VAV terminal boxes in each zone have reheat capabilities if necessary. Separating the ventilation stream represents a new trend in building HVAC systems and has shown promise in reducing energy usage between 10-40% [149, 150] as subsystems can be downsized and/or other cooling technologies utilized for return air conditioning.

Historical trended data for this building is not available due to software limitations. However, dynamic trending of critical points was facilitated by the Texas A&M Utilities Office. This method of data collection records point values in real time with a maximum sampling time of 2 minutes and/or when point values change above a threshold. Data was collected from approximately 10 am to 4 pm from November through December 2017 to capture original building operations. The nature of dynamic trending resulted in data sets with random sampling times. To utilize the hunting algorithm of Section 5.1, each dataset was resampled to enforce a 2 minute sampling time.

Even though the TTI Building is less than 20 years old and has an advanced HVAC system design, the AHU chilled water valve controls still have significant hunting issues. As seen in Figures 5.26 and 5.27, each floors AHU valve control experiences some level of hunting behavior. AHU1 has a hunting period of approximately 60 minutes, AHU2 30 minutes, and AHU3 20 minutes. The level of hunting, in terms of amplitude and period, is again correlated with system load as seen when outdoor air temperature approached 70°F.

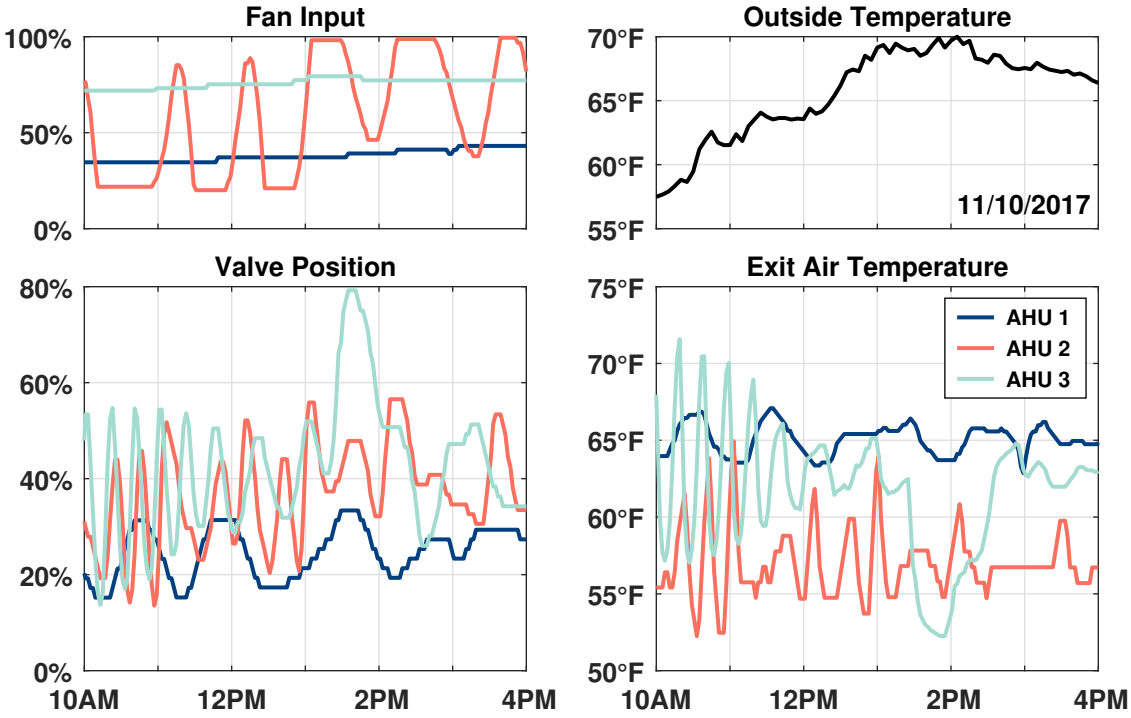

Figure 5.26: Chilled water valve hunting becomes less prominent as outside air warms.

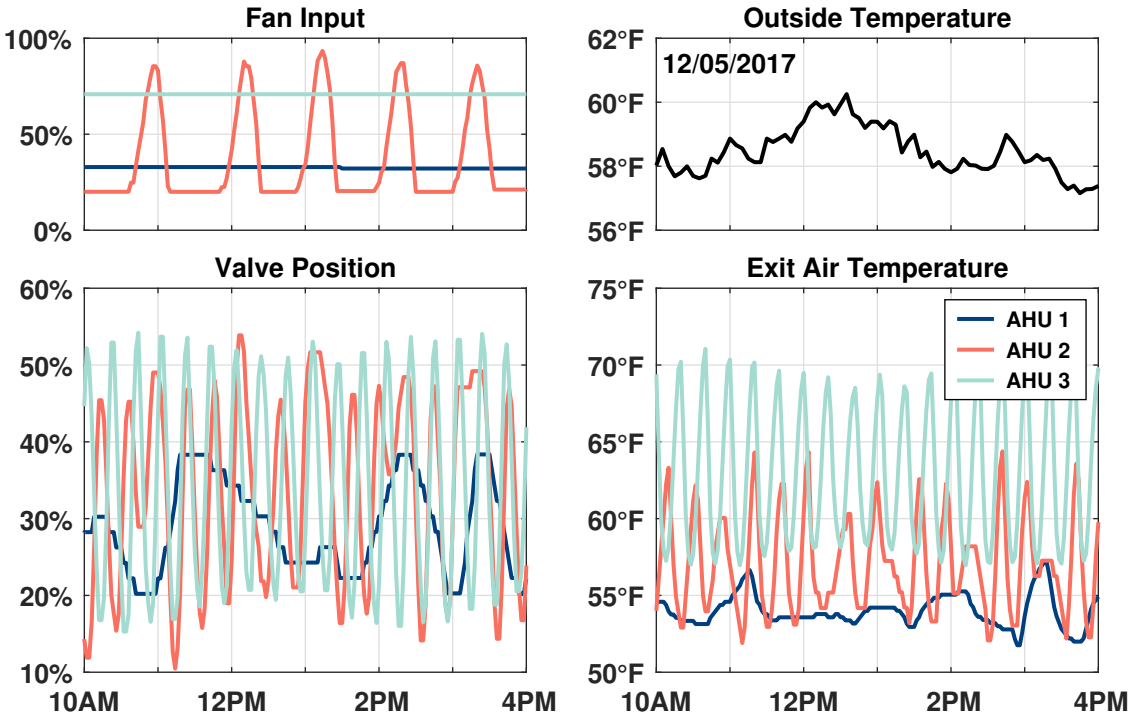

Figure 5.27: All three AHU CHW valve controllers hunt continuously on cool days.

Also apparent from the figures, is that the supply air fan for AHU2 has a large issue with hunting. Fan speeds are allowed to very within $\omega \in [20\%, 100\%]$ which accounts for the saturated appearance of the signal. Fan speeds for AHUs 1 and 2 vary only slightly or are constant during a normal day. Note that access to record data for the DOAS was given in early 2018, well after the time frame of these nominal plots.

The tuning process at the TTI Building highlights several fundamental issues of practical building control. In particular how hunting controllers can mask multiple system faults. The following sections detail issues discovered at the TTI as they arose and how implementing cascaded control revealed several other underlying problems.

5.7.1 Problem 1 - Poorly Tuned Control Gains

Parsing the Gilchrist Building control code, the chilled water LOOP command settings for each AHU were found to vary widely as seen below. At issue are the vastly different sampling times seen in the upper floors. Due to the multiplication of the integral gain and sampling time (see Equation 5.4), the effective k_i gain for these systems is 30 times larger for those floors than the first floor. Differences in gains help to explain the variation in loop performance between AHUs. Most likely, hunting behavior was observed in AHU3 and to compensate the magnitude of **pg** was reduced by an order of magnitude. Similarly, the integral gain for AHU1 was reduced to avoid oscillations.

AHU 1:	**pg** = 600,	**ig** = 7.5,	t_s = 1 sec	$\Rightarrow$	k_p = 0.6	$k_i t_s = 0.0075$
AHU 2:	**pg** = 600,	**ig** = 15,	t_s = 15 sec	$\Rightarrow$	k_p = 0.6	$k_i t_s = 0.225$
AHU 3:	**pg** = 60,	**ig** = 15,	t_s = 15 sec	$\Rightarrow$	k_p = 0.06	$k_i t_s = 0.225$
DOAS:	**pg** = 600,	**ig** = 20,	t_s = 1 sec	$\Rightarrow$	k_p = 0.6	$k_i t_s = 0.020$

The main culprit of the nearly constant hunting in the initial dynamic data is therefore the large effective integral gains. However, as seen in Figure 5.26, there is still a demonstrated reliance on operating conditions as warmer ambient temperatures reduce the prevalence of hunting. Implementing a properly tuned cascaded controller will there-

fore inherently eliminate oscillations due to poor tuning as well as reduce variations in performance due to changing operating conditions.

For initial cascaded tuning, the LOOP sampling time will be $t_s = 1$ second with an initial inner loop gain of $k_L = 0.5$. The gains **pg** and **ig** for AHU1 will be used as initial nominal gains for the tuning process. The cascaded loop gains are therefore $k_{pc} = 0.2$ and $k_{ic} = 0.015$ which correspond to the initial LOOP gains $\mathbf{pg_c} = 100$ and $\mathbf{ig_c} = 7.5$ to be used with with Algorithm 5.2. These calculations, including for the LOOP bias term, are given by Equations 5.10 and 5.11.

$$\mathbf{pg_c} = \mathbf{pg} - 1000k_L = 100 \qquad \& \qquad \mathbf{ig_c} = \mathbf{ig} = 7.5 \tag{5.10}$$

$$\mathbf{B} = B_2 - k_L B_1 = 50\% - \left(0.5\frac{\%}{^\circ\mathrm{F}}\right)\left(\frac{65^\circ\mathrm{F} + 55^\circ\mathrm{F}}{2}\right) = 20\% \tag{5.11}$$

After some initial testing, the inner loop gain was increased to $k_L = 1$ to amplify the linearization effect of the cascaded controller. Due to the additional issues discussed below, the integral gain was slowly decreased to $\mathbf{ig_c} = 2.5$. With these gains, the system showed a qualitative improvement in performance as seen in Figure 5.28. This improvement represents incremental progress with notable reductions in oscillation period and magnitude. After the remaining issues were fixed, the final integral gains for each unit were increased to 7.5, 10, 10, and 7.5 respectively.

5.7.2 Problem 2 - Failed End Static Pressure Sensors

As seen in Figure 5.28, fan speed for AHU2 hunts periodically throughout a normal day. The architecture of Figure 5.9 shows that the fan speed is used to maintain a certain static pressure at given points in the system ducting. Usually End Static Pressure (ESP) sensors are located at a point two-thirds along the longest path of the ducting. Given the L-shape of the TTI Building, floors 2 and 3 have two ESP sensors.

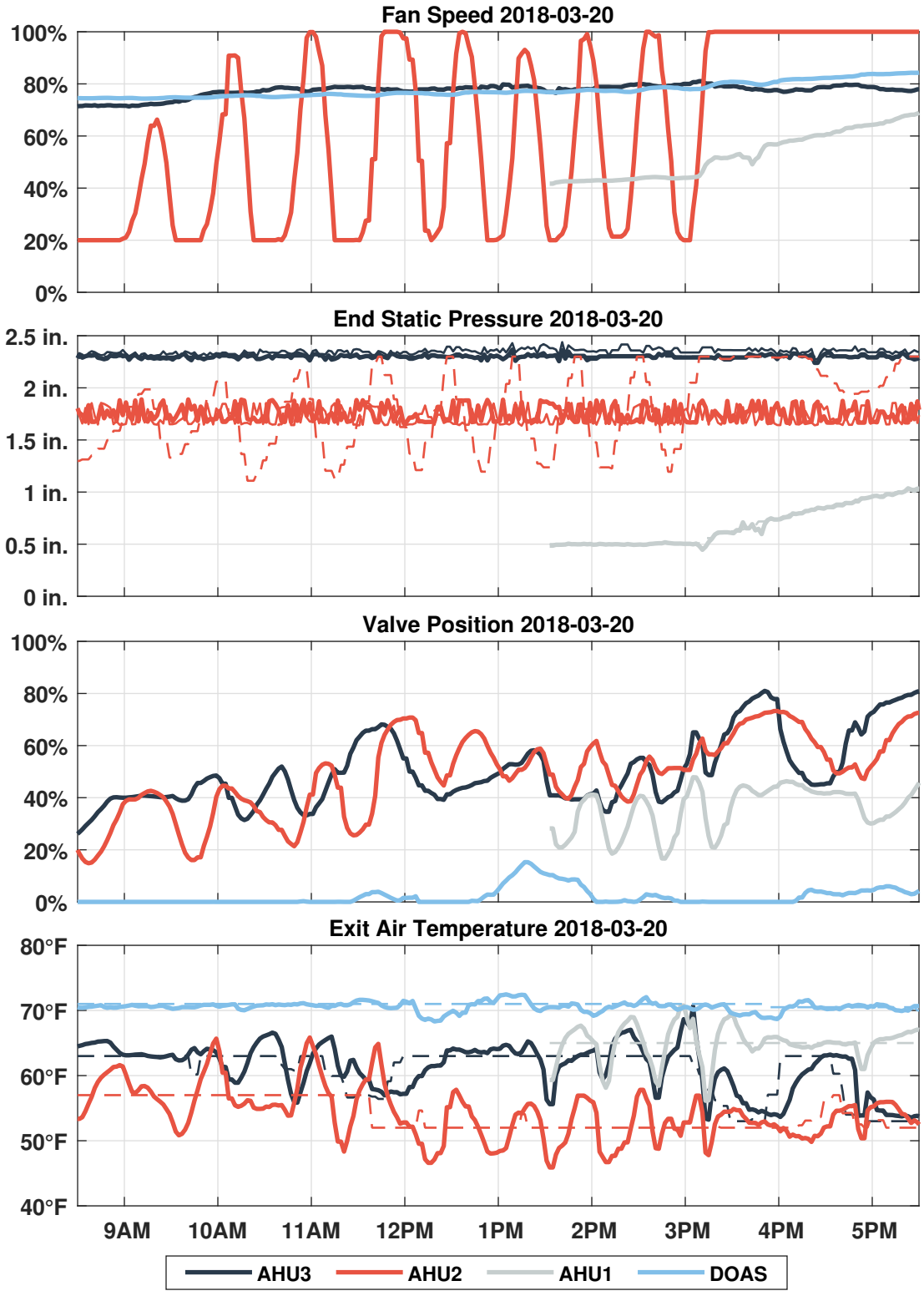

Figure 5.28: ESP setpoint for AHU2 oscillates throughout the day due broken ESP sensors.

In normal operation, PPCL code takes the minimum reading from the two ESP sensors as the input to the static pressure control loop. On floor 2 however, a comment in the system code indicated that one of the sensors had failed at an earlier date. Given that the second sensor continuously read a similar value to the failed sensor and both showed no reaction to drastic changes in supply fan speed, the failure of both ESP sensors was determined. This has the effect of breaking the ESP feedback loop at the red 'x' in Figure 5.9, thereby effectively introducing a constant disturbance between ESP SP and fan speed controllers. While unmeasurable from the failed ESP sensors, the effect of the hunting fan speed was still observable through the damper command calculation. As dampers at each zones VAV box closed to accommodate rising ESP due to the increased fan speed, the ESP SP controller would lower the ESP setpoint. This process would reverse and eventually cause the observed sustained oscillation in the ESP setpoint. As soon as one of the ESP sensors on floor 2 was replaced, the oscillations in AHU2 fan speed were eliminated giving the slightly improved results of Figure 5.29 where fan speed hunting has been eliminated. Note that although AHU2 is parallel to AHU1 and AHU3, the hunting fan speed acted as a disturbance, affecting the distribution of fresh air being delivered to each AHU.

5.7.3 Problem 3 - Failed CHW System Pressure Sensor & Control Issue

After fixing the ESP sensor, a synchronized oscillation in all four AHUs at the Gilchrist Building began to manifest (see Figure 5.29). Due to the configuration of the system, an issue with the DOAS was suspected as oscillations in discharge air temperature for that unit could propagate to the other three units. Trouble shooting proved inconclusive as simple valve stiction tests such as [151] failed to positively identify the issue.

In early April 2018, weather conditions in College Station were cold enough that no conditioning of fresh air was needed from the DOAS. Despite the stable supply fresh air temperature being delivered to AHUs 1-3, discharge air temperatures still displayed the

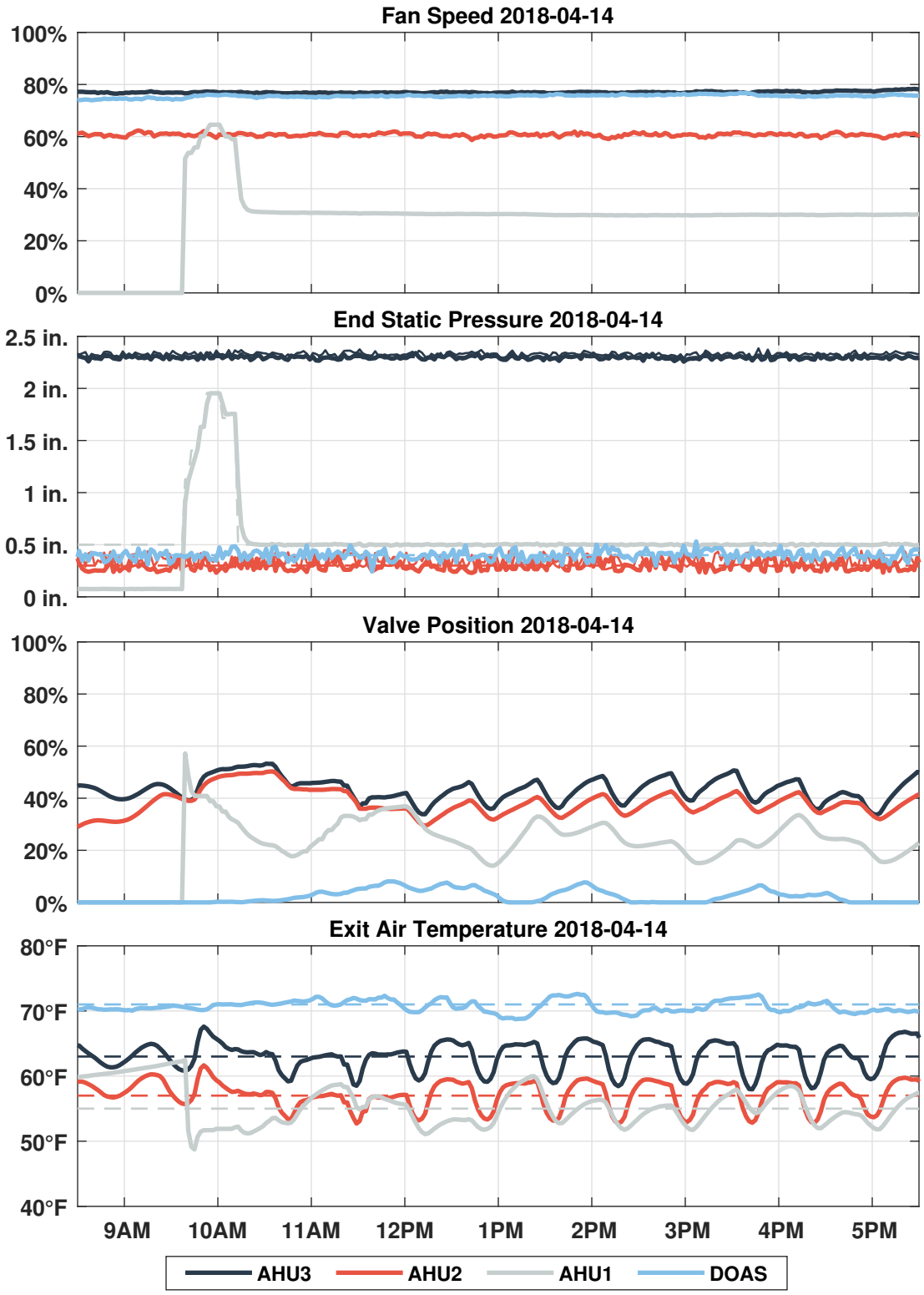

Figure 5.29: Synchronized disturbances in all AHUs point to an common upstream disturbance determined to be CHW supply system.

same synchronized oscillations. Their persistence strongly indicated that another upstream disturbance besides the DOAS was causing the oscillations.

Such a disturbance was determined to be coming from the buildling CHW supply system. As seen in Figure 5.30(a), the system consists of two actuators (a pump and a valve), four pressure sensors, and two temperature sensors. The CHW control architecture seen in Figure 5.31 seeks to maintain a Differential Pressure (DP) between supply and return water. The DP setpoint is determined through a rule set that uses a time averaged

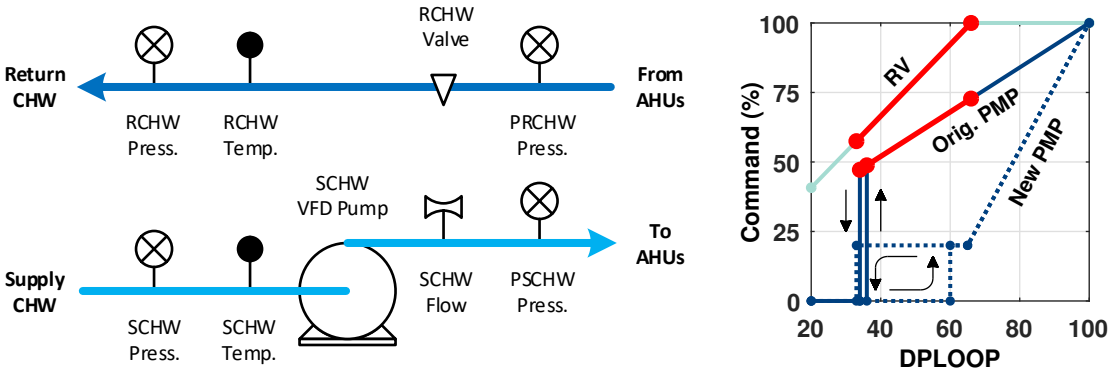

(a) (b)

Figure 5.30: (a) Schematic of CHW supply system. (b) Original CHW supply control had a significant region (shown in red) where the return valve and pump actuated simultaneously. New pump control settings fixed this issue.

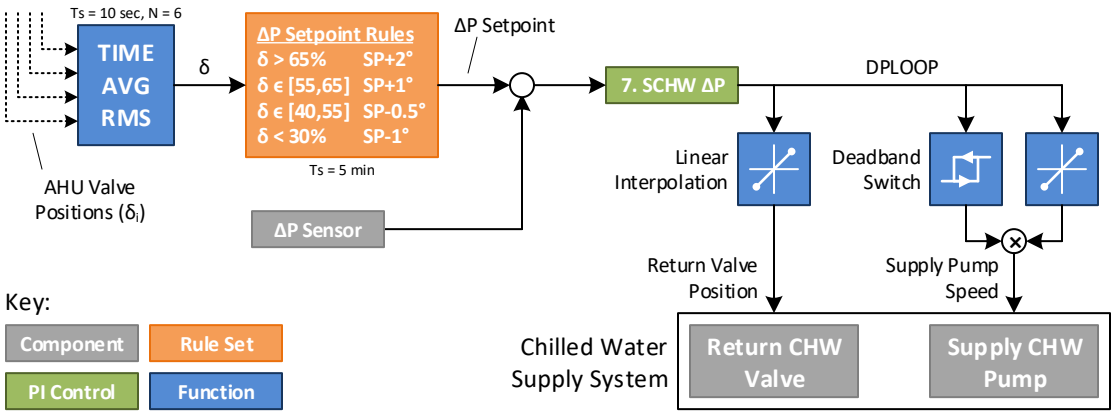

Figure 5.31: Control digram of TTI Building CHW supply control architecture.

Root-Mean-Square (RMS) valve position for the four AHUs. A PI controller operates on DP error to output DPLOOP $\in [20, 100]$, a demand variable that is interpolated to determine settings for the return water valve position and pump speed. The deadband block in the pump control is meant to prevent short cycling of the pump and to ensure that the pump and valve are actuating separately.

As seen in Figure 5.32, the building CHW pump short cycles ON/OFF several times throughout the day. These cycles correspond to the periodic oscillations seen in AHU discharge air temperature. The sudden changes in pump speed cause sharp changes in building CHW flow rate which affects flows to individual AHUs. This causes the sudden, synchronized drops in exit air temperatures.

The short cycling was due to several concurrent system issues. Firstly, the deadband region meant to prevent rapid pump cycles was extremely small turning the pump ON when DPLOOP rose above 36 and OFF when it dropped below 34. As DPLOOP would drop below 34 almost immediate after the pump switched ON, the pump would cycle OFF after the five minute sampling time of the DP Setpoint rules block. Also because the linear interpolation for the return water valve was for 20 $\leq$ DPLOOP $\leq$ 66, both the pump and the valve were actuating simultaneously for a significant range of operation shown graphically in Figure 5.30(b). Secondly, the return CHW pressure sensor had a fault causing large swings in measurements. The resulting oscillation was propagated through the SCHW PI controller causing the pump and valve to oscillate. Finally, the integral gain in the SCHW PI loop was **ig** = 125 with a sampling time t_s = 1. The large integral gain caused DPLOOP to hunt even for small errors in DP. Each of these identified issues was fixed by working with TAMU Utilities. The CHW program was changed to expand the the deadband zone and alter the interpolations to regions where the pump and valve actuate separately (see Figure 5.30(b))). The return pressure sensor was also replaced and calibrated and the DPLOOP PI controller was returned.

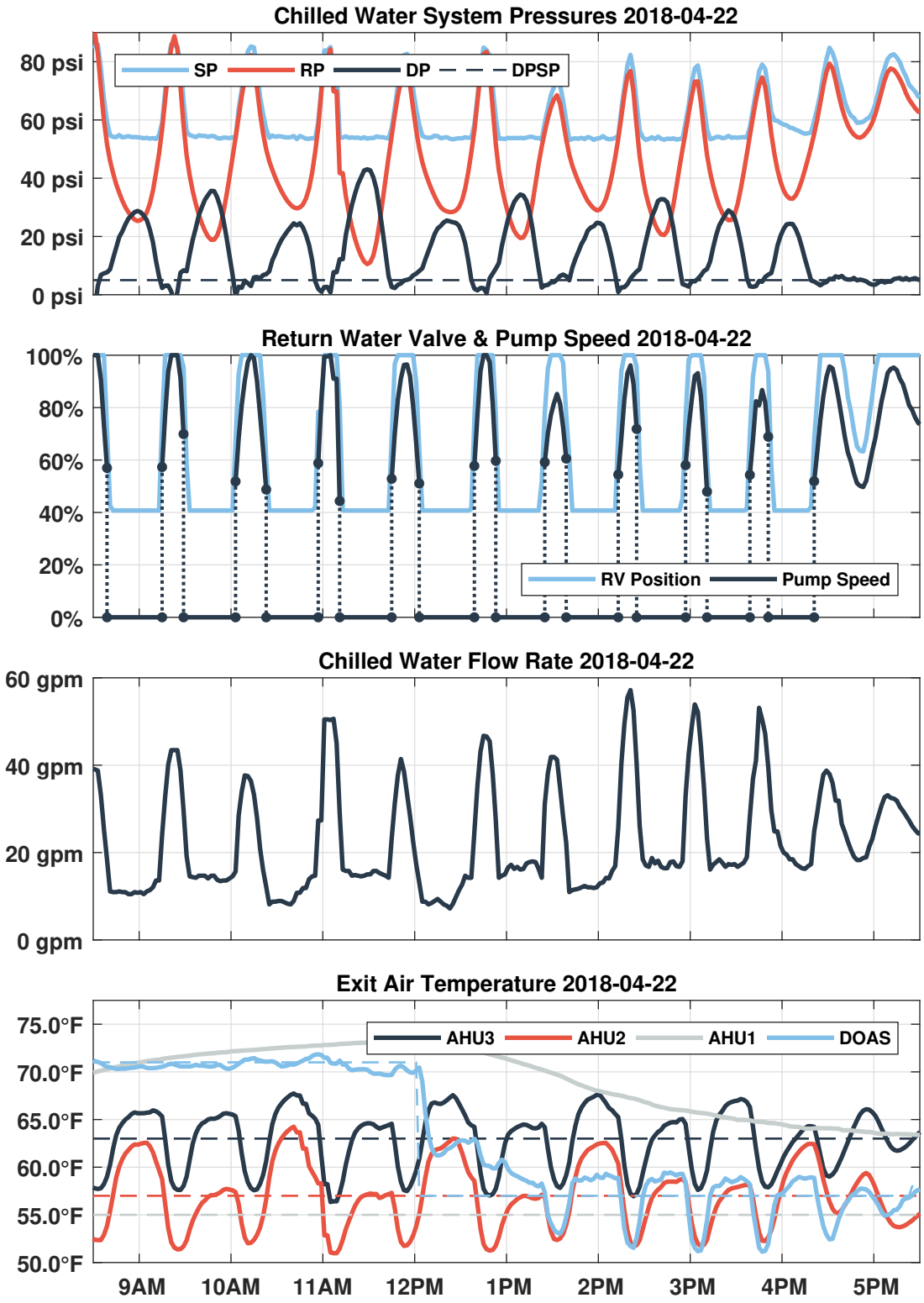

Figure 5.32: The CHW system pump short cycled throughout the day causing large disturbances to DAT control loops.

After fixing CHW supply issues, the system began to operate fault free. Initial results showed that hunting had been completely eliminated and that large disturbance oscillations from system faults had been removed. However, tracking performance was poor as cascaded controllers had been detuned to tolerate the many system faults. After retuning the controllers to improve tracking performance, system results are similar to those from Figure 5.33. Comparing with the original performance seen in Figure 5.26 and 5.27, fixing the multiple faults and implementing cascaded control has significantly improved building performance. At the end of the tuning process, final cascaded PPCL gains were k_L = 1, $\mathbf{pg_c}$ = 100, and $\mathbf{ig_c}$= 10 except for the DOAS whose integral gain was $\mathbf{ig_c}$ = 7.5.

5.8 Estimated Energy Savings

Having established that cascaded control has significantly improved the performance of AHU exit air temperature, one question that can now be answered is how much energy poor AHU control wastes. The trouble shooting from the previous section has, for the time being, left the Gilchrist Building HVAC system operating fault free and a comparison of daily energy usage and costs can be made by alternating between the original PI and new cascaded controllers. As the only difference will be the AHU exit air control architecture, assuming similar loads, any differences in usages will be due to control alone.

To estimate daily resource consumption, additional information about the building HVAC system is required. From the building HVAC floor plans, the nominal power of the four AHU fans and CHW pump are known (Table 5.5). Each of these motors are variable speed, normally operating at some fraction of their top speed. The part load power

Table 5.5: Gilchrist Building HVAC Motor List

Unit	AHU1	AHU2	AHU3	DOAS	SCHW
Type	Fan	Fan	Fan	Fan	Pump
Power	25 HP	25 HP	20 HP	7.5 HP	20 HP

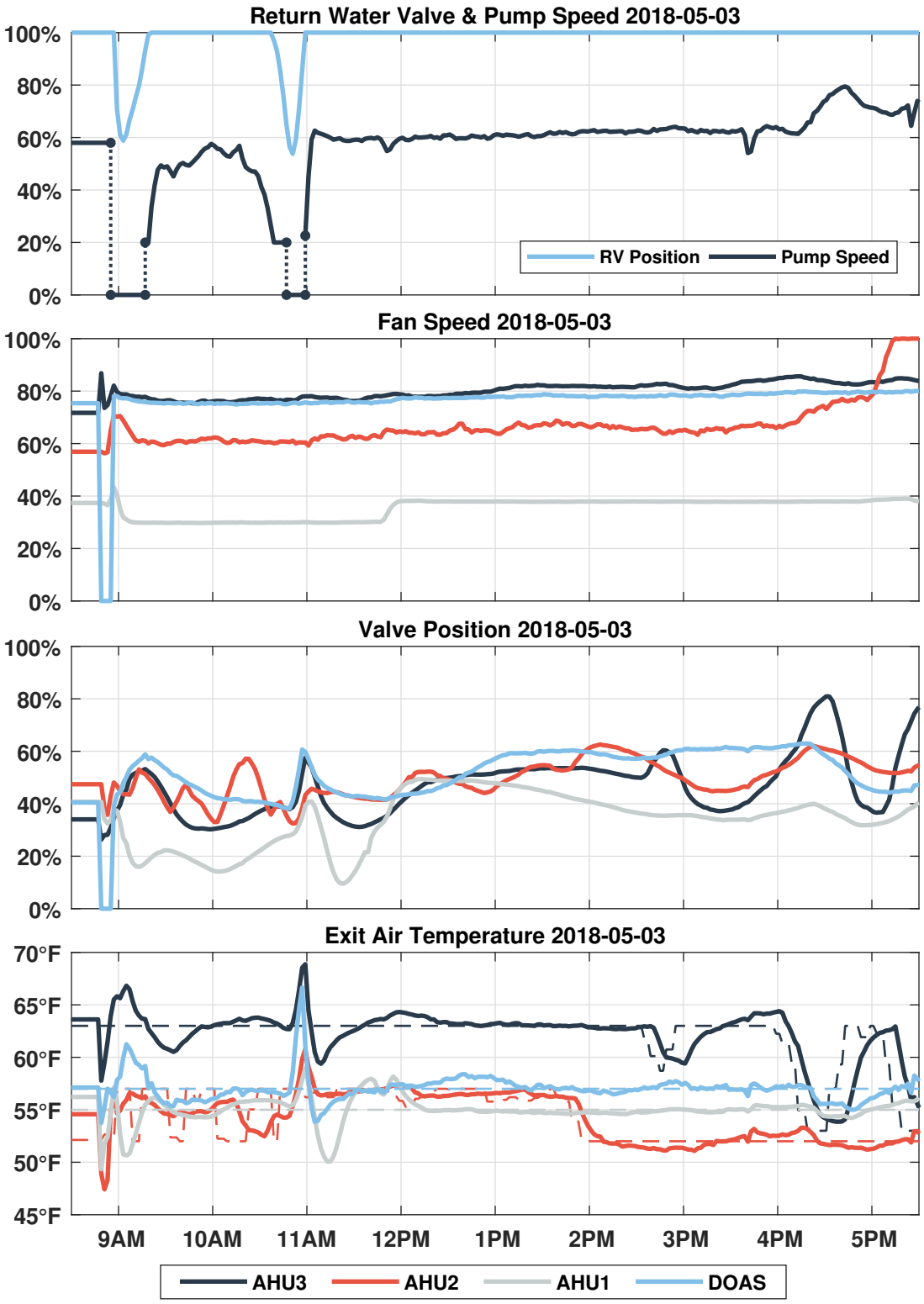

Figure 5.33: Example of improved DAT control from fixing system faults and implementing cascaded control.

can be found using standard fan/pump affinity laws leading to the instantaneous electrical power estimate of Equation 5.12 where $\omega_i \in [0, 100]$ are speeds and the subscripts '*oa*' and '*p*' are for the DOAS fan and CHW pump respectively. Each building on campus is billed at a rate of approximately \$0.08/kWh of electricity which represents the average cost of electricity production at the campus generation sites.

$$P_{elec} = 18.65\,\omega_1^3 + 18.65\,\omega_2^3 + 14.92\,\omega_3^3 + 5.595\,\omega_{oa}^3 + 14.92\,\omega_p^3 \quad kW \tag{5.12}$$

The volume of chilled water used daily by the Gilchrist HVAC system is relatively easy to compute as CHW flow is monitored in real time. However, estimating cost is slightly more complicated as Texas A&M Utilities does not bill by volume but by energy content. As all conditioning water is returned to the central processing plants, buildings that require more cooling will return warmer water. Solely billing on volume usage therefore does not capture the additional cost of re-cooling warmer return water. Calculating energy used by the HVAC system requires monitoring chilled water flow rate as well as the temperature differential between supply and return water. Instantaneous CHW power consumed by the HVAC system is given by Equation 5.13 and has an associated cost of approximately \$0.052/kWh of chilled water which represents the average cost of cold water production.

$$P_{CHW} = c_p\,\rho\,\dot{V}\Delta T = 0.1463\,\dot{V}\Delta T \quad kW \tag{5.13}$$

Starting in May 2018, the AHU discharge air temperature control was switched between the original PI control and the new cascaded control approximately every two weeks. Energy consumption, costs, and cooling degree days were calculated daily to generate plots comparing the two control architectures. As seen in Figures 5.34 and 5.35, there are two distinct schedules at the Gilchrist Building: weekday and weekend. The weekend schedule completely shuts down the first floor AHU resulting in the bifurcation. On particularly hot days AHU1 will however operate on Saturdays.

Preliminary results show that for high demand conditions (CCD > 10), the PI and cascaded controllers result in similar daily energy consumption. Analysis of control performance in these conditions shows that the PI controllers are well tuned for such conditions. Under these loads, mixed air temperatures are higher and discharge air temperature set points are in the low $50°$F range. It is expected though that in cooler conditions (CCD < 10) that PI hunting will be come more prominent. Under such conditions discharge temperature set points will be in the mid to low $60°$F range with the system operating in much higher response gain region.

Expected trends for PI and cascaded control on weekday schedules are shown by dotted lines in both Figures 5.34 and 5.35. As shown, the cost of operating with PI control is expected to level off in cooler weather with respect to CCDs. Cascaded control should eliminate hunting behavior and therefore avoid the extra cost due to the nonlinear power consumption of the fans and pump. Should the shaded region in the cost plot prove correct, hunting could cost up to $100 per day depending on outside weather conditions.

5.9 Summary of Cascaded Control Testing

This chapter has detailed detection of hunting behavior in several buildings on the Texas A&M Campus and the implementation of cascaded control loops to eliminate that problem. Hunting at the UBO and TTI buildings was virtually eliminated through a combination of troubleshooting and cascaded control design. Results at the YMCA building were more mixed, but a general trend in improved tracking performance without introducing control oscillations was observed. The basis for an estimation of hunting/poor control costs was started at the TTI building. Data will continue to be recorded in order to capture differences in PI and cascaded control in cool weather conditions.

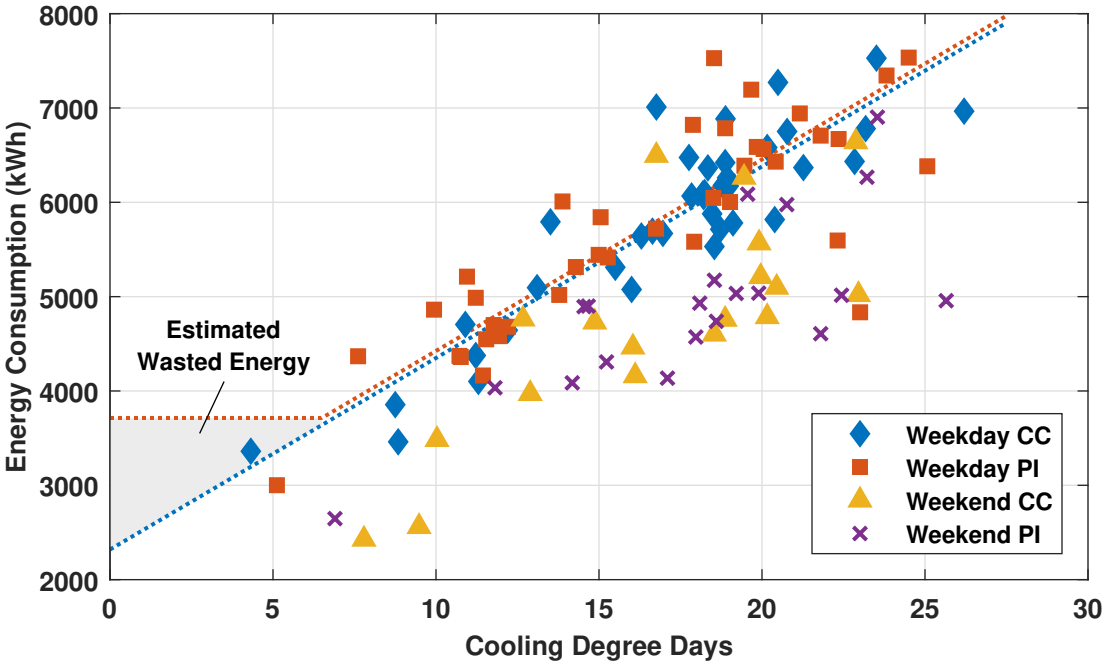

Figure 5.34: Daily control energy comparison at Gilchrist Building.

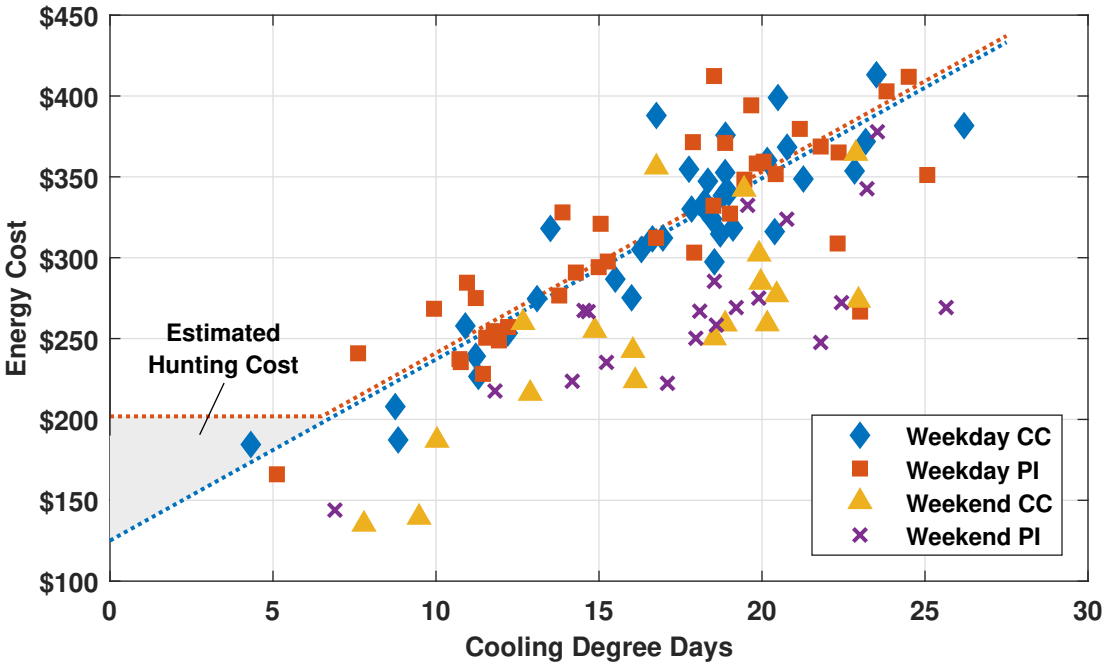

Figure 5.35: Daily control cost comparison at Gilchrist Building.

6. CONCLUSIONS & FUTURE WORK

6.1 Summary of Contributions & Conclusions

This dissertation has developed the cascaded control architecture for building HVAC systems. A thorough analysis of the current state of building HVAC controls was discussed, placing the proposed architecture in context and identifying issues with current PI controllers. The structure and benefits of cascaded loops were outlined and quantified by defining new Nonlinear Gap Metrics. Those metrics were used in the development of simple tuning techniques and in the generation of an optimal LQ tuning framework. Several case studies on both simulated and experimental systems highlighted the benefits of the architecture and the proposed tuning techniques. Analysis of several implementation approaches were studied taking advantage of the developed Dual Youla parameterization of a generalized static output feedback cascaded controller. Also a mathematical analysis of performance guarantees of the cascaded loop was outlined using LMIs and a polytopic representation of plant dynamics. Finally, results from a series of pilot cascaded loop implementations in several campus Air Handling Units were presented showing improved performance.

While this dissertation demonstrates the ability of the cascaded architecture to improve the operation of a wide array of HVAC equipment, there are many opportunities to further develop the control methodology. The following sections outline continued work and possible avenues for future research.

6.2 Performance & Optimization Opportunities

The analysis in Chapter 4 developed soft cascaded implementation techniques and analyzed simple control interpolation approaches. The analysis pointed to cascaded control being a simple control method that can be widely adopted by the HVAC field. Experimen-

tal results in three campus buildings shows that cascaded loops can easily be incorporated into existing architectures and provide better performance and even help to uncover additional system faults. A survey of campus AHUs show that hunting and poor PI control are widespread issues and easily fixed with cascaded control.

The LMI analysis in Chapter 4.7 also points to synthesis opportunities for cascaded control. Similar to the work presented there, consider the general cascaded loop controller of Equation 6.1. After substitution, the resulting closed loop LMI can be written as Equation 6.2 where F_{ol} is the open loop $\mathcal{H}_\infty$ LMI and each LMI equation F_i is defined by the control feedback. Unlike Chapter 2.6 where the cost function was constrained to LQ, the LMI expression allows for a minimization based off of I/O filter selection. Also, the order of the controller is unaffected unlike in full $\mathcal{H}_\infty$ synthesis. Further development of optimal control methodologies could further improve cascaded loop performance and reveal simple tuning techniques for HVAC systems.

$$D_K = k_1 \begin{bmatrix} 1 & 0 & 0 \end{bmatrix} + k_2 \begin{bmatrix} 0 & 1 & 0 \end{bmatrix} + k_3 \begin{bmatrix} 0 & 0 & 1 \end{bmatrix} = k_1 D_{\Delta 1} + k_2 D_{\Delta 2} + k_3 D_{\Delta 3} \quad (6.1)$$

$$F_{ol}(x) + \sum_{i=1}^{3} k_i F_i(x, D_{\Delta i}) < \gamma \bar{I} \quad (6.2)$$

6.3 Application of Cascaded Control on Building Systems

In Chapter 5 cascaded control was applied to Air Handling Unit (AHU) chilled water valve control. Results showed an improvement in control performance due to three unique issues associated with PI control hunting: hunting due to changing loads, hunting due to supervisory control oscillations, and poor initial control tuning. The three buildings identified as a test set for this project were selected by the Texas A&M Building facilities. Poor performance was not the main criteria for building selection but ultimately convenience and testing risk minimization. Hunting behavior in these buildings was merely coincidental and a symptom of fundamental issues with PI control with HVAC systems.

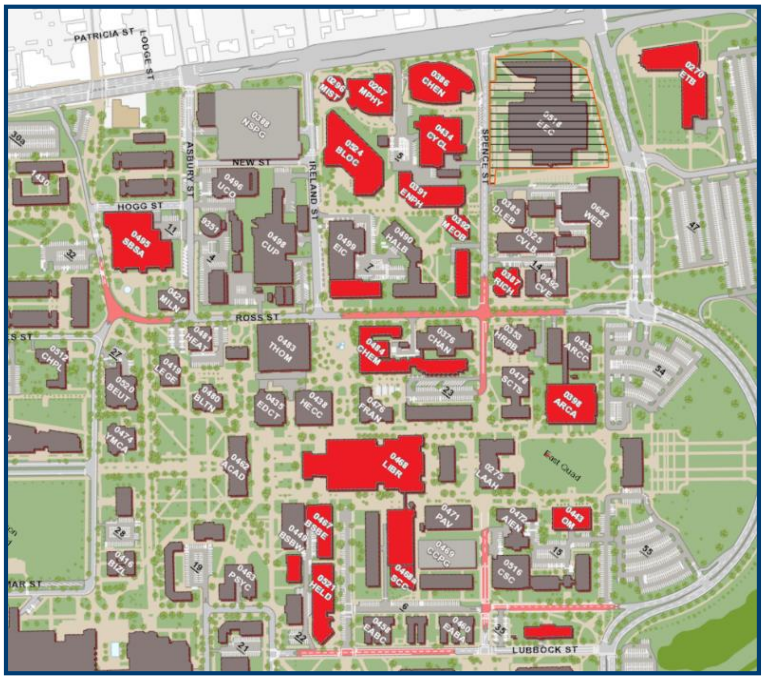

Figure 6.1: Texas A&M East Campus buildings with identified AHU valve and/or fan hunting issues (red).

Hunting issues on the Texas A&M campus are not confined to the buildings studied. A survey of HVAC control performance on East Campus focusing mainly on buildings in the engineering section found more than a dozen additional buildings with some level of hunting (Figure 6.1). Important to note is that these identified buildings are not a complete list and represent only buildings that have points trended for historical analysis. Several buildings had no data on control performance and thus could not be analyzed. Results from this building survey indicate that there is significant opportunity to apply cascaded control across campus and improve building chilled water valve performance.

Chapter 5 results also highlighted the opportunity for cascaded control in other HVAC control loops. Several AHU supply air fans had distinct periods of speed hunting and many setpoint loops had oscillations such as in the YMCA Building discharge air temperature setpoint control. Applying cascaded control to these loops would further improve

overall HVAC system performance. Implementing these loops would also help leaning to distinguish the ultimate cause of hunting in a given system. The dynamics of an AHU are inherently coupled, not to mention the highly coupled control structure employed in campus buildings (see Figure 5.9). Piecewise cascaded control roll-out would allow future projects to develop tools to identify the source of large oscillations.

Application of cascaded control at the test facilities underscored the overall lack of common metrics to assess building control performance. There are only a handful of papers dedicated to performance measures and detection of hunting behavior in HVAC systems (see [27, 30]) and no definitive ASHRAE standard exists. Going forward, especially as more advanced HVAC control paradigms are developed, a common building operating metric will become necessary to both measure current energy/comfort and to quantify improvement.

Along with developing such metrics, fault detection in building controls needs to be developed. While there are numerous equipment fault detection methods for HVAC systems, particularly for AHUs and VCC systems, there is very little development of tools for identifying faulty controls. As seen with cascaded control implementation at the Gilchrist Building, fundamental control architecture issues can significantly hamper HVAC operation. For example, incorrect settings for the deadband region in the Gilchrist CHW supply system caused short cycling of the CHW pump that manifested as a large synchronized disturbance in all four AHUs. Future work in the HVAC field should include development of holistic diagnostic tools that can identify such oscillations and pinpoint problem systems. Whether this takes the form of machine learning algorithms or diagnostic decision trees is an open question.

Given development of performance metrics and diagnostics tools, an additional area of future work with cascaded control is the development of automated deployment procedures. Ideally, this would be a form of plug-and-play device or software package that

would incorporate easily into existing building controls. Such a module would need to identify several factors for proper implementation. Firstly, identification of candidate control loops needs to be understood. If existing controls offer satisfactory performance, the additional time and cost of implementing cascaded control may not be feasible. Also, as seen in Chapter 5, oscillations in a signal may not be the result of poor control but due to rejecting upstream disturbances. Locating upstream control faults will point to the correct candidate for cascaded loop implementation. Second, automating the structure of cascaded control needs to be developed. For example, there may be several intermediate signals that can be utilized to linearize system responses (e.g. air flow rate for VAV dampers) or the inner and outer loops could take feedback on the same signal (e.g. cascaded control for AHU exit air temperature control). Finally, tuning of the cascaded control loop gains would need to be automated. This can proceed in multiple directions such as adaptive control paradigms or auto-tuning algorithms.

REFERENCES

[1] Office of Energy Efficiency and Renewable Energy Buildings Technologies Program, "Building Energy Data Book," tech. rep., U.S. Department of Energy, 2011.

[2] R. E. Brown and J. G. Koomey, "Electricity use in California: Past trends and present usage patterns," *Energy Policy*, vol. 31, pp. 849–864, July 2003.

[3] U.S. Environmental Protection Agency, "Overview of Greenhouse Gases," April 14, 2017. https://www.epa.gov/ghgemissions/overview-greenhouse-gases.

[4] Office of Air Quality Planing and Standards Clean Air Technology Center, "Nitrogen Oxides (NO_x), Why and How They Are Controlled," Technical Bulletin EPA 456/F-99-006R, U.S. Environmental Protection Agency, Nov. 1999.

[5] N. Klepeis, W. Nelson, W. Ott, J. Robinson, A. Tsang, P. Switzer, J. Behar, S. Hern, and W. Engelmann, "The national human activity pattern survey (NHAPS): A resource for assessing exposure to environmental pollutants," *Journal of Exposure Analysis and Environmental Epidemiology*, vol. 11, no. 3, pp. 231–252, 2001.

[6] D. Sarigiannis, "Combined or Multiple Exposure to Health Stressors in Indoor Built Environments," tech. rep., World Health Organization, Regional Office for Europe, 2013.

[7] W. Goetzler, R. Zogg, J. Young, and J. Schmidt, "Energy Savings Potential and Research, Development, & Demonstration Opportunities for Residential Building Heating, Ventilation, and Air Conditioning Systems," tech. rep., U.S. Department of Energy Office of Energy Efficiency and Renewable Energy Buildings Technologies Program, Oct. 2012.

[8] W. Goetzler, R. Zogg, H. Hiraiwa, J. Burgos, and J. Young, "Energy Savings Potential and Research, Development, & Demonstration Opportunities for Commercial Building Heating, Ventilation, and Air Conditioning Systems," tech. rep., U.S. Department of Energy Office of Energy Efficiency and Renewable Energy Buildings Technologies Program, Sept. 2011.

[9] M. Brambley, P. Haves, S. McDonald, P. Torcellini, D. Hansen, D. Holmberg, and K. Roth, "Advanced Sensors and Controls for Building Applications: Market Assessment and Potential R&D Pathways," Tech. Rep. PNNL-15149, Pacific Northwest National Laboratory, 2005.

[10] U.S. Energy Information Administration (EIA), "A look at the u.s. commercial building stock: Results from eia's 2012 commercial buildings energy consumption survey (cbecs)," 2015.

[11] U. Berardi, "Building energy consumption in us, eu, and bric countries," *Procedia Engineering*, vol. 118, pp. 128 – 136, 2015. Defining the future of sustainability and resilience in design, engineering and construction.

[12] M. Aksoezen, M. Daniel, U. Hassler, and N. Kohler, "Building age as an indicator for energy consumption," *Energy and Buildings*, vol. 87, pp. 74 – 86, 2015.

[13] The American Society for Heating, Refrigerating, & Air-conditioning Engineers, "ANSI/ASHRAE Standard 62.1," 2016.

[14] Siemens Global, "Texas A&M university - a detailed account of how one university is improving its energy efficiency and campus environment through effective management and performance contracting," *White Paper*, 2011.

[15] B. P. Rasmussen, C. Price, J. Koeln, B. Keating, and A. Alleyne, *HVAC System Modeling and Control: Vapor Compression System Modeling and Control*, ch. 4, pp. 73–103. Cham: Springer International Publishing, 2018.

[16] M. Headley, "Guidelines for selecting the proper valve characteristics," *Valve Magazine*, vol. 15, no. 2, 2003.

[17] J. Monsen, "Part 1: An insider's guide to valve sizing & selection," *Flow Control Magazine*, vol. XXI, Feb 2015.

[18] R. W. Haines and D. C. Hittle, *Control Systems for Heating, Ventilating, and Air Conditioning*. New York, NY: Springer, 6th ed., 2006.

[19] Y. Yamakawa, T. Yamazaki, K. Kamimura, and S. Kurosu, "Compensation of manual reset to offset thermal loads change for pid controller," *ASHRAE Transactions*, vol. 116, no. 1, pp. 303–315, 2010.

[20] P. M. T. Broersen and M. F. G. Van der Jagt, "Hunting of evaporators controlled by a thermostatic expansion valve," *Journal of Dynamic Systems, Measurement, and Control*, vol. 102, no. 2, pp. 130–135, 1980.

[21] A. Singhal and T. I. Salsbury, "Characterization and cancellation of static nonlinearity in HVAC systems," *ASHRAE Transactions*, vol. 113, no. 1, pp. 391–399, 2007.

[22] R. Chintala, C. R. Price, S. Liang, and B. P. Rasmussen, "Identification and elimination of hunting behavior in HVAC systems," *ASHRAE Transactions*, vol. 121, pp. 294–305, 2015.

[23] S. Katipamula and M. R. Brambley, "Methods for fault detection, diagnostics, and prognostics for building systems - a review, part I," *HVAC&R Research*, vol. 11, no. 1, pp. 3–25, 2005.

[24] J. Granderson, R. Singla, E. Mayhorn, P. Ehrlich, D. Vrabie, and S. Frank, "Characterization and survey of automated fault detection and diagnostics tools," tech. rep., Lawrence Berkeley National Laboratory, Berkeley, CA, Nov. 2017.

[25] S. Katipamula and M. R. Brambley, "Methods for fault detection, diagnostics, and prognostics for building systems - a review, part II," *HVAC&R Research*, vol. 11, no. 2, pp. 169–187, 2005.

[26] W. Kim and S. Katipamula, "A review of fault detection and diagnostics methods for building systems," *Science and Technology for the Built Environment*, vol. 24, no. 1, pp. 3–21, 2018.

[27] Z. O'Neill, Y. Li, and K. Williams, "Hvac control loop performance assessment: A critical review (1587-RP)," *Science and Technology for the Built Environment*, vol. 23, no. 4, pp. 619–636, 2017.

[28] T. J. Harris, "Assessment of control loop performance," *The Canadian Journal of Chemical Engineering*, vol. 67, no. 5, pp. 856–861, 1989.

[29] T. Salsbury, "A practical algorithm for diagnosing control loop problems," *Energy and Buildings*, vol. 29, no. 3, pp. 217 – 227, 1999.

[30] R. Chintala, *A Methodology for Automating the Implementation of Advanced Control Algorithms Such as Model Predictive Control on Large Scale Building HVAC Systems*. PhD thesis, Texas A&M University, 2017.

[31] Q. P. He, J. Wang, M. Pottmann, and S. J. Qin, "A curve fitting method for detecting valve stiction in oscillating control loops," *Industrial & Engineering Chemistry Research*, vol. 46, no. 13, pp. 4549–4560, 2007.

[32] A. Singhal and T. I. Salsbury, "A simple method for detecting valve stiction in oscillating control loops," *Journal of Process Control*, vol. 15, no. 4, pp. 371 – 382, 2005.

[33] A. Horch, "A simple method for detection of stiction in control valves," *Control Engineering Practice*, vol. 7, no. 10, pp. 1221 – 1231, 1999.

[34] M. Kano, H. Maruta, H. Kugemoto, and K. Shimizu, "Practical model and detection algorithm for valve stiction," *IFAC Proceedings Volumes*, vol. 37, no. 9, pp. 859 – 864, 2004. 7th IFAC Symposium on Dynamics and Control of Process Systems 2004 (DYCOPS -7), Cambridge, USA, 5-7 July, 2004.

[35] R. Wisniewski, L. Chen, and L. F. Larsen, "Synchronization analysis of the supermarket refrigeration system," in *Proceedings of the 48th IEEE Conference on Decision and Control Held Jointly with the 28th Chinese Control Conference CDC/CCC*, pp. 5562–5567, IEEE, 2009.

[36] R. Wisniewski, J. Leth, and J. G. Rasmussen, "Analysis of synchronization in a supermarket refrigeration system," *Control Theory and Technology*, vol. 12, pp. 154–162, May 2014.

[37] The American Society of Heating, Refrigerating, and Air-Conditioning Engineers, *ASHRAE Handbook: Refrigeration*. Atlanta, GA: ASHRAE, SI ed., 2010.

[38] L. Desborough and R. Miller, "Increasing customer value of industrial control performance monitoring-Honeywell's experience," in *AIChE Symposium Series*, pp. 169–189, New York; American Institute of Chemical Engineers; 1998, 2002.

[39] K. Åström and T. Hägglund, "The future of PID control," *Control Engineering Practice*, vol. 9, no. 11, pp. 1163–1175, 2001.

[40] K. Åström, T. Hägglund, C. C. Hang, and W. K. Ho, "Automatic tuning and adaptation for pid controllers - A Survey," *Control Engineering Practice*, vol. 1, no. 4, pp. 699–714, 1993.

[41] K. H. Ang, G. Chong, and Y. Li, "PID control system analysis, design, and technology," *IEEE Transactions on Control Systems Technology*, vol. 13, no. 4, pp. 559–576, 2005.

[42] K. J. Åström and T. Hägglund, *Advanced PID Control*. The Instrumentation, Systems, and Automation Society (ISA), 2006.

[43] A. Visioli, *Practical PID Control*. Advances in Industrial Control, London: Springer, 2006.

[44] J. G. Ziegler and N. B. Nichols, "Optimum settings for automatic controllers," *ASME Transactions*, vol. 64, pp. 759–768, 1942.

[45] The American Society of Heating, Refrigerating, and Air-Conditioning Engineers, *ASHRAE Handbook: Fundamentals*. Atlanta, GA: ASHRAE, si ed., 2017.

[46] C. C. Hang, K. J. Astrom, and W. K. Ho, "Refinements of the Ziegler-Nichols tuning formula," *IEE Proceedings D - Control Theory and Applications*, vol. 138, pp. 111–118, Mar. 1991.

[47] D. Xue, Y. Chen, and D. P. Atherton, *Linear Feedback Control: Analysis and Design with MATLAB*. Advances in Design and Control, Philadelphia, PA: Society for Industrial and Applied Mathematics, 2007.

[48] R. Rakshamare, G. Kamble, and R. Chile, "Some tuning methods of PID controller for different processes," in *Proceedings of the International Conference on Information Engineering, Management and Security*, pp. 282–288, 2015.

[49] J. Lee, W. Cho, and T. F. Edgar, "An improved technique for PID controller tuning from closed-loop tests," *American Institute of Chemical Engineers (AIChE) Journal*, vol. 36, pp. 1891–1895, Dec. 1990.

[50] C. A. Smith and A. B. Corripio, *Principles and Practice of Automatic Process Control*. Hoboken, NJ: Wiley, 3rd ed., 2006.

[51] G. Cohen and G. Coon, "Theoretical consideration of retarded control," *ASME Transactions*, vol. 75, pp. 827–834, 1953.

[52] A. O'Dwyer, *Handbook of PI and PID Controller Tuning Rules*. London, UK: Imperial College Press, 3rd ed., 2009.

[53] H. Fertik, "Tuning controllers for noisy processes," *ISA Transactions*, vol. 14, pp. 292–304, 1975.

[54] R. Ciancone and T. Marlin, "Tune controllers to meet plant objectives," *Control*, vol. 5, pp. 50–57, 1992.

[55] A. M. Lopez, P. W. Murrill, and C. L. Smith, "Controller tuning relationships based on integral performance criteria," *Instrumentation Technology*, vol. 14, Nov. 1967.

[56] A. Jutan, "A comparison of three closed-loop PID tuning algorithms," *AIChE Journal*, vol. 35, pp. 1912–1914, Nov. 1989.

[57] R. Kumar, S. K. Singla, and V. Chopra, "Comparison among some well known control schemes with different tuning methods," *Journal of Applied Research and Technology*, vol. 13, no. 3, pp. 409–415, 2015.

[58] D. E. Rivera and M. E. Flores, "Internal Model Control," in *Control Systems, Robotics, and Automation: System Analysis and Control: Classical Approaches II*,

vol. 2, pp. 80–108, Encyclopedia of Life Support Systems (EOLSS) Publications, 2009.

[59] G. F. Franklin, J. D. Powell, and A. Emami-Naeini, *Feedback Control of Dynamic Systems*. Pearson, 7th ed., 2015.

[60] MathWorks, "Control of Processes with Long Dead Time: The Smith Predictor - MATLAB & Simulink Example." https://www.mathworks.com/help/control/examples/control-of-processes-with-long-dead-time-the-smith-predictor.html, Accessed on 8/4/2017.

[61] S. Skogestad, "Simple analytic rules for model reduction and PID controller tuning," *Journal of Process Control*, vol. 13, no. 4, pp. 291–309, 2003.

[62] W. Levine, *Control System Applications*. CRC Press, Illustrated ed., 1999.

[63] K. J. Åström and T. Hägglund, *PID Controllers: Theory, Design, and Tuning*. Research Triangle Park, N.C. : International Society for Measurement and Control, 2nd ed., 1995.

[64] T. Hägglund and K. J. Åström, "Revisiting the Ziegler-Nichols Tuning Rules for PI Control," *Asian Journal of Control*, vol. 4, pp. 364–380, 2002.

[65] K. J. Åström and T. Hägglund, "Revisiting the Ziegler-Nichols step response method for PID control," *Journal of Process Control*, vol. 14, pp. 635–650, 2004.

[66] D. Lim, B. P. Rasmussen, and D. Swaroop, "Selecting PID control gains for nonlinear HVAC&R systems," *HVAC&R Research*, vol. 15, no. 6, pp. 991–1019, 2009.

[67] S. P. Bhattacharyya, H. Chapellat, and L. H. Keel, *Robust Control: The Parametric Approach*. Prentice-Hall Information and System Sciences Series, Upper Saddle, NJ: Prentice Hall, 1995.

[68] C.-C. Yu, *Autotuning of PID Controllers: A Relay Feedback Approach*. Advances in Industrial Control, London: Springer, 2nd ed., 2006.

[69] S. W. Sung and J. H. Lee, "Pseudo-random binary sequence design for finite impulse response identification," *Control Engineering Practice*, vol. 11, pp. 935–947, 2003.

[70] M. A. Johnson and M. H. Moradi, *PID Control: New Identification and Design Methods*. New York: Springer, 2005.

[71] J. Singh, N. Singh, and J. Sharma, "Fuzzy modeling and control of HVAC systems - A Review," *Journal of Scientific & Industrial Research*, vol. 65, pp. 470–476, June 2006.

[72] G. Ulpiani, M. Borgognoni, A. Romagnoli, and C. Di Perna, "Comparing the performance of ON/OFF, PID and fuzzy controllers applied to the heating system of an energy-efficient building," *Energy and Buildings*, vol. 116, pp. 1–17, Mar. 2016.

[73] S. Bhattacharya, A. Chatterjee, and S. Munshi, "An improved PID-type fuzzy controller employing individual fuzzy P, fuzzy I and fuzzy D controllers," *Transactions of the Institute of Measurement and Control*, vol. 25, pp. 352–372, Sept. 2003.

[74] S. Purdon, B. Kusy, R. Jurdak, and G. Challen, "Model-free HVAC control using occupant feedback," in *38th Annual IEEE Conference on Local Computer Networks - Workshops*, pp. 84–92, 2013.

[75] C. Lin, D. Auslander, and C. Federspiel, "Multi-sensor single-actuator control of HVAC systems," in *Proceedings of the Second International Conference for Enhanced Building Operations*, 2002.

[76] T. I. Salsbury and R. C. Diamond, "Fault detection in HVAC systems using model-based feedforward control," *Energy and Buildings*, vol. 33, no. 4, pp. 403–415, 2001.

[77] B. Thomas, M. Soleimani-Mohseni, and P. Fahlén, "Feed-forward in temperature control of buildings," *Energy and Buildings*, vol. 37, no. 7, pp. 755–761, 2005-07.

[78] K. Zhou, J. C. Doyle, and K. Glover, *Robust and Optimal Control*. Prentice-Hall, Inc., 1st ed., 1996.

[79] X.-D. He, S. Liu, H. H. Asada, and H. Itoh, "Multivariable control of vapor compression systems," *HVAC&R Research*, vol. 4, no. 3, pp. 205–230, 1998.

[80] S. Al-Assadi, R. Patel, M. Zaheer-uddin, M. Verma, and J. Breitinger, "Robust decentralized control of HVAC systems using H_∞-performance measures," *Journal of the Franklin Institute*, vol. 341, no. 7, pp. 543 – 567, 2004.

[81] G. Qu and M. Zaheeruddin, "Real-time tuning of PI controllers in HVAC systems," *International Journal of Energy Research*, vol. 28, no. 15, pp. 1313–1327, 2004.

[82] M. Kasahara, T. Matsuba, Y. Kuzuu, T. Yamazaki, Y. Hashimoto, K. Kamimura, and S. Kurosu, "Design and tuning of robust PID controller for HVAC systems," *ASHRAE Transactions*, vol. 105, p. 154, 1999.

[83] M. Anderson, M. Buehner, P. Young, D. Hittle, C. Anderson, J. Tu, and D. Hodgson, "MIMO robust control for hvac systems," *IEEE Transactions on Control Systems Technology*, vol. 16, no. 3, pp. 475–483, 2008.

[84] G.-R. Duan and H.-H. Yu, *LMIs in Control Systems: Analysis, Design and Applications*. CRC Press, June 2013.

[85] B. Li, N. Jain, and A. G. Alleyne, "LMI control design for nonlinear vapor compression cycle systems," in *Proceedings of the 5th Dynamic Systems and Controls Conference (DSCC)*, vol. 2, pp. 711–718, 2012.

[86] C. Price and B. P. Rasmussen, "Optimal tuning of cascaded control architectures for nonlinear HVAC systems," *Science and Technology for the Built Environment*, vol. 23, no. 8, pp. 1190–1202, 2017.

[87] F. Tahersima, J. Stoustrup, and H. Rasmussen, "An analytical solution for stability-performance dilemma of hydronic radiators," *Energy and Buildings*, vol. 64, pp. 439 – 446, 2013.

[88] J. Zhu, Q. Yang, X. Xu, and J. Lu, "A LPV model-based chilled water temperature controller for HVAC systems," *Building Services Engineering Research and Technology*, vol. 36, no. 3, pp. 368–385, 2015.

[89] C. Hoffmann and H. Werner, "A survey of linear parameter-varying control applications validated by experiments or high-fidelity simulations," *IEEE Transactions on Control Systems Technology*, vol. 23, pp. 416–433, Mar. 2015.

[90] D. Finn and C. Doyle, "Control and optimization issues associated with algorithm-controlled refrigerant throttling devices," *ASHRAE Transactions*, vol. 106, pp. 524–533, 2000.

[91] A. Outtagarts, P. Haberschill, and M. Lallemand, "The transient response of an evaporator fed through an electronic expansion valve," *International Journal of Energy Research*, vol. 21, no. 9, pp. 793–807, 1997.

[92] F. Oldewurtel, A. Parisio, C. N. Jones, D. Gyalistras, M. Gwerder, V. Stauch, B. Lehmann, and M. Morari, "Use of model predictive control and weather forecasts for energy efficient building climate control," *Energy and Buildings*, vol. 45, pp. 15 – 27, 2012.

[93] C. Bay, *Advancing Embedded and Extrinsic Solutions for Optimal Control and Efficiency of Energy Systems in Buildings*. PhD thesis, Texas A&M University, 2017.

[94] A. Afram and F. Janabi-Sharifi, "Theory and applications of HVAC control systems - A review of model predictive control (MPC)," *Building and Environment*, vol. 72, pp. 343 – 355, 2014.

[95] Y. Ma, F. Borrelli, B. Hencey, B. Coffey, S. Bengea, and P. Haves, "Model predictive control for the operation of building cooling systems," *IEEE Transactions on Control Systems Technology*, vol. 20, pp. 796–803, May 2012.

[96] J. Široký, F. Oldewurtel, J. Cigler, and S. Prívara, "Experimental analysis of model predictive control for an energy efficient building heating system," *Applied Energy*, vol. 88, no. 9, pp. 3079 – 3087, 2011.

[97] S. R. West, J. K. Ward, and J. Wall, "Trial results from a model predictive control and optimisation system for commercial building HVAC," *Energy and Buildings*, vol. 72, pp. 271 – 279, 2014.

[98] M. G. Na, "Auto-tuned PID controller using a model predictive control method for the steam generator water level," *IEEE Transactions on Nuclear Science*, vol. 48, pp. 1664–1671, Oct 2001.

[99] M. Xu, S. Li, W. jian Cai, and L. Lu, "Effects of a GPC-PID control strategy with hierarchical structure for a cooling coil unit," *Energy Conversion and Management*, vol. 47, no. 1, pp. 132 – 145, 2006.

[100] M. S. Elliott and B. P. Rasmussen, "Optimal setpoints for HVAC systems via iterative cooperative neighbor communication," *Journal of Dynamic Systems, Measurement, and Control*, vol. 137, no. 1, 2015.

[101] M. S. Elliott and B. P. Rasmussen, "Decentralized model predictive control of a multi-evaporator air conditioning system," *Control Engineering Practice*, vol. 21, no. 12, pp. 1665 – 1677, 2013.

[102] R. E. Jalal and B. P. Rasmussen, "Neighbor-communication distributed model predictive control for coupled and constrained subsystems in networks," in *2015 American Control Conference (ACC)*, pp. 743–749, July 2015.

[103] S. A. Kalogirou, "Artificial neural networks and genetic algorithms in energy applications in buildings," *Advances in Building Energy Research*, vol. 3, no. 1, pp. 83–119, 2009.

[104] S. Song, W. Cai, and Y.-G. Wang, "Auto-tuning of cascade control systems," *ISA Transactions*, vol. 42, no. 1, pp. 63 – 72, 2003.

[105] T. I. Salsbury, "A survey of control technologies in the building automation industry," *IFAC Proceedings Volumes*, vol. 38, no. 1, pp. 90 – 100, 2005. 16th IFAC World Congress.

[106] K. Phalak and G. Wang, "Performance comparison of cascade control with conventional controls in air handling units for building pressurization," in *ASHRAE Winter Conference. Orlando, FL. January*, pp. 26–29, 2016.

[107] C. Guo, Q. Song, and W. Cai, "Supply air temperature control of AHU with a cascade control strategy and a SPSA based neural controller," in *Proceedings. 2005 IEEE International Joint Conference on Neural Networks, 2005.*, vol. 4, pp. 2243–2248 vol. 4, July 2005.

[108] C. Rentel-Gomez and M. Velez-Reyes, "Decoupled control of temperature and relative humidity using a variable-air-volume HVAC system and non-interacting control," in *Control Applications, 2001. (CCA 2001). Proceedings of the 2001 IEEE International Conference on*, pp. 1147–1151, 2001.

[109] M. S. Elliott and B. P. Rasmussen, "On reducing evaporator superheat nonlinearity with control architecture," *International Journal of Refrigeration*, vol. 33, no. 3, pp. 607 – 614, 2010.

[110] M. S. Elliott, C. Estrada, and B. P. Rasmussen, "Cascaded superheat control with a multiple evaporator refrigeration system," in *Proceedings of the 2011 American Control Conference*, pp. 2065–2070, June 2011.

[111] H. Rasmussen, C. Thybo, and L. Larsen, "Nonlinear superheat and evaporation temperature control of a refrigeration plant," *IFAC Proceedings Volumes*, vol. 39, no. 19, pp. 251 – 254, 2006. 1st IFAC Workshop on Energy Saving Control in Plants and Buildings.

[112] Y. I. Son, I. H. Kim, D. S. Choi, and H. Shim, "Robust cascade control of electric motor drives using dual reduced-order pi observer," *IEEE Transactions on Industrial Electronics*, vol. 62, pp. 3672–3682, June 2015.

[113] A. Hildebrandt, O. Sawodny, R. Neumann, and A. Hartmann, "Cascaded control concept of a robot with two degrees of freedom driven by four artificial pneumatic muscle actuators," in *Proceedings of the 2005, American Control Conference, 2005.*, pp. 680–685 vol. 1, June 2005.

[114] M. Bergerman, O. Amidi, J. R. Miller, N. Vallidis, and T. Dudek, "Cascaded position and heading control of a robotic helicopter," in *2007 IEEE/RSJ International Conference on Intelligent Robots and Systems*, pp. 135–140, Oct 2007.

[115] C. R. Price and B. P. Rasmussen, "Effective Tuning of Cascaded Control Loops for Nonlinear HVAC Systems," in *ASME 2015 Dynamic Systems and Control Conference*, vol. 2, (Columbus, OH), Oct. 2015.

[116] C. R. Price, S. Liang, and B. Rasmussen, "HVAC Nonlinearity Compensation Using Cascaded Control Architectures," *ASHRAE Transactions*, vol. 121, pp. 217–231, 2015.

[117] D. Goswami and F. Kreith, *Energy Efficiency and Renewable Energy Handbook*. Mechanical and Aerospace Engineering Series, CRC Press, 2nd ed., 2015.

[118] B. P. Rasmussen, "Dynamic modeling for vapor compression systems - Part I: Literature review," *HVAC&R Research*, vol. 18, no. 5, pp. 934–955, 2012.

[119] J. Lee, D. Hyun Kim, and T. F. Edgar, "Static decouplers for control of multivariable processes," *AIChE Journal*, vol. 51, no. 10, pp. 2712–2720, 2005.

[120] N. Jain, B. Li, M. Keir, B. Hencey, and A. Alleyne, "Decentralized feedback structures of a vapor compression cycle system," *IEEE Transactions on Control Systems Technology*, vol. 18, pp. 185–193, Jan 2010.

[121] S. Skogestad and I. Postlethwaite, *Multivariable Feedback Control: Analysis and Design*. John Wiley & Sons, 2nd ed., 2005.

[122] E. Bristol, "On a new measure of interaction for multivariable process control," *IEEE Transactions on Automatic Control*, vol. 11, pp. 133–134, Jan 1966.

[123] F. L. Lewis and V. L. Syrmos, *Optimal Control*. Wiley, 2nd ed., 1995.

[124] K. Ogata, *Discrete-Time Control Systems*. Englewood Cliffs, NJ: Prentice Hall, 2nd ed., 1995.

[125] C. R. Price and B. P. Rasmussen, "Decoupling of MIMO systems using cascaded control architectures with application for HVAC systems," in *2017 American Control Conference (ACC)*, pp. 2907–2912, May 2017.

[126] Anaheim Automation, "BLK42 Series Brushless DC Motors: Model 170v-300," 2011.

[127] I. Khoo, G. Levermore, and K. Letherman, "Variable-air-volume terminal units 1: Steady-state models," *Building Services Engineering Research and Technology*, vol. 19, pp. 155–162, Jan. 1998.

[128] X. Zhou and J. E. Braun, "A simplified dynamic model for chilled-water cooling and dehumidifying coils - Part 1: Development (RP-1194)," *HVAC&R Research*, vol. 13, no. 5, pp. 785–804, 2007.

[129] X. Zhou and J. Braun, "A simplified dynamic model for chilled-water cooling and dehumidifying coils - Part 2: Experimental validation (RP-1194)," *HVAC&R Research*, vol. 13, pp. 805–817, Sept. 2007.

[130] L. Hansen, *Stochastic Modeling of Central Heating Systems*. Phd thesis, Department of Mathematical Modeling at the Technical University of Denmark, Kongens Lyngby, Denmark, 1997.

[131] Air-Conditioning, Heating, & Refrigeration Institute (AHRI), "Monthly air conditioning & heat pump system shipment data," 2011. http://www.ahrinet.org/Resources/Statistics/Monthly-Shipments.aspx.

[132] X.-M. Guo, Y.-G. Chen, W.-H. Wang, and C.-Z. Chen, "Experimental study on frost growth and dynamic performance of air source heat pump system," *Applied Thermal Engineering*, vol. 28, pp. 2267–2278, Dec. 2008.

[133] J. Zhu, Y. Sun, W. Wang, S. Deng, Y. Ge, and L. Li, "Developing a new frosting map to guide defrosting control for air-source heat pump units," *Applied Thermal Engineering*, vol. 90, pp. 782–791, Nov. 2015.

[134] Emerson Climate Technologies, "Electronic Expansion Valves EXM/L Series," 2015. http://www.emersonclimate.com/europe/ProductDocuments/AlcoLiterature/EN_EXML%20TB.pdf.

[135] T.-T. Tay, I. Mareels, and J. B. Moore, *High Performance Control*. Systems & Control: Foundations & Applications, Birkhauser Boston, 1998.

[136] B. P. Rasmussen and A. G. Alleyne, "Gain scheduled control of an air conditioning system using the youla parameterization," *IEEE Transactions on Control Systems Technology*, vol. 18, pp. 1216–1225, Sept 2010.

[137] A. Tayebi, S. Abdul, M. B. Zaremba, and Y. Ye, "Robust iterative learning control design: Application to a robot manipulator," *IEEE/ASME Transactions on Mechatronics*, vol. 13, pp. 608–613, Oct 2008.

[138] J. Stoustrup and H. Nieman, "Fault tolerant feedback control using the youla parameterization," in *2001 European Control Conference (ECC)*, pp. 1970–1974, Sept 2001.

[139] J. Ma, T. Wang, S. Wang, X. Gao, X. Zhu, Z. Wang, and J. S. Thorp, "Application of dual youla parameterization based adaptive wide-area damping control for power system oscillations," *IEEE Transactions on Power Systems*, vol. 29, pp. 1602–1610, July 2014.

[140] B. P. Rasmussen and Y. J. Chang, "Stable controller interpolation and controller switching for lpv systems," *Journal of Dynamic Systems, Measurement and Control*, vol. 132, no. 1, pp. 1–12, 2010.

[141] S. P. Boyd, L. El Gahoui, E. Feron, and V. Balakrishnan, *Linear Matrix Inequalities in System and Control Theory*, vol. 15 of *SIAM Studies in Applied Mathematics*. Philadelphia: Society for Industrial and Applied Mathematics (SIAM), 1994.

[142] T. Hagglund, "A control-loop performance monitor," *Control Engineering Practice*, vol. 3, no. 11, pp. 1543 – 1551, 1995.

[143] N. Thornhill and T. Hagglund, "Detection and diagnosis of oscillation in control loops," *Control Engineering Practice*, vol. 5, no. 10, pp. 1343 – 1354, 1997.

[144] T. Miao and D. E. Seborg, "Automatic detection of excessively oscillatory feedback control loops," in *Proceedings of the 1999 IEEE International Conference on Control Applications (Cat. No.99CH36328)*, vol. 1, pp. 359–364 vol. 1, 1999.

[145] N. Thornhill, B. Huang, and H. Zhang, "Detection of multiple oscillations in control loops," *Journal of Process Control*, vol. 13, no. 1, pp. 91 – 100, 2003.

[146] Siemens Building Technologies, *APOGEE Powers Process Control Language (PPCL) User's Manual*, Oct. 2000.

[147] Siemens Building Technologies, *Adaptive Control Application Guide*, Apr. 2008.

[148] S. Walker, "The Academic Building and the YMCA," *The Texas A&M Association of Former Students Newsletter*, Sept. 2014.

[149] M. K. Khattar and M. J. Brandemuehl, "Separating the V in HVAC: A dual-path approach," *ASHRAE Journal*, vol. 44, p. 37, May 2002.

[150] S. J. Emmerich and T. McDowell, "Initial evaluation of displacement ventilation and dedicated outdoor air systems for U.S. commercial buildings," Tech. Rep. NISTIR 7244, National Institute of Standards and Technology, July 2005.

[151] M. A. S. Choudhury, V. Kariwala, S. L. Shah, H. Douke, H. Takada, and N. F. Thornhill, "A simple test to confirm control valve stiction," *IFAC Proceedings Volumes*, vol. 38, no. 1, pp. 81 – 86, 2005. 16th IFAC World Congress.

APPENDIX A

JURY STABILITY CRITERIA FOR SECOND ORDER SYSTEMS

A.1 Under & Over Damped Case ($\zeta \neq 1$)

$$G_{zoh}(z) = Z\left\{\frac{1-e^{-sT}}{s}\left(\frac{\psi(\sigma)\omega_n^2}{s^2+2\zeta\omega_n s+\omega_n^2}\right)\right\}$$
$$= \psi(\sigma)\left\{1-\frac{z-1}{\sqrt{1-\zeta^2}}\cdot\frac{z\sqrt{1-\zeta^2}+e^{-\zeta\omega_n T}\sin(\omega_n\sqrt{1-\zeta^2}T-\phi)}{z^2-2ze^{-\zeta\omega_n T}\cos(\omega_n\sqrt{1-\zeta^2}T)z+e^{-2\zeta\omega_n T}}\right\}$$

where $\phi = \arccos(\zeta)$ and T is the hold time.

Jury Test #1-2:

$$K^*_{1-2} = \frac{\pm 1 - e^{-2\zeta\omega_n T}}{e^{-2\zeta\omega_n T} + \frac{e^{-\zeta\omega_n T}}{\sqrt{1-\zeta^2}}\sin(\omega_n\sqrt{1-\zeta^2}T-\phi)}$$

Jury Test #3-4:

$$K^*_{3-4} = \frac{-1-e^{-2\zeta\omega_n T}\pm 2e^{-\zeta\omega_n T}\cos(\omega_n\sqrt{1-\zeta^2}T)}{e^{-2\zeta\omega_n T}+\frac{e^{-\zeta\omega_n T}}{\sqrt{1-\zeta^2}}\left[\sin(\omega_n\sqrt{1-\zeta^2}T-\phi)\mp\sin(\omega_n\sqrt{1-\zeta^2}T+\phi)\right]\pm 1}$$

A.2 Critically Damped Case ($\zeta = 1$)

$$G_{zoh}(z) = Z\left\{\frac{1-e^{-sT}}{s}\left(\frac{a^2\psi(\sigma)}{(s+a)^2}\right)\right\}$$
$$= \psi(\sigma)\frac{[1-e^{-aT}(1+aT)]z+e^{-aT}(-1+aT+e^{-aT})}{(z-e^{-aT})^2}$$

Jury Test #1-2: $K^*_{1-2} = \frac{1}{\psi(\sigma)}\cdot\frac{\pm 2e^{-aT}\mp e^{-2aT}\mp 1}{\pm 1\mp 2e^{-aT}+e^{-2aT}}$

Jury Test #3-4: $K^*_{3-4} = \frac{\pm 1-e^{-2aT}}{e^{-aT}(-1+aT+e^{-aT})}$

APPENDIX B

MODELS FOR CHAPTER 2 CASE STUDIES

B.1 Case Study #1: Tuning Models

$$\begin{cases} \dot{x}_T = \begin{bmatrix} -2 & 0 & 0 \\ 0 & -5 & 0 \\ 0.7071 & 0 & -1 \end{bmatrix} x_T + \begin{bmatrix} 2.8284 \\ 5 \\ 0 \end{bmatrix} u_i \\ y = \begin{bmatrix} 0 & 1 & 0 \\ 0 & 0 & 1 \end{bmatrix} x_T \end{cases}$$

$$\begin{cases} \dot{x}_A = \begin{bmatrix} -2 & 0 & 0 & 0 \\ 0 & -5 & 0 & 0 \\ 0.7071 & 0 & -1 & 0 \end{bmatrix} x_A + \begin{bmatrix} 2.8284 \\ 5 \\ 0 \\ 0 \end{bmatrix} u_i \\ y = \begin{bmatrix} 0 & 1 & 0 & 0 \\ 0 & 0 & 1 & 0 \\ 0 & 0 & 0 & 1 \end{bmatrix} x_A \end{cases}$$

Final Tuning Parameters: $R = 3.16$, $q_1 = 1\text{x}10^{-5}$, $q_2 = q_3 = 1$, $q_4 = 1.25\text{x}10^{4}$

B.2 Case Study #7: Heat Pump Models

Demand	State-Space	Steady-State
Low	$\left[\begin{array}{cc\|c} -0.00327 & 0.00233 & 6.99\text{x}10^{-5} \\ -0.00482 & -0.00084 & 1.19\text{x}10^{-4} \\ \hline -24.92 & 5.238 & 0 \\ 197.9 & 76.42 & 0 \end{array}\right]$	$y_{ss} = \begin{bmatrix} -0.42 \\ 6.26 \end{bmatrix}$
Moderate	$\left[\begin{array}{cc\|c} -0.00488 & 0.00304 & 1.31\text{x}10^{-4} \\ -0.00447 & -0.00412 & 1.09\text{x}10^{-4} \\ \hline -9.972 & 1.619 & 0 \\ 96.22 & 55.29 & 0 \end{array}\right]$	$y_{ss} = \begin{bmatrix} -0.33 \\ 2.53 \end{bmatrix}$
High	$\left[\begin{array}{cc\|c} -0.00420 & -0.00083 & 7.43\text{x}10^{-5} \\ 0.00027 & -0.00221 & -1.86\text{x}10^{-6} \\ \hline -17.92 & -1.515 & 0 \\ 80.85 & -54.74 & 0 \end{array}\right]$	$y_{ss} = \begin{bmatrix} -0.29 \\ 0.94 \end{bmatrix}$

APPENDIX C

TABLES FOR CHAPTER 4.5 EXAMPLE

LQN stands for Linear-Q Network and LCN stands for Linear Controller Network. These are defined respectively by interpolating the Youla parameter Q or the controller directly. Note that θ and ϕ are the plant and controller scheduling variables respectively.

Table C.1: Single Plant with Single Controller and LSN-LQN Network ($P_0 = 0.6$)

$\theta \setminus \phi$	0 (PI)	0.25	0.5	0.75	1 (CC)	PI - CC
0.2	1.2712	1.0849	0.9415	0.8329	0.7547	0.5165
0.4	0.9677	0.9151	0.8698	0.8332	0.8067	0.1611
0.6	1.0147	0.9851	0.9561	0.9290	0.9059	0.1088
0.8	1.1317	1.1080	1.0823	1.0552	1.0284	0.1033
1	1.2368	1.2192	1.1991	1.1761	1.1508	0.0860

Table C.2: Single Plant with Single Controller and LSN-LCN Network ($P_0 = 0.6$)

$\theta \setminus \phi$	0 (PI)	0.25	0.5	0.75	1 (CC)	PI - CC
0.2	1.2712	1.0556	0.9144	0.8150	0.7547	0.5165
0.4	0.9677	0.8956	0.8501	0.8227	0.8067	0.1611
0.6	1.0147	0.9751	0.9454	0.9230	0.9059	0.1088
0.8	1.1317	1.0993	1.0719	1.0485	1.0284	0.1033
1	1.2368	1.2121	1.1898	1.1694	1.1508	0.0860

Table C.3: Single Plant with Polytopic Controller and LSN-LQN Network

$\theta \setminus P_0$	0 (PI)	0.25	0.5	0.75	1 (CC)
0.2	2.7699	2.4114	2.4061	2.4693	2.5196
0.4	2.2844	1.9317	1.7966	1.7966	1.7966
0.6	2.9579	2.9579	2.9579	2.9579	2.9579
0.8	6.4954	6.4954	6.4954	6.4954	6.4954
1	13.8410	13.8410	13.8410	13.8410	13.8410

Table C.4: Single Plant with Polytopic Controller and LSN-LCN Network

$\theta \setminus P_0$	0 (PI)	0.25	0.5	0.75	1 (CC)
0.2	2.5491	2.5491	2.5491	2.5491	2.5491
0.4	1.5834	1.5834	1.5834	1.5834	1.5834
0.6	2.1601	2.1601	2.1601	2.1601	2.1601
0.8	4.7436	4.7436	4.7436	4.7436	4.7436
1	10.1081	10.1081	10.1081	10.1081	10.1081

Table C.5: Polytopic Plant with Single Controller and LSN-LQN Network

$P_0 \setminus \phi$	0 (PI)	0.25	0.5	0.75	1 (CC)
0.2	2.2735	2.1515	2.0227	1.8821	1.7245
0.4	2.2735	2.1106	1.9679	1.8392	1.7245
0.6	2.2735	2.0703	1.9174	1.8033	1.7245
0.8	2.2735	2.0381	1.8853	1.7858	1.7245
1	2.2735	2.0273	1.8791	1.7846	1.7245

Table C.6: Polytopic Plant with Single Controller and LSN-LCN Network

$P_0 \setminus \phi$	0 (PI)	0.25	0.5	0.75	1 (CC)
0.2	2.2735	2.0496	1.9021	1.7988	1.7246
0.4	2.27353	2.04955	1.90211	1.79882	1.7245
0.6	2.27353	2.0495	1.9021	1.7988	1.7245
0.8	2.27353	2.0495	1.9021	1.7988	1.7245
1	2.27353	2.0495	1.9021	1.7988	1.7245

Table C.7: Comparison of full Polytopic Plant & Controller Combination

P_0	0.2	0.4	0.6	0.8	1.0
LSN + LQN	15.1023	14.6304	14.6273	14.7174	14.8266
LSN + LCN	10.7169	10.7168	10.7168	10.7168	10.7168

APPENDIX D

HUNTING DETECTION ALGORITHM

The following code implements the hunting detection algorithm developed by [30]. This implementation builds upon the one discussed there by adding additional features including excluding off-time from the hunting percentage calculation and reducing false positives by checking the forward and previous magnitudes between oscillations to exclude large step changes.

```
function [hunting_amt] = FNC_IdentifyHunting_CRP(t,data,Alim,Tlim,h)
% Alim is peak-to-peak minimum amplitude
% Tlim is the index window for two oscillations

% Indices of identified hunting & total length of data
data_loc = [];
data_len = length(data);

% Step 1: Calculate sign changes
sgns_bck = sign(data(2:end-1) - data(1:end-2));
sgns_fwd = sign(data(3:end+0) - data(2:end-1));
sgns_bck(sgns_bck == 0) = 1;
sgns_fwd(sgns_fwd == 0) = 1;
sgns = find(sgns_bck ~= sgns_fwd);

% Step 2: Initialize Hunting Variables
if ~isempty(sgns)
    i_h = 1;
    i_o = sgns(1);
    n_osc = 0;

    % Step 3: Detect hunting behavior
    for i = 3:2:length(sgns)
        i_c = sgns(i);

        % Calculate peak-to-peak amplitude of oscillation
        A = abs([data(i_c)-data(sgns(i-1)) data(sgns(i-1))-data(i_o)]);

        % Check in inside hunting window
        if (i_c - i_h) > Tlim
            i_h = sgns(i-2);
            i_o = i_c;
            n_osc = 0;
```

```
        % Check forward & back magnitude of oscillation
        elseif all(A > Alim)
            % If first large oscillation, set up window variables...
            if n_osc == 0
                n_osc = 1;
                i_h = sgns(i-2);
                i_o = i_c;
            % Otherwise there is hunting...
            else
                data_loc = [data_loc; i_h i_c];
                i_h = i_o;
                i_o = i_c;
            end
        end
    end
end

% Check if there was any hunting...
if ~isempty(data_loc)
    i = 2:data_len-1;

    % Check if last index of hunting is within Tlim of end...
    if (data_len - data_loc(end,2)) < Tlim
        data_loc(end,2) = data_len-1;
    end

    % Create logical index variable with identified hunting locations
    j = i >= data_loc(:,1);
    k = i <= data_loc(:,2);
    data_loc = sum(logical(j.*k),1) > 0;

    % Look for times when the system is off & sum off time
    offtime = find(data ~= 0)';
    offtime = diff(offtime);
    i = offtime > 36;
    offtime = sum(offtime(i));

    % Plot hunting periods
    data(data_loc == 0) = nan;
    plot(h,t,data,'r-','linewidth',2)

    % Calculate time spent hunting while on
    % (the -1 is to fix earlist index of 2...)
    hunting_amt = sum(data_loc)/(data_len - 2 - offtime)*100;
else
    hunting_amt = 0;
end
```

APPENDIX E

PPCL BUILDING CODE

The following code is from the TTI Building and is representative of PPCL code for normal building HVAC control. Sections are grouped by shading and annotated to improve understanding. See Figure 5.9 for control diagram.

```
00001 C --- START OF CODE ---
00100 C --- DEFININTIONS ---
00101 DEFINE(RM, "TTI1600.FV3")
00102 DEFINE(DN, ":DAY.NGT")
00103 DEFINE(CLO, ":CLG LOOPOUT")
00104 DEFINE(DMP, ":DMPR COMD")
00105 DEFINE(VLV, ":VLV COMD")
00106 DEFINE(NOV, ":NGT OVRD")
00107 DEFINE(MODE,"1600_AHU3")
00108 DEFINE(OAT,"1600_VOADBT")
00109 DEFINE(OAD,"TTI1600.A3OAD")
00110 DEFINE(SFSS,"TTI1600.A3SS")
00111 DEFINE(SVF,"TTI1600.A3VFD")
00112 DEFINE(SVFV,"1600_A3.SVF.V")
00113 DEFINE(DAT,"TTI1600.A3DT")
00114 DEFINE(DATS,"1600_A3.DAT.S")
00114 DEFINE(CCV,"TTI1600.A3CDV")
00115 DEFINE(CCVV,"1600_A3.CCV.V")
00116 DEFINE(DAS1,"TTI1600.A3SP1")
00117 DEFINE(DAS2,"TTI1600.A3SP2")
00118 DEFINE(DASS,"TTI1600.A3SSP")
00119 DEFINE(DSMK,"TTI1600.A3DSM")
00120 DEFINE(ACLP,"1600_A3.ACLP")
00121 DEFINE(ACDMP,"1600_A3.ACDMP")
00200 C --- DEFINE LOCAL VARIABLES ---
00210 LOCAL(XDATS,NDATS,XDASS,NDASS,CLPTTL,DMPTTL,MDAS,TECCNT)
00300 C --- CONVERT PERCENTAGES TO VOLTAGES ---
00310 TABLE("1600_A3.CCV.V","TTI1600.A3CDV",0,10,100,0)
00320 TABLE("%SVFV%","%SVF%",0,0,100,10)
00400 C --- CALCULATE GLOBAL VARIABLES ---
00410 C find smallest end static pressure value
00411 MIN($MDAS,"%DAS1%","%DAS2%")
00420 C caltulate damper and flow demand every 30 seconds
00421 SAMPLE(30) GOTO 500
00430 C initialize values for damper and flow demand
00430 IF("%ACLP%" .EQ. 0 .AND. "%ACDMP%" .EQ. 0) THEN GOTO 325
00440 GOTO 700
```

```
00500 C --- CALCULATE DEMAND VALUES (FOR LOOP) ---
00505 SET(0,"$TECCNT","$CLPTTL","$DMPTTL",$LOC10,$LOC11,$LOC12,$LOC1)
00510 GOSUB 700 "%RM%01%DN","%RM%01%CLO","%RM%01%DMP"
  :
00590 GOSUB 700 "%RM%99%DN","%RM%99%CLO","%RM%99%DMP"
00595 GOTO 800
00700 C --- SUBROUTINE TO SUM VAV BOX VALUES ---
00710 IF($ARG1 .EQ. FAILED) THEN GOTO 770
00720 C count number of boxes
00721 "$TECCNT" = "$TECCNT" + 1
00730 C sum flow commands and find max
00731 "$CLPTTL" = "$CLPTTL" + $ARG2
00732 MAX($LOC10,$LOC10,$ARG2)
00740 C sum damper commands and find max
00741 "$DMPTTL" = "$DMPTTL" + $ARG3
00742 MAX($LOC11,$LOC11,$ARG3)
00750 RETURN
00800 C --- CALCULATE WEIGHTED AVG ---
00810 "%ACLP%" = "$CLPTTL" / "$TECCNT" * (2 / 5) + $LOC10 * (3 / 5)
00820 "%ACDMP%" = "$DMPTTL" / "$TECCNT" * (2 / 5) + $LOC11 * (3 / 5)
00900 C --- FIRE SAFETY CHECK ---
00910 IF("%RMSMK%" .NE. ON .AND. "%DSMK%" .NE. ON) THEN GOTO 950
00920 OFF(@SMOKE,"%SFSS%","%OAD%")
00930 SET(0,"%CCVV%","%SVFV%")
00940 GOTO 1700
00950 RELEAS(@SMOKE,"%SFSS%","%OAD%")
01000 C --- DETERMINE MODE / REDIRECT ---
01010 IF("%MODE%" .EQ. 0) THEN GOTO 1100
01020 IF("%MODE%" .EQ. 1) THEN GOTO 1200
01030 IF("%MODE%" .GE. 2 .AND. "%MODE%" .LE. 11) THEN GOTO 1300
01040 IF("%MODE%" .EQ. 12) THEN GOTO 1400
01050 GOTO 1300
01100 C --- UNOCC - ESSENTIAL ONLY ---
01110 ON("%SFSS%")
01120 OFF("%OAD%")
01130 $XDATS = 70
01140 $NDATS = 53
01150 $XDASS = 1.5
01160 $NDASS = 0.5
01170 GOSUB 1500
01180 GOTO 1600
01200 C --- NORMAL OCCUPATION ---
01210 ON("%SFSS%")
01220 IF("%OAT%" .LT. 50) THEN OFF("%OAD%") ELSE ON("%OAD%")
01230 $NDATS = 53
01240 $XDATS = 57
01250 $XDASS = 2.3
01260 $NDASS = 0.5
01270 GOSUB 1500
01280 GOTO 1600
```

```
01300 C --- LOW OCCUPATION ---
01310 ON("%SFSS%")
01320 OFF("%OAD%")
01330 $XDATS = 70
01340 $NDATS = 55
01350 $XDASS = 1.75
01360 $NDASS = 0.5
01370 GOSUB 1500
01380 GOTO 1600
01400 C --- OCC3 - OCC5 ---
01410 C --- WARMUP ---
01420 C --- COOLDOWN ---
01430 C --- NIGHT HEATING/COOLING ---
01440 C --- STOP HEATING/COOLING ---
01450 C --- HIBERNATE (CAMPUS BREAK) ---
01460 OFF("%SFSS%","%OAD%")
01470 SET(0,"%CCVV%","%SVFV%")
01480 GOTO 1600
01500 C --- SUBROUTINE TO RESET SETPOINTS AND MODULATE FAN/VALVE ---
01505 C discharge air temperature setpoint
01515 $XDATS = 63
01520 $LOC1 = $NDATS + ($XDATS - $NDATS) / 2
01525 LOOP(128,"%ACLP%","%DATS%",50,15,1.5,0,300,$LOC1,$NDATS,$XDATS,0)
01530 C chilled water valve position
01535 C PI control is line 1540, CC is lines 1545 and 1550
01540 C LOOP(0,"%DAT%","%CCVV%","%DATS%",60,15,0,15,50,0,100,0)
01545 $LOC2 = 20+1.0*"%DAT%"
01550 LOOP(0,"%DAT%","%CCVV%","%DATS%",100,5,0,1,$LOC2,0,100,0)
01555 C end static pressure setpoint
01560 $NDASS = 0.5
01565 $LOC11 = $NDASS + ($XDASS - $NDASS) / 2
01570 LOOP(0,"%ACDMP%","%DASS%",58,.5,.05,0,300,$LOC11,$NDASS,$XDASS,0)
01575 C fan speed
01580 LOOP(128,$MDAS,"%SVFV%","%DASS%",2500,250,20,15,60,20,100,0)
01585 RETURN
01600 C --- END OF CODE---
01601 GOTO 1
```